

Sum Frequency Generation Vibrational Spectroscopy of Adsorbed Amino Acids,  
Peptides, and Proteins at Hydrophilic and Hydrophobic Solid-Water Interfaces

By

George Joseph Holinga IV

A dissertation submitted in partial satisfaction of the

requirements for the degree of

Doctor of Philosophy

in

Chemistry

in the

Graduate Division

of the

University of California, Berkeley

Committee in charge:

Professor Gabor A. Somorjai, Chair  
Professor Ronald C. Cohen  
Professor Kevin E. Healy

Fall 2010

Sum Frequency Generation Vibrational Spectroscopy of Adsorbed Amino Acids,  
Peptides, and Proteins at Hydrophilic and Hydrophobic Solid-Water Interfaces

Copyright © 2010

by

George Joseph Holinga IV

## Abstract

### Sum Frequency Generation Vibrational Spectroscopy of Adsorbed Amino Acids, Peptides, and Proteins at Hydrophilic and Hydrophobic Solid-Water Interfaces

by

George Joseph Holinga IV

Doctor of Philosophy in Chemistry

University of California, Berkeley

Professor Gabor A. Somorjai, Chair

Sum frequency generation (SFG) vibrational spectroscopy was used to investigate the interfacial properties of several amino acids, peptides, and proteins adsorbed at the hydrophilic polystyrene solid-liquid and the hydrophobic silica solid-liquid interfaces. The influence of experimental geometry on the sensitivity and resolution of the SFG vibrational spectroscopy technique was investigated both theoretically and experimentally. SFG was implemented to investigate the adsorption and organization of eight individual amino acids at model hydrophilic and hydrophobic surfaces under physiological conditions. Biointerface studies were conducted using a combination of SFG and quartz crystal microbalance (QCM) comparing the interfacial structure and concentration of two amino acids and their corresponding homopeptides at two model liquid-solid interfaces as a function of their concentration in aqueous solutions. The influence of temperature, concentration, equilibration time, and electrical bias on the extent of adsorption and interfacial structure of biomolecules were explored at the liquid-solid interface via QCM and SFG. QCM was utilized to quantify the biological activity of heparin functionalized surfaces. A novel optical parametric amplifier was developed and utilized in SFG experiments to investigate the secondary structure of an adsorbed model peptide at the solid-liquid interface.

# Table of Contents

List of Figures.....	iv
List of Tables.....	x
Acknowledgements.....	xi
<b>Chapter 1. Introduction.....</b>	<b>1</b>
<b>Chapter 2. Sum Frequency Generation Vibrational Spectroscopy.....</b>	<b>4</b>
2.1. Sum Frequency Generation Vibrational Spectroscopy Introduction.....	4
2.2. Sum Frequency Generation Theoretical Background.....	4
2.3. Sum Frequency Generation from a Surface.....	7
2.4. Sum Frequency Generation Instrumentation.....	8
2.5. Sum Frequency Generation Sample Substrate Preparation.....	9
References.....	11
<b>Chapter 3. Sum Frequency Generation Vibrational Spectroscopy and the Influence of Experimental Sample Geometry on Technique Sensitivity for an Absorptive Medium or Media.....</b>	<b>12</b>
3.1. Introduction.....	12
3.2. Experimental.....	13
3.2.1. SFG Theoretical Analysis.....	13
3.2.2. SFG Experimental Measurements.....	16
3.2.3. SFG Sample Preparation.....	17
3.3. Results and Discussion.....	17
3.4. Conclusions.....	25
References.....	26
<b>Chapter 4. Quartz Crystal Microbalance.....</b>	<b>29</b>
4.1. Quartz Crystal Microbalance Introduction.....	29
4.2. Quartz Crystal Microbalance Theoretical Background.....	29
4.3. Quartz Crystal Microbalance Instrumentation.....	31
4.4. Quartz Crystal Microbalance Sample Substrate Preparation.....	33
References.....	34
<b>Chapter 5. A SFG Study of Interfacial Amino Acids at the Hydrophilic SiO<sub>2</sub> and Hydrophobic Deuterated Polystyrene Surfaces.....</b>	<b>35</b>
5.1. Introduction.....	35
5.2. Experimental.....	36
5.2.1. SFG Experimental Measurements.....	36
5.2.2. Chemicals.....	36
5.2.3. SFG Sample Preparation.....	37
5.3. Results and Discussion.....	37

5.3.1. SFG of Phosphate Buffered Saline at the Hydrophobic Deuterated Polystyrene and the Hydrophilic SiO <sub>2</sub> Surfaces.....	37
5.3.2. SFG at the Hydrophobic Deuterated Polystyrene Surface.....	40
5.3.3. SFG Data at the Hydrophilic SiO <sub>2</sub> Surface.....	49
5.4. Conclusions.....	57
References.....	59

**Chapter 6. A Study of the Influence of Amino Acid Side Functional Group on the Adsorption of Interfacial Homopeptides and Their Constituent Amino Acids on Hydrophilic SiO<sub>2</sub> and Hydrophobic Polystyrene Surfaces Studied by SFG and QCM.....61**

6.1. Introduction.....	61
6.2. Experimental.....	62
6.2.1. QCM Experimental Measurements.....	62
6.2.2. SFG Experimental Measurements.....	63
6.2.3. Chemicals.....	63
6.2.4. Sample Preparation.....	64
6.3. Results and Discussion.....	64
6.3.1. QCM Data and Analysis.....	64
6.3.2. SFG Data and Analysis.....	67
6.3.3. Discussion of Combined QCM and SFG Results.....	74
6.4. Conclusions.....	77
References.....	78

**Chapter 7. A SFG and QCM Investigation of the Influence of Temperature, Concentration, Competitive Adsorption, Amino Acid Residue Structure, Electrical Bias, and Equilibration Time on the Adsorption and Interfacial Organization of Several Amino Acids and Peptides.....80**

7.1. Introduction.....	80
7.2. Experimental.....	81
7.2.1. QCM Experimental Measurements.....	81
7.2.2. SFG Experimental Measurements.....	81
7.2.3. Chemicals.....	82
7.2.4. Sample Surface Preparation.....	82
7.3. Results and Discussion.....	82
7.3.1. SFG Investigation of Amino Acid Coadsorption on Hydrophilic and Hydrophobic Surfaces.....	82
7.3.2. Langmuir-Type Adsorption Behavior of Amino Acids as a Function of Side Chain, Solution Concentration, and Interface Character.....	89
7.3.3. SFG Spectrum of L-Proline Amino Acid as a Function of Interface Temperature.....	93
7.3.4. The Time-Dependent Nature of SFG Experiments in the Laboratory.....	96
7.3.5. SFG Comparison of Poly-L-Proline and the Collagen-Like Peptide Ac-(PPG) <sub>4</sub> -NH <sub>2</sub> .....	97
7.3.6. SFG Investigation of H <sub>2</sub> O, PBS, and L-Arginine at the Platinum Electrode Surface.....	98
7.4. Conclusions.....	103

References.....	104
<b>Chapter 8. An SFG and QCM Study of Biologically Active Heparin Functionalized Surfaces.....106</b>	
8.1. Introduction.....	106
8.2. Experimental.....	108
8.2.1. QCM Experimental Measurements.....	108
8.2.2. SFG Experimental Measurements.....	108
8.2.3. Chemicals.....	109
8.2.4. Heparin Functionalized Surface Preparation.....	109
8.3. Results and Discussion.....	110
8.3.1. QCM Data and Analysis.....	110
8.3.2. SFG Data and Analysis.....	114
8.4. Conclusions.....	115
References.....	116
<b>Chapter 9. The Development and Implementation of a Novel Optical Parametric Amplifier Utilizing Lithium Thioindate to Probe the Amide I Mode of a Model Amphiphilic Peptide.....118</b>	
9.1. Introduction.....	118
9.2. Experimental.....	119
9.2.1. SFG Experimental Details.....	119
9.2.2. Peptide Synthesis and Sample Preparation Details.....	122
9.3. Results and Discussion.....	122
9.4. Conclusions.....	126
References.....	127

## List of Figures

Figure 2.1. Schematic of the Laservision OPG/OPA laser setup used for SFG experiments.....	9
Figure 2.2. Diagram of SFG sample substrate in slab geometry.....	10
Figure 2.3. Diagram of SFG sample substrate in prism geometry.....	10
Figure 3.1. SiO <sub>2</sub> sample substrate diagram for slab geometry used in SFG experiments.....	13
Figure 3.2. SiO <sub>2</sub> sample substrate diagram for prism geometry used in SFG experiments.....	13
Figure 3.3. Diagram of SFG beam geometry at the interface between medium 1 and medium 2 with a thin interfacial layer between them.....	15
Figure 3.4. Plot of real (blue line) and imaginary (green line) components of the index of refraction of liquid H <sub>2</sub> O in the infrared wavelength region 2800 cm <sup>-1</sup> to 3600 cm <sup>-1</sup> .....	16
Figure 3.5. Plot of the geometric factor, $G(\beta')$ , at infrared frequencies of 2800 cm <sup>-1</sup> (blue line), 3200 cm <sup>-1</sup> (green line) and 3600 cm <sup>-1</sup> , respectively, as a function of the average angle of incidence of the input laser beams $\beta' = (\beta_{IR} + \beta_{vis})/2$ , and normalized by the G factor at $\beta' = 35^\circ$ .....	18
Figure 3.6. Plot of ratio of geometric factor for the prism geometry, $G_{prism}$ , normalized by the geometric factor value for the slab geometry, $G_{slab}$ , as a function of incident infrared wavelength in the region 2800 - 3600 cm <sup>-1</sup> .....	19
Figure 3.7. Plot of the ratios of Fresnel transmission coefficients for the prism geometry relative to the slab geometry as a function of infrared wavelength.....	20
Figure 3.8. Plot of the Fresnel coefficient for transmitted infrared light as a function of the infrared beams' angle of incidence.....	21
Figure 3.9. Plot of ratios of simulated geometry related terms, $ \sin(\beta_{IR}) ^2$ (blue line) and $ \sec(\beta) ^2$ (green line), comparing prism and slab geometries as a function of infrared frequency.....	21
Figure 3.10. SFG spectra of the polystyrene-air interface in the slab (black circles) and prism (red squares) experimental beam geometries.....	23
Figure 3.11. SFG spectra of the SiO <sub>2</sub> - H <sub>2</sub> O solid-liquid interface at room temperature in slab (black circles) and prism (red squares) experimental beam geometries.....	24
Figure 3.12. Comparison of predicted theoretical (red circles) and experimentally measured (black squares) ratio of SFG signal enhancement obtained in the prism sample geometry relative to the slab geometry.....	25

Figure 4.1. Schematic of QCM sensor surface displacement with externally applied surface potential.....	30
Figure 4.2. Schematic of Q-sense QCM instrument measurement process.....	32
Figure 4.3. Diagram of Q-sense QCM instrument's liquid measurement chamber and sensor crystal as experimentally used.....	33
Figure 5.1. SFG spectrum of PBS at the hydrophobic $d_8$ -PS surface.....	38
Figure 5.2. SFG spectrum of PBS at the hydrophilic $\text{SiO}_2$ surface.....	39
Figure 5.3. SFG spectrum of $d_8$ -PS/PBS solid-liquid interface before (black squares) and after (red circles) addition of L-phenylalanine (5 mg/mL).....	40
Figure 5.4. SFG spectrum of the $d_8$ -PS/PBS solid-liquid interface before (black squares) and after (red circles) the addition of L-leucine (5 mg/mL).....	41
Figure 5.5. SFG spectrum of the $d_8$ -PS/PBS solid-liquid interface before (black squares) and after (red circles) the addition of glycine (100 mg/mL).....	43
Figure 5.6. SFG spectrum of the $d_8$ -PS/PBS solid-liquid interface before (black squares) and after (red circles) the addition of L-lysine (15 mg/mL).....	44
Figure 5.7. SFG spectrum of the $d_8$ -PS/PBS solid-liquid interface before (black squares) and after (red circles) the addition of L-arginine (15 mg/mL).....	45
Figure 5.8. SFG spectrum of the $d_8$ -PS/PBS solid-liquid interface before (black squares) and after (red circles) the addition of L-cysteine (25 mg/mL).....	46
Figure 5.9. SFG spectrum of the $d_8$ -PS/PBS solid-liquid interface before (black squares) and after (red circles) the addition of L-alanine (40 mg/mL).....	47
Figure 5.10. SFG spectrum of the $d_8$ -PS/PBS solid-liquid interface before (black squares) and after (red circles) the addition of L-proline (15 mg/mL).....	48
Figure 5.11. SFG spectrum of PBS/ $\text{SiO}_2$ liquid-solid interface before (black squares) and after (red circles) addition of L-phenylalanine (5mg/mL).....	50
Figure 5.12. SFG spectrum of PBS/ $\text{SiO}_2$ liquid-solid interface before (black squares) and after (red circles) addition of L-leucine (5mg/mL).....	51
Figure 5.13. SFG spectrum of PBS/ $\text{SiO}_2$ liquid-solid interface before (black squares) and after (red circles) addition of L-arginine (15mg/mL).....	52

Figure 5.14. SFG spectrum of PBS/SiO <sub>2</sub> liquid-solid interface before (black squares) and after (red circles) addition of L-lysine (15mg/mL).....	53
Figure 5.15. SFG spectrum of the SiO <sub>2</sub> /PBS solid-liquid interface before (black squares) and after (red circles) the addition of glycine (100 mg/mL).....	54
Figure 5.16. SFG spectrum of the SiO <sub>2</sub> /PBS solid-liquid interface before (black squares) and after (red circles) the addition of L-cysteine (25 mg/mL).....	55
Figure 5.17. SFG spectrum of the SiO <sub>2</sub> /PBS solid-liquid interface before (black squares) and after (red circles) the addition of L-alanine (40 mg/mL).....	56
Figure 5.18. SFG spectrum of the SiO <sub>2</sub> /PBS solid-liquid interface before (black squares) and after (red circles) the addition of L-proline (15 mg/mL).....	57
Figure 6.1. Raw QCM measurement data for the frequency (green squares) and dissipation (blue circles) values for the third harmonic of a SiO <sub>2</sub> coated sensor crystal in PBS prior to, during, and after addition of a solution of poly-L-lysine homopeptide.....	65
Figure 6.2. Plot summarizing biomolecule surface concentrations upon adsorption on polystyrene (red bars) and SiO <sub>2</sub> (blue bars) surfaces as determined by QCM experiment.....	66
Figure 6.3. The SFG spectrum of the <i>d</i> <sub>8</sub> -PS/PBS interface before (black squares) and after the addition of poly-L-lysine (12.5 mg/mL) (red circles).....	67
Figure 6.4. The SFG spectrum of the <i>d</i> <sub>8</sub> -PS/PBS interface before (black squares) and after the addition of L-lysine amino acid (red circles) at a solution concentration of 16.5 mg/mL.....	68
Figure 6.5. The SFG spectrum of the <i>d</i> <sub>8</sub> -PS/PBS interface before (black squares) and after (red circles) the addition of a solution of poly-L-proline at a concentration of 0.5 mg/mL.....	69
Figure 6.6. The SFG spectrum of the <i>d</i> <sub>8</sub> -PS/PBS interface before (black squares) and after (red circles) the addition of L-proline amino acid at a final solution concentration of 500 mg/mL.....	70
Figure 6.7. The SFG spectrum of the SiO <sub>2</sub> /PBS interface before (black squares) and after (red circles) the addition of poly-L-lysine at a concentration of 12.5 mg/mL.....	71
Figure 6.8. The SFG spectrum of the SiO <sub>2</sub> /PBS interface before (black squares) and after (red circles) the addition of L-lysine amino acid at a solution concentration of 16.5 mg/mL.....	72
Figure 6.9. The SFG spectrum of the SiO <sub>2</sub> /PBS interface before (black squares) and after (red circles) the addition of poly-L-proline at a solution concentration of 0.5 mg/mL.....	73
Figure 6.10. The SFG spectrum of the SiO <sub>2</sub> /PBS interface before (black squares) and after (red circles) the addition of L-proline amino acid at a solution concentration of 500 mg/mL.....	74

Figure 7.1. SFG spectrum of the hydrophobic $d_8$ -PS/PBS interface in the presence of pure L-proline (red circles), pure L-arginine (back squares), and an equal concentration mixture of L-proline and L-arginine (blue triangles).....	83
Figure 7.2. SFG spectrum of the hydrophobic $d_8$ -PS/PBS interface in the presence of pure PBS (black squares), with 15 mg/mL L-arginine (red circles), and subsequently an equal concentration mixture (both 15 mg/mL) of L-proline and L-arginine (blue triangles).....	84
Figure 7.3. SFG spectrum of the hydrophobic $d_8$ -PS/PBS interface in the presence of pure PBS (black squares), with L-proline at 15 mg/mL (red circles), and subsequently a solution of equal concentrations of L-proline and L-arginine at 15 mg/mL (blue triangles).....	85
Figure 7.4. SFG spectrum of the hydrophilic $SiO_2$ /PBS interface in the presence of pure PBS (black squares), with L-proline at 15 mg/mL (red circles), and an equal concentrations mixture of L-proline and L-arginine at 15 mg/mL (blue triangles).....	86
Figure 7.5. SFG spectrum of the hydrophilic $SiO_2$ /PBS interface in the presence of pure PBS (black squares), with L-arginine amino acid at 1 mg/mL (red circles), and an equal concentration mixture of L-arginine and L-proline both at 1 mg/mL (blue triangles).....	87
Figure 7.6. SFG spectrum of the hydrophobic $d_8$ -PS/PBS interface in the presence of pure PBS (black squares), L-arginine (red circles) at 3 mg/mL concentration, and an equal concentration mixture of L-arginine and L-phenylalanine both at 3 mg/mL (blue triangles).....	88
Figure 7.7. SFG spectrum of the hydrophilic $SiO_2$ /PBS interface in the presence of pure PBS (black squares), with 2 mg/mL L-phenylalanine (red circles), and an equal concentration mixture of L-arginine and L-phenylalanine both at 2 mg/mL (blue triangles).....	89
Figure 7.8. QCM data of L-arginine adsorption on the hydrophilic $SiO_2$ surface as a function of amino acid concentration in PBS at pH 7.4 and 24 °C.....	90
Figure 7.9. QCM data of L-leucine adsorption on the hydrophobic PS surface as a function of amino acid concentration in PBS at pH 7.4 and 24 °C.....	91
Figure 7.10. QCM data of L-proline adsorption on the hydrophobic PS surface as a function of amino acid concentration in PBS at pH 7.4 and 20 °C.....	92
Figure 7.11. SFG spectrum of the hydrophilic $SiO_2$ /PBS interface before (white boxes), and after addition of L-arginine solutions at 0.5 mg/mL (red circles), 1 mg/mL (blue triangles), and 15 mg/mL (olive triangles).....	93
Figure 7.12. SFG spectrum of the hydrophobic $d_8$ -PS/PBS interface before (black squares) and after addition of L-proline at 5 mg/mL (red squares) at 20 °C, and again after the subsequent elevation of interface temperature to 30 °C (blue squares).....	94

Figure 7.13. SFG spectrum of the hydrophobic $d_8$ -PS/PBS interface before (black squares) and after addition of L-proline at 5 mg/mL (red circles) at 30 °C, and again after the subsequent reduction of interface temperature to 20 °C (blue triangles).....	95
Figure 7.14. The SFG spectrum of the $d_8$ -PS/PBS solid-liquid interface before (black squares) and at 45 minutes (red circles), 90 minutes (blue triangles), and 165 minutes (olive triangles) after the addition of L-arginine and L-proline (15 mg/mL each).....	97
Figure 7.15. The SFG spectra of 0.5 mg/mL solutions of the collagen-like peptide Ac-(PPG) <sub>4</sub> -NH <sub>2</sub> (black squares) and poly-L-proline at the $d_8$ -PS/PBS solid-liquid interface.....	98
Figure 7.16. Schematic of the platinum electrode prism and experimental arrangement during SFG measurement.....	99
Figure 7.17. The SFG spectra of the Pt electrode-PBS interface at zero bias (black squares), at +5 V potential (red circles), and at -5 V potential (blue triangles).....	100
Figure 7.18. SFG spectra of the Pt electrode-H <sub>2</sub> O interface at zero bias (black squares), at +10 V potential (red circles), and at -10 V potential (blue triangles).....	101
Figure 7.19. SFG spectra of the Pt electrode-H <sub>2</sub> O interface in the presence of L-arginine amino acid (2 mg/mL) at zero bias (black squares), at +10 V potential (red circles), and at -10 V potential (blue triangles).....	102
Figure 8.1. Angioplasty balloons with and without surface treatment to minimize blood clotting.....	106
Figure 8.2. Schematic of the biocatalytic action of heparin for the deactivation of thrombin clotting factor by the simultaneous binding of the antithrombin-III and thrombin.....	107
Figure 8.3. Schematic of QCM binding experiment performed for the determination of surface loading capacity of bare polystyrene and heparin coated surfaces for TNF- $\alpha$ .....	110
Figure 8.4. QCM experimental data of showing TNF- $\alpha$ binding from a protein solution (83 $\mu$ g/L in PBS) flowed across bare polystyrene and heparin coated surfaces (100 $\mu$ L/min) at 37 °C....	111
Figure 8.5. Schematic of QCM binding experiment performed for the determination of surface loading capacity of bare polystyrene and heparin coated surfaces for AT-III before and after the introduction of a solution of TNF- $\alpha$ .....	112
Figure 8.6. QCM experimental data showing the binding AT-III from a solution (1 UN or 200 mg/L in PBS) flowed across bare polystyrene and heparin coated surfaces (50 $\mu$ L/min) at 37 °C.....	113
Figure 8.7. SFG spectrum of heparin coated glass microscope cover slip in air.....	115

Figure 9.1. Diagram of OPG/OPA laser setup utilizing LIS crystals.....	120
Figure 9.2. Infrared energy output for LIS based OPA.....	121
Figure 9.3. Amide I SFG spectrum of 1X PBS (high ionic strength) the hydrophobic $d_8$ -PS solid-liquid interface before (black circles) and after (red squares) the addition of LK <sub>14</sub> peptide (0.15mg/mL).....	123
Figure 9.4. The SFG amide I spectrum of the low ionic strength (0.01X PBS) buffer at the $d_8$ -PS hydrophobic solid-liquid interface before (black circles) and after (red squares) the addition of LK <sub>14</sub> peptide (0.15 mg/mL).....	124
Figure 9.5. The amide I SFG spectrum of 1X PBS (high ionic strength) at the hydrophilic CaF <sub>2</sub> solid-liquid interface before (black circles) and after (red squares) addition of LK <sub>14</sub> peptide (0.15 mg/mL).....	125

## List of Tables

Table 3.1. Angles of incidence relative to sample surface normal for input visible and infrared beams, $\beta_{\text{vis}}$ and $\beta_{\text{IR}}$ , respectively, for slab and prism sample substrate geometries.....	15
Table 6.1. Summary QCM data quantifying the surface concentration of each adsorbed biomolecule on the polystyrene and SiO <sub>2</sub> substrate surfaces.....	66
Table 7.1. Summary of QCM data quantifying the surface concentration of L-proline adsorbed on the hydrophobic polystyrene surface as a function of interface temperature.....	96
Table 8.1. Summary of TNF- $\alpha$ binding capacity of polystyrene and heparin coated surfaces as determined by QCM measurements at 37 °C.....	111
Table 8.1. Summary of the AT-III and subsequent TNF- $\alpha$ binding capacity of polystyrene and heparin coated surfaces as determined by QCM measurements at 37 °C.....	113

## Acknowledgements

I would like to thank Professor Gabor A. Somorjai for the opportunity and the privilege to work in his research group. Working for Professor Somorjai has been a rewarding experience and from his mentorship, encouragement, and advice and I have learned a great deal about research, science, and life.

I would also like to thank all of the members of the Somorjai group both past and present for their advice, help, discussions, ideas, and friendship. Specifically, I want to thank Roger York, Cesar Aliaga, Yuri Borodko, Yimin Li, Derek Butcher, Russ Renzas, Keith McCrea, Chris Kliewer, Will Browne, Chris Thompson, Chris Hahn, Nic Webb, Alfred Yoon, and Inger Coble who together have made my research experience in the Somorjai group so rewarding and productive. Additional researchers I would like to acknowledge for helping to make this research possible are Professor Kevin Healy, Naomi Kohen, Professor Phillip Geissler, Ron Zuchermann, David King, Marco Rolandi, Anfeng Wang, and Bob Ward.

During graduate school I was blessed to meet a very special woman, Sarah Ross. I am grateful for all of her love, kindness, humor, patience, and support. Sarah, I love you and thank you for being such a wonderful part of my life.

I am honored to have met Derek Butcher, Melissa Fardy, Dan Work, David Okawa, and Chanda Ho during graduate school and I am grateful for their friendship and for making my life outside of the lab during the past five years such a fun and rich experience. I consider you all my second family.

I would like to thank my parents for all of their love and lifelong dedication to helping me pursue my dream of becoming a scientist. I would also like to thank Professor Todd L. Lowary and Professor Matthew S. Platz for the opportunities to work in their research groups as well as for their continued encouragement, advice, and friendship over the past several years. Lastly, I would like to express my appreciation and gratitude to David Dao for all of his help, guidance, and support during graduate school all of which have made both my professional life and my personal life more rewarding than I ever expected.

This work was supported by the Director, Office of Science, Office of Basic Energy Sciences, of the U.S. Department of Energy under Contract DE-AC02-05CH11231.

## Chapter 1

### Introduction

The study of biomolecules and biomaterials at biological interfaces under physiological conditions provides a remarkable opportunity to combine the exploration of important and complex biological processes with the development of new materials.<sup>1, 2</sup> When taken together these areas of research have the potential to improve the everyday quality of life for countless numbers of people. A few examples of biomaterials illustrating this point include the development of contact lenses, artificial hip joints, and coronary stents all of which have had a profound impact on both the duration and the quality of life.<sup>3, 4</sup> Despite these advances in biological surface technology over the past decades, the chemical and physical processes which make these developments possible are, to a large extent, still poorly understood at the molecular level.<sup>5-8</sup> Since proteins have high molecular weight and complex structures we decided to study their building blocks, amino acids and peptides, to delineate their molecular structures and conformations on model polystyrene hydrophobic and hydrophilic SiO<sub>2</sub> surfaces. The recent development of several surface-sensitive analysis techniques, particularly sum frequency generation (SFG) vibrational spectroscopy and quartz crystal microbalance (QCM) have proven power tools for the characterization of biological interfaces under physiological conditions. In this dissertation, SFG vibrational spectroscopy and QCM are implemented in the study of amino acid, peptide, and protein adsorption at several model liquid-solid biointerfaces.

Chapter 2 provides a theoretical background for the sum frequency generation (SFG) vibrational spectroscopy technique utilized in later chapters to characterize biological interfaces. This nonlinear optical technique is particularly powerful laser spectroscopy due to its inherent surface-sensitivity and ability to be implemented in situ across a wide range of temperatures, pressures, and interfaces. The versatility of SFG vibrational spectroscopy is particularly well suited for studying biological interfaces under physiological conditions that would prove challenging using most other surface sensitive analytical techniques.

Chapter 3 introduces the quartz crystal microbalance (QCM) technique along with a fundamental physical and experimental background for its implementation at the biological liquid-solid interface. QCM is a robust, gravimetric analytical tool that can be used to quantify the amount of material adsorbed on a surface in a variety of experimental conditions. In later chapters, the QCM is utilized to quantify the adsorption of amino acids, peptides, and proteins adsorbed from solution onto several different surfaces.

Chapter 4 deals with a theoretical and experimental study of the influence of experimental laser beam geometry on the sensitivity of the SFG technique. A thorough theoretical investigation was performed in this investigation to allow the prediction of the optimal SFG beam geometry for maximizing the sensitivity of the technique and minimizing the influence of competing optical processes. The theoretically calculated optimal beam orientations were experimentally implemented and found to provide a dramatic enhancement in the sensitivity and resolution of the SFG instrument.

Chapter 5 discusses an SFG study of eight individual amino acids in aqueous solutions at model hydrophilic silica (SiO<sub>2</sub>) and hydrophobic polystyrene surfaces. This experimental study was made possible by the SFG spectroscopy technique developments included in the previous

chapter. In this study, SFG vibrational spectra were obtained for the first time for several of the amino acids at the solid-liquid interface under physiological conditions. These results provided experimental evidence for feasibility of utilizing SFG to characterize the interfacial structure and ordering of amino acids at biologically important interfaces.

Chapter 6 describes an SFG and QCM study conducted on L-lysine and L-proline amino acids and their corresponding homopeptides, poly-L-lysine and poly-L-proline, at the liquid-solid interface. In this study, the SFG spectra of the amino acids were found to be qualitatively similar to their corresponding homopeptides despite the smaller molecular mass amino acid species generating less signal intensity from C-H vibrational modes on a hydrophobic polystyrene surface. On the same surface, QCM measurements indicated that the origin of these differences in SFG signal intensity were due, in part, to the more massive homopeptides exhibiting a greater degree of interfacial ordering. Additionally, both the SFG spectra and the QCM data collected at the hydrophilic SiO<sub>2</sub> surface in this study suggest that adsorbed biomolecules exert a substantial influence on the structure of interfacial water on at a hydrophilic interface.

Chapter 7 focuses on a number of exploratory SFG and QCM studies of biological molecules at several model liquid-solid interfaces. Specifically, these investigations explore the influence of a number of experimental parameters on the adsorption and surface ordering of several amino acids and peptides at the liquid-solid interface. This chapter provides experimental evidence for a number of promising future directions for biointerface research.

Chapter 8 presents an investigation of the biological activity and protein binding ability heparin coated surfaces utilizing QCM and SFG. In this study, the surface binding capacities of both heparin and polystyrene coated surfaces were quantitatively determined for two biologically important proteins, tumor necrosis factor alpha and antithrombin III, under physiological conditions. The first known SFG vibrational spectrum of a heparin functionalized surface was also obtained in this study. The findings of this investigation support further exploration of heparin functionalized surfaces for the removal of pathogens and the purification of blood.

Chapter 9 discusses the development and implementation of a new optical parametric amplifier (OPA) using lithium thioindate. In this study, the new OPA was utilized for the SFG investigation of the interfacial secondary structure of a model peptide in the amide I frequency region. This model peptide was found to exhibit a SFG vibrational mode in the amide I spectral region indicative of an  $\alpha$ -helical secondary structure at the liquid-solid interface.

## References

1. Anderson, J. M., *Annual Review of Materials Research* **2001**, *31*, 81-110.
2. Castner, D. G.; Ratner, B. D., *Surface Science* **2002**, *500* (1-3), 28-60.
3. Grasel, T. G.; Cooper, S. L., *Journal of Biomedical Materials Research* **1989**, *23* (3), 311-338.
4. Chen, Z.; Ward, R.; Tian, Y.; Malizia, F.; Gracias, D. H.; Shen, Y. R.; Somorjai, G. A., *Journal of Biomedical Materials Research* **2002**, *62* (2), 254-264.
5. Baier, R. E.; American Chemical Society.; American Chemical Society. Division of Colloid and Surface Chemistry., *Applied chemistry at protein interfaces : a symposium at the 166th meeting of the American Chemical Society, Chicago, Ill., August 29-31, 1973*. American Chemical Society: Washington, 1975; p viii, 399 p.
6. Horbett, T. A.; Brash, J. L.; American Chemical Society. Division of Colloid and Surface Chemistry.; American Chemical Society. Meeting, *Proteins at interfaces II : fundamentals and applications*. American Chemical Society: Washington, DC, 1995; p xiv, 561 p.
7. Feast, W. J.; Munro, H. S., *Polymer surfaces and interfaces*. Wiley: Chichester, 1987; p xii, 257p.
8. Brash, J. L., *Current Opinion in Colloid & Interface Science* **1996**, *1* (5), 682-688.

## Chapter 2

### Sum Frequency Generation Vibrational Spectroscopy

#### 2.1. Sum Frequency Generation Vibrational Spectroscopy Introduction

Sum frequency generation (SFG) vibrational spectroscopy is a nonlinear optical technique which allows the direct measurement of a vibrational spectrum of an interface or surface and its adsorbates. What makes SFG vibrational spectroscopy a particularly powerful technique is its inherent sensitivity to non-centrosymmetric regions including boundaries, interfaces, and surfaces while remaining insensitive to regions of centrosymmetry including most bulk solids, liquids, and gasses. This ability of SFG to resolve vibrational spectra of interfacial regions and species present at their boundaries makes it a remarkably sensitive and well-suited technique for investigation of a surface's chemistry, physics, and biology including catalysis, molecular adsorption, surface restructuring, in addition to a number of other surface phenomena.

#### 2.2. Sum Frequency Generation Theoretical Background

Sum frequency generation (SFG) vibrational spectroscopy was first experimentally implemented in 1987 by Shen<sup>1, 2</sup> and Harris,<sup>3</sup> but the SFG process itself was first reported 25 years earlier in 1962.<sup>4, 5</sup> This process has been made experimentally feasible with the advent of ultrafast pulsed lasers because SFG requires the spatial and temporal overlap of two electric fields at peak intensities not easily produced using conventional light sources.

A derivation and explanation of the theoretical basis of the SFG process is presented below, but a more detailed derivation is can be found elsewhere.<sup>6-15</sup> The theoretical background for the SFG process is complex and can developed by first examining a simpler system involving a single weak electric field impinging on a surface. When the weak electric field is incident on a material it can induce a surface polarization,  $\vec{P}$ , which is approximated by the sum of the material's static polarization,  $\vec{P}^{(0)}$ , and the first-order linear polarization,  $\vec{P}^{(1)}$ , as shown in equations (2.1) and (2.2).

$$\vec{P} \cong \vec{P}^{(0)} + \vec{P}^{(1)} \quad (2.1)$$

$$\vec{P}^{(0)} = \text{constant} \quad (2.2)$$

As indicated in equation (2.3), the first-order polarization term is dependent on the linear susceptibility,  $\vec{\chi}^{(1)}$ , as well as the field strength and oscillation frequency  $\vec{E}(r)$  and  $\omega$ , respectively, where  $\epsilon_0$  is the permittivity of free space.

$$\vec{P}^{(1)} = \epsilon_0 \vec{\chi}^{(1)} \vec{E}(r) \cos(\omega t) \quad (2.3)$$

Equation 2.1 is a sufficient approximation to describe the polarization induced on a surface by a weak applied electric field which is responsible for linear optical phenomena including both Raman and infrared spectroscopies. However, for incident electric fields of sufficient strength such that the forces felt by the surface material's electrons from the applied field are on the order of those exerted by the proton, the induced polarization on a surface is not sufficiently approximated by equation (2.1) and must be expanded to include higher order terms as shown in equation (2.4).

$$\bar{P} = \bar{P}^{(0)} + \bar{P}^{(1)} + \bar{P}^{(2)} + \bar{P}^{(3)} + \dots \quad (2.4)$$

The second-order nonlinear polarization,  $\bar{P}^{(2)}$ , represented by equation (2.5) is responsible for sum frequency generation (SFG), second harmonic generation (SHG), difference frequency generation (DFG), and the production of a constant bias polarization. In the equation (2.5),  $\chi_{ijk}^{(2)}$  represents the second-order nonlinear susceptibility of the system in a coordinate system with axes  $i$ ,  $j$ , and  $k$ . The terms,  $\bar{E}_j(r)\cos(\omega_1 t)$  and  $\bar{E}_k(r)\cos(\omega_2 t)$  refer to the applied electric fields (i.e. laser beam or beams in this case) incident on the surface where the  $\bar{E}_i(r)$  and  $\bar{E}_j(r)$  terms correspond to the strength of each field, and  $\omega_1$  and  $\omega_2$  correspond to the angular frequencies of these oscillating fields.

$$\bar{P}_i^{(2)} = \epsilon_0 \sum_{j,k} \chi_{ijk}^{(2)} \bar{E}_j(r) \cos(\omega_1 t) \bar{E}_k(r) \cos(\omega_2 t) \quad (2.5)$$

In the case where  $\omega_1 = \omega_2$ , equation (2.5) simplifies into the form of equation (2.6) describing a special case of SFG known as second harmonic generation or SHG. For incident electric fields at different frequencies, equation (2.5) can be expanded as presented in equation (2.7) where the  $\cos[(\omega_1 + \omega_2)t]$  and  $\cos[(\omega_1 - \omega_2)t]$  terms are responsible for SFG and DFG processes, respectively.

$$\bar{P}_i^{(2)} = \frac{\epsilon_0}{2} \sum_{j,k} \chi_{ijk}^{(2)} \bar{E}_j(r) \bar{E}_k(r) [1 + \cos(2\omega t)] \quad (2.6)$$

$$\bar{P}_i^{(2)} = \frac{\epsilon_0}{2} \sum_{j,k} \chi_{ijk}^{(2)} \bar{E}_j(r) \bar{E}_k(r) [\cos[(\omega_1 + \omega_2)t] + \cos[(\omega_1 - \omega_2)t]] \quad (2.7)$$

The probability of the SFG process and subsequently the intensity of the emitted sum frequency light generated is dependent upon the product of the input beam intensities as well as  $\chi^{(2)}$  shown by equations (2.8) and (2.9).

$$\bar{P}^{(2)}(\omega_{sfg}) = \bar{\chi}^{(2)}(\omega_{sfg}) : \bar{E}_{(vis)} \bar{E}_{(ir)} \quad (2.8)$$

$$I_{\text{sfg}} \propto |\chi^{(2)}|^2 \quad (2.9)$$

The second-order nonlinear susceptibility,  $\chi^{(2)}$ , is a third rank tensor and therefore is subject to the equalities presented in equations (2.10) and (2.11).

$$\chi_{ijk}^{(2)} = \chi_{-i-j-k}^{(2)} \quad (2.10)$$

$$\chi_{ijk}^{(2)} = -\chi_{-i-j-k}^{(2)} \quad (2.11)$$

In a centrosymmetric environment such as a bulk medium  $\chi^{(2)}$  can only obey both of the required conditions presented above if and only if its value is zero. Therefore, the SFG process which is inherently dependent upon  $\chi^{(2)}$  can only occur in a non-centrosymmetric environment such as at surface or interface. This property is directly responsible for the inherent surface sensitivity of the SFG process which makes it such a powerful and practical spectroscopic technique.

As presented in equation (2.12)  $\chi^{(2)}$  is composed of both resonant and non-resonant components  $\chi_{NR}^{(2)}$  and  $\chi_R^{(2)}$ , respectively.

$$\chi^{(2)} = \chi_{NR}^{(2)} + \chi_R^{(2)} \quad (2.12)$$

The non-resonant component is typically approximated as being constant across the range of frequencies spanned in an experiment. Additionally,  $\chi_{NR}^{(2)}$  is substantially smaller than  $\chi_R^{(2)}$  for dielectric sample substrates and it generally only contributes a small amount to overall SFG intensity with the exception of conducting sample surfaces such as silver and gold which can exhibit surface plasmon phenomena. These typical characteristics of  $\chi_{NR}^{(2)}$  are summarized in equations (2.13) and (2.14).

$$\chi_{NR}^{(2)} \ll \chi_R^{(2)} \quad (2.13)$$

$$\chi_{NR}^{(2)} \sim \text{constant} \quad (2.14)$$

The resonant component of the second-order nonlinear susceptibility,  $\chi_R^{(2)}$ , for a given system is dependant upon the number of surface oscillators,  $N$ , and the second-order hyperpolarizability of the oscillator system,  $\alpha_{lmn}^{(2)}$ , as presented in equation (2.15). Additionally,  $\chi_R^{(2)}$  is determined by the ensemble average orientation of the oscillators in a molecular coordinate system with axes  $l$ ,  $m$ , and  $n$  transformed into a laboratory coordinate system with axes  $i$ ,  $j$ , and  $k$  as expressed by the  $\langle (\hat{i} \cdot \hat{l})(\hat{j} \cdot \hat{m})(\hat{k} \cdot \hat{n}) \rangle$  term in equation (2.15). This term is responsible for the SFG selection rule requiring a population of SFG active oscillators have an

overall net orientation as the ensemble average of a completely random orientation of oscillators would otherwise be zero.

$$\chi_R^{(2)} = N \chi_{ijk}^{(2)} \sum_q \sum_{l,m,n} \langle (\hat{i} \cdot \hat{l})(\hat{j} \cdot \hat{m})(\hat{k} \cdot \hat{n}) \rangle \alpha_{lmn,q}^{(2)} \quad (2.15)$$

The hyperpolarizability term for the  $q^{\text{th}}$  vibrational mode,  $\alpha_{lmn,q}^{(2)}$ , is determined by the frequency of the incident infrared beam,  $\omega_{\text{IR}}$ , the frequency of the  $q^{\text{th}}$  vibrational mode,  $\omega_q$ , the damping constant for the  $q^{\text{th}}$  vibrational mode,  $\Gamma_q$ , the difference between the populations of the ground vibrational state and the first excited vibrational state,  $\Delta\rho_{gq}$ , and the oscillator strength for the  $q^{\text{th}}$  vibrational mode,  $A_q$ , as shown in equation (2.16).

$$\alpha_{lmn,q}^{(2)} = \frac{A_q}{(\omega_{\text{IR}} - \omega_q + i\Gamma_q)} \Delta\rho_{gq} \quad (2.16)$$

The oscillator strength for the  $q^{\text{th}}$  vibrational mode,  $A_q$ , is a function of the frequency of that mode,  $\omega_q$ , and the partial derivatives of the dipole moment,  $\mu_n$ , and the linear polarizability  $\alpha_{lm}^{(1)}$  of the system. Equation (2.17) highlights the origin of the SFG selection rule requiring the  $q^{\text{th}}$  vibrational mode be both Raman and infrared active as either of these partial derivative being zero results in  $A_q$ ,  $\alpha_{lmn,q}^{(2)}$ , and ultimately  $\chi_R^{(2)}$  also being zero for that mode.

$$A_q = \frac{1}{2\omega_q} \frac{\partial \mu_n}{\partial q} \frac{\partial \alpha_{lm}^{(1)}}{\partial q} \quad (2.17)$$

### 2.3. Sum Frequency Generation from a Surface

In an SFG experiment, the polarizations of the two input fields and the emitted field are represented by the indices of  $\chi^{(2)}$  and determine whether or not the SFG process is forbidden or allowed. As a third rank tensor  $\chi^{(2)}$  is composed of three fields each of which can have a projection in three orthogonal directions resulting in a matrix representation with a total of 27 polarization elements.<sup>15</sup> Specifically,  $\chi_{xyz}^{(2)}$  represents the second-order nonlinear hyperpolarizability for a system where the polarization of the SFG emitted, visible input beam, and the infrared input beams are represented by the indices x, y, z, respectively. Fields with a polarization parallel to the surface are designated as *s*-polarized while fields with a polarization perpendicular to the sample surface are designated as *p*-polarized. Therefore, a SFG experiment conducted in the *ssp* polarization combination, involve an emitted SFG beam that is *s*-polarized, an input visible beam that is *s*-polarized, and an input infrared beam that is *p*-polarized. While  $\chi^{(2)}$  represents a matrix with 27 polarization elements, performing an experiment on a flat surface with  $C_\infty$  symmetry imposes symmetry conditions eliminating all but 7 of these polarization elements. Three of the remaining 7 matrix elements result in unique polarization

combinations, *pss*, *sps*, and *ssp*, and the remaining four elements contribute to the total signal generated in experiments utilizing the *ppp* polarization combination.

The unique SFG sensitivity of a system relative the polarization combination implemented can allow the molecular orientation of interfacial species to be determined simply by comparing the spectral data from a given system utilizing different polarizations.<sup>6, 10, 16-18</sup> Specifically, one can determine the relative orientation of an interfacial species' dipole moment simply by changing the polarization of the applied infrared beam. For example, a positive SFG spectral feature indicates a molecular dipole aligned with the incident infrared field, a negative SFG feature indicates a dipole anti-aligned with the incident field, and the absence of a feature indicates a dipole orthogonal to the applied field provided all other SFG selection rules are satisfied.

While the basic principle of orientational analysis is straight-forward, the application of this theory is non-trivial as the mathematical operations involved introduce relatively large uncertainties and the number of closely spaced spectral features quickly grows with increasing number of atoms for a given molecule. In all of the SFG experiments included herein the *ssp* polarization combination was utilized exclusively.

## 2.4. Sum Frequency Generation Instrumentation

Sum frequency generation vibrational spectroscopy typically requires the use of ultrafast pulsed lasers to obtain electric fields of sufficient intensity to induce a detectable number of SFG events. In these experiments, a Continuum (Santa Clara, CA) Leopard D-20 Nd:YAG laser with a 20 Hz output at 1064 nm and 22 picosecond pulse width was used at an approximate energy of 22 mJ per pulse. The Nd:YAG laser output was sent through both Optical Parametric Generator (OPG) and Optical Parametric Amplifier (OPA) stages in a Laservision (Bellevue, WA) OPG/OPA where both the visible and infrared beams used in experiments were produced as shown in Figure 2.1. The 1064 nm Nd:YAG output is sent into the OPG/OPA where it is split into two beams, I and II, respectively. Beam I is sent through a potassium di-deuterium phosphate (KD\*P) crystal,  $\text{KD}_2\text{PO}_4$ , where the 1064nm beam is frequency doubled and converted to a 532 nm beam subsequently split into beams Ia and Ib. Beam Ia is then output and directly used as the visible beam,  $\omega_{\text{vis}}$ , in experiments at an energy of approximately 200  $\mu\text{J}$  per pulse. The other 532 nm laser beam, Ib, is then passed through a set of angle-tunable potassium titanyl phosphate (KTP) crystals,  $\text{KTiOPO}_4$ , where it is converted into tunable infrared signal and idler beams between 720 - 870 nm and 1370 - 2040 nm, respectively. The signal beam is dumped, and the idler beam, 2b, is then mixed with beam II in a set of angle-tunable potassium titanyl arsenate (KTA) crystals,  $\text{KTiOAsO}_4$ , generating a tunable infrared beam, 3b, in the region 2500 - 4000  $\text{cm}^{-1}$  (4.0 - 2.5  $\mu\text{m}$ ). Beam 3b is directly used as the infrared beam in experiments,  $\omega_{\text{IR}}$ , at an energy of approximately 200  $\mu\text{J}$  per pulse. Upon irradiation from beams Ia and 3b, the resulting SFG signal generated at sample surface is passed through a polarizer and Jovin-Yvon monochromator (France) before being detected by a Hamamatsu (Japan) photomultiplier tube (PMT). After each laser pulse, the output signal from the PMT is passed through a Stanford Research Systems (Sunnyvale, CA) lock-in amplifier before being averaged and recorded on a desktop computer.

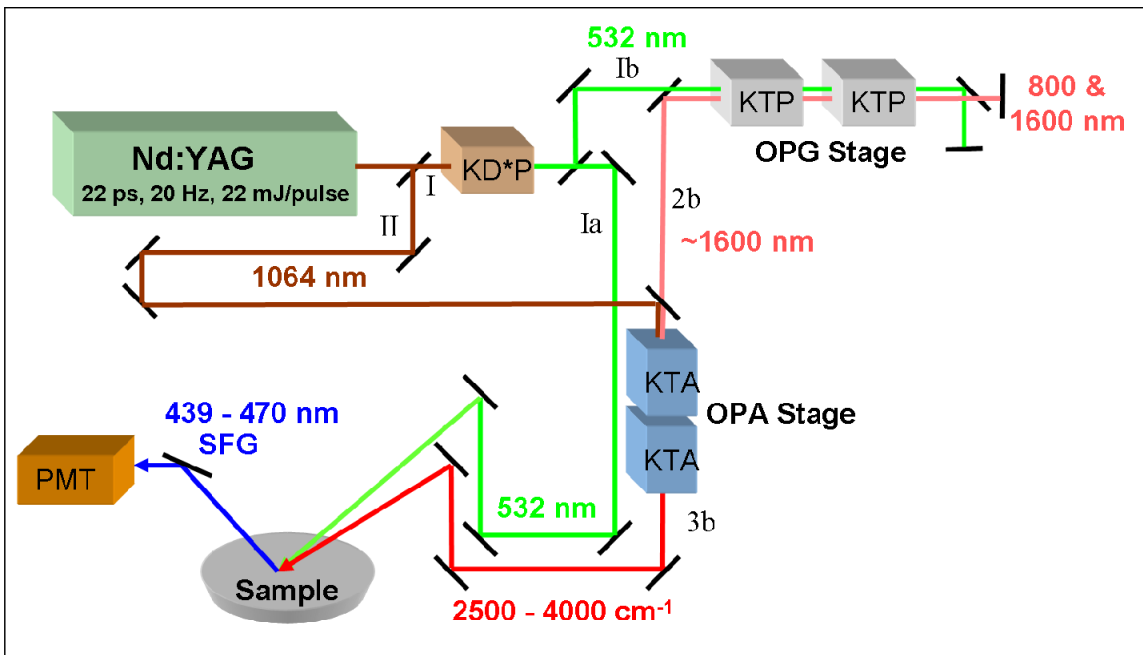


Figure 2.1. Schematic of the Laservision OPG/OPA laser setup used for SFG experiments. A picosecond Nd:YAG laser with 1064 nm output and split into two beams, I and II. Beam I is passed through a frequency doubling KD\*P crystal producing 532 nm output which is then split into beams Ia and Ib. Beam Ia is sent directly to the sample surface where it is used as the visible beam in the SFG experiment. Beam Ib is sent directly to the OPG stage where it passes through two angle-tunable KTP crystals and produces both a signal and an idler beam. The higher energy signal beam is dumped, and the lower energy idler beam, 2b, is then sent to the OPA stage. Beam II and beam 2b are mixed in two angle-tunable KTA crystals producing 3b consisting of mid-infrared laser light at the difference frequency of the two input beams. Beam 3b is then sent directly to the sample and used as the infrared beam in the SFG experiment.

## 2.5. Sum Frequency Generation Sample Substrate Preparation

All SFG experiments were conducted using fused silica,  $\text{SiO}_2$ , substrates which were cleaned by soaking overnight in a bath of concentrated  $\text{H}_2\text{SO}_4$  (97%) (Sigma-Aldrich) and Nochromix (Godax). Subsequently, the substrates were rinsed with distilled, de-ionized water and then treated with a Herrick oxygen plasma cleaner (Ithaca, NY) (18 W RF, 200 mtorr  $\text{O}_2$ ) for 60 s to remove any surface contaminants and to maximize the extent of Si/ $\text{SiO}_2$  prism surface oxidation. For SFG measurements on  $d_8$ -deuterated polystyrene ( $d_8$ -PS) surfaces, the plasma cleaned prisms were then spin-coated with a 3 % weight solution of deuterated  $d_8$ -polystyrene (MW  $\approx$  300,000) (Polymer Source) in toluene (Sigma-Aldrich). Similarly,  $h_8$ -polystyrene (PS) surfaces were prepared by coating 3 % weight solutions of PS (MW  $\approx$  280,000) (Aldrich) in toluene (Sigma-Aldrich). Spin-coating was carried out at 3000 rpm for 45 s using a Specialty Coating Systems (Indianapolis, IN) spin-coater and was followed by annealing at 120 °C for 12 hours. Ellipsometry and atomic force microscopy measurements were performed and the resulting thicknesses of the  $d_8$ -PS and PS films were determined to be  $\sim$ 105 nm. Diagrams of the slab and prism shaped substrates used in SFG experiments are presented in Figures 2.1 and 2.2 and detailed descriptions explaining their use are included in the text of Chapter 3.

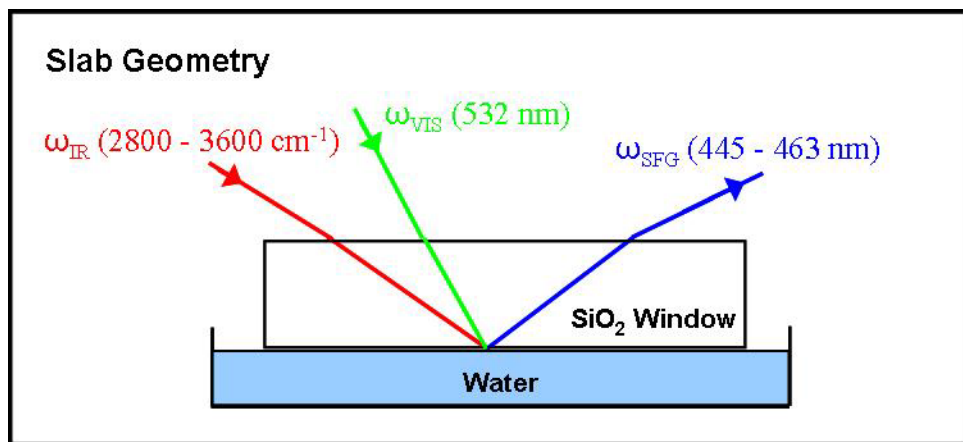


Figure 2.2. Diagram of SFG sample substrate in slab geometry.

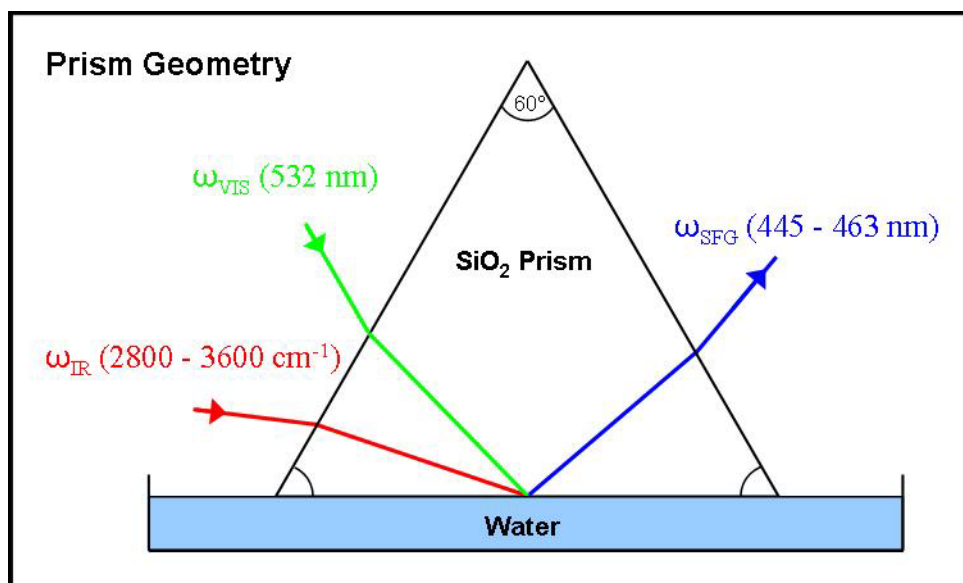


Figure 2.3. Diagram of SFG sample substrate in prism geometry.

## References

1. Hunt, J. H.; Guyot-Sionnest, P.; Shen, Y. R., *Chemical Physics Letters* **1987**, *133* (3), 189-192.
2. Zhu, X. D.; Suhr, H.; Shen, Y. R., *Physical Review B* **1987**, *35* (6), 3047-3050.
3. Harris, A. L.; Chidsey, C. E. D.; Levinos, N. J.; Loiacono, D. N., *Chemical Physics Letters* **1987**, *141* (4), 350-356.
4. Bloembergen, N.; Pershan, P. S., *Physical Review* **1962**, *128* (2), 606-&.
5. Bass, M.; Hill, A. E.; Franken, P. A.; Peters, C. W.; Weinreich, G., *Physical Review Letters* **1962**, *8* (1), 18.
6. Hirose, C.; Yamamoto, H.; Akamatsu, N.; Domen, K., *Journal of Physical Chemistry* **1993**, *97* (39), 10064-10069.
7. Du, Q.; Superfine, R.; Freysz, E.; Shen, Y. R., *Physical Review Letters* **1993**, *70* (15), 2313-2316.
8. Shen, Y. R., *Nature* **1989**, *337* (6207), 519-525.
9. Shen, Y. R., *Surface Science* **1994**, *300* (1-3), 551-562.
10. Moad, A. J.; Simpson, G. J., *Journal of Physical Chemistry B* **2004**, *108* (11), 3548-3562.
11. Mazely, T. L.; Hetherington, W. M., *Journal of Chemical Physics* **1987**, *86* (6), 3640-3647.
12. Bain, C. D., *Journal of the Chemical Society-Faraday Transactions* **1995**, *91* (9), 1281-1296.
13. Dick, B., *Chemical Physics* **1985**, *96* (2), 199-215.
14. Boyd, R. W., *Nonlinear optics*. 2nd ed.; Academic Press: San Diego, CA, 2003; p xvii, 578 p.
15. Lambert, A. G.; Davies, P. B.; Neivandt, D. J., *Applied Spectroscopy Reviews* **2005**, *40* (2), 103-145.
16. Moad, A. J.; Moad, C. W.; Perry, J. M.; Wampler, R. D.; Goeken, G. S.; Begue, N. J.; Shen, T.; Heiland, R.; Simpson, G. J., *Journal of Computational Chemistry* **2007**, *28* (12), 1996-2002.
17. Eisenthal, K. B., *Chemical Reviews* **1996**, *96* (4), 1343-1360.
18. Watry, M. R.; Richmond, G. L., *Journal of Physical Chemistry B* **2002**, *106* (48), 12517-12523.

## Chapter 3

### Sum Frequency Generation Vibrational Spectroscopy and the Influence of Experimental Sample Geometry on Technique Sensitivity for an Absorptive Medium or Media

The influence of experimental geometry on the sensitivity of sum frequency generation (SFG) vibrational spectroscopy was investigated theoretically and experimentally. Theoretical analysis predicted the substantial SFG signal enhancement for sample geometries at or near the critical angle for incident light would be attenuated by systems and media with complex indices of refraction if not proper experimental compensations were not made. SFG experiments were conducted on both fused silica and polystyrene substrates at two experimental geometries each. Experimental data was compared and found to agree well with theoretical predictions for SFG measurements conducted in the  $S_{\text{SFG}}S_{\text{Vis}}P_{\text{IR}}$  laser polarization.

#### 3.1. Introduction

Sum frequency generation (SFG) was first experimentally implemented as a nonlinear surface-sensitive vibrational spectroscopy in 1987 and it has rapidly become a powerful and versatile tool for the study of a wide range of surfaces and interfaces.<sup>1-34</sup> It has been well documented by a number of research groups that the amount of SFG signal detected in a given experiment can be dramatically enhanced by careful selection of the angles of incidence for the input laser beams.<sup>35-54</sup> In many of these experiments, a total internal reflection (TIR) input beam geometry has been utilized to enhance the amount of SFG signal detected from sample systems with weak signal. However, the interpretation of SFG spectra collected in this beam geometry can prove challenging when one of the boundary materials is absorptive in the region of interest.<sup>55-57</sup> In this study, we perform a theoretical and experimental analysis of the influence angle of incidence for infrared and visible wavelength laser beams used in SFG experiments.<sup>58</sup> Specifically, we explore two specific beam geometries, slab and prism, where a change in the angle of incidence for the input laser beams has a dramatic influence on the amount of SFG signal that is detected at the  $\text{SiO}_2$  -  $\text{H}_2\text{O}$  and the polystyrene-air interfaces. The sample substrates in the slab sample geometry (Figure 3.1) provide angles of incidence far away from the critical angle for both of the input laser beams. Meanwhile, the substrates with a prism geometry (Figure 3.2) provide beam orientations where the infrared beam is near its critical angle and the visible angle is approximately  $10^\circ$  away from TIR. These two geometries were implemented in this study because they allowed reproducible changing of experimental beam geometries without requiring the movement or modification of any additional optics. Furthermore, the use of two different substrate shapes allowed us to have a well defined set of parameters for reference in our theoretical analysis.

We found that for a medium with a complex index of refraction the Fresnel coefficients for a system can change substantially with a small change in input beam geometry. Subsequently, this change in Fresnel coefficients can have a dramatic effect on the amount of SFG signal that results from the input beams. These results provide a basis for a better understanding of why a SFG signal enhancement is experienced in TIR beam geometries. Additionally, our findings lend insights as to input beam geometries which could be

implemented with absorptive materials to maximize detectable SFG signal while avoiding any frequency dependence in the signal response.

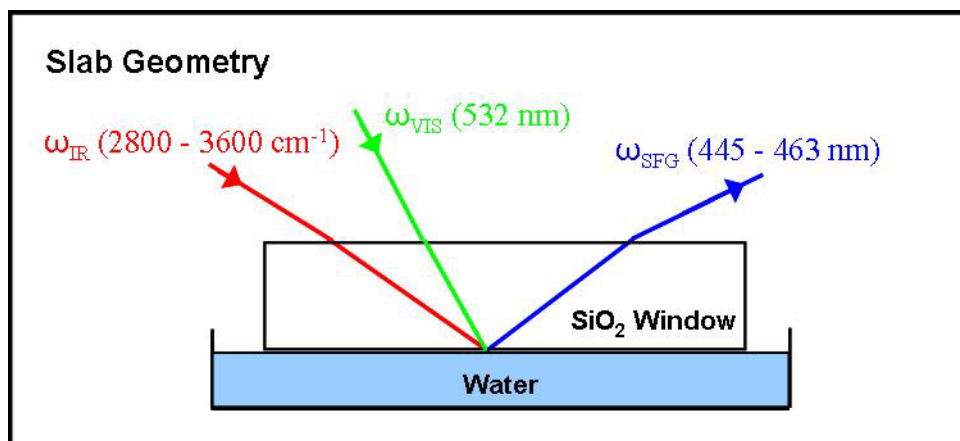


Figure 3.1. SiO<sub>2</sub> sample substrate diagram for slab geometry used in SFG experiments. Angles of incidence for infrared and visible laser beams are included in Table 3.1.

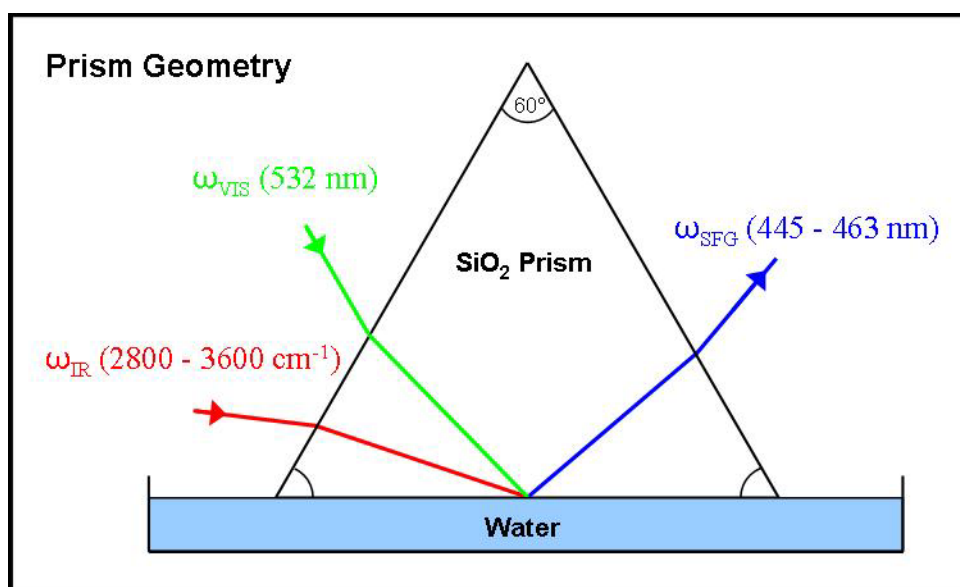


Figure 3.2. SiO<sub>2</sub> sample substrate diagram for prism geometry used in SFG experiments. Angles of incidence for infrared and visible laser beams are included in Table 3.1.

## 3.2. Experimental

### 3.2.1. SFG Theoretical Analysis

The aim of this investigation was to determine the origin of the SFG signal intensity enhancement with a change in experimental geometry. Furthermore, it was unclear if the observed enhancement was frequency dependent, influenced by the absorption of interfacial infrared light, or if the prism geometry was optimal for attaining maximal SFG intensity.

Experimentally, the intensity of SFG signal output,  $I$ , is measured as a function of infrared frequency,  $\omega_{IR}$ . In the theoretical portion of this study, we employed a previously published three-layer thin film model for SFG for measurements conducted in  $S_{SFG}S_{Vis}P_{IR}$  polarization. Under these conditions the SFG signal intensity can be expressed as presented in Equation (3.1).<sup>59, 60</sup>

$$I_{ssp}^{SFG} = \frac{32\pi^3 \omega_s^2}{c^3} \frac{\text{Re}[\epsilon_1^{1/2}(\omega_s)]}{|\epsilon_1(\omega_s)| \text{Re}[\epsilon_1^{1/2}(\omega_{Vis})\epsilon_1^{1/2}(\omega_{IR})]} \quad (3.1)$$

$$\times |\chi_{yyz}^{(2)}(\omega_s) \sec \beta \sin \beta_{IR} L^S L_T^{Vis} L_T^{IR} \frac{\epsilon_1^{1/2}(\omega_{IR})\epsilon_2^{1/2}(\omega_{IR})}{\epsilon_M(\omega_{IR})}|^2 I^{Vis} I^{IR}$$

This equation shows the intensity of SFG light output depends on the intensity of the two input beams,  $I^{Vis}$  and  $I^{IR}$ , and  $\chi^{(2)}$ , the nonlinear hyperpolarizability for the system. The  $\chi^{(2)}$  term for a given system is dependent upon the Raman polarizability and infrared activity as well as population number and net orientation of the interfacial species.<sup>1-3</sup> However, this nonlinear hyperpolarizability term will remain the same for two systems that differ only in sample geometry. Additionally, the intensity of SFG generated at an interface depends upon the Fresnel coefficients for the input and SFG beams as well as the physical properties  $\epsilon$ ,  $\omega$ , and  $\beta$  that determine them as shown in Figure 3.3. Medium 1, medium 2, and medium M represent SiO<sub>2</sub>, liquid H<sub>2</sub>O, and a thin film layer where they meet, respectively. The Fresnel coefficient,  $L$ , describes the amplitude or intensity of light reflected and transmitted when an input field is impinges on an interface. The magnitude of a Fresnel coefficient depends upon the polarization, angle, and wavelength, of light incident at the interface as well as the dielectric constant of the medium or media at the interface. Equation 3.2 represents the Fresnel coefficient of SFG light in the  $S_{SFG}S_{Vis}P_{IR}$  polarization combination generated at the boundary of two media where  $\epsilon$ ,  $\omega$ ,  $\beta$ , and  $\gamma$ , are the dielectric constants, wavelengths, reflection angles, and transmission angles for the system, respectively.

$$L^S = \frac{2\epsilon_1^{1/2}(\omega_s) \cos \beta}{\epsilon_2^{1/2}(\omega_s) \cos \gamma + \epsilon_1^{1/2}(\omega_s) \cos \beta} \quad (3.2)$$

Similarly, Equations 3.3 and 3.4 represent the Fresnel coefficients for  $s$ -polarized visible light and  $p$ -polarized infrared light, respectively, transmitted through the boundary of two media.

$$L_T^{Vis} = \frac{2\epsilon_1^{1/2}(\omega_{Vis}) \cos \beta_{Vis}}{\epsilon_2^{1/2}(\omega_{Vis}) \cos \gamma_{Vis} + \epsilon_1^{1/2}(\omega_{Vis}) \cos \beta_{Vis}} \quad (3.3)$$

$$L_T^{IR} = \frac{2\epsilon_1^{1/2}(\omega_{IR}) \cos \beta_{IR}}{\epsilon_2^{1/2}(\omega_{IR}) \cos \beta_{IR} + \epsilon_1^{1/2}(\omega_{IR}) \cos \gamma_{IR}} \quad (3.4)$$

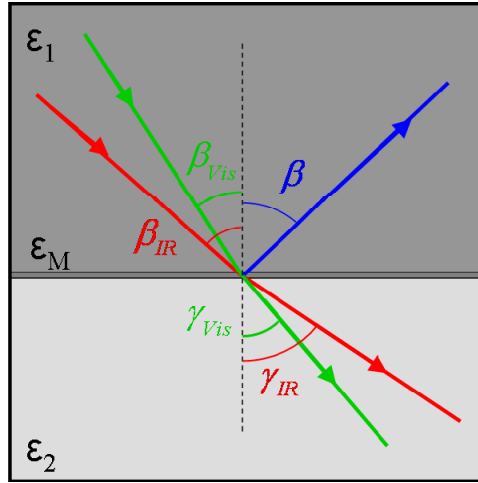


Figure 3.3. Diagram of SFG beam geometry at the interface between medium 1 and medium 2 with a thin interfacial layer between them. Input visible and infrared laser light approaches the interface through medium 1 at incident angles  $\beta_{Vis}$  and  $\beta_{IR}$ , respectively, and SFG generated at the interface exits the system through medium I at angle  $\beta$ . Angles  $\gamma_{Vis}$  and  $\gamma_{IR}$  correspond to the angle of transmission of the visible and infrared beams through medium 2.

The validity of Equation 3.1 depends upon its substituent terms being largely frequency invariant. However, this condition is not met in certain circumstance where an interfacial medium is absorptive at the wavelengths of interest. In the frequency region explored herein, water absorbs infrared light to a varying extent at the  $\text{SiO}_2$  -  $\text{H}_2\text{O}$  solid-liquid interface. Therefore, it was necessary to conduct a theoretical analysis of the frequency-dependent terms in Equation 3.1 to determine the origin of the geometry dependent SFG signal enhancement. The infrared and visible beam angles used in this investigation were fixed for the theoretical simulations and experimental measurements as shown in Table 3.1.

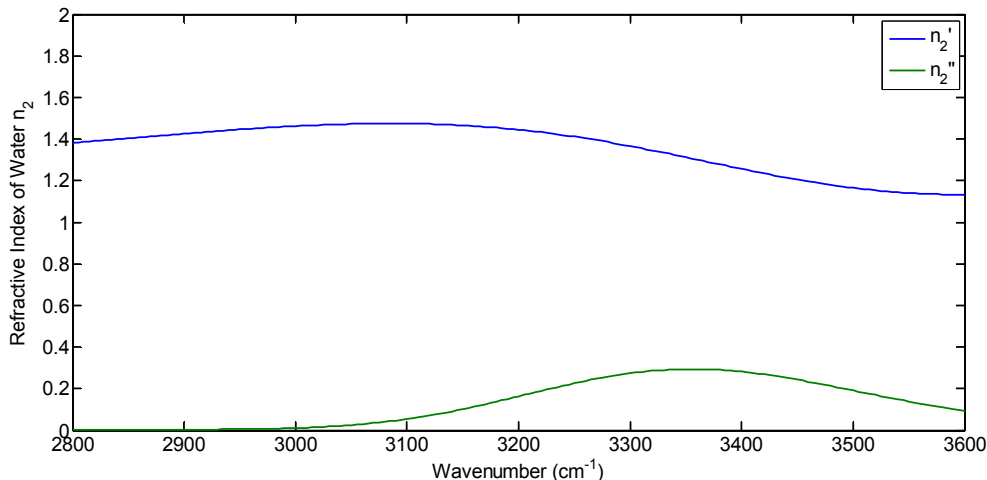
Substrate Geometry	Slab	Prism
$\beta_{Vis}$	$36^\circ$	$57^\circ$
$\beta_{IR}$	$39^\circ$	$64^\circ$

Table 3.1. Angles of incidence relative to sample surface normal for input visible and infrared beams,  $\beta_{Vis}$  and  $\beta_{IR}$ , respectively, for slab and prism sample substrate geometries.

A dimensionless geometric quantity,  $G(\beta_{Vis}, \beta_{IR})$ , shown in Equation (3.5) was defined to simplify the theoretical analysis while maintaining its theoretical and experimental relevance because of the complexity and number of terms included in equation A. This quantity relates the geometry dependent terms in Equation (3.1) to the overall SFG activity of a system in a simplified form.

$$G(\beta_{Vis}, \beta_{IR}) = \left| \sec \beta \sin \beta_{IR} L^S L_T^{Vis} L_T^{IR} \right|^2 \quad (3.5)$$

Utilizing Equation (3.5) for two different beam geometries it was then possible to theoretically compare expected differences in detectable SFG signal between them. Simulations were then carried out for a system consisting of the interface between silica,  $\text{SiO}_2$ , and water by calculation of  $G(\beta_{\text{vis}}, \beta_{\text{IR}})$  for two different geometries. The incident angles for the visible and infrared light used in the prism and slab geometries are included in Table (3.1). The value for the index of refraction of silica,  $\epsilon_1^{1/2}$  (or  $\eta_1$ ), used for SFG and visible beam wavelengths was 1.46, while the value used for infrared wavelengths was 1.41. For the refractive index of liquid water,  $\epsilon_2^{1/2}$  (or  $\eta_2$ ), the value of 1.34 was used for SFG and visible wavelengths. The dielectric constant for water in the infrared region varies substantially with wavelength in the region between  $2800 \text{ cm}^{-1}$  and  $3600 \text{ cm}^{-1}$  as demonstrated by the fitting of experimental data presented in Figure 3.4.<sup>57</sup> Subsequently, the wavelength dependent values used for  $\epsilon_2^{1/2}$  in the infrared region were taken directly from this plot. The index of refraction for the interfacial thin film layer,  $\epsilon_M^{1/2}$ , was estimated to be 1.40 for the SFG and visible beams and 1.38 for the infrared beam. However, when directly comparing the one geometric factor to another the  $\epsilon_M^{1/2}$  terms are equivalent and thus cancel along with the  $\chi^{(2)}$  terms.



**Figure 3.4.** Plot of real (blue line) and imaginary (green line) components of the index of refraction of liquid  $\text{H}_2\text{O}$  in the infrared wavelength region  $2800 \text{ cm}^{-1}$  to  $3600 \text{ cm}^{-1}$ . In the spectral region  $3300 - 3450 \text{ cm}^{-1}$  the imaginary component of the index of refraction approaches 30% the magnitude of the real component.

### 3.2.2. SFG Experimental Measurements

Sum Frequency Generation (SFG) vibrational spectroscopy is a surface-sensitive nonlinear optical laser technique which typically requires the use of high-intensity, pulsed ultrafast lasers. In these experiments, a 22 picosecond pulse width Continuum (Santa Clara, CA) Leopard D-20 Nd:YAG laser was used. This laser was operated at a 20 Hz repetition rate and produced an output beam at 1064 nm and approximately 22 mJ per pulse. This near-infrared output was sent through a Laservision (Bellevue, WA) Optical Parametric Generator (OPG)/Optical Parametric Amplifier (OPA) optical system. In the OPG/OPA system, a portion

of the 1064 nm light was frequency doubled and converted to a 532 nm beam and directly used as the visible beam,  $\omega_{\text{vis}}$ , in experiments. The remainder of the input light from the Nd:YAG laser was passed through a series of angle-tunable nonlinear crystals to generate an infrared beam tunable in the region 2500 - 4000  $\text{cm}^{-1}$  (4.0 - 2.5  $\mu\text{m}$ ),  $\omega_{\text{IR}}$ . At the experimental interface, laser beams at energy of approximately 200  $\mu\text{J}$  per pulse was used for both the visible and tunable infrared frequencies. The resulting SFG signal generated at the prism and slab sample surfaces was detected by a photomultiplier tube (PMT) after passing through a polarizer and monochromator. SFG signal from the PMT was processed, averaged, and recorded on a desktop computer. All SFG experiments were carried out at room temperature and under standard conditions. Due to the experimental challenges associated with reproducibly realigning high-intensity laser beams back and forth between two experimental geometries, we instead utilized  $\text{SiO}_2$  sample substrates with prism and slab geometric shapes (Figures 3.1 and 3.2). This practice allowed the angle of incidence for incoming laser beams to be experimentally changed reproducibly without necessitating the modification or movement of mirrors or other optics.

### 3.2.3. SFG Sample Preparation

SFG samples were prepared by first soaking fused silica,  $\text{SiO}_2$ , equilateral prisms and windows overnight in a solution of concentrated  $\text{H}_2\text{SO}_4$  (97%) (Sigma-Aldrich) and Nochromix (Godax). Next, the silica substrates were washed with distilled, de-ionized water. All sample substrates were then subjected to oxygen plasma treatment using a Herrick plasma cleaner (Ithaca, NY) (18 W RF, 200 mtorr  $\text{O}_2$ ) for 60 s. This process was implemented to ensure the full oxidation and subsequent removal of any organic surface contaminants remaining after acid bath treatment. The  $\text{O}_2$  plasma treatment also served to maximize the oxidation of the silica surfaces. SFG substrates coated with polystyrene (PS) thin films were prepared by spin-coating the plasma cleaned prisms and slabs with a 3 % weight solution of PS (MW  $\approx$  280,000) (Aldrich) dissolved in toluene (Sigma-Aldrich). For the spin-coating process a Specialty Coating Systems (Indianapolis, IN) instrument was utilized for 45 s at a speed of 3000 rpm. The resulting polystyrene thin films were then annealed at a temperature of 120  $^\circ\text{C}$  for 12 hours. The thickness of the PS films was determined to be  $\sim$ 105 nm by ellipsometry and atomic force microscopy.

## 3.3. Results and Discussion

We present in Figure 3.5 plots of the simulated geometry factor,  $G$ , as a function of angle  $\beta'$  at three different infrared wavelengths in the region 2800 - 3600  $\text{cm}^{-1}$ . In these plots,  $\beta$  was taken to be the average angle of incidence of two input beams,  $\beta' = (\beta_{\text{IR}} + \beta_{\text{vis}})/2$ , and calculated  $G$  values were normalized by the  $G$  factor at  $\beta' = 35^\circ$ . Additionally, the difference in angle of incidence between the input beams,  $\beta_{\text{IR}} - \beta_{\text{vis}}$ , was fixed at  $6^\circ$  in the simulations. As shown in Figure 3.5, the  $G$  values calculated for all three infrared wavelengths indicate a substantial enhancement in SFG intensity for input infrared beams approaching total internal reflection angle of incidence (or critical angle) near  $67^\circ$ . At the critical angle, total internal reflection is achieved and the theory predicts that the  $L_T^{\text{IR}}$  coefficient reaches a maximum at this value for materials with purely real (i.e. non-complex) indices of refraction. This effect has been exploited by a number of research groups to increase experimental SFG intensity. However, this

enhancement is not uniform across the three wavelengths and suggests an enhancement at 2800  $\text{cm}^{-1}$  which is nearly 3 times that at 3200  $\text{cm}^{-1}$  and 4 times that at 3600  $\text{cm}^{-1}$ . This result suggests that while nearly an order of magnitude enhancement in SFG signal can be obtained by positioning the incident infrared beam at or near its critical angle as this enhancement would not be uniform across the scanning range. Therefore conducting experiments near the critical angle in this infrared frequency region and subsequently attempting to perform quantitative data analysis would prove challenging. Figure 3.6 emphasizes this result and shows the infrared frequency dependence of the  $G$  factor enhancement for the prism geometry when normalized by the slab geometry  $G$  factor.

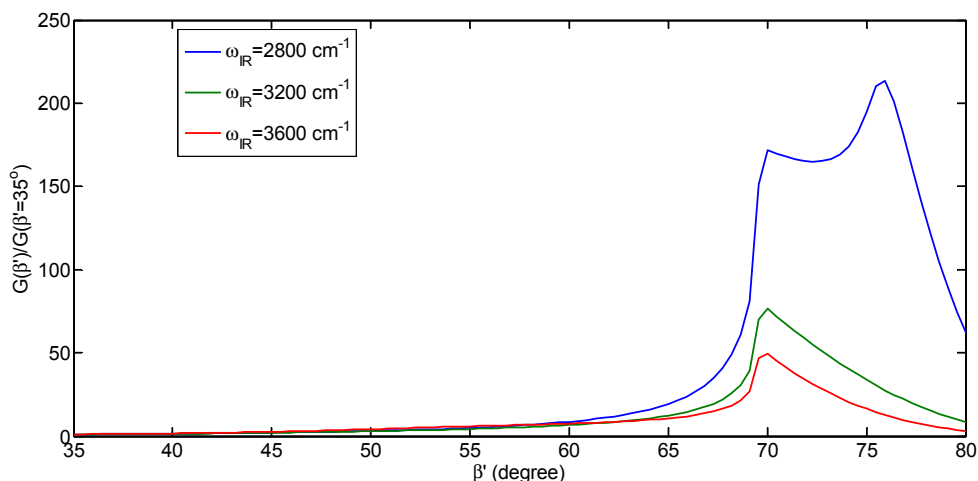


**Figure 3.5.** Plot of the geometric factor,  $G(\beta')$ , at infrared frequencies of 2800  $\text{cm}^{-1}$  (blue line), 3200  $\text{cm}^{-1}$  (green line) and 3600  $\text{cm}^{-1}$ , respectively, as a function of the average angle of incidence of the input laser beams  $\beta' = (\beta_{\text{IR}} + \beta_{\text{vis}})/2$ , and normalized by the  $G$  factor at  $\beta' = 35^\circ$ . In these simulations the difference between the angle of incidence for the infrared and visible beams was fixed at  $\beta_{\text{IR}} - \beta_{\text{vis}} = 6^\circ$ . This simulation data suggests that a dramatic increase in SFG signal can be obtained experimentally in systems with  $\beta'$  values near  $67^\circ$  where the infrared light approaches its critical angle. However, the magnitude of this enhancement in SFG signal is highly frequency dependent at angles of incidence approaching total internal refraction in infrared frequency region 2800 - 3600  $\text{cm}^{-1}$ .

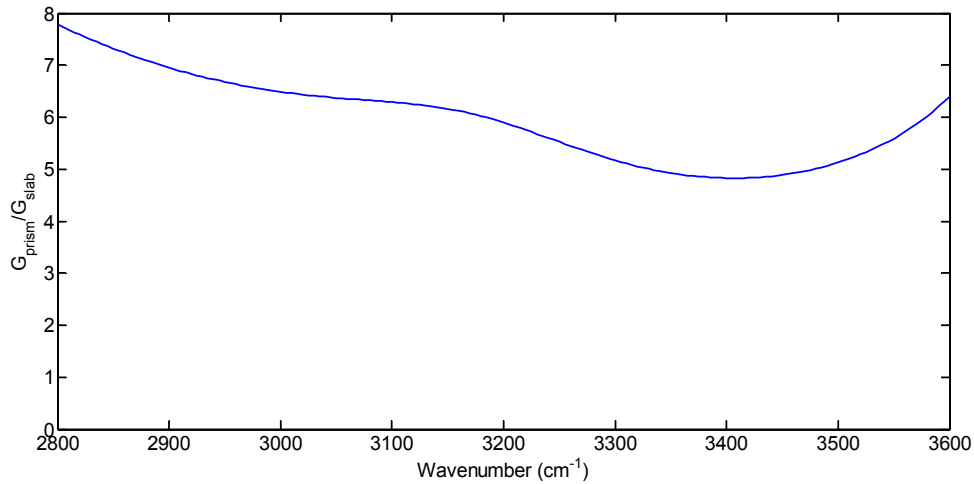


**Figure 3.6. Plot of ratio of geometric factor for the prism geometry,  $G_{\text{prism}}$ , normalized by the geometric factor value for the slab geometry,  $G_{\text{slab}}$ , as a function of incident infrared wavelength in the region 2800 - 3600  $\text{cm}^{-1}$ . This data indicates the relative enhancement in experimental SFG signal intensity obtained when switching from the slab to the prism geometry is non-uniform across in the infrared frequency region of interest.**

Since the SFG experiments conducted in the prism geometry had an angle of incidence for the infrared beam at approximately  $\sim 64^\circ$ , a dramatic enhancement in the transmitted electric field would be expected as a result of being very near the total internal reflection angle. Despite this prediction, the modulus squared of the Fresnel coefficient calculated for the infrared beam in the prism geometry is slightly less than that of the slab geometry in a majority of the region shown in Figure 3.7. The reduction in the ratio  $\left| L_{T,\text{prism}}^{\text{IR}} / L_{T,\text{slab}}^{\text{IR}} \right|^2$  for the infrared beam was attributed primarily to the complex index of refraction shown in Figure 3.4. However, the further examination described below was required to confirm this hypothesis. Despite this finding, the Fresnel coefficients were predicted to increase slightly for both the visible and SFG beams as plotted in Figure 3.7.

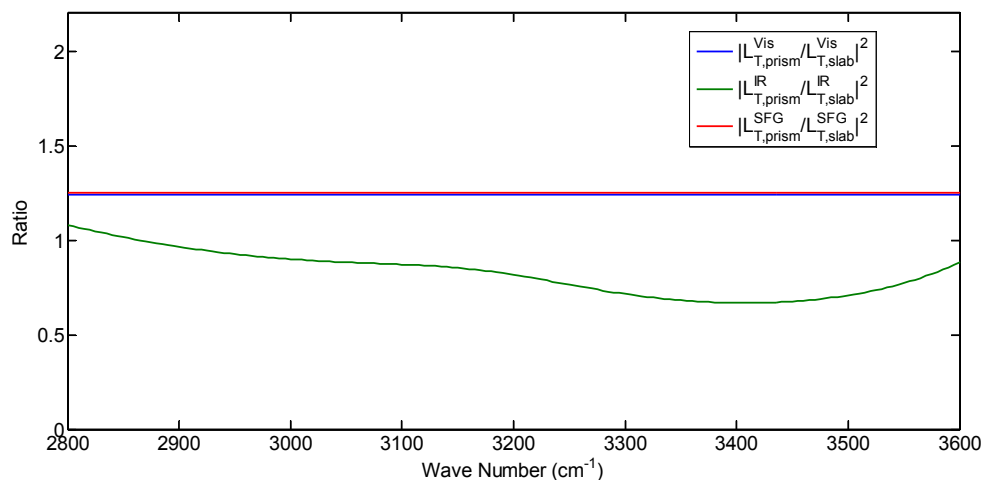


**Figure 3.7. Plot of the ratios of Fresnel transmission coefficients for the prism geometry relative to the slab geometry as a function of infrared wavelength. The simulated Fresnel transmission coefficient ratios for the visible (blue line) and SFG (red line) beams are frequency independent, but the ratio for the infrared (green line) transmission varies majority with wavelength. This data predicts a slight decrease in magnitude of infrared transmission across a majority of the frequency region 2800 - 3600  $\text{cm}^{-1}$ .**

To better understand the nature of Fresnel coefficients, it is important to recall that the index of refraction,  $\eta$ , is defined as the ratio of the speed of light propagating in a vacuum relative to the speed in a medium.<sup>61</sup> For non-magnetic substances, such as the materials used in this study, the index of refraction is equivalent to the square root of the substance's dielectric constant,  $\epsilon^{1/2}$ . This physical property of a material is wavelength dependent and it can also be a complex quantity. For materials with a complex index of refraction, the imaginary part is characterized by the absorption of light by that material.

In many circumstances, the imaginary component of a material's index of refraction may be neglected when it is approximately 10% or less in magnitude than the real component. However, in the case of water in the infrared frequency range 2800 - 3600  $\text{cm}^{-1}$  the imaginary part of the index cannot be neglected as it is nearly 30% the magnitude of the real part at frequencies approaching 3400  $\text{cm}^{-1}$  as shown in Figure 3.4. With this knowledge we then simulated the Fresnel coefficient for the infrared beam as a function of angle of incidence several complex indices of refraction as presented in Figure 3.8. From this plot it is apparent that as the Fresnel coefficient for the transmitted infrared decreases with an increase in magnitude of the imaginary component of the index of refraction at angles approaching and exceeding the critical angle.

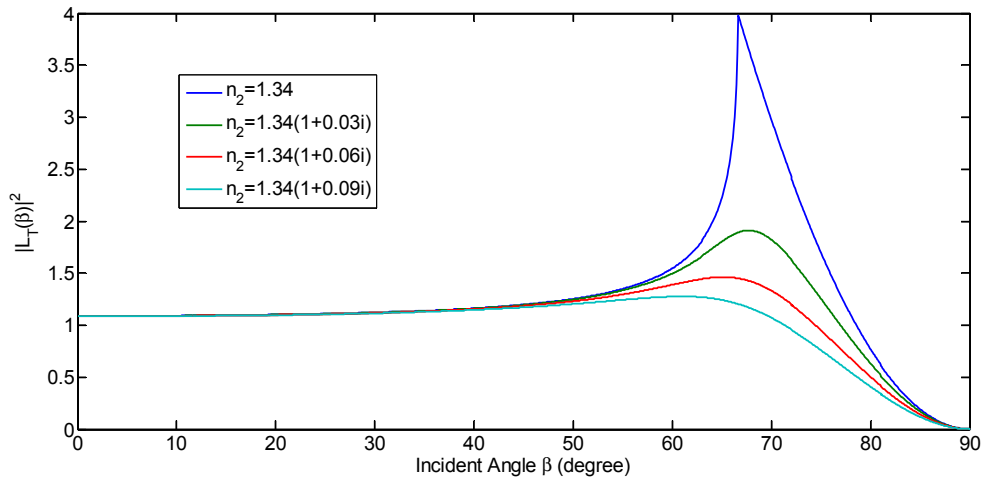


**Figure 3.8.** Plot of the Fresnel coefficient for transmitted infrared light as a function of the infrared beams' angle of incidence. This simulation data indicates the magnitude of enhancement for Fresnel coefficient varies with frequency and is strongly influenced by the magnitude of the imaginary component of index of refraction at angles approaching total internal reflection.

When comparing the incident infrared angle dependent  $G$  factor term for the two geometries, we find that the value of  $|\sin(\beta_{IR, \text{prism}})|^2$  is approximately 2.05 times that of  $|\sin(\beta_{IR, \text{slab}})|^2$  as shown in Figure 3.9. Also demonstrated in Figure 3.9, the  $G$  factor term dependant on the angle of the emitted SFG,  $|\sec(\beta)|^2$ , is more than twice as large for the prism geometry as it is for the slab geometry. Subsequently, the theoretical calculations predict a more than four-fold combined increase in the magnitude of the  $G$  value when changing from the slab to the prism geometry.

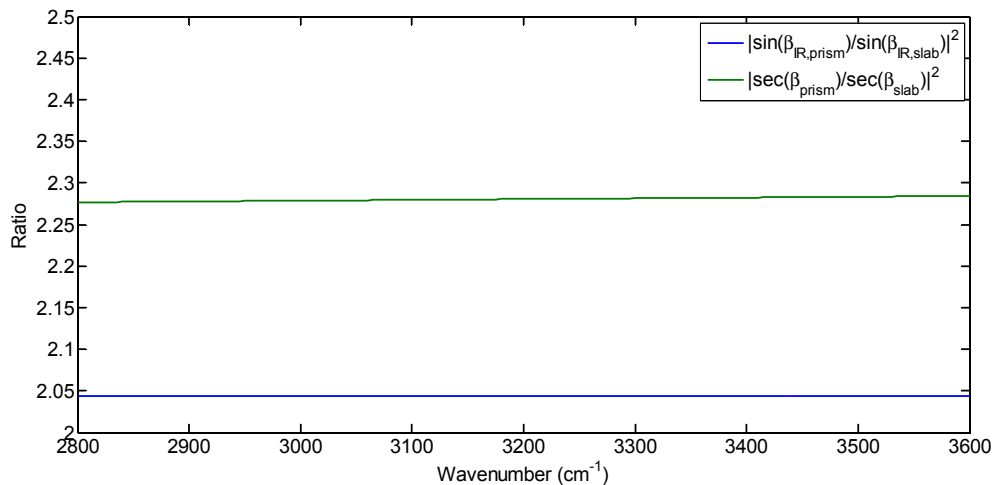


**Figure 3.9.** Plot of ratios of simulated geometry related terms,  $|\sin(\beta_{IR})|^2$  (blue line) and  $|\sec(\beta)|^2$  (green line), comparing prism and slab geometries as a function of infrared frequency. Simulation data for both terms predicts an approximate two-fold enhancement that is largely frequency independent for the prism geometry.

All of this theoretical data taken together provides strong evidence that the frequency dependence of the Fresnel coefficient for the infrared beam is the result of the complex and wavelength dependent index of refraction of water. Additionally, the proximity of the beam to the critical angle enhances this phenomenon. However, this Fresnel coefficient frequency dependence can be eliminated at an infrared beam angle of incidence far away from the critical angle. In such a case, an experimental beam geometry where the visible and SFG beams were both near the critical angle could be utilized to compensate for the loss in overall SFG intensity that would accompany a reduction in the infrared beam angle.

The theoretical predictions for the origin of the SFG signal enhancement as a function of incident beam geometry were experimentally tested using both polystyrene coated and bare SiO<sub>2</sub> prism and slab sample substrates. The SFG spectrum of the polystyrene-air interface was measured for samples in the prism and slab geometries and is included in Figure 3.10. Each data point in the figure is the average of 200 laser shots, and both spectra show the strong vibrational mode centered at 3060 cm<sup>-1</sup> observed in previous SFG studies of the polystyrene-air interface.<sup>59</sup> Specifically, this spectra peak is attributed to the  $\nu_2$  aromatic C-H vibrational mode of the polystyrene's six-member rings. The SFG signal detected from this  $\nu_2$  mode in the prism geometry is enhanced by more than an order of magnitude relative to the slab geometry. Additionally, the dramatic enhancement in SFG intensity with the prism geometry also enabled the resolution of two additional vibrational modes at 2915 cm<sup>-1</sup> and 3010 cm<sup>-1</sup> corresponding to a CH<sub>2</sub> asymmetric stretch from the polystyrene backbone and a combination band, respectively. Finally, the data collected in the slab and prism geometries had signal-to-noise ratios of 24 and 29, respectively, indicating that experimental data collected while using the prism geometry had less noise than that collected when using the slab geometry.

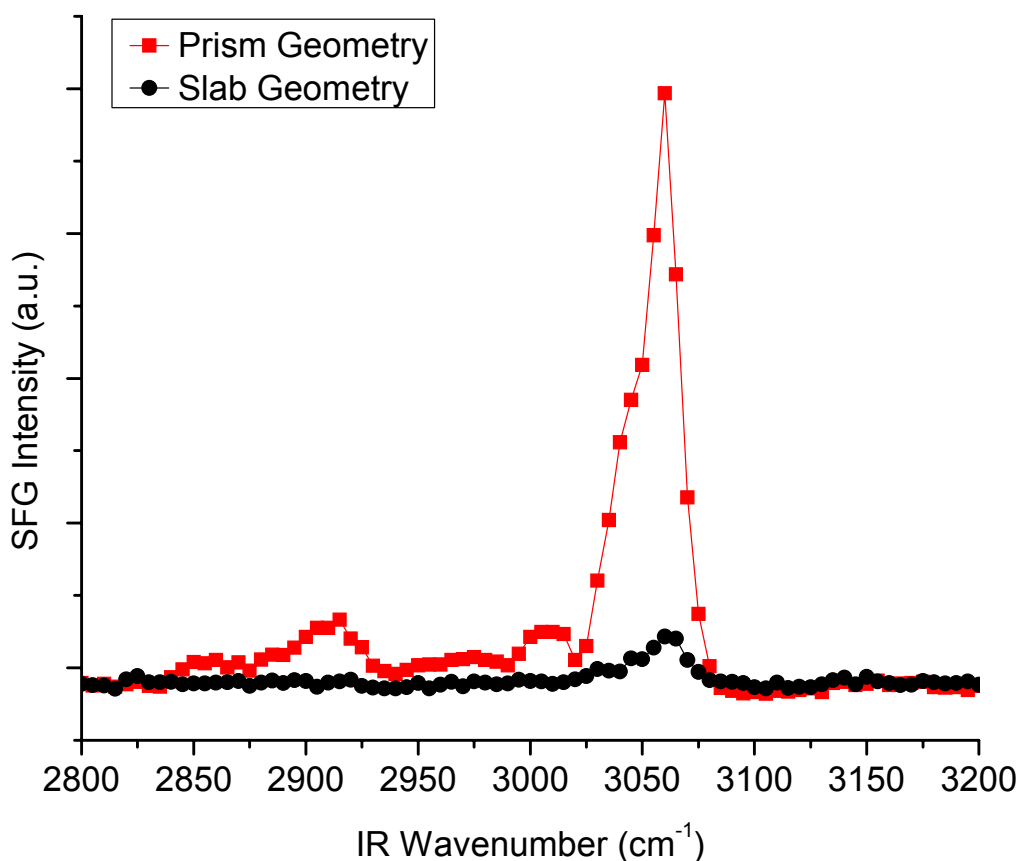


Figure 3.10. SFG spectra of the polystyrene-air interface in the slab (black circles) and prism (red squares) experimental beam geometries. The spectral peak centered at  $3060\text{ cm}^{-1}$  corresponding to the  $\nu_2$  aromatic C-H stretching mode on the phenyl ring is enhanced by more than an order of magnitude in the prism geometry. Additionally, the spectrum collected in the prism geometry shows C-H vibrational modes at  $2915\text{ cm}^{-1}$  and  $3010\text{ cm}^{-1}$  which are not observed in the slab geometry. The presence of these two vibrational modes is attributed to an enhanced resolution and improved signal-to-noise ratio obtained in the prism geometry.

A second set of experiments was conducted at the  $\text{SiO}_2 - \text{H}_2\text{O}$  interface to compare the influence of experimental geometry on SFG intensity for prism and slab substrates. SFG spectra from this study are presented in Figure 3.11, and the spectral features observed are similar to previous studies.<sup>13, 56</sup> Broad O-H vibrational modes are observed at  $3200\text{ cm}^{-1}$  and  $3400\text{ cm}^{-1}$  attributed to “ice-like” tetrahedrally coordinated and “liquid-like” less than tetrahedrally coordinated interfacial water molecules, respectively. Data in Figure 3.11 shows over an order of magnitude enhancement in SFG signal for the prism geometry. This result is remarkably similar to the increase in SFG signal at the polystyrene-air interface. However, for the measurements conducted at the  $\text{SiO}_2 - \text{H}_2\text{O}$  interface each data point for the prism geometry was the average of 1000 laser shots while each data point for the slab geometry was the average of 1600 laser shots.

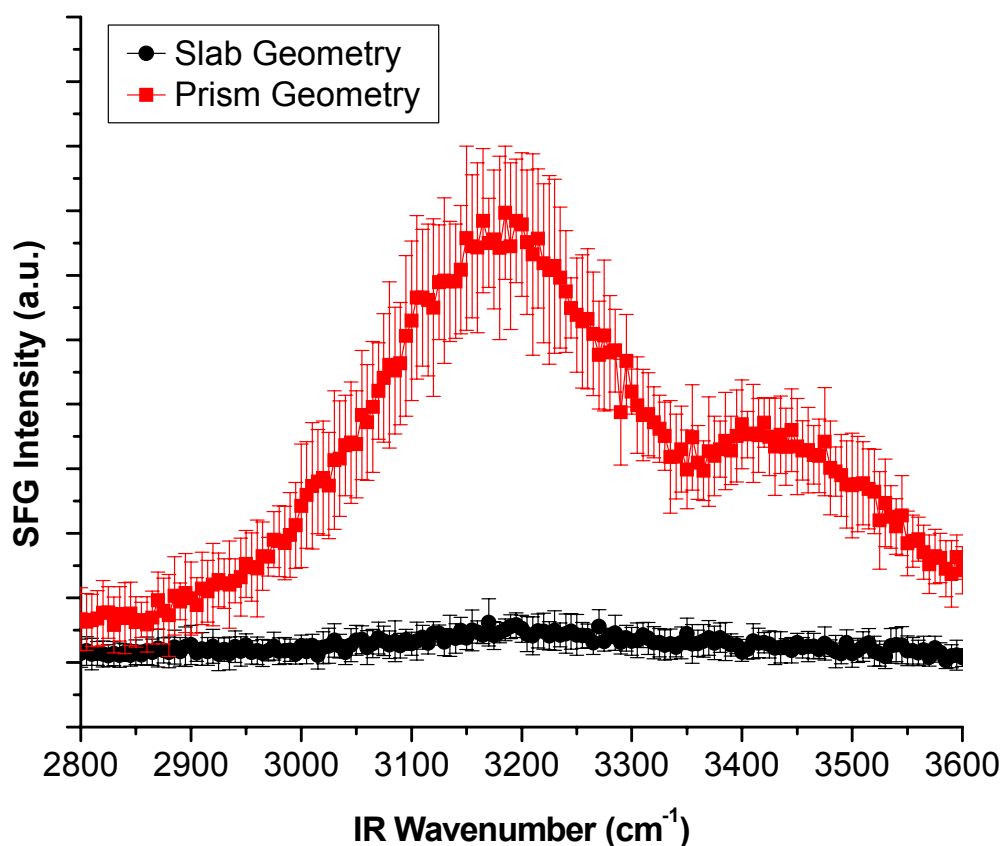


Figure 3.11. SFG spectra of the  $\text{SiO}_2$  -  $\text{H}_2\text{O}$  solid-liquid interface at room temperature in slab (black circles) and prism (red squares) experimental beam geometries. The broad peaks centered around  $3200\text{ cm}^{-1}$  and  $3400\text{ cm}^{-1}$  are attributed to O-H stretches of “ice-like” tetrahedrally coordinated and “liquid-like” less than tetrahedrally coordinated interfacial water, respectively. The spectrum collected in the prism geometry shows more than an order of magnitude enhancement in SFG signal intensity compared to the slab geometry.

While a comparison of Figures 3.10 and 3.11 indicates that the experimental noise was substantially smaller at the solid-air interface than at the solid-liquid interface, a quantitative comparison directly between these two data sets is not appropriate due to differences in number of measurements between geometries and interfaces. However, a qualitative comparison between the prism-to-slab SFG signal ratio experimentally and theoretically determined is included in Figure 3.12. As demonstrated in this figure, the theoretical prediction and experimental data compare quite well to within experimental error as both indicate approximately an order of magnitude enhancement in SFG signal for measurements conducted utilizing the prism when compared to the slab geometry. Figure 3.12 shows the theoretical prediction for the enhancement of SFG signal in the region  $2800 - 2900\text{ cm}^{-1}$  is slightly larger than what was experimentally observed at the  $\text{SiO}_2$  -  $\text{H}_2\text{O}$  solid-liquid interface and slightly smaller in the region  $2900 - 3600\text{ cm}^{-1}$ . While a slightly improved theoretical model may be needed as evidenced by these slight deviations, the overall agreement between theory and experiment in this study is strong evidence for the current model’s utility.

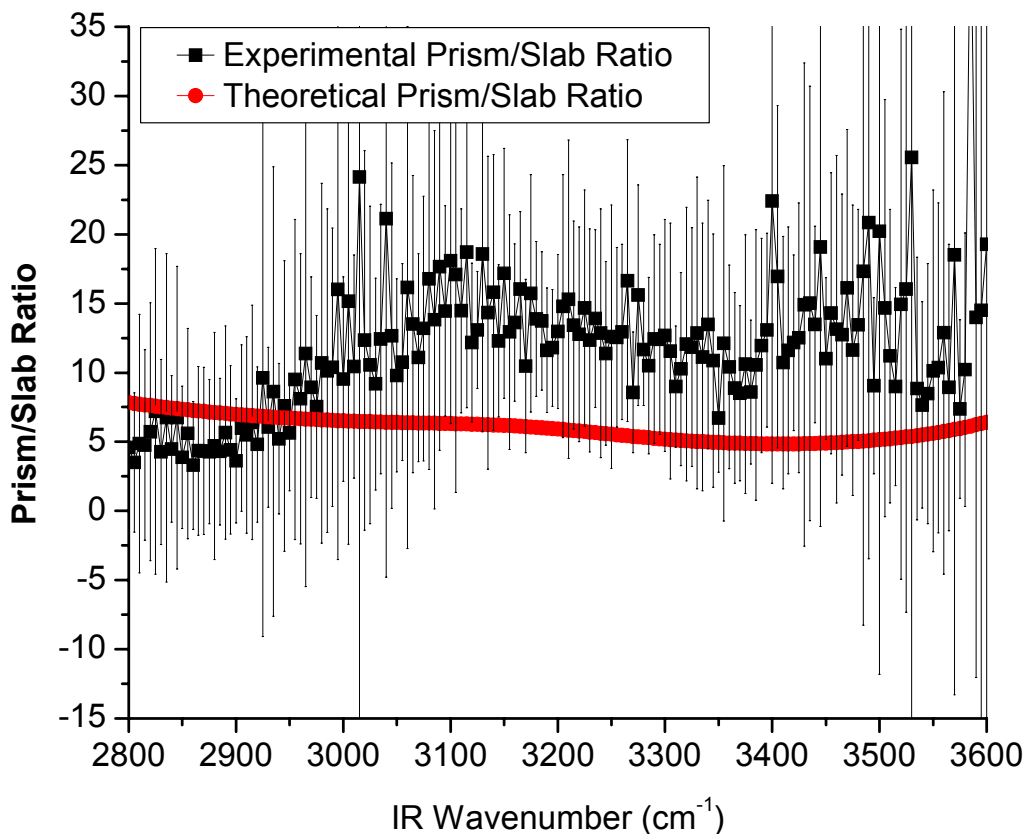


Figure 3.12. Comparison of predicted theoretical (red circles) and experimentally measured (black squares) ratio of SFG signal enhancement obtained in the prism sample geometry relative to the slab geometry. Theoretical predictions slightly underestimate the SFG signal enhancement observed in experiments in most of the region studied, but the theory and experiment agree to within experimental error for nearly all data points.

### 3.4. Conclusions

The influence of experimental laser beam geometry on SFG signal was studied at the interface between absorbing and non-absorbing media. The imaginary portion of an absorptive medium's complex index of refraction was found to have dramatic influence on the magnitude of Fresnel coefficients for that system. Because the magnitude of a system's Fresnel coefficients can substantially influence the amount of SFG intensity measured experimentally, this influence should be carefully considered when selecting the desired beam geometry for a given experiment. Additionally, the magnitude of this effect was predicted by numerical simulation and confirmed experimentally to be dramatically enhanced in systems where incident light impinges on an interface at or near the critical angle for the system. As a result, caution should be exercised when utilizing beam geometries where the angle of incidence of one or more input beams is near the critical angle.

## References

1. Hunt, J. H.; Guyot-Sionnest, P.; Shen, Y. R., *Chemical Physics Letters* **1987**, *133* (3), 189-192.
2. Harris, A. L.; Chidsey, C. E. D.; Levinos, N. J.; Loiacono, D. N., *Chemical Physics Letters* **1987**, *141* (4), 350-356.
3. Zhu, X. D.; Suhr, H.; Shen, Y. R., *Physical Review B* **1987**, *35* (6), 3047-3050.
4. Shen, Y. R., *Nature* **1989**, *337* (6207), 519-525.
5. Shen, Y. R., *Solid State Communications* **1997**, *102* (2-3), 221-229.
6. Gracias, D. H.; Chen, Z.; Shen, Y. R.; Somorjai, G. A., *Accounts of Chemical Research* **1999**, *32* (11), 930-940.
7. Chen, Z.; Shen, Y. R.; Somorjai, G. A., *Annual Review of Physical Chemistry* **2002**, *53*, 437-465.
8. Eisenthal, K. B., *Chemical Reviews* **1996**, *96* (4), 1343-1360.
9. Lambert, A. G.; Davies, P. B.; Neivandt, D. J., *Applied Spectroscopy Reviews* **2005**, *40* (2), 103-145.
10. Wang, H. F.; Gan, W.; Lu, R.; Rao, Y.; Wu, B. H., *International Reviews in Physical Chemistry* **2005**, *24* (2), 191-256.
11. York, R. L.; Browne, W. K.; Geissler, P. L.; Somorjai, G. A., *Israel Journal of Chemistry* **2007**, *47* (1), 51-58.
12. Wampler, R. D.; Moad, A. J.; Moad, C. W.; Heiland, R.; Simpson, G. J., *Accounts of Chemical Research* **2007**, *40* (10), 953-960.
13. Hopkins, A. J.; McFearin, C. L.; Richmond, G. L., *Current Opinion in Solid State & Materials Science* **2005**, *9* (1-2), 19-27.
14. Chen, X. Y.; Chen, Z., *Biochimica Et Biophysica Acta-Biomembranes* **2006**, *1758* (9), 1257-1273.
15. Baldelli, S., *Accounts of Chemical Research* **2008**, *41* (3), 421-431.
16. Kubota, J.; Domen, K., *Analytical and Bioanalytical Chemistry* **2007**, *388* (1), 17-27.
17. Raschke, M. B.; Shen, Y. R., *Current Opinion in Solid State & Materials Science* **2004**, *8* (5), 343-352.
18. Eisenthal, K. B., *Annual Review of Physical Chemistry* **1992**, *43*, 627-661.
19. Somorjai, G. A.; Rupprechter, G., *Journal of Physical Chemistry B* **1999**, *103* (10), 1623-1638.
20. Shultz, M. J.; Baldelli, S.; Schnitzer, C.; Simonelli, D., *Journal of Physical Chemistry B* **2002**, *106* (21), 5313-5324.
21. Koffas, T. S.; Amitay-Sadovsky, E.; Kim, J.; Somorjai, G. A., *Journal of Biomaterials Science-Polymer Edition* **2004**, *15* (4), 475-509.
22. Opdahl, A.; Koffas, T. S.; Amitay-Sadovsky, E.; Kim, J.; Somorjai, G. A., *Journal of Physics-Condensed Matter* **2004**, *16* (21), R659-R677.
23. Vidal, F.; Tadjeddine, A., *Reports on Progress in Physics* **2005**, *68* (5), 1095-1127.
24. Buck, M.; Himmelhaus, M., *Journal of Vacuum Science & Technology a-Vacuum Surfaces and Films* **2001**, *19* (6), 2717-2736.
25. Allen, H. C.; Raymond, E. A.; Richmond, G. L., *Current Opinion in Colloid & Interface Science* **2000**, *5* (1-2), 74-80.
26. Somorjai, G. A.; McCrea, K. R., *Advances in Catalysis, Vol 45* **2000**, *45*, 385-438.
27. Bain, C. D., *Current Opinion in Colloid & Interface Science* **1998**, *3* (3), 287-292.

28. Shultz, M. J.; Schnitzer, C.; Simonelli, D.; Baldelli, S., *International Reviews in Physical Chemistry* **2000**, *19* (1), 123-153.
29. Richmond, G. L., *Annual Review of Physical Chemistry* **2001**, *52*, 357-389.
30. Richmond, G. L., *Chemical Reviews* **2002**, *102* (8), 2693-2724.
31. Chen, X. Y.; Clarke, M. L.; Wang, J.; Chen, Z., *International Journal of Modern Physics B* **2005**, *19* (4), 691-713.
32. Gopalakrishnan, S.; Liu, D. F.; Allen, H. C.; Kuo, M.; Shultz, M. J., *Chemical Reviews* **2006**, *106* (4), 1155-1175.
33. Ma, G.; Allen, H. C., *Photochem. Photobiol.* **2006**, *82* (6), 1517-1529.
34. Chen, Z., *Polym. Int.* **2007**, *56* (5), 577-587.
35. Hatch, S. R.; Polizzotti, R. S.; Dougal, S.; Rabinowitz, P., *Chemical Physics Letters* **1992**, *196* (1-2), 97-102.
36. Hatch, S. R.; Polizzotti, R. S.; Dougal, S.; Rabinowitz, P., *Journal of Vacuum Science & Technology a-Vacuum Surfaces and Films* **1993**, *11* (4), 2232-2238.
37. Wang, J.; Chen, X. Y.; Clarke, M. L.; Chen, Z., *Proceedings of the National Academy of Sciences of the United States of America* **2005**, *102* (14), 4978-4983.
38. Lobau, J.; Wolfrum, K., *Laser Physics* **1998**, *8* (3), 582-592.
39. Lobau, J.; Wolfrum, K., *Journal of the Optical Society of America B-Optical Physics* **1997**, *14* (10), 2505-2512.
40. Conboy, J. C.; Messmer, M. C.; Richmond, G. L., *Journal of Physical Chemistry* **1996**, *100* (18), 7617-7622.
41. Conboy, J. C.; Messmer, M. C.; Richmond, G. L., *Journal of Physical Chemistry B* **1997**, *101* (34), 6724-6733.
42. Yang, Y. J.; Pizzolatto, R. L.; Messmer, M. C., *Journal of the Optical Society of America B-Optical Physics* **2000**, *17* (4), 638-645.
43. Gautam, K. S.; Schwab, A. D.; Dhinojwala, A.; Zhang, D.; Dougal, S. M.; Yeganeh, M. S., *Physical Review Letters* **2000**, *85* (18), 3854-3857.
44. Nishi, N.; Hobara, D.; Yamamoto, M.; Kakiuchi, T., *Analytical Sciences* **2003**, *19* (6), 887-890.
45. Harp, G. P.; Rangwalla, H.; Yeganeh, M. S.; Dhinojwala, A., *Journal of the American Chemical Society* **2003**, *125* (37), 11283-11290.
46. Knock, M. M.; Bell, G. R.; Hill, E. K.; Turner, H. J.; Bain, C. D., *Journal of Physical Chemistry B* **2003**, *107* (39), 10801-10814.
47. Strunk, M. R.; Williams, C. T., *Langmuir* **2003**, *19* (22), 9210-9215.
48. Rangwalla, H.; Dhinojwala, A., *Journal of Adhesion* **2004**, *80* (1-2), 37-59.
49. Dreesen, L.; Sartenaer, Y.; Humbert, C.; Mani, A. A.; Lemaire, J. J.; Methivier, C.; Pradier, C. M.; Thiry, P. A.; Peremans, A., *Thin Solid Films* **2004**, *464-65*, 373-378.
50. Kweskin, S. J.; Komvopoulos, K.; Somorjai, G. A., *Langmuir* **2005**, *21* (8), 3647-3652.
51. Kweskin, S. J.; Rioux, R. M.; Habas, S. E.; Komvopoulos, K.; Yang, P.; Somorjai, G. A., *Journal of Physical Chemistry B* **2006**, *110* (32), 15920-15925.
52. Yeganeh, M. S.; Dougal, S. A.; Silbernagel, B. G., *Langmuir* **2006**, *22* (2), 637-641.
53. Wang, J.; Even, M. A.; Chen, X. Y.; Schmaier, A. H.; Waite, J. H.; Chen, Z., *Journal of the American Chemical Society* **2003**, *125* (33), 9914-9915.
54. Chen, X. Y.; Wang, J.; Sniadecki, J. J.; Even, M. A.; Chen, Z., *Langmuir* **2005**, *21* (7), 2662-2664.
55. Miranda, P. B.; Shen, Y. R., *Journal of Physical Chemistry B* **1999**, *103* (17), 3292-3307.

56. Shen, Y. R.; Ostroverkhov, V., *Chemical Reviews* **2006**, *106* (4), 1140-1154.
57. Downing, H. D.; Williams, D., *Journal of Geophysical Research* **1975**, *80* (12), 1656-1661.
58. York, R. L.; Li, Y. M.; Holinga, G. J.; Somorjai, G. A., *Journal of Physical Chemistry A* **2009**, *113* (12), 2768-2774.
59. Briggman, K. A.; Stephenson, J. C.; Wallace, W. E.; Richter, L. J., *Journal of Physical Chemistry B* **2001**, *105* (14), 2785-2791.
60. Heinz, T. F., *University of California, Berkeley, Thesis* **1982**, 1-149.
61. Hecht, E., *Optics*. 4th ed.; Addison-Wesley: Reading, Mass., 2002; p vi, 698 p.

## Chapter 4

### Quartz Crystal Microbalance

#### 4.1. Quartz Crystal Microbalance Introduction

The quartz crystal microbalance (QCM) is a powerful, gravimetric analytical tool that allows quantitative measurement of the amount of material adsorbed on a surface. This experimental technique has proven to be a particularly useful tool for surface scientists because of its surface sensitivity on the order of nanograms per square centimeter coupled with its efficacy across a broad range of experimental conditions where many other surface analysis techniques are ineffective.<sup>1, 2</sup> QCM has proven an effective technique in environments ranging from ultra-high vacuum chambers to liquid-solid interfaces at atmospheric temperatures and pressures, and it has been utilized for in-situ investigation of systems ranging from protein absorption and biocompatibility to gas-phase thin-film deposition.<sup>3-10</sup> Fundamentally based on the piezoelectric nature of crystalline quartz, QCM has the added advantage of being a remarkably robust due to its simplicity in implementation as well as the minimal need for data analysis relative to other surface sensitive analytical techniques such as Auger electron and x-ray photoelectron spectroscopies (AES and XPS). Finally, the QCM technique has the practical advantage that the surface of sensor crystals can be coated or modified with a diverse range of materials including metals, metal oxides, semiconductors, and polymers allowing measurement of scientifically, medically, and industrially relevant surfaces.<sup>11-13</sup>

#### 4.2. Quartz Crystal Microbalance Theoretical Background

The QCM measurement technique is based on the two physical phenomena of piezoelectricity and oscillator resonance. The piezoelectric effect which was first reported by Pierre and Jacques Curie in 1880.<sup>14</sup> This phenomenon is characterized by a material which exhibits a polarization when under mechanical strain, and exhibits a mechanical strain when a polarization is applied.<sup>15</sup> Resonance can be defined as the phenomenon when the frequency oscillator is driven matches the natural frequency of the oscillator.<sup>16</sup> Typically, an oscillator exhibits its maximal displacement amplitude relative to its equilibrium position when driven at its resonance frequency. This is a result of the oscillator being able to accept the transfer of energy applied at the resonant frequency into a larger number of allowed energy eigenstates than at other frequencies where some of the oscillation modes are either not supported or forbidden. In 1889, Lord Rayleigh reported that the resonance frequency of an oscillating crystal can be modified by changing its inertia.<sup>17</sup>

The phenomena of oscillator resonance and piezoelectricity were utilized by Sauerbrey in 1959 to develop a linear relationship now bearing his name that directly correlates the change in resonant frequency of a quartz oscillator with the mass of material adsorbed on its surface.<sup>18</sup> The Sauerbrey Equation, equation (4.1), correlates the change in the resonant frequency of a QCM resonator's  $n^{\text{th}}$  harmonic,  $\Delta f_n$ , the harmonic number of the resonance,  $n$ , and a constant dependant upon the physical properties of the resonator,  $C$ , to the mass added to the resonator's surface,  $\Delta m$ . The Sauerbrey equation is valid for resonator systems when the temperature is held

constant and the added surface mass is elastically bound, less than 2% of the crystal mass, and evenly distributed across the crystal resonator surface.

$$\Delta m = -\frac{C}{n} \Delta f_n \quad (4.1)$$

A typical QCM measurement begins when a piezoelectric crystal resonator is driven to oscillation by applying a high-frequency AC potential. Each alternating polarization applied produces subsequent mechanical deformation in the lateral direction of the crystal oscillator as shown in Figure 4.1. Next the driving AC polarization is turned off and the piezoelectric sensor continues to vibrate generating a subsequent surface charge which changes polarization with each half oscillation cycle. This surface polarization of the sensor crystal is directly measured as an AC voltage at oscillating at the crystal's resonance frequency. The magnitude of the resonator's surface AC polarization with each successive oscillation is related the crystal's displacement in the plane of vibration. This oscillation displacement is a function of the system's total inertia. As a non-ideal oscillator system, the crystal's inertial energy is gradually lost with each successive vibration in the absence of a driving frequency. Experimentally, this loss in energy is referred to as the dissipation factor,  $D$ , and is measured as the decay in magnitude of the AC surface polarization with time. Specifically, the dissipation factor is defined as the amount of energy lost in one resonator oscillation divided by  $2\pi$  times the total energy stored in the oscillating system as shown in equation (4.2).<sup>6</sup>

$$D = \frac{1}{Q} = \frac{E_{Dissipated}}{2\pi E_{Stored}} \quad (4.2)$$

The non-ideality of all physical oscillator systems restricts the valid of use of the Sauerbrey equation alone when analyzing experimental QCM data to systems exhibiting small dissipation values and high surface elasticity.<sup>19, 20</sup> For all QCM experimental data included herein, the criteria necessary for valid use of the Sauerbrey equation were satisfied.

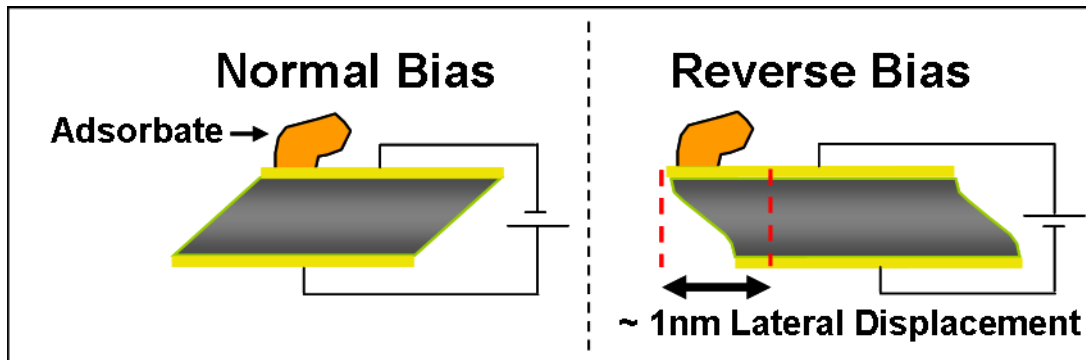


Figure 4.1. Schematic of QCM sensor surface displacement with externally applied surface potential. Crystal surface and adsorbate move laterally in response to oscillating voltage. After driving AC voltage is turned off, the resonator and adsorbate system continues to vibrate at its resonant frequency.

### 4.3. Quartz Crystal Microbalance Instrumentation

Quartz crystal microbalance measurements were carried out using commercial Q-sense (Glen Burnie, MD) D300 and E4 model instruments. The QCM resonance frequency and dissipation for a given harmonic of each quartz crystal resonator is measured and recorded in 5 ms intervals by the Q-Sense instruments resulting in an overall data collection frequency of 200 Hz. Each 5 ms data acquisition interval for the QCM instruments is subdivided into three consecutive sub-intervals where a resonator is driven, measured while freely oscillating, and the measured data is communicated and processed by desktop computer as shown in Figure 4.2. During the first data collection sub-interval, a range of high-frequency AC potentials are applied to energize a quartz crystal resonator for a 2 ms period. The specific driving frequencies used are unique and individually determined for each individual crystal and are centered in the expected frequency ranges for the fundamental and several odd harmonic frequencies. Next, the driving high-frequency AC field is turned off for 2 ms while the resonator oscillation frequency is measured in the second data acquisition sub-interval. This is accomplished by monitoring the frequency of crystal surface polarization resulting from the continued resonant oscillation of the piezoelectric quartz sensor crystal. As a non-ideal simple harmonic oscillator, the QCM sensor crystal loses a portion of its total kinetic energy with each subsequent oscillation until it comes to rest. This energy loss is measured and recorded as the dissipation number,  $D$ , for each resonant frequency. Finally, in the third data acquisition sub-interval the resonance frequencies and dissipation values measured are communicated to a desktop computer where the data is processed and recorded. This procedure occurs over a time period of 1 ms and upon completion the QCM instrument begins the next data acquisition interval. During measurements conducted with the D300 instrument, the resonances and dissipation values of each sensor crystal were measured and recorded at the fundamental as well as the 3<sup>rd</sup>, 5<sup>th</sup>, and 7<sup>th</sup> harmonic frequencies at approximately 5 MHz, 15 MHz, 25 MHz, and 35 MHz, respectively. QCM experiments utilizing the E4 instrument were performed while measuring and recording the fundamental, 3<sup>rd</sup>, 5<sup>th</sup>, 7<sup>th</sup>, 9<sup>th</sup>, 11<sup>th</sup>, and 13<sup>th</sup> harmonic frequencies and dissipation values. All measurements were performed inside of temperature controlled measurement chambers. This instrumentation capability allowed all data collection to be conducted at fixed temperature maintained to within 0.1 °C for the duration of each QCM experiment.

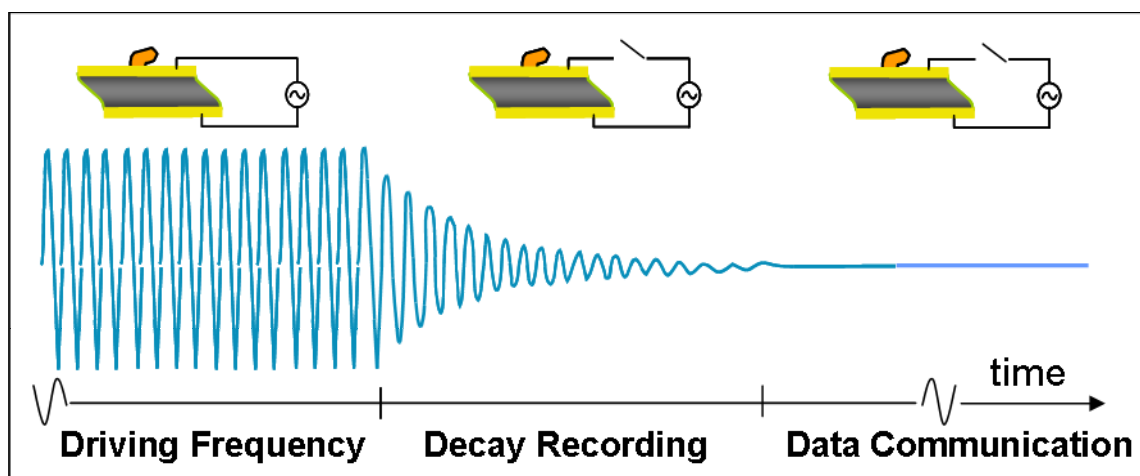


Figure 4.2. Schematic of Q-sense QCM instrument measurement process. Initially, a high-frequency AC field is applied to the sensor crystal for 2 ms to drive its lateral oscillation. Subsequently, the applied field is removed and the crystal continues to oscillate at its resonant frequency. This oscillation is directly measured for 2 ms as an AC surface potential generated by the quartz resonator and is then recorded. Finally, the frequency, magnitude, and decay of the sensor crystal's surface polarization is communicated to a desktop computer over a period of 1 ms and then the measurement process begins again.

Both gold and SiO<sub>2</sub> coated Q-sense QCM sensor crystals were used for all measurements. All QCM crystals were made of AT-cut quartz and had fundamental resonance frequencies at ~5 MHz. Each Q-sense crystal sensor was manufactured from AT-cut quartz to the specification that its resonance constant for the Sauerbrey equation,  $C$ , is 17.7 ng•cm<sup>-2</sup>•Hz<sup>-1</sup>. Immediately prior to all measurements, the exact resonance frequencies and dissipation values for each individual sensor crystal was experimentally determined in air and in solution.

Reagent and rinse solutions were introduced and passed through the D300 instrument using a gravity fed 5 mL solution reservoir, and a high-precision peristaltic pump (Ismatec, Switzerland) was used to pass solutions through the E4 instrument. During measurement, solutions were flowed through QCM instrument sensor chambers to ensure complete liquid exchange prior to stopping solution flow and data collection of the static liquid-solid system as shown in Figure 4.3. Between measurements, the QCM instruments were thoroughly rinsed with distilled, de-ionized water before and after being cleaned with a 2% volume solution of Hellmanex II detergent (Hellma GmbH) in water.

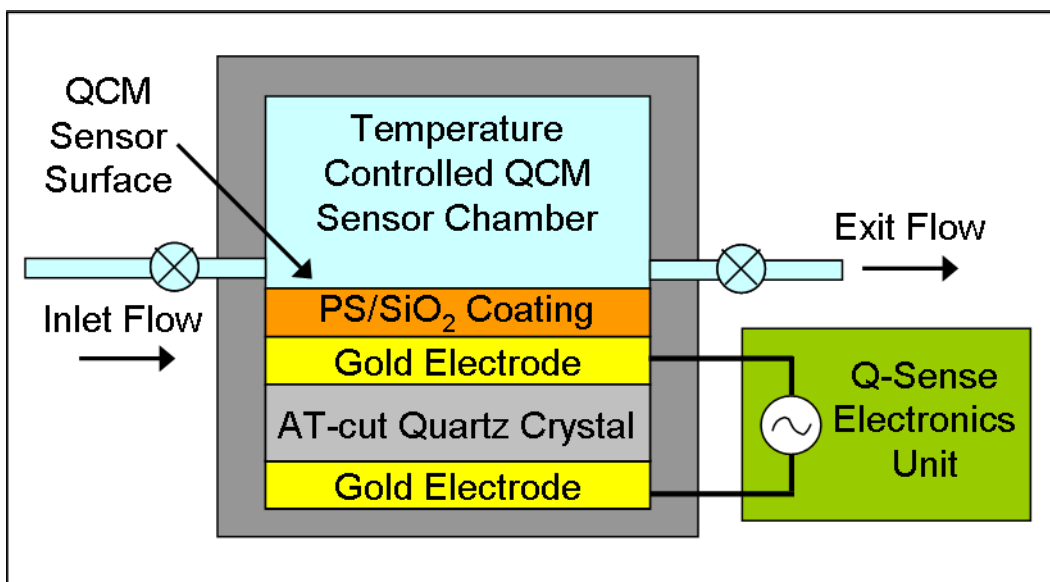


Figure 4.3. Diagram of Q-sense QCM instrument's liquid measurement chamber and sensor crystal as experimentally used. A quartz sensor crystal is mounted in the bottom of a temperature controlled measurement chamber which can be filled with a static or a flowing solution. The crystal surfaces have a gold electrode coating on each side allowing an AC potential to be applied and subsequently by an external electronics unit. The gold coated sensor surface in contact with the solution can be coated with polystyrene (PS), silica (SiO<sub>2</sub>), or a variety of other materials allowing measurement of the liquid-solid interface of interest.

#### 4.4. Quartz Crystal Microbalance Sample Substrate Preparation

QCM measurements were carried out on gold and SiO<sub>2</sub> coated Q-Sense (Glen Burnie, MD) sensors. Prior to each use QCM sensor crystals were cleaned with a Herrick oxygen plasma cleaner (Ithaca, NY) (18 W RF, 200 mtorr O<sub>2</sub>) for 60 s to remove any organic surface contaminants and to also ensure the full surface oxidation of the crystal surfaces in the case of SiO<sub>2</sub> sensor crystals. After plasma treatment, SiO<sub>2</sub> crystals were used directly, and polystyrene (PS) surfaces were then prepared on the clean gold coated sensor crystals. PS films were prepared by spin coating a 2 % weight solution of polystyrene (PS) (MW ≈ 280,000) (Aldrich) in toluene (Sigma-Aldrich) on the gold surfaces. The spin-coating procedure was carried out at 3000 rpm for 45 s using a Specialty Coating Systems (Indianapolis, IN) spin coater, and the resulting films were then annealed for 12 hours at 120 °C. Both ellipsometry and atomic force microscopy measurements were conducted on the PS coated substrates which were subsequently found to have polymer coatings ~95 nm thick.

## References

1. Marx, K. A., *Biomacromolecules* **2003**, *4* (5), 1099-1120.
2. O'Sullivan, C. K.; Guilbault, G. G., *Biosensors & Bioelectronics* **1999**, *14* (8-9), 663-670.
3. Andersson, J.; Ekdahl, K. N.; Lambris, J. D.; Nilsson, B., *Biomaterials* **2005**, *26* (13), 1477-1485.
4. Lord, M. S.; Stenzel, M. H.; Simmons, A.; Milthorpe, B. K., *Biomaterials* **2006**, *27* (4), 567-575.
5. Irwin, E. F.; Ho, J. E.; Kane, S. R.; Healy, K. E., *Langmuir* **2005**, *21* (12), 5529-5536.
6. Rodahl, M.; Kasemo, B., *Review of Scientific Instruments* **1996**, *67* (9), 3238-3241.
7. Rodahl, M.; Hook, F.; Fredriksson, C.; Keller, C. A.; Krozer, A.; Brzezinski, P.; Voinova, M.; Kasemo, B., *Faraday Discussions* **1997**, *107*, 229-246.
8. Groner, M. D.; Fabreguette, F. H.; Elam, J. W.; George, S. M., *Chem. Mat.* **2004**, *16* (4), 639-645.
9. Aarik, J.; Aidla, A.; Uustare, T.; Ritala, M.; Leskela, M., *Applied Surface Science* **2000**, *161* (3-4), 385-395.
10. Kukli, K.; Aarik, J.; Aidla, A.; Siimon, H.; Ritala, M.; Leskela, M., *Applied Surface Science* **1997**, *112*, 236-242.
11. York, R. L.; Holinga, G. J.; Somorjai, G. A., *Langmuir* **2009**, *25* (16), 9369-9374.
12. Phillips, D. C.; York, R. L.; Mermut, O.; McCrea, K. R.; Ward, R. S.; Somorjai, G. A., *Journal of Physical Chemistry C* **2007**, *111* (1), 255-261.
13. Mermut, O.; Phillips, D. C.; York, R. L.; McCrea, K. R.; Ward, R. S.; Somorjai, G. A., *Journal of the American Chemical Society* **2006**, *128* (11), 3598-3607.
14. Curie, J.; Curie, P., *Comptes Rendus Hebdomadaires Des Seances De L Academie Des Sciences* **1880**, *91*, 294-295.
15. Simpson, R. E., *Introductory electronics for scientists and engineers*. 2nd ed.; Allyn and Bacon: Boston, 1987; p xvi, 939 p.
16. Halliday, D.; Resnick, R.; Walker, J., *Fundamentals of physics*. 5th ed.; Wiley: New York, 1997; p xxix, 1142 p.
17. Rayleigh, L., *Proc. London Math. Soc.* **1888**, *s1-20* (1), 225-237.
18. Sauerbrey, G., *Zeitschrift Fur Physik* **1959**, *155* (2), 206-222.
19. Hook, F.; Rodahl, M.; Brzezinski, P.; Kasemo, B., *Langmuir* **1998**, *14* (4), 729-734.
20. Hook, F.; Kasemo, B.; Nylander, T.; Fant, C.; Sott, K.; Elwing, H., *Analytical Chemistry* **2001**, *73* (24), 5796-5804.

## Chapter 5

### A SFG Study of Interfacial Amino Acids at the Hydrophilic SiO<sub>2</sub> and Hydrophobic Deuterated Polystyrene Surfaces

Sum frequency generation (SFG) vibrational spectroscopy was employed to characterize the interfacial structure of eight individual amino acids in aqueous solution at model hydrophilic and hydrophobic surfaces. Specifically, SFG vibrational spectra were obtained for L-phenylalanine, L-leucine, glycine, L-lysine, L-arginine, L-cysteine, L-alanine, and L-proline amino acids at the solid-liquid interface between both hydrophobic *d*<sub>8</sub>-polystyrene (*d*<sub>8</sub>-PS) and SiO<sub>2</sub> model surfaces and phosphate buffered saline (PBS) at pH 7.4. At the hydrophobic *d*<sub>8</sub>-PS surface, seven of the amino acids solutions investigated showed clear and identifiable C-H vibrational modes. In the SFG spectra obtained at the hydrophilic SiO<sub>2</sub> surface, no C-H vibrational modes were observed from any of the amino acids studied. Nonetheless, the amino acid solutions were found to have a detectable and widely varying influence on the magnitude of SFG signal from adsorbed water at the SiO<sub>2</sub>/PBS interface. This study provides the first known SFG spectra of several individual amino acids in aqueous solution at the solid-liquid interface and under physiological conditions.

#### 5.1. Introduction

Biological surface science and biomaterials is an active area of research in the academic, medical, and commercial communities because of the crucial role surfaces play in maintaining and improving our everyday quality of life.<sup>1, 2</sup> A biomaterial has been defined as “a nonviable material used in a medical device, intended to interact with biological systems.”<sup>3</sup> Several biomaterials have been developed over the past decades which are used to accomplish tasks as complex as keeping coronary arteries from collapsing or as simple as allowing an individual to trade in glasses for contact lenses. A common and fundamental approach to developing better biomaterials has been through the functionalizing of surfaces to exhibit specific properties which have been found to reduce or eliminate a host organism’s immune response and other complexities. However, this is a challenging problem due to vast array of molecules, proteins, and cells within an organism. Our approach to this problem was to start with small, model systems which are experimentally tractable and to move gradually toward systems with increasing complexity as we learned more about the fundamental parameters governing the interactions between a biomaterials and biomolecules. By studying amino acids at the liquid-solid interface we seek to understand the chemical and physical interactions of these molecules which are the fundamental building blocks of peptides and proteins. In the past, there were few experimental techniques available to surface scientists to quantitatively probe the chemistry and surface physics of biological interfaces under physiological conditions. However, several surface sensitive analysis techniques, particularly sum frequency generation vibrational spectroscopy (SFG), second harmonic generation spectroscopy (SHG), quartz crystal microbalance (QCM), and surface plasmon resonance (SPR) have proven invaluable to studying the interactions between surfaces and biomolecules in their native systems at ambient temperatures and pressures and free from contributions from a bulk or surrounding environment.

Recent advances in SFG techniques have enabled the detection of amino acids at the liquid-solid interface. In this study, we employ SFG vibrational spectroscopy to characterize the adsorption and interaction of eight amino acids with an aqueous solvent at the hydrophobic  $d_8$ -polystyrene ( $d_8$ -PS) and  $\text{SiO}_2$  model surfaces. This experimental investigation documents the first known evidence of SFG activity of several individual amino acids at the solid-liquid interface under physiological conditions.

## 5.2. Experimental

### 5.2.1. SFG Experimental Measurements

Sum Frequency Generation (SFG) experiments were conducted using a Continuum (Santa Clara, CA) Leopard D-20 Nd:YAG laser with a pulsed 1064 nm output at 20 Hz and with 22 picosecond pulse width. This pulsed, near-infrared output was then sent to a Laservision (Bellevue, WA) Optical Parametric Generator (OPG)/Optical Parametric Amplifier (OPA) optical system. The OPG/OPA system produced both a 532 nm visible beam,  $\omega_{\text{vis}}$ , as well as a tunable infrared beam,  $\omega_{\text{IR}}$ , with an output of 2800 - 3600  $\text{cm}^{-1}$ . Both of these beams were directly used in SFG measurements at pulse energies of  $\sim 200$   $\mu\text{J}$ . Equilateral prism sample substrates made of fused  $\text{SiO}_2$  were utilized with experimental beam orientations of  $65^\circ$  and  $42^\circ$  off surface normal for the incoming visible and infrared beams, respectively. These angles were specifically chosen to maximize the collection of SFG signal generated at the liquid-solid interface while minimizing wavelength dependent fluctuations of Fresnel coefficients due to the imaginary components of the index of refraction of water over infrared wavelengths.<sup>4</sup> The prism substrates were placed on top of a PBS/biomolecule solution filled Viton o-ring in a clean Petri dish to prevent solvent evaporation and contamination during measurement. SFG signal generated at the solution-prism interface was subsequently detected by a photomultiplier tube before being processed and recorded on a desktop computer. All SFG measurements were conducted in the  $S_{\text{SFG}}S_{\text{VIS}}P_{\text{IR}}$  polarization combination. A more detailed theoretical background of the SFG process is provided in Chapter 2,<sup>5</sup> and a complete description of the Laservision OPG/OPA system as well as the SFG sample substrate arrangement is provided in Chapter 3.

### 5.2.2. Chemicals

All experiments were conducted at pH 7.4 and solutions were made with phosphate buffered saline (PBS) (Sigma-Aldrich). All amino acids used were purchased directly from Sigma-Aldrich and were used as received. Biomolecule solutions of L-phenylalanine and L-leucine were both used at 5 mg/mL in PBS. Solutions of L-proline, L-lysine and L-arginine were all studied at 15 mg/mL in PBS. Finally, L-cysteine, L-alanine, and glycine were all investigated in PBS at final solution concentrations of 25 mg/mL, 40 mg/mL, and 100 mg/mL, respectively. The experimental amino acid concentrations used in this study were selected to maximize SFG signal while still maintaining solubility. All SFG measurements were carried out in pure PBS or amino acid/PBS solutions at pH 7.4 and maintained at 20  $^\circ\text{C}$ .

### 5.2.3. SFG Sample Preparation

SFG sample substrates were prepared from fused SiO<sub>2</sub> equilateral prisms which were cleaned by soaking for 12 hours in a solution of concentrated H<sub>2</sub>SO<sub>4</sub> (97%) (Sigma-Aldrich) and Nochromix (Godax). Subsequently, the SiO<sub>2</sub> prism substrates were washed with distilled, de-ionized water prior to being cleaned using a Herrick (Ithaca, NY) oxygen plasma cleaner for 60 s (18 W RF, 200 mtorr O<sub>2</sub>). The O<sub>2</sub> plasma treatment was employed to remove any residual organic surface contaminants and to maximize the extent of Si/SiO<sub>2</sub> prism surface oxidation. After plasma treatment the clean SiO<sub>2</sub> prisms were either used directly for SFG measurements of the SiO<sub>2</sub>-PBS interface or were prepared with deuterated polystyrene (*d*<sub>8</sub>-PS) thin films. The thin films were prepared on the SFG prism substrates by spin-coating 3 % weight solution of *d*<sub>8</sub>-PS (MW ≈ 300,000) (Polymer Source) dissolved in toluene (Sigma-Aldrich). The spin-coating was followed by annealing at 120 °C for 12 hours ensure surface flatness and to fully remove any residual toluene solvent from the spin coating solution. The thickness of the resulting *d*<sub>8</sub>-PS films were determined to be ~105 nm by ellipsometry and atomic force microscopy.

## 5.3. Results and Discussion

### 5.3.1. SFG of Phosphate Buffered Saline at the Hydrophobic Deuterated Polystyrene and the Hydrophilic SiO<sub>2</sub> Surfaces

*Phosphate Buffered Saline (PBS) at the Hydrophobic *d*<sub>8</sub>-PS Surface:* The SFG spectrum of pure pH 7.4 PBS at the hydrophilic-hydrophobic PBS/*d*<sub>8</sub>-PS liquid-solid interface is presented in Figure 5.1 and in the background spectra of Figures 5.3 - 5.10. In these SFG spectra the *d*<sub>8</sub>-PS/PBS interface shows a broad spectral feature centered at ~3100 cm<sup>-1</sup>. This broad peak is attributed to a continuum of O-H stretching vibrational modes of ordered interfacial water on a hydrophobic surface and is consistent with previous SFG studies of PBS solutions at the hydrophobic *d*<sub>8</sub>-PS surface under similar conditions.<sup>6-13</sup>

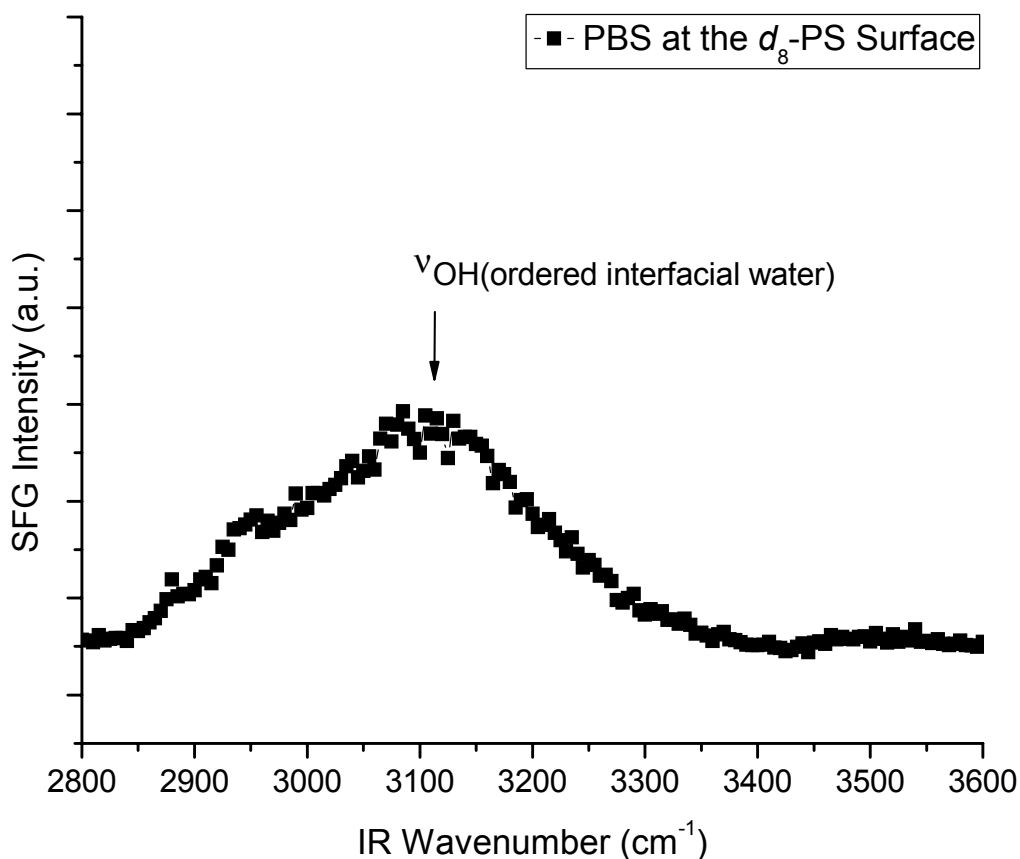


**Figure 5.1.** SFG spectrum of PBS at the hydrophobic  $d_8$ -PS surface. The broad spectral feature centered at  $\sim 3100\text{ cm}^{-1}$  is attributed to a continuum of O-H stretching modes from water at a hydrophobic surface.

*Phosphate Buffered Saline (PBS) at the Hydrophilic  $\text{SiO}_2$  Surface:* The SFG spectrum of pure pH 7.4 PBS at the hydrophilic  $\text{SiO}_2$ /PBS solid-liquid interface is presented in Figure 5.2 and in the background spectra of Figures 5.11 - 5.18. In these plots, the SFG spectra of PBS at the hydrophilic interface show two strong, broad spectral features centered at the  $\sim 3200\text{ cm}^{-1}$  and  $\sim 3400\text{ cm}^{-1}$  attributed to a continuum of O-H stretching modes of interfacial water. Both of these spectral features are consistent with previous SFG studies of PBS solutions at the hydrophilic  $\text{SiO}_2$  surface under similar conditions, and the peak at  $\sim 3200\text{ cm}^{-1}$  is identified as corresponding to “ice-like” tetrahedrally coordinated interfacial water, while the peak at  $\sim 3400\text{ cm}^{-1}$  is indicative of “water-like” less than tetrahedrally coordinated interfacial water.<sup>4, 6, 7, 9-12, 14</sup> None of amino acids investigated at the hydrophilic  $\text{SiO}_2$  surface were observed to have clear C-H vibrational modes at this interface. However, the addition of these biomolecules to the hydrophilic solid-PBS interface was found to have a varying and measurable range of influence on the SFG signal from interfacial water as a function of amino acid identity. The absence of observable C-H vibrational modes at the  $\text{SiO}_2$ /PBS interface for these species is attributed to the zwitterionic nature of amino acids in aqueous solution at pH 7.4. These amino acids have their amine portions protonated and their carboxylic acid portions deprotonated leaving charged NH-

$3^+$ -R and C-O $^-$  groups present at the two ends of each molecule, respectively.<sup>15</sup> Yeganeh *et al.* using SFG observed SiO $_2$  in an aqueous environment transitioning with decreasing pH from having a negative surface charge to becoming electrically neutral at its isoelectric point, pI  $\sim$ 2.<sup>16</sup> As a zwitterionic amino acid comes close to the negatively charged and hydrophilic SiO $_2$  surface, cumbic forces between the two are expected to drive adsorption via the charged ends of the amino acid instead of through the side chain as expected in the case with the hydrophobic  $d_8$ -PS surface. This phenomenon is highlighted in the case of solvated glycine at pH 7.4 where each molecule has a total of two charged moieties and only nine covalently bound atoms.

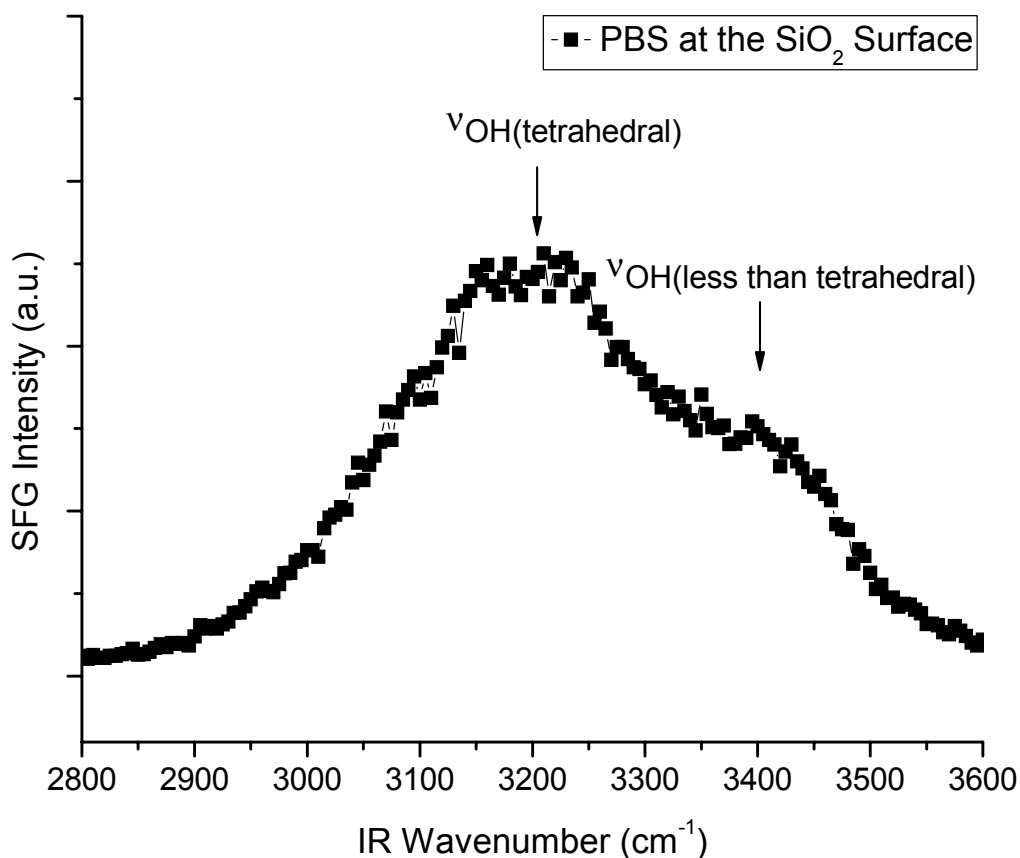


**Figure 5.2.** SFG spectrum of PBS at the hydrophilic SiO $_2$  surface. The broad spectral features centered at  $\sim$ 3200  $\text{cm}^{-1}$  and  $\sim$ 3400  $\text{cm}^{-1}$  are attributed to a continuum of O-H stretching modes from “ice-like” tetrahedrally coordinated and “liquid-like” less than tetrahedrally coordinated interfacial water at a hydrophobic surface, respectively.

### 5.3.2. SFG at the Hydrophobic Deuterated Polystyrene Surface

*L-Phenylalanine*: The SFG spectrum of L-phenylalanine (5 mg/mL) in PBS at the hydrophobic  $d_8$ -PS/PBS solid-liquid interface is shown in Figure 5.3. Each data point in this plot is the average of 500 laser shots. Upon the addition of L-phenylalanine, an enhancement in the SFG signal of ordered water is observed and attributed to the presence of solvated amino acid species at the hydrophobic interface. Additionally, three C-H vibrational peaks are present in this spectrum at infrared frequencies of  $2880\text{ cm}^{-1}$ ,  $2945\text{ cm}^{-1}$ , and  $3070\text{ cm}^{-1}$ . The first and second peaks at  $2880\text{ cm}^{-1}$  and  $2945\text{ cm}^{-1}$  are attributed to  $\text{CH}_2(\text{s})$  and  $\text{CH}_2(\text{as})$  stretching modes of the carbon atom connecting the phenyl group to the amino acid backbone, respectively. The stronger third peak at  $3070\text{ cm}^{-1}$  is attributed to an aromatic C-H  $\nu_2$  stretch from the phenyl group.<sup>17</sup> This aromatic SFG peak from phenylalanine was observed at  $3064\text{ cm}^{-1}$  at the hydrophilic-hydrophobic  $\text{CCl}_4/\text{D}_2\text{O}$  buffer liquid-liquid interface by Watry and Richmond,<sup>18</sup> but the  $\text{CH}_2(\text{s})$  vibrational mode at  $2880\text{ cm}^{-1}$  was not reported in that study. Phillips *et al.* also observed also observed an aromatic C-H stretch at  $3050\text{ cm}^{-1}$  attributed to phenylalanine in the

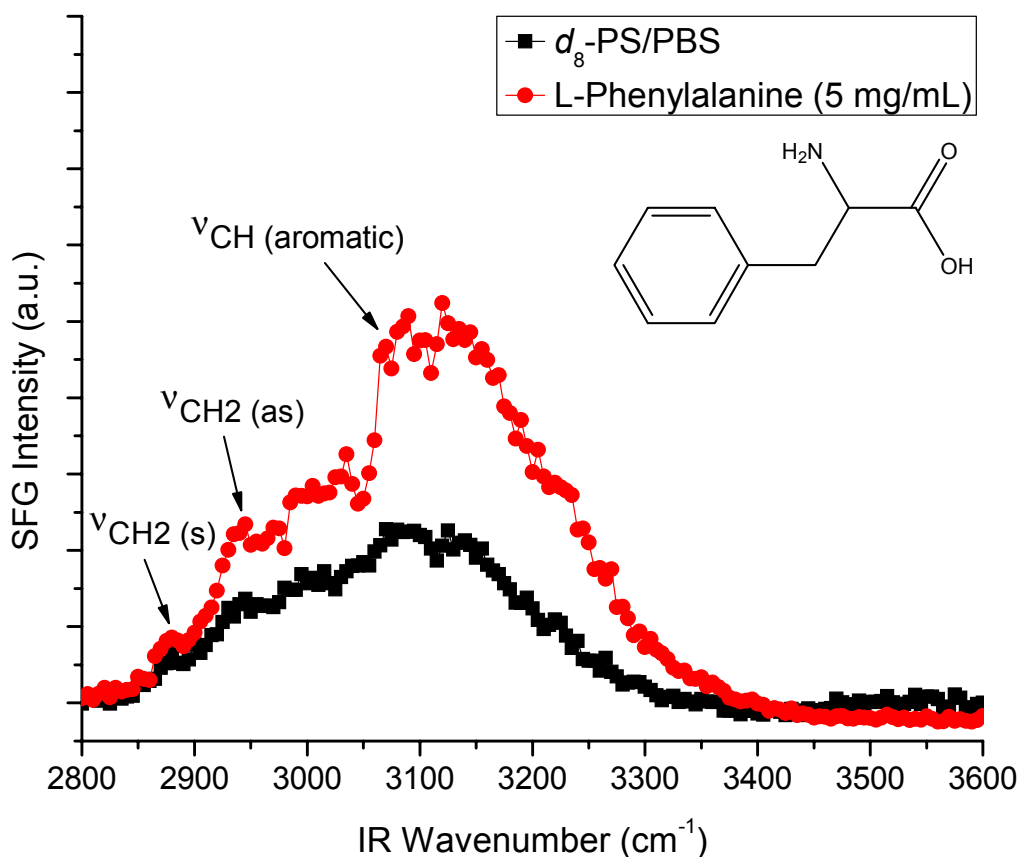


Figure 5.3. SFG spectrum of  $d_8$ -PS/PBS solid-liquid interface before (black squares) and after (red circles) addition of L-phenylalanine (5 mg/mL). The vibrational modes at  $2880\text{ cm}^{-1}$  and  $2945\text{ cm}^{-1}$  are attributed to  $\text{CH}_2$  symmetric and asymmetric stretches, respectively. The largest peak at  $3070\text{ cm}^{-1}$  indicative of the aromatic C-H  $\nu_2$  stretch of the amino acid phenyl side chain.

SFG spectrum of an amphiphilic peptide containing only phenylalanine and arginine residues.<sup>9</sup> The  $20\text{ cm}^{-1}$  peak shift of the aromatic C-H stretches of phenylalanine between these studies is attributed to the substantial structural differences between the individual amino acids and those bound together in a peptide which have geometric conformational restrictions, substantially less molecular charge per residue in solution at pH 7.4 and individual amino acids which are zwitterionic, and may form secondary structures as a result of intramolecular forces between adjacent residue side chains in the peptide. However, Phillips *et al.* did not observe the  $\text{CH}_2$  (s) modes at  $2880\text{ cm}^{-1}$  and  $2945\text{ cm}^{-1}$ , suggesting that the ability to resolve these peaks in this study but not in earlier studies may be due to the implementation of near-total internal reflection sample geometry herein.<sup>4</sup>

*L-Leucine*: The SFG spectrum of L-leucine (5 mg/mL) in PBS at the hydrophilic-hydrophobic PBS/ $d_8$ -PS liquid-solid interface is shown in Figure 5.4. In this figure, every data point is the average of 500 experimental measurements. Two prominent C-H stretching vibrational modes appear in this spectrum, but the identification of these is somewhat ambiguous

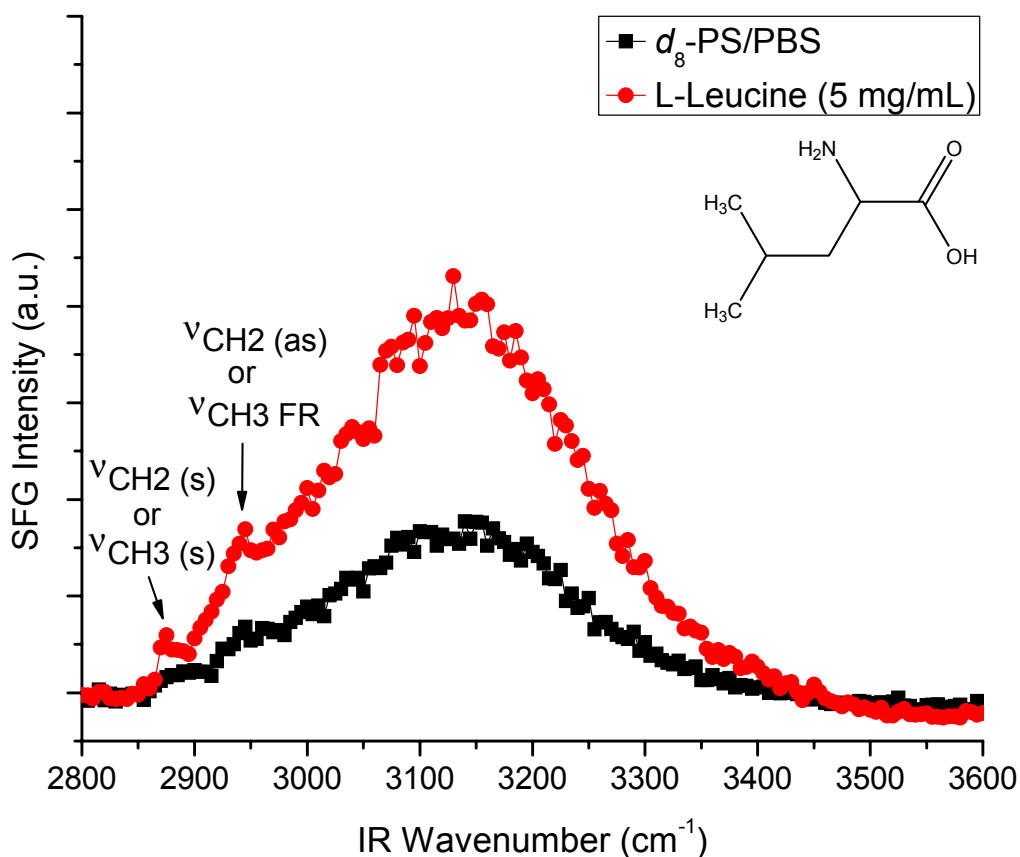
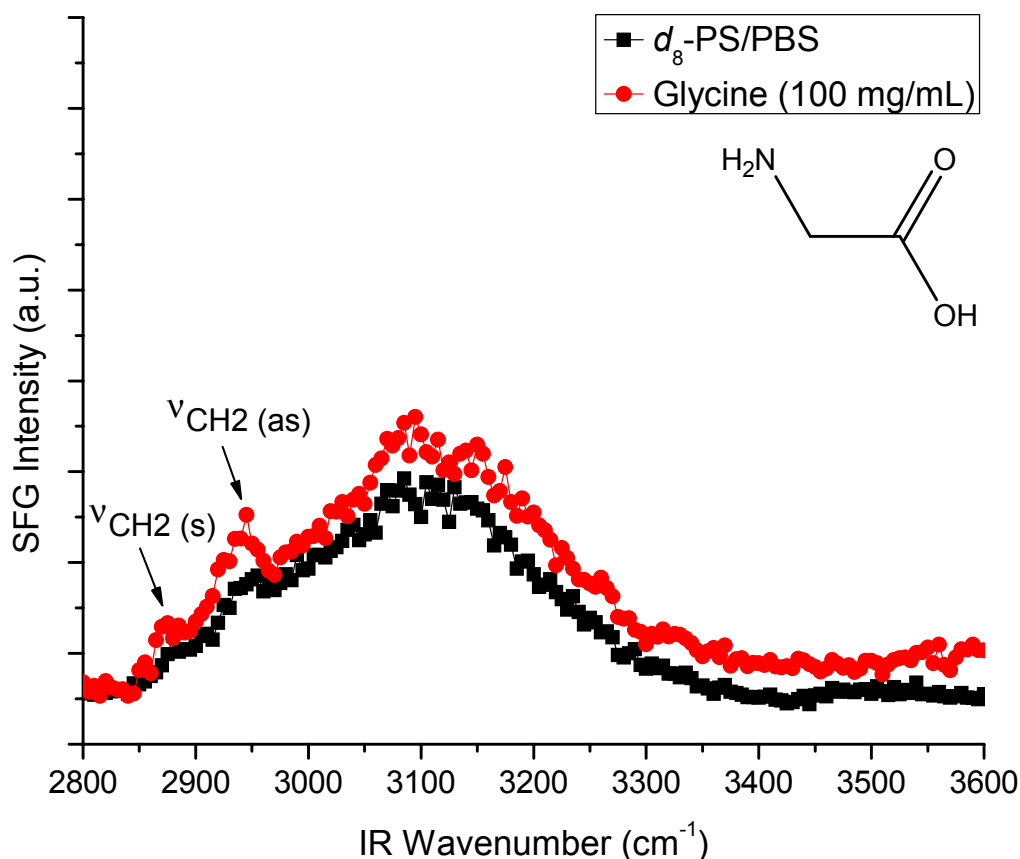


Figure 5.4. SFG spectrum of the  $d_8$ -PS/PBS solid-liquid interface before (black squares) and after (red circles) the addition of L-leucine (5 mg/mL). The vibrational mode at  $2875\text{ cm}^{-1}$  is attributed to either a  $\text{CH}_3$  symmetric stretch from the terminal methyl groups or a  $\text{CH}_2$  symmetric stretching mode. The larger peak at  $2945\text{ cm}^{-1}$  is indicative of a  $\text{CH}_3$  Fermi resonance or a  $\text{CH}_2$  asymmetric stretch.

as both could be reasonably be attributed to either CH<sub>2</sub> or CH<sub>3</sub> SFG active vibrational modes. While previous studies have assigned the peak centered at 2875 cm<sup>-1</sup> for L-leucine as a CH<sub>3</sub>(s) mode,<sup>7-9, 12, 18, 19</sup> the findings of this study indicate that it may also originate from a CH<sub>2</sub>(s) mode, or a combination of both CH<sub>2</sub>(s) and CH<sub>3</sub>(s) vibrations. Similarly, the vibrational mode observed at 2945 cm<sup>-1</sup> has been identified as a CH<sub>3</sub> Fermi resonance in those other studies. However, the spectrum of L-phenylalanine (which has no CH<sub>3</sub> groups) shown in Figure 5.3 also has a peak at 2945 cm<sup>-1</sup> which leaves open the possibility of this being a CH<sub>2</sub>(as) mode of L-leucine. Interestingly, several additional peaks previously observed in SFG studies of L-leucine amino acid and peptides with L-leucine residues at 2847 cm<sup>-1</sup>, 2895 cm<sup>-1</sup>, 2910 cm<sup>-1</sup>, and 2960 cm<sup>-1</sup> were not observed.<sup>7-9, 12, 18, 19</sup> The absence of these peaks may be due to a reduced amino acid concentration at the interface leading to signal being generated by a more uniformly distributed population at the interface where multilayer formation or secondary structures present surface molecular conformations where atypical adsorbate geometries may manifest themselves. Similar to the spectrum of phenylalanine, the SFG spectrum of the *d*<sub>8</sub>-PS/PBS interface shows a substantial increase in SFG signal from ordered interfacial water with the presence of L-leucine. This phenomenon is also attributed to an increase in the concentration of ordered interfacial water due to the presence of the solvated amino acid at the hydrophobic solid-liquid interface.

*Glycine:* The SFG spectrum of a solution of the simplest amino acid, glycine (100 mg/mL in PBS), at the hydrophobic *d*<sub>8</sub>-PS surface is presented in Figure 5.5. Each data point in this plot is the average of 500 laser shots. This SFG spectrum shows two C-H vibrational modes at 2875 cm<sup>-1</sup> and 2945 cm<sup>-1</sup> which are readily identified as a CH<sub>2</sub>(s) and a CH<sub>2</sub>(as) vibrations, respectively, due to the molecular simplicity of glycine. These peak assignments coupled with the only carbon atom of the molecule directly bonded to hydrogen atoms being a CH<sub>2</sub> group supports the attribution of the 2945 cm<sup>-1</sup> stretch of L-leucine in this study to a CH<sub>2</sub>(as) mode. However, the high amino acid concentration necessary to observe SFG activity of glycine amino acid may have influenced the frequency of this CH<sub>2</sub>(as) mode and still leaves open the possibility of the Fermi resonance peak assignment of leucine in other studies to stand as reasonable.<sup>7-9, 12, 18, 19</sup> The SFG signal from the O-H stretches of ordered interfacial water is largely unchanged in Figure 5.3 upon the introduction of the amino acid which is remarkably different than in the case of L-phenylalanine and L-leucine. While the reason for this is unclear, it may be due to the high concentration of glycine used as a similar phenomena was previously observed in SFG spectrum of concentrated L-proline (500 mg/mL in PBS) at the same *d*<sub>8</sub>-PS interface.<sup>11</sup> Alternatively, the relatively minor change in water signal may be explained as a minimal disruption of the solid-liquid interface after addition of the amino acid. However, this case is unlikely due to the presence of C-H vibrational modes in this spectrum.



**Figure 5.5.** SFG spectrum of the  $d_8$ -PS/PBS solid-liquid interface before (black squares) and after (red circles) the addition of glycine (100 mg/mL). The vibrational mode at  $2875\text{ cm}^{-1}$  is attributed to a  $\text{CH}_2$  symmetric stretching mode, and the larger peak at  $2945\text{ cm}^{-1}$  is identified as originating from a  $\text{CH}_2$  asymmetric stretch.

*L-Lysine:* The SFG spectrum of L-lysine (15 mg/mL) in PBS at the  $d_8$ -PS/PBS solid-liquid interface is shown in Figure 5.6. In these spectra, every data point is the average of 600 measurements. Upon introduction of L-lysine, the SFG spectrum shows peaks at  $2875\text{ cm}^{-1}$  and  $2940\text{ cm}^{-1}$  which have been previously reported by our group as corresponding to a  $\text{CH}_2(\text{s})$  and  $\text{CH}_2(\text{as})$  vibrational modes, respectively.<sup>11</sup> Additionally, the amino acid spectrum shows a substantial SFG signal increase in the water region between  $3100 - 3300\text{ cm}^{-1}$  when compared to the SFG spectrum of the pure PBS/ $d_8$ -PS hydrophobic interface.<sup>6</sup> Interestingly, the broadened and enhanced O-H peak is indicative of an increase in the concentration of ordered interfacial water. This is explained by the terminal amine group on the lysine side chain which is protonated under these experimental conditions and in turn will be well solvated due to both N-H hydrogen bonding and coulombic forces between the aqueous solvent and the protonated amine.<sup>15</sup> This hypothesis is further supported by the apparent blue-shift of the ordered water peak and which is consistent with the presence of an N-H Amide B stretch hidden in the shoulder of the O-

H peak and located at  $\sim 3100\text{ cm}^{-1}$ .<sup>20, 21</sup> Thus the dramatic signal increase in the water region is most likely due to the presence of interfacial amine groups. This large enhancement was not detected in previous studies by our group, but the new resolution is attributed to the recent rebuilding of the experimental setup and an upgrade of the collection optics which has resulted in improved signal-to-noise for experimental SFG measurements.

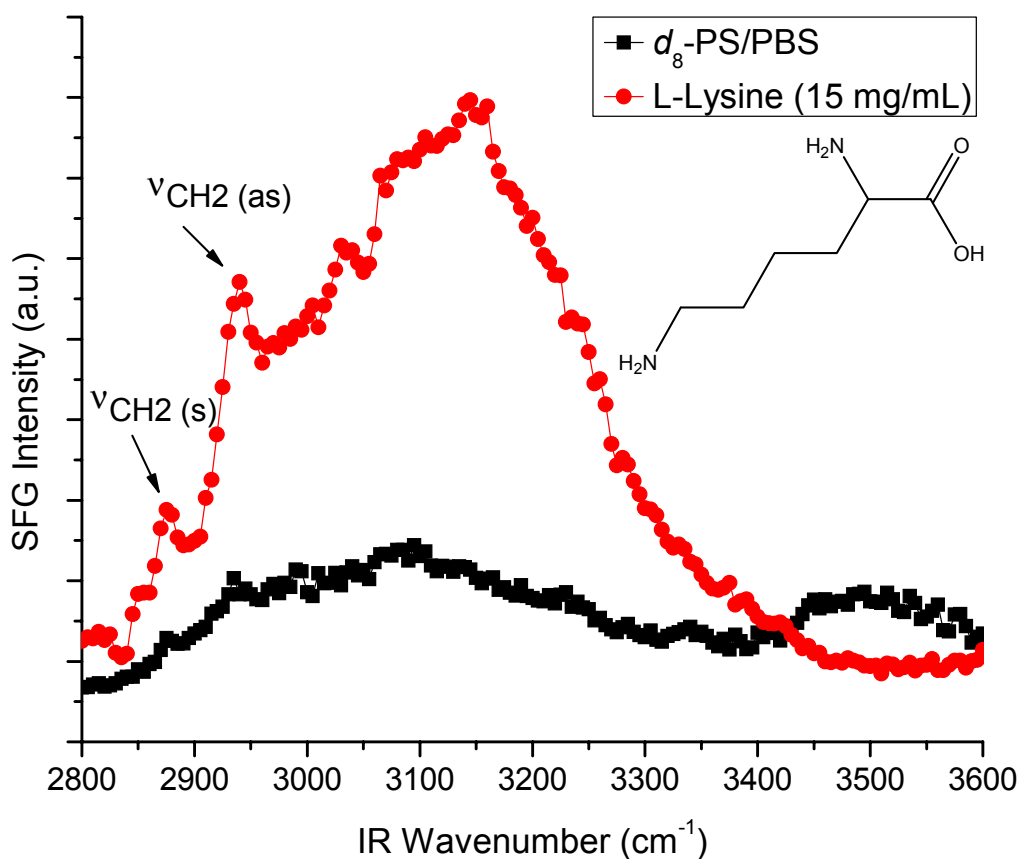


**Figure 5.6.** SFG spectrum of the  $d_8$ -PS/PBS solid-liquid interface before (black squares) and after (red circles) the addition of L-lysine (15 mg/mL). The vibrational mode at  $2875\text{ cm}^{-1}$  is attributed to a  $\text{CH}_2$  symmetric stretch and a larger peak at  $2940\text{ cm}^{-1}$  indicative of a  $\text{CH}_2$  asymmetric stretch from the lysine side chain. The dramatic increase in signal in the range  $3100 - 3300\text{ cm}^{-1}$  upon the addition of L-lysine is attributed to an increase in the concentration of ordered interfacial water as well as an N-H Amide B stretch of the acid's terminal amine group.

*L-Arginine:* The SFG spectrum of L-arginine (15 mg/mL) in PBS at the hydrophilic-hydrophobic PBS/ $d_8$ -PS liquid-solid interface is shown in Figure 5.7. Individual data points in these spectra are the average of 300 SFG experimental measurements. The amino acid spectrum shows two  $\text{CH}_2$  vibrational modes centered at  $2875\text{ cm}^{-1}$  and  $2935\text{ cm}^{-1}$  which are attributed to symmetric and asymmetric stretches of the L-arginine side chain, respectively. The spectrum also shows a substantial increase in signal at  $\sim 3070\text{ cm}^{-1}$  attributed to an increase in the

concentration of organized interfacial water and dominated by the N-H Amide B stretch of the charged terminal guanidino group. This explanation is supported by the spectrum of L-lysine (Figure 5.6) which shares both vibrational modes and structural features (terminal amine groups) with L-arginine.

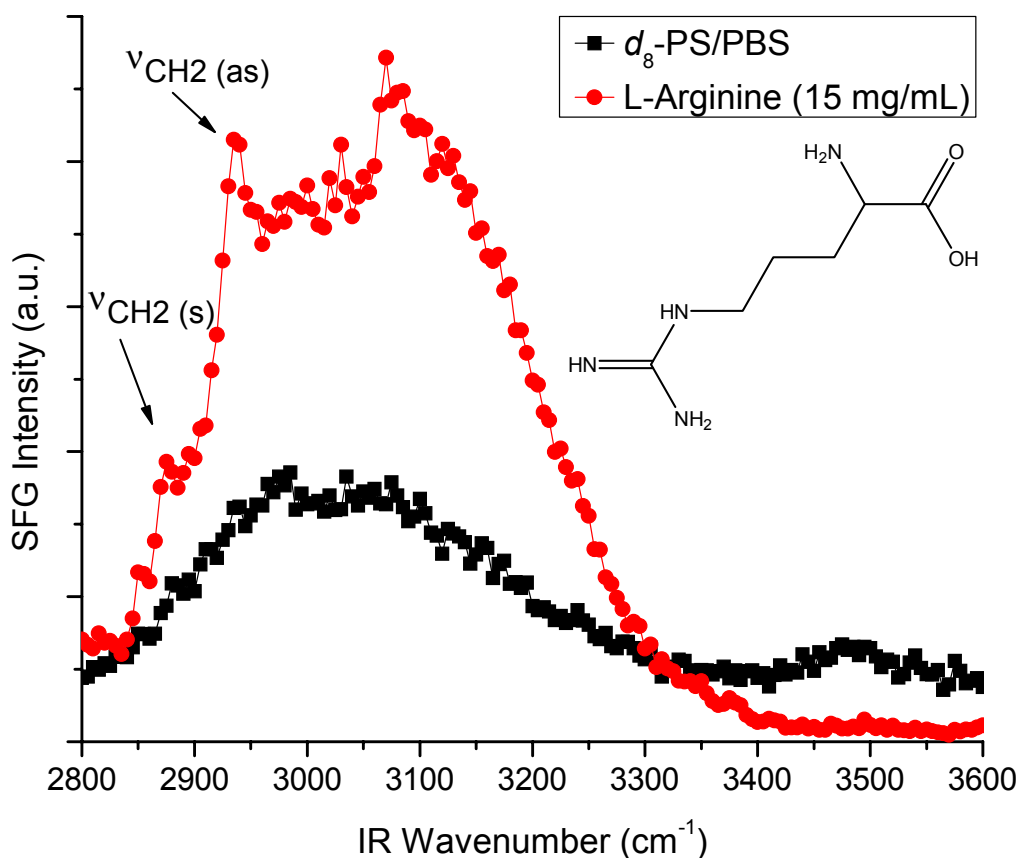


Figure 5.7. SFG spectrum of the  $d_8$ -PS/PBS solid-liquid interface before (black squares) and after (red circles) the addition of L-arginine (15 mg/mL). The vibrational mode at  $2875\text{ cm}^{-1}$  is attributed to a  $\text{CH}_2$  symmetric stretch and a larger peak at  $2935\text{ cm}^{-1}$  indicative of a  $\text{CH}_2$  asymmetric stretch. The dramatic increase in signal at approximately  $3070\text{ cm}^{-1}$  upon the addition of L-arginine is attributed to an increase in the concentration of ordered interfacial water as well as an N-H Amide B stretch of the amino acid's terminal guanidino group.

*L-Cysteine:* The SFG spectrum of L-cysteine (25 mg/mL) in PBS at the hydrophilic-hydrophobic PBS/ $d_8$ -PS liquid-solid interface is shown in Figure 5.8. Each data point in this figure is the average of 300 laser shots. The L-cysteine amino acid shows  $\text{CH}_2$  symmetric and asymmetric stretches at  $2870\text{ cm}^{-1}$  and  $2935\text{ cm}^{-1}$ , respectively. Interestingly, the SFG spectrum of L-cysteine also shows a C-H peak at  $2990\text{ cm}^{-1}$  for which the peak assignment is non-trivial. However, recent theoretical studies have predicted a vibrational modes of L-cysteine at this approximate infrared frequency originating from a perturbed  $\text{CH}_2$  (as) vibrational mode,<sup>22</sup> or from a combination of the  $\text{CH}_2$ (s) mode and the CH mode from the carbon atom connecting the

thiol group to the amino acid backbone.<sup>22, 23</sup> Similar to glycine, the SFG spectrum of L-cysteine shows only a minimal change in the O-H signal from ordered interfacial water at the hydrophobic  $d_8$ -PS surface.

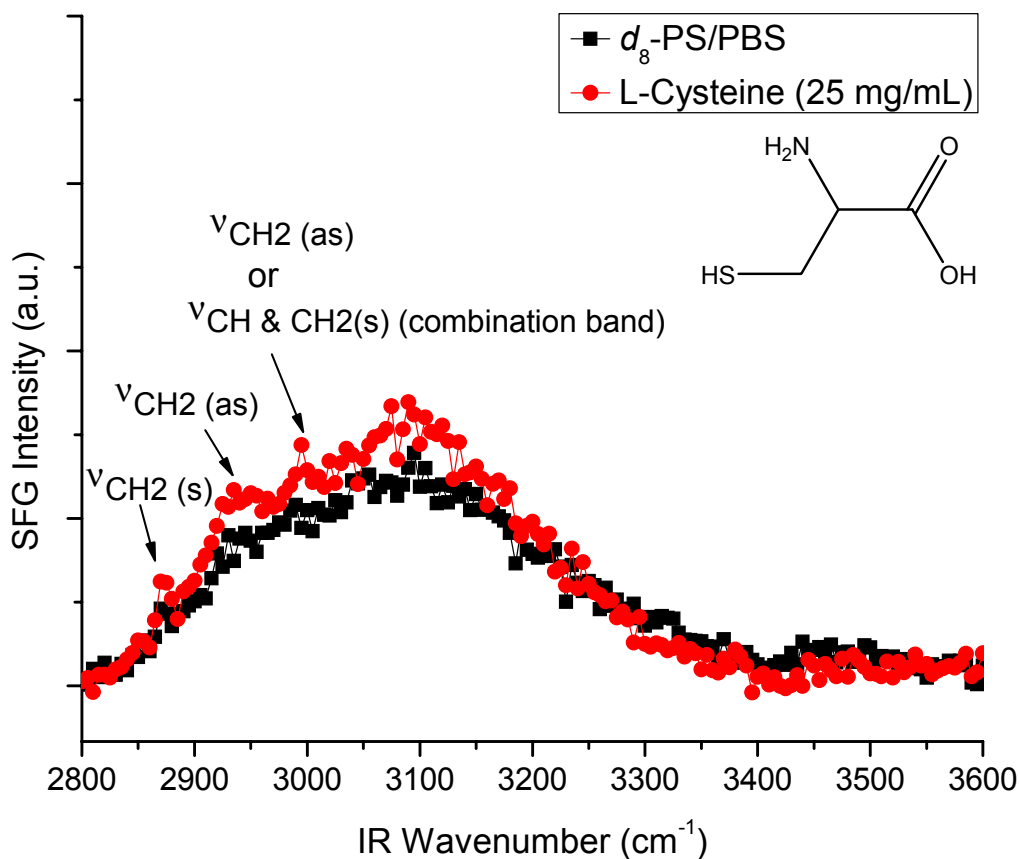


Figure 5.8. SFG spectrum of the  $d_8$ -PS/PBS solid-liquid interface before (black squares) and after (red circles) the addition of L-cysteine (25 mg/mL). The vibrational mode at  $2870\text{ cm}^{-1}$  is attributed to a  $\text{CH}_2$  symmetric stretching mode, and the peak at  $2935\text{ cm}^{-1}$  is identified as originating from a  $\text{CH}_2$  asymmetric stretch. A third C-H vibrational mode is observed at  $2990\text{ cm}^{-1}$  and is assigned as either a perturbed  $\text{CH}_2$ (as) mode, or a combination band of the  $\text{CH}_2$ (s) and CH stretches of solvated L-cysteine molecules.

*L-Alanine*: The SFG spectrum of a solution of L-alanine (40 mg/mL) in PBS at the hydrophobic  $d_8$ -PS liquid-solid interface is presented in Figure 5.9. Each data point in these spectra is the average of 600 laser shots. Interestingly, the spectrum of L-alanine does not show any SFG active modes at this hydrophobic. Furthermore, the background and amino acid spectra are indistinguishable as both show a broad continuum of SFG signal centered around  $3100\text{ cm}^{-1}$  is attributed to O-H stretching vibrational modes of ordered interfacial water at the hydrophobic solid-liquid interface. The similarity between the pure PBS and the L-alanine spectra suggest that any attractive forces between this molecule and the hydrophobic surface are not sufficiently strong to overcome the energy required to displace interfacial water. Using arguments based purely on the hydrophobic nature expected to be exhibited by an amino acid with a methyl side

chain, one might expect this small molecular species to readily adsorb to the deuterated polystyrene surface. Therefore, the absence of SFG active C-H modes in this spectrum is likely due to a lack of interfacial L-alanine ordering and not an all together absence of interfacial amino acid species.

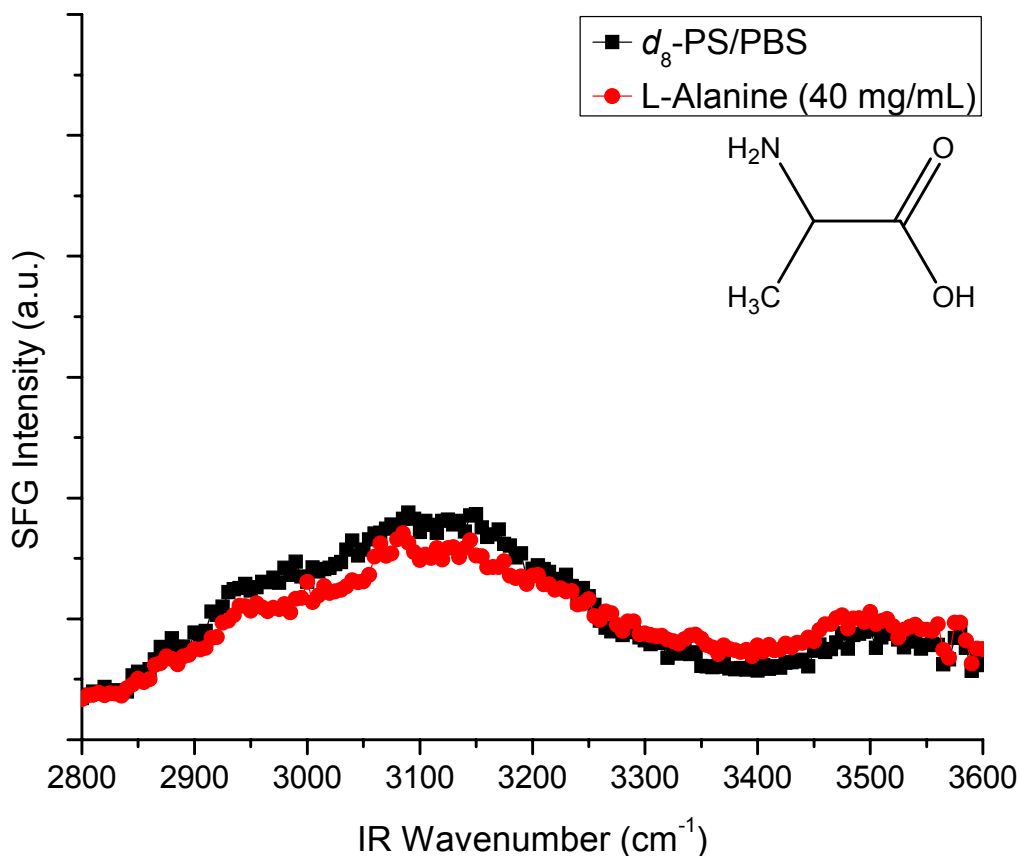


Figure 5.9. SFG spectrum of the  $d_8$ -PS/PBS solid-liquid interface before (black squares) and after (red circles) the addition of L-alanine (40 mg/mL), and no C-H vibrational modes are observed.

*L-Proline*: The SFG spectrum of L-proline (15mg/mL) is presented in Figure 5.10 where each data point in is the average of 600 measurements. This spectrum shows C-H vibrational modes at the  $d_8$ -PS hydrophobic interface at  $2880\text{ cm}^{-1}$  indicative of a combination of  $C_\beta\text{H}_2$  (s),  $C_\gamma\text{H}_2$  (s), and  $C_\delta\text{H}_2$  (s) modes,  $2935\text{ cm}^{-1}$  also indicative of a combination mode from  $C_\beta\text{H}_2$  (s) and  $C_\gamma\text{H}_2$  (s) vibrations, and finally a mode at  $2995\text{ cm}^{-1}$  from a combination of  $C_\beta\text{H}_2$  (as) and  $C_\gamma\text{H}_2$  (as) modes.<sup>11, 24</sup> The asymmetric  $\text{CH}_2$  modes are observed at a higher frequency than for all other amino acids in this study due to the strained nature of the five-member proline ring from which they originate. Additionally, the spectrum shows a dramatic increase in the region  $\sim 3000 - 3400\text{ cm}^{-1}$ . The origin of this signal enhancement is attributed to one vibrational mode from ordered interfacial water O-H ( $\sim 3100\text{ cm}^{-1}$ ), and two N-H stretches identified as the Amide B ( $\sim 3050 - 3100\text{ cm}^{-1}$ ) and the Amide A ( $\sim 3300\text{ cm}^{-1}$ ) modes from L-proline.<sup>20, 21, 25</sup> While these are

identified as individual modes responsible for the increase in SFG signal, these modes are not distinctive in the broad peak because both the N-H group from L-proline and O-H from the aqueous solvent (carboxylic acid portion of the amino acid is deprotonated at pH 7.4)<sup>15</sup> readily participate in hydrogen bonding which leads to line broadening for each of the three modes to the extent that they are substantially overlapping.

In a previous SFG study of similar L-proline solutions at the hydrophilic  $d_8$ -PS interface we only observed a small peak in this region around 3100  $\text{cm}^{-1}$  attributed to “ordered OH” groups which was only about half of the intensity of the 2995  $\text{cm}^{-1}$  mode.<sup>11</sup> This discrepancy between the L-proline spectra is partially attributed to differences in the solution concentrations used in these studies. Previously, it was previously necessary for us to perform our SFG experiments on L-proline at 500 mg/mL concentrations to resolve any spectral features in the 2800 - 3600  $\text{cm}^{-1}$  region, but subsequent beam realignments and the replacement of several signal collection optics allowed the amino acid to be easily resolved in this study at 15 mg/mL

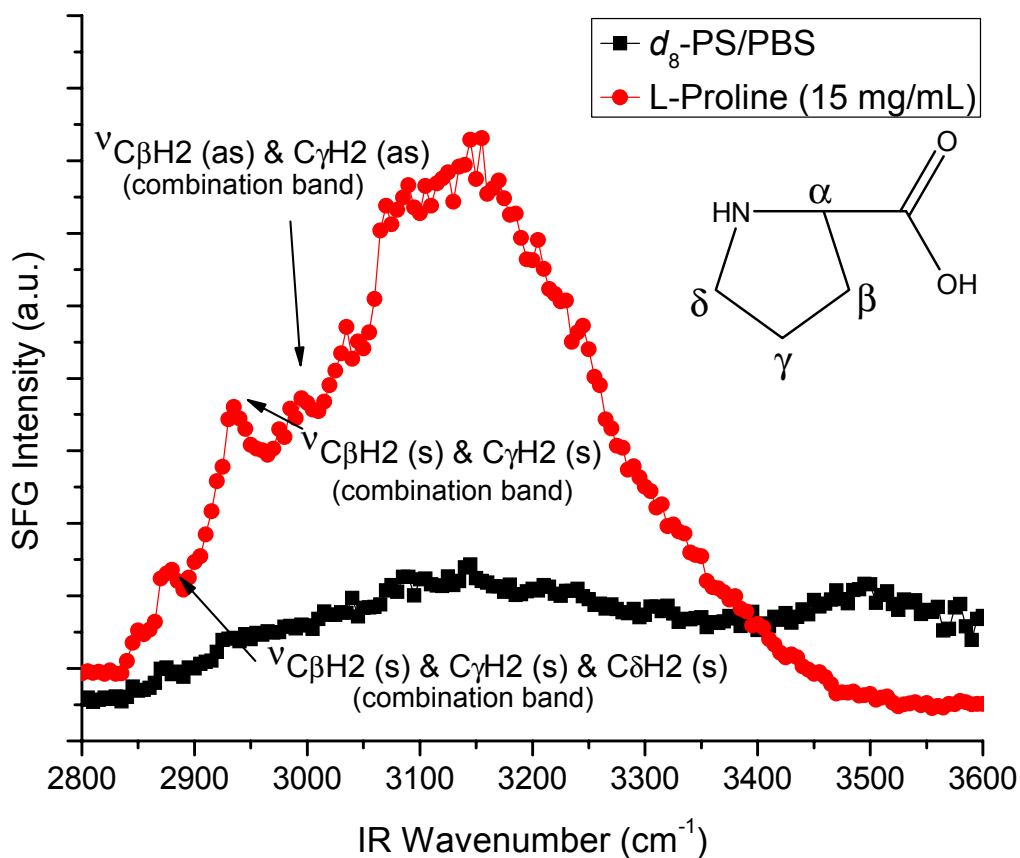


Figure 5.10. SFG spectrum of the  $d_8$ -PS/PBS solid-liquid interface before (black squares) and after (red circles) the addition of L-proline (15 mg/mL). The vibrational mode at 2880  $\text{cm}^{-1}$  is attributed to a combination of  $C_\beta\text{H}_2$  (s),  $C_\gamma\text{H}_2$  (s), and  $C_\delta\text{H}_2$  (s) modes. The peak at 2935  $\text{cm}^{-1}$  identified as combination mode from  $C_\beta\text{H}_2$  (s) and  $C_\gamma\text{H}_2$  (s) vibrations. Finally, the combination mode at 2995  $\text{cm}^{-1}$  originates from  $C_\beta\text{H}_2$  (as) and  $C_\gamma\text{H}_2$  (as) vibrations. The broad increase of SFG signal in the region 3000 - 3400  $\text{cm}^{-1}$  upon the addition of L-proline is attributed to an increase in the concentration of ordered interfacial water as well as N-H Amide A and Amide B stretches of the heterocyclic amino acid.

concentration. The substantial reduction of solution concentration used may have reduced the incidence of adsorbate accumulation on the substrate surface thus providing a more appropriate liquid-solid interface to probe with SFG by minimizing the probability of signal contributions from a potential multilayer build-up of amino acid molecules.

### 5.3.3. SFG Data at the Hydrophilic SiO<sub>2</sub> Surface

*L-Phenylalanine, L-Leucine, L-Arginine, L-Lysine:* At the hydrophilic SiO<sub>2</sub>/PBS solid-liquid interface Figures 5.11 - 5.14 show the SFG spectra of solutions of L-phenylalanine (5 mg/mL), L-leucine (5 mg/mL), L-arginine (15 mg/mL), and L-lysine (15 mg/mL) in PBS, respectively. Upon the addition of amino acid solutions, each of these spectra show an enhancement in the SFG signal from ordered “ice-like” tetrahedrally coordinated and “liquid-like” less than tetrahedrally coordinated interfacial water at  $\sim 3200\text{ cm}^{-1}$  and  $\sim 3400\text{ cm}^{-1}$  relative to the spectrum of pure PBS at the SiO<sub>2</sub> surface. These four amino acids have side chains of substantially differing chemical structure and character making this finding unanticipated. The origin of the water signal enhancement is indicative of an increase in either the concentration or ordering of interfacial water, or both. However, due to the aforementioned negative surface charge exhibited by SiO<sub>2</sub> in contact with aqueous solutions at pH 7.4 it is unexpected that the addition of an amino acid would drive more water to the polar and hydrophilic surface than in the case of pure PBS. Instead, it appears more probable that the increase in SFG signal from interfacial water observed here is due to adsorbed of the amino acid species seeding the reorganization of water into a more structured population at the SiO<sub>2</sub> surface. Each data point in the spectra of L-phenylalanine, L-leucine, and L-arginine are the average of 500 laser shots, while the spectrum of L-lysine is the average of 600 measurements.

Interestingly, in a previous SFG study of phenylalanine at the glassy carbon electrode/D<sub>2</sub>O liquid-solid interface the observation of an aromatic C-H stretch was expected but not observed. The absence of this spectral feature was hypothesized to be due to an insufficiently strong dipole of this vibrational mode.<sup>26</sup> However, the presence of the  $3070\text{ cm}^{-1}$  peak at the *d*<sub>8</sub>-PS/PBS interface in Figure 5.3 demonstrates the dipole of the aromatic C-H bonds in L-phenylalanine is of sufficient strength to be SFG active. This indicates that the inability to resolve this aromatic C-H vibrational mode in previous studies was likely due to insufficient ordering of the interfacial species or a low surface concentration. Further supporting this hypothesis is the observation of the aromatic C-H  $\nu_2$  stretching mode of L-phenylalanine in systems where attractive intermolecular forces between the aromatic ring and hydrophobic interfacial surface species (i.e. *d*<sub>8</sub>-polystyrene or CCl<sub>4</sub>) would be expected to be thermodynamically favorable,<sup>9, 18</sup> but only minimal or a complete lack of signal at hydrophilic-hydrophilic interfacial environments (i.e. SiO<sub>2</sub>/PBS or TiO<sub>2</sub>/D<sub>2</sub>O) where these forces would be substantially smaller.<sup>27, 28</sup> This finding underscores the sensitivity of SFG vibrational spectroscopy to a species' interfacial orientation and the intermolecular forces that can affect it.

The SFG data of L-arginine (Figure 5.13) and L-lysine (Figure 5.14) additionally shows a minor spectral shift from having two broad but defined peaks at  $3200\text{ cm}^{-1}$  and  $3400\text{ cm}^{-1}$  in the case of pure PBS to having larger and much broader peaks. This spectral change may be indicative of a weak N-H vibrational mode from these amino acids which is distinctive and shared characteristic of having amine terminated side chains overlapping with the existing O-H modes. The amino terminated chain of L-lysine and the guanidino terminated side chain of L-

arginine are both capable of directly participating in hydrogen bonding in aqueous solution and both are expected to be protonated in a solution of PBS at pH 7.4.<sup>15</sup> The presence of these additional charged groups on the amino acids may also lead to an enhancement in the frequency and strength of attractive interactions with the hydrophilic and charged SiO<sub>2</sub> substrate in addition to coordinating and organizing the water molecules solvating them as they approach the substrate in an adsorption event.

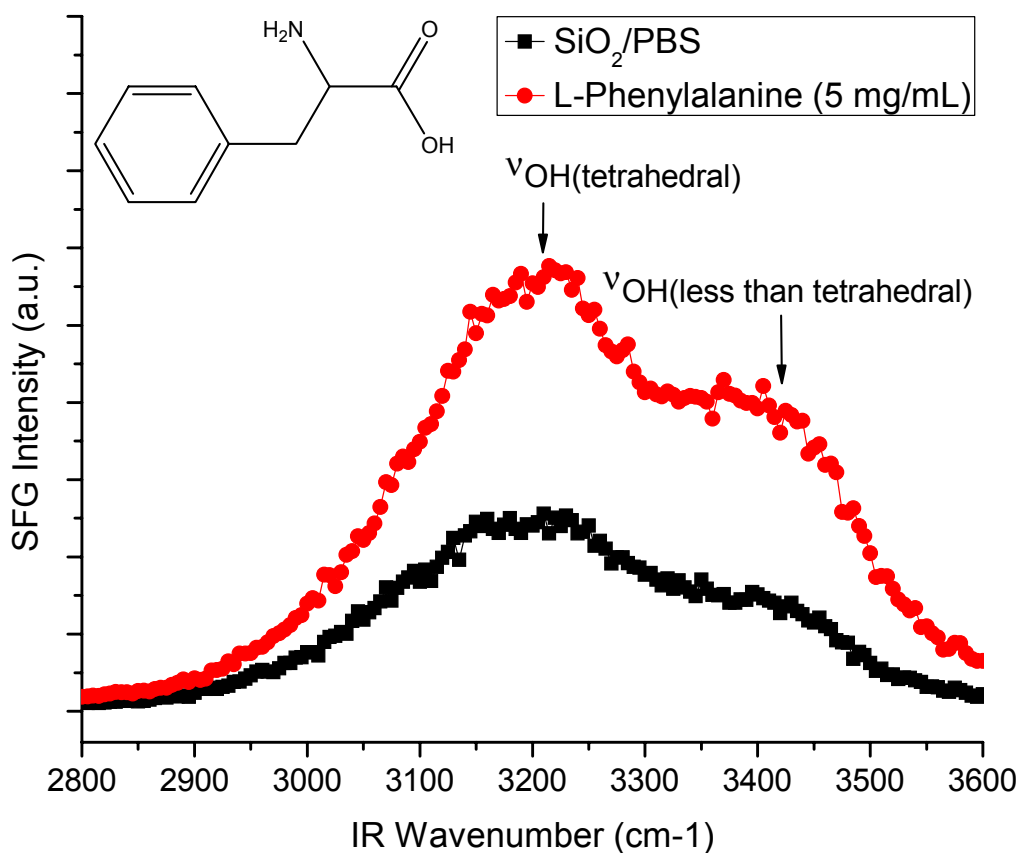


**Figure 5.11.** SFG spectrum of PBS/SiO<sub>2</sub> liquid-solid interface before (black squares) and after (red circles) addition of L-phenylalanine (5mg/mL). No hydrocarbon vibrational modes are observed, but an enhancement in the broad spectral features at ~3200 cm<sup>-1</sup> and ~3400 cm<sup>-1</sup> indicative of O-H stretching modes of “ice-like” tetrahedrally coordinated water and “liquid-like” less than tetrahedrally coordinated water, respectively, occurs upon the addition of amino acid. This finding suggests that the presence of L-phenylalanine can induce an increase in the extent of water ordering at the SiO<sub>2</sub>/PBS interface.

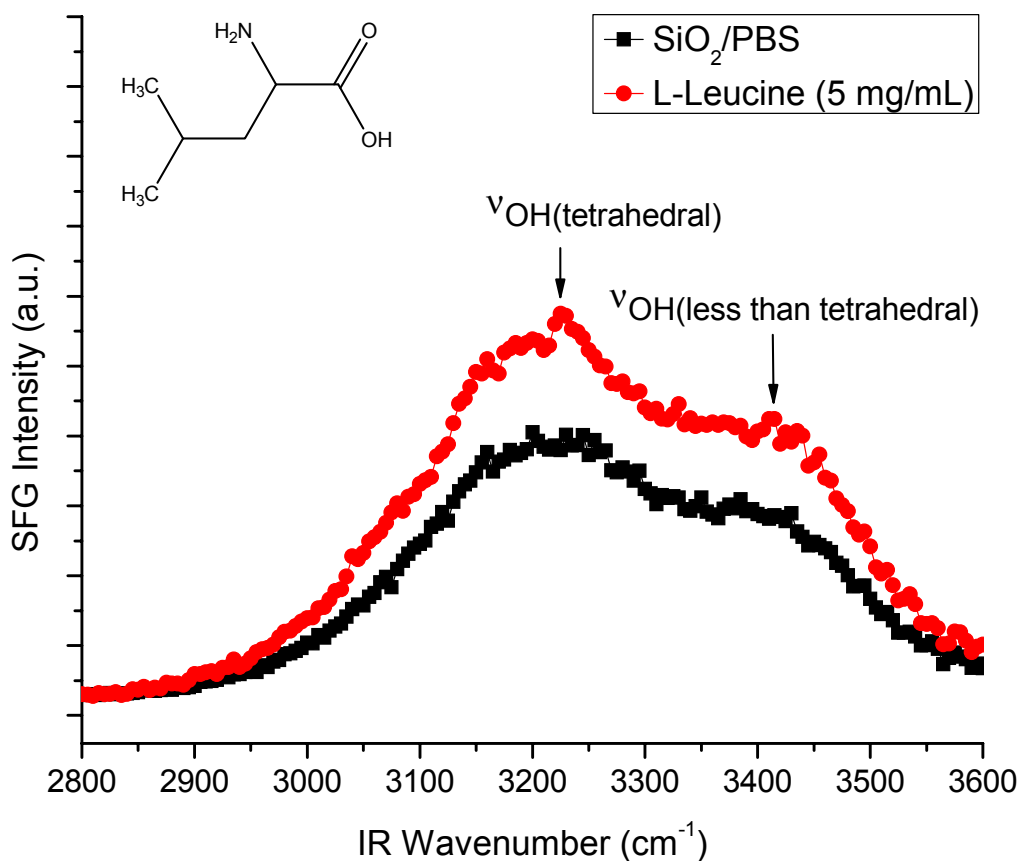
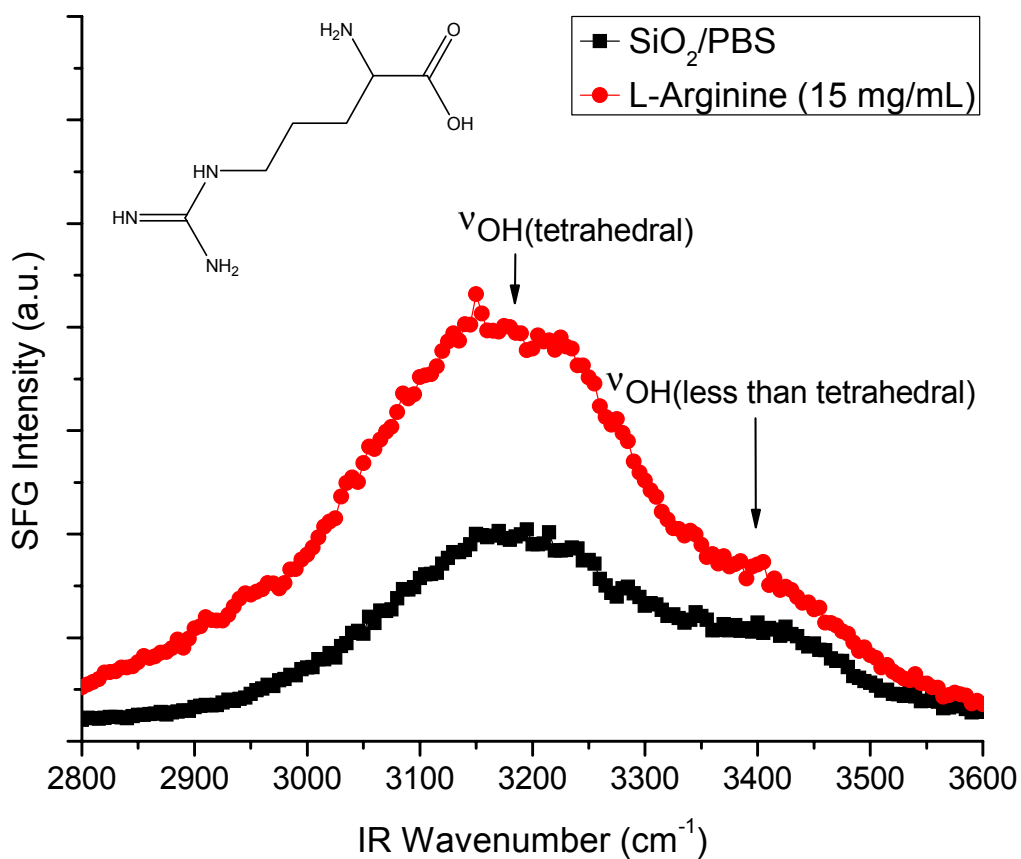


Figure 5.12. SFG spectrum of  $\text{PBS}/\text{SiO}_2$  liquid-solid interface before (black squares) and after (red circles) addition of L-leucine (5mg/mL). No hydrocarbon vibrational modes are observed, but an enhancement in the broad spectral features at  $\sim 3200 \text{ cm}^{-1}$  and  $\sim 3400 \text{ cm}^{-1}$  indicative of O-H stretching modes of “ice-like” tetrahedrally coordinated water and “liquid-like” less than tetrahedrally coordinated water, respectively, occurs upon the addition of leucine. This result suggests that the presence of the hydrophobic amino acid can cause an increase in the extent of water ordering at the  $\text{SiO}_2/\text{PBS}$  interface.



**Figure 5.13.** SFG spectrum of  $\text{PBS}/\text{SiO}_2$  liquid-solid interface before (black squares) and after (red circles) addition of L-arginine (15mg/mL). No hydrocarbon vibrational modes are observed upon the addition of arginine, but an enhancement and substantial peak broadening occurs in the spectral features at  $\sim 3200 \text{ cm}^{-1}$  and  $\sim 3400 \text{ cm}^{-1}$  originating from O-H stretching modes of “ice-like” tetrahedrally coordinated water and “liquid-like” less than tetrahedrally coordinated water, respectively. This result suggests that the presence of the L-arginine can cause an increase in the extent of water ordering at the  $\text{SiO}_2/\text{PBS}$  interface.

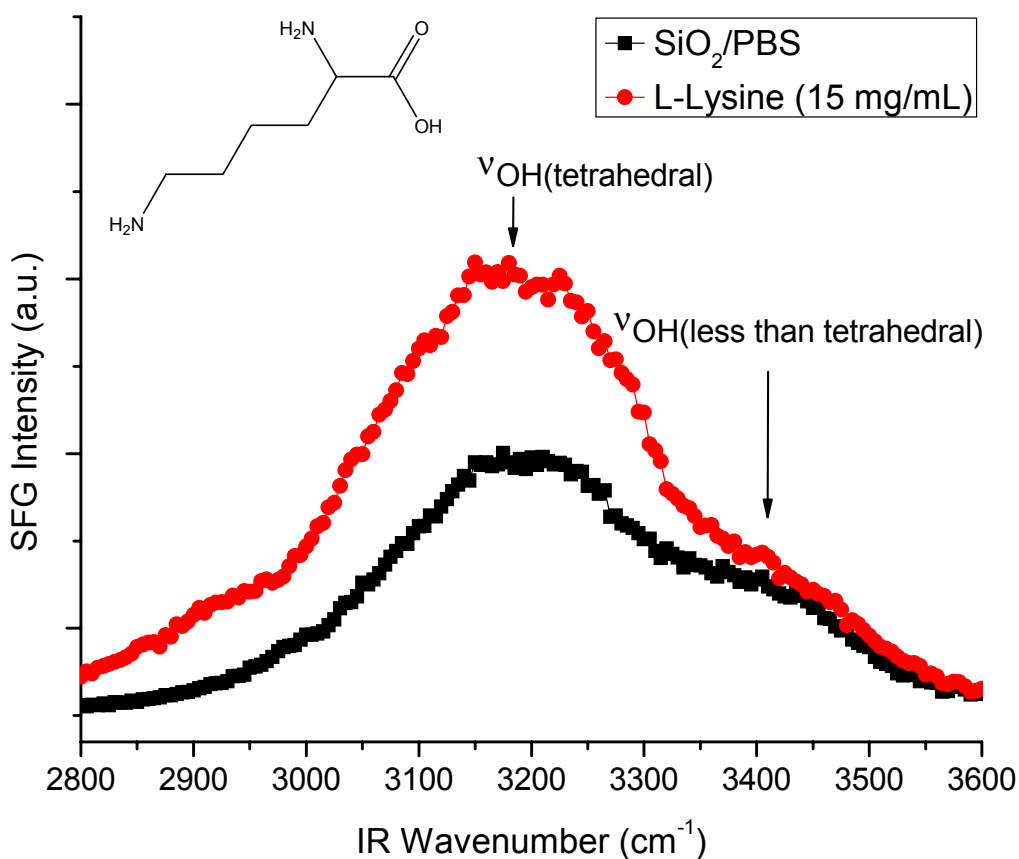


Figure 5.14. SFG spectrum of PBS/SiO<sub>2</sub> liquid-solid interface before (black squares) and after (red circles) addition of L-lysine (15mg/mL). No hydrocarbon vibrational modes are observed upon the addition of arginine. However, similar to the SFG spectrum of L-arginine at the SiO<sub>2</sub>/PBS interface, this spectrum shows a significant enhancement and peak broadening occurring in the spectral features at ~3200 cm<sup>-1</sup> and ~3400 cm<sup>-1</sup> from O-H stretching modes of “ice-like” tetrahedrally coordinated water and “liquid-like” less than tetrahedrally coordinated water, respectively. This result suggests that the presence of the L-lysine amino acid molecules may increase the extent of water ordering at the SiO<sub>2</sub>/PBS interface.

*Glycine, L-Cysteine, and L-Alanine:* The SFG spectra of glycine (100 mg/mL), L-cysteine (25 mg/mL), and L-alanine (40 mg/mL) at the SiO<sub>2</sub> surface all show a reduction in interfacial water SFG signals relative to their pure PBS background scans presented in Figures 5.15 - 5.17, respectively. This was an unanticipated similarity between the spectra based on their remarkably different molecular structures and varying hydrophilic nature of the three amino acids. The absence of C-H modes from glycine goes along with previous SFG and FTIR experiments on another hydrophilic surface, TiO<sub>2</sub>, at the liquid-solid interface.<sup>27, 29</sup> However, the decrease in SFG water signal in these three spectra may be attributed to the higher solution concentration of these amino acids than all others in this study. An elevated level of biomolecule solution concentration could result in an enhancement in the level of their interaction with interfacial water molecules. At high concentrations, these amino acid-water interactions could become sufficiently strong to result in either a disruption of the surface arrangement or, more

dramatically, the displacement of the previously ordered interfacial water molecules. Either of these potential circumstances would directly result in a decrease in the SFG signal intensity observed from water. This hypothesis is supported by the observed reduction in water signal upon addition of a high concentration L-proline at the  $\text{SiO}_2/\text{PBS}$  interface in a previous study.<sup>11</sup> Each data point in the spectra of glycine and L-alanine are the average of 500 laser shots, while the spectrum of L-cysteine is an average of 600 measurements.

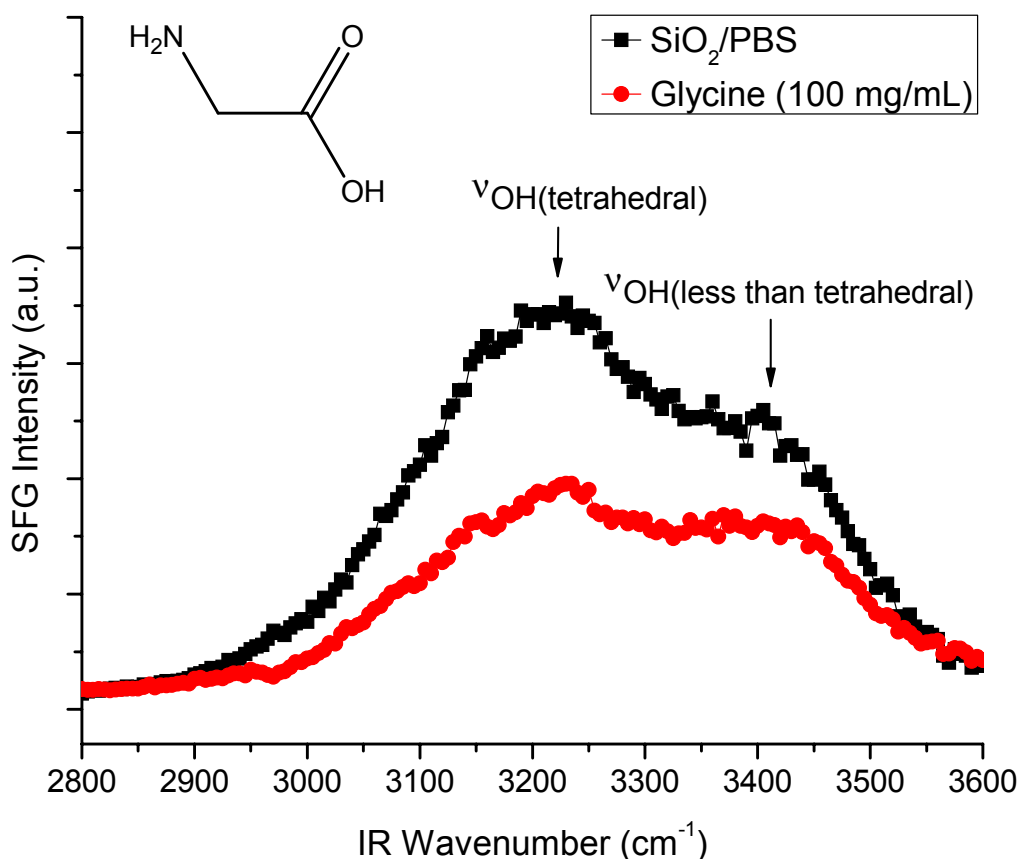


Figure 5.15. SFG spectrum of the  $\text{SiO}_2/\text{PBS}$  solid-liquid interface before (black squares) and after (red circles) the addition of glycine (100 mg/mL). SFG signal at  $\sim 3200 \text{ cm}^{-1}$  and  $\sim 3400 \text{ cm}^{-1}$  from “ice-like” tetrahedrally coordinated water and “liquid-like” less than tetrahedrally coordinated water, respectively, are reduced upon addition of the amino acid.

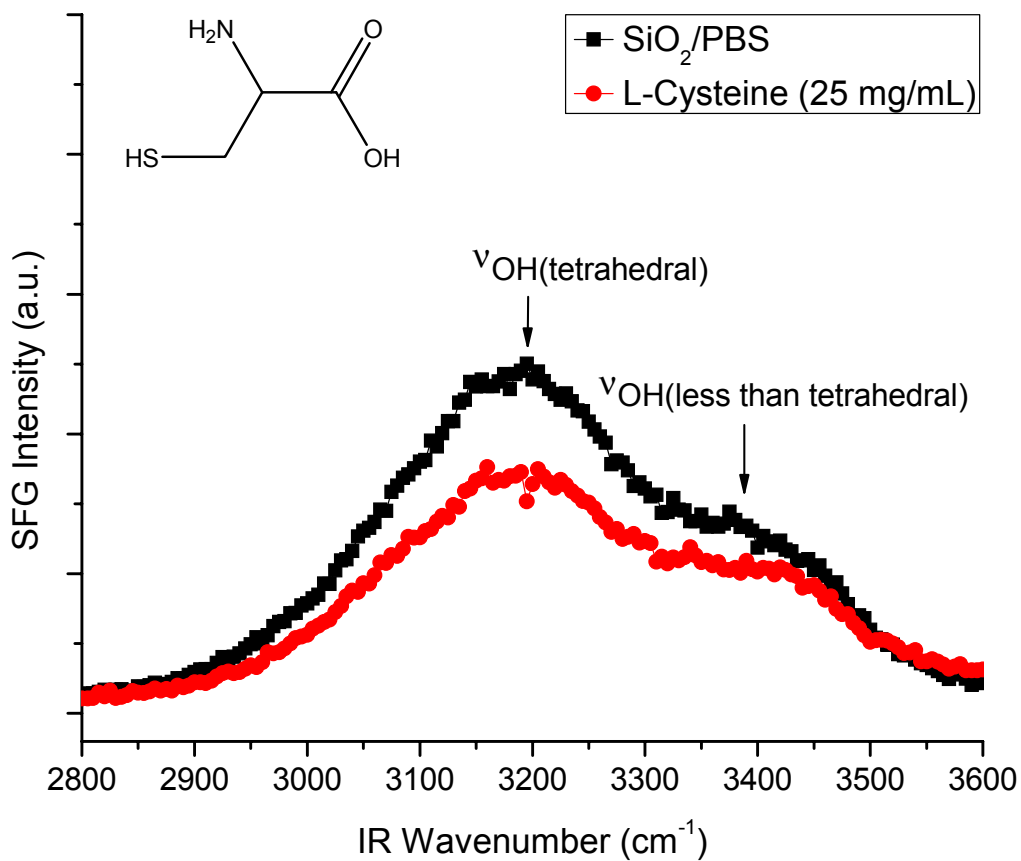
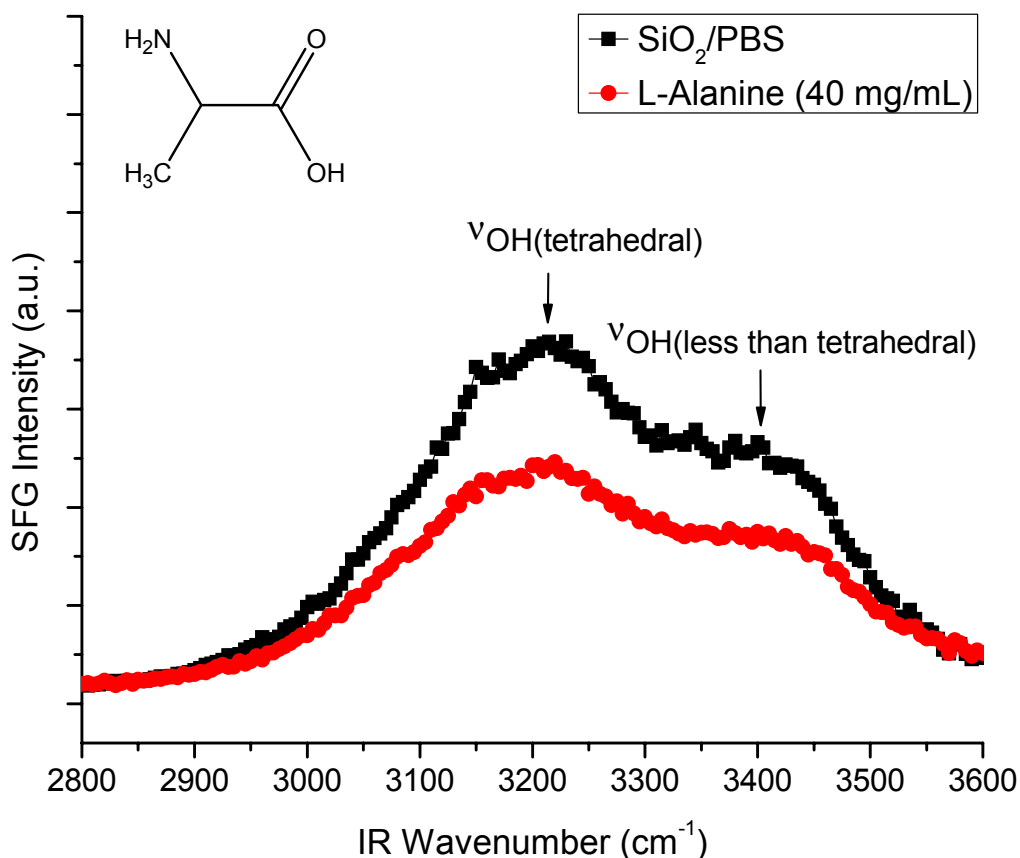


Figure 5.16. SFG spectrum of the SiO<sub>2</sub>/PBS solid-liquid interface before (black squares) and after (red circles) the addition of L-cysteine (25 mg/mL). SFG signal at ~3200 cm<sup>-1</sup> and ~3400 cm<sup>-1</sup> from “ice-like” tetrahedrally coordinated water and “liquid-like” less than tetrahedrally coordinated water, respectively, are reduced upon addition of the amino acid.



**Figure 5.17.** SFG spectrum of the SiO<sub>2</sub>/PBS solid-liquid interface before (black squares) and after (red circles) the addition of L-alanine (40 mg/mL). SFG signal at ~3200 cm<sup>-1</sup> and ~3400 cm<sup>-1</sup> from “ice-like” tetrahedrally coordinated water and “liquid-like” less than tetrahedrally coordinated water, respectively, are reduced upon addition of the amino acid.

*L-Proline:* The SFG spectrum of L-proline (15 mg/mL) in Figure 5.18 is unique from the other amino acids studied at the hydrophilic SiO<sub>2</sub> surface in that its spectrum is not different from that of pure PBS. Neither the “ice-like” tetrahedrally coordinated interfacial water signal at 3200 cm<sup>-1</sup> nor the “liquid-like” less than tetrahedrally coordinated water peak at 3400 cm<sup>-1</sup> show any change upon the addition of amino acid. This is in contrast to a previous SFG study of L-proline at much higher concentration (500 mg/mL) where both a C-H vibrational mode and a substantially reduced water signal were observed at the hydrophilic SiO<sub>2</sub>/PBS interface in the presence of the L-proline amino acid.<sup>11</sup> In that study, a small peak at 2985 cm<sup>-1</sup> was identified as originating from an asymmetric CH<sub>2</sub> stretch from the C<sub>β</sub> and C<sub>γ</sub> carbons on the strained, five-member proline ring.<sup>11, 24</sup> Some of the reduction in water signal in that study was attributed to the relatively high concentration of amino acid used which may have led to the displacement of interfacial water molecules from the SiO<sub>2</sub> surface. This hypothesis is supported by the absence

in observed change of the water signal upon addition of L-proline at a much lower solution concentration of 15 mg/mL used in this study. Each data point in Figure 5.18 is the average of 500 laser measurements.

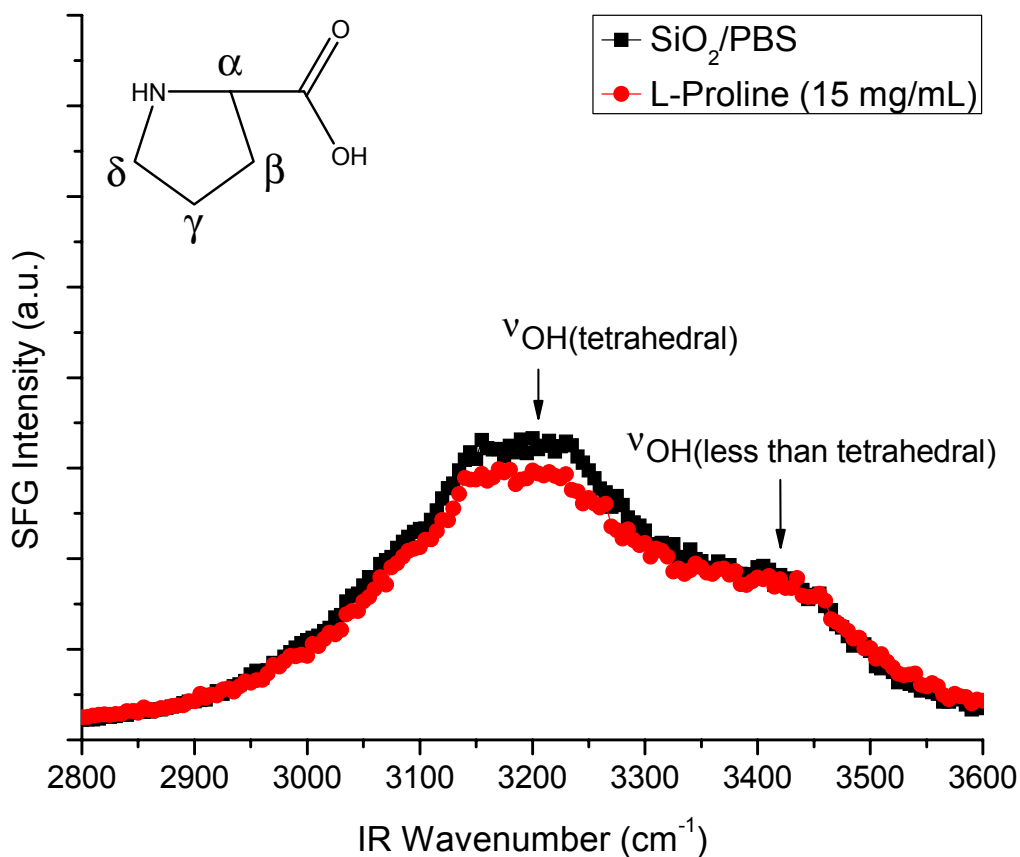


Figure 5.18. SFG spectrum of the SiO<sub>2</sub>/PBS solid-liquid interface before (black squares) and after (red circles) the addition of L-proline (15 mg/mL). No changes in water signal at ~3200 cm<sup>-1</sup> or ~3400 cm<sup>-1</sup> are observed upon the addition of amino acid.

#### 5.4. Conclusions

This investigation demonstrated the feasibility of investigating amino acids, the building blocks of both peptides and proteins, using sum frequency generation vibrational spectroscopy. Furthermore, the SFG spectra of aqueous solutions of eight amino acids were obtained at the hydrophilic SiO<sub>2</sub> and hydrophobic *d*<sub>8</sub>-polystyrene surfaces. This finding is significant because it includes the first known SFG signal obtained from several of these individual amino acids in aqueous solutions at the solid-liquid interface and at physiological pH. Seven of the eight amino acids showed identifiable C-H vibrational modes at the hydrophobic *d*<sub>8</sub>-polystyrene surface. Additionally, several of the amino acids spectra included vibrational modes indicative of amide moieties at the hydrophobic *d*<sub>8</sub>-PS/PBS interface. At the hydrophilic SiO<sub>2</sub> surface, no C-H

vibrational modes were observed from any of the amino acids studied. However, the presence of amino acids in buffer solutions was found to have a varying influence on the SFG signal from interfacial water at the SiO<sub>2</sub> surface. The spectra obtained at the SiO<sub>2</sub>/PBS interface showed enhancement in the SFG signal from ordered, interfacial water in the presence of L-phenylalanine, L-leucine, L-arginine, and L-lysine amino acid molecules when compared to background levels. The spectral features from both “ice-like” tetrahedral and “liquid-like” less than tetrahedrally coordinated interfacial water were found to decrease in magnitude from levels observed at the pure PBS/SiO<sub>2</sub> interface for solutions of glycine, L-cysteine, and L-alanine. This finding is attributed to these three amino acids being studied at relatively high solution concentrations of 25 mg/mL and above which may lead to an increase in the number and frequency of interactions with interfacial water molecules. Such a circumstance could result in a disruption displacement of the ordered water molecules at the hydrophilic SiO<sub>2</sub> surface. Lastly, the SFG spectra of a solution of L-proline at the SiO<sub>2</sub>/PBS interface showed no evidence of the amino acid disrupting the organization or concentration of adsorbed water.

## References

1. Anderson, J. M., *Annual Review of Materials Research* **2001**, *31*, 81-110.
2. Castner, D. G.; Ratner, B. D., *Surface Science* **2002**, *500* (1-3), 28-60.
3. Williams, D. F.; European Society for Biomaterials., *Definitions in biomaterials : proceedings of a consensus conference of the European Society for Biomaterials, Chester, England, March 3-5, 1986*. Elsevier: Amsterdam ; New York, 1987; p vii, 72 p.
4. York, R. L.; Li, Y. M.; Holinga, G. J.; Somorjai, G. A., *Journal of Physical Chemistry A* **2009**, *113* (12), 2768-2774.
5. Lambert, A. G.; Davies, P. B.; Neivandt, D. J., *Applied Spectroscopy Reviews* **2005**, *40* (2), 103-145.
6. Shen, Y. R.; Ostroverkhov, V., *Chemical Reviews* **2006**, *106* (4), 1140-1154.
7. Mermut, O.; Phillips, D. C.; York, R. L.; McCrea, K. R.; Ward, R. S.; Somorjai, G. A., *Journal of the American Chemical Society* **2006**, *128* (11), 3598-3607.
8. Mermut, O.; York, R. L.; Phillips, D. C.; McCrea, K. R.; Ward, R. S.; Somorjai, G. A., *Biointerphases* **2006**, *1* (2), P5-P11.
9. Phillips, D. C.; York, R. L.; Mermut, O.; McCrea, K. R.; Ward, R. S.; Somorjai, G. A., *Journal of Physical Chemistry C* **2007**, *111* (1), 255-261.
10. York, R. L.; Browne, W. K.; Geissler, P. L.; Somorjai, G. A., *Israel Journal of Chemistry* **2007**, *47* (1), 51-58.
11. York, R. L.; Holinga, G. J.; Somorjai, G. A., *Langmuir* **2009**, *25* (16), 9369-9374.
12. York, R. L.; Mermut, O.; Phillips, D. C.; McCrea, K. R.; Ward, R. S.; Somorjai, G. A., *J. Phys. Chem. C* **2007**, *111* (25), 8866-8871.
13. Shen, Y. R.; Ostroverkhov, V.; Chen, E. C. Y.; Ji, N.; Waychunas, G., *Abstracts of Papers of the American Chemical Society* **2006**, *231*, -.
14. Miranda, P. B.; Shen, Y. R., *Journal of Physical Chemistry B* **1999**, *103* (17), 3292-3307.
15. Voet, D.; Voet, J. G.; Pratt, C. W., *Fundamentals of biochemistry upgrade*. [Rev. ed.; Wiley: New York, 2002; p 1 v. (various pagings).
16. Yeganeh, M. S.; Dougal, S. M.; Pink, H. S., *Physical Review Letters* **1999**, *83* (6), 1179-1182.
17. Briggman, K. A.; Stephenson, J. C.; Wallace, W. E.; Richter, L. J., *Journal of Physical Chemistry B* **2001**, *105* (14), 2785-2791.
18. Watry, M. R.; Richmond, G. L., *Journal of Physical Chemistry B* **2002**, *106* (48), 12517-12523.
19. Breen, N. F.; Weidner, T.; Li, K.; Castner, D. G.; Drobny, G. P., *Journal of the American Chemical Society* **2009**, *131* (40), 14148-+.
20. Krimm, S.; Dwivedi, A. M., *Journal of Raman Spectroscopy* **1982**, *12* (2), 133-137.
21. Miyazawa, T., *Journal of Molecular Spectroscopy* **1960**, *4* (2), 168-172.
22. Pawlukoje, A.; Leciejewicz, J.; Ramirez-Cuesta, A. J.; Nowicka-Scheibe, J., *Spectrochimica Acta Part A: Molecular and Biomolecular Spectroscopy* **2005**, *61* (11-12), 2474-2481.
23. Tiwari, S.; Mishra, P. C., *Spectrochimica Acta Part A: Molecular and Biomolecular Spectroscopy* **2009**, *73* (4), 719-729.
24. Reva, I. D.; Stepanian, S. G.; Plokhotnichenko, A. M.; Radchenko, E. D.; Sheina, G. G.; Blagoi, Y. P., *Journal of Molecular Structure* **1994**, *318*, 1-13.
25. Krimm, S.; Bandekar, J., *Advances in Protein Chemistry* **1986**, *38*, 181-364.

26. Kim, J.; Chou, K. C.; Somorjai, G. A., *Journal of Physical Chemistry B* **2002**, *106* (36), 9198-9200.
27. Paszti, Z.; Keszthelyi, T.; Hakkel, O.; Guzzi, L., *Journal of Physics-Condensed Matter* **2008**, *20* (224014), -.
28. Paszti, Z.; Guzzi, L., *Vibrational Spectroscopy* **2009**, *50* (1), 48-56.
29. Ojamae, L.; Aulin, C.; Pedersen, H.; Kall, P. O., *Journal of Colloid and Interface Science* **2006**, *296* (1), 71-78.

## Chapter 6

### **A Study of the Influence of Amino Acid Side Functional Group on the Adsorption of Interfacial Homopeptides and Their Constituent Amino Acids on Hydrophilic SiO<sub>2</sub> and Hydrophobic Polystyrene Surfaces Studied by SFG and QCM**

Sum frequency generation (SFG) vibrational spectroscopy and quartz crystal microbalance (QCM) experiments were carried out in the investigation of the interfacial structure and adsorbed amount of L-lysine and L-proline amino acids and their corresponding homopeptides, poly-L-lysine and poly-L-proline, at two liquid-solid interfaces. The SFG and QCM experiments were performed on these biomolecules at the liquid-solid interface between phosphate buffered saline at pH 7.4 (PBS) and the hydrophobic deuterated polystyrene (*d*<sub>8</sub>-PS) surface as well as the interface between PBS and hydrophilic fused SiO<sub>2</sub>. The SFG spectra of the amino acids studied here were qualitatively similar to their corresponding homopeptides. However, SFG signal from the amino acids at the solid/PBS interface was smaller in magnitude than that of the more massive corresponding homopeptides at the concentrations studied. Substantial differences were observed in the SFG spectra for each species between the hydrophobic *d*<sub>8</sub>-PS and the hydrophilic SiO<sub>2</sub> liquid-solid interfaces suggesting a surface-dependent interfacial ordering of the biomolecules. QCM measurements indicated that on both surfaces poly-L-lysine adsorbs to a greater extent than its constituent amino acid L-lysine over the range of concentrations used in this study. Interestingly, the opposite trend was demonstrated by poly-L-proline which was found to adsorb to both surfaces less extensively than its corresponding amino acid, L-proline. Lastly, the SFG spectra obtained in this study indicated that the adsorbed biomolecule species exert a strong influence on the structure of interfacial water.

#### **6.1. Introduction**

The study of interfacial biomolecules, particularly proteins and peptides, at interfaces is currently an active area of research for both the surface science and biomedical communities.<sup>1-3</sup> Recently, the surface-specific nonlinear optical technique of sum frequency generation (SFG) vibrational spectroscopy has been utilized in the study of adsorbed biomolecules at the solid-liquid interface.<sup>4-8</sup> Of the most common interfaces studied in the research literature two stand out as being experimentally challenging to investigate: biomolecules at the SiO<sub>2</sub>/liquid interface and amino acids at physiological pH at any solid/liquid interface.<sup>5</sup> These two biological interfaces have proven to be experimentally challenging to study due to the fact that C-H modes were not observed in the SFG spectra. While the origin of these systems' SFG inactivity in the C-H stretching region has not been well understood, it has been postulated to result from absence of adsorbed amino acids or the absence of side chain ordering in these biomolecules.<sup>5</sup> In the case of biomolecules at the SiO<sub>2</sub>/phosphate buffered saline (PBS) interface, both the aqueous solvent and the silica surface are hydrophilic while a peptides and proteins contain side chains that generally are more hydrophobic. It was found in previous studies that these hydrophobic side chains lacked sufficient thermodynamic driving force to exhibit sufficient ordering at the

hydrophilic SiO<sub>2</sub>/PBS interface to be observable by SFG vibrational spectroscopy.<sup>9</sup> This has been demonstrated for biomolecules of various chain-lengths ranging from individual amino acids to large proteins.<sup>5, 9-11</sup> Amino acids, the individual building blocks of proteins, have been previously studied at the CCl<sub>4</sub>/H<sub>2</sub>O interface using SFG by Watry and Richmond,<sup>12</sup> Ji and Shen utilized SFG vibrational spectroscopy to quantitatively study leucine at the air/H<sub>2</sub>O interface;<sup>13</sup> Kim and co-workers studied phenylalanine at the glassy carbon electrode using SFG;<sup>14</sup> and recently Paszti and co-workers utilized SFG spectroscopy to examine several different amino acids adsorbed on different hydrophilic solid surfaces.<sup>15</sup> In the case of amino acids at the hydrophobic solid/liquid interface, no SFG active C-H vibrational mode ordering has been reported in the research literature with the exception of electrochemical interfaces.<sup>14</sup> The reason for this inability to resolve amino acids is unclear as ordered C-H modes of proteins and peptides have been observed at the hydrophobic solid/buffer interface previously.

In this investigation C-H ordering in the SFG spectra of L-lysine and L-proline amino acids is experimentally observed at the deuterated polystyrene (*d*<sub>8</sub>-PS)/PBS interface. Furthermore, SFG spectra demonstrating C-H ordering of poly-L-lysine at the hydrophilic SiO<sub>2</sub>/PBS interface is presented herein. These SFG spectra were obtained utilizing both high biomolecule solution concentrations and a near total internal reflection (nTIR) experimental laser beam geometry. Similar to earlier findings of the Cremer group,<sup>10</sup> the SFG spectra obtained in this study indicated differences in the adsorbates' interfacial structures on both hydrophilic and hydrophobic surfaces. The influence of peptide chain length on the interfacial structure of L-lysine and L-proline homopeptides was also investigated at both hydrophobic and hydrophilic surfaces in this study. Additionally, the interfacial structure of homopeptides was compared to that of amphiphilic peptides adsorbed to both hydrophobic and hydrophilic surfaces. Lastly, this investigation explored the influence of an adsorbed biomolecule on the ordering of interfacial water molecules at both *d*<sub>8</sub>-PS and SiO<sub>2</sub> substrate surfaces.

## 6.2. Experimental

### 6.2.1. QCM Experimental Measurements

Quartz crystal microbalance experiments in this study were carried out using a commercial Q-sense (Glen Burnie, MD) model D300 QCM instrument. At the beginning of each QCM experiment the resonance and dissipation values of each individual sensor crystal was measured and recorded in pure phosphate buffered saline (PBS) solution at pH 7.4. During the entire measurement process, the fundamental as well as the 3<sup>rd</sup>, 5<sup>th</sup>, and 7<sup>th</sup> harmonic frequencies and dissipations were monitored at approximately 5 MHz, 15 MHz, 25 MHz, and 35 MHz, respectively. After establishing a stable baseline values for sensor resonance frequencies and dissipations in PBS, the sensor crystals were then exposed to solutions of biomolecules dissolved in PBS. QCM data collection was performed inside a temperature controlled measurement chamber maintained at a constant temperature of 20.3 ± 0.2 °C. Biomolecule surface concentrations were determined from the experimentally measured 3<sup>rd</sup> harmonic frequency data using the Sauerbrey relationship, Equation (6.1).<sup>16</sup>

$$\Delta m = -\frac{C}{n} \Delta f_n \quad (6.1)$$

This equation correlates the change in the resonant frequency of a QCM resonator's  $n^{\text{th}}$  harmonic,  $\Delta f_n$ , the harmonic number of the resonance,  $n$ , and a constant dependant upon the physical properties of the resonator,  $C$ , to the mass added to the resonator's surface,  $\Delta m$ . In these measurements, the value of  $C = 17.7 \text{ ng s cm}^{-2}$  was used as prescribed by the QCM sensor's manufacturer. A theoretical background for the QCM technique is provided in Chapter 4 along with a detailed description of the Q-sense QCM instrument, sensor crystals, and specific experimental procedures used in this study.<sup>16-20</sup>

## 6.2.2. SFG Experimental Measurements

Sum Frequency Generation (SFG) experiments were carried out utilizing a Continuum (Santa Clara, CA) Leopard D-20 Nd:YAG laser with a pulsed 1064 nm output beam with 22 picosecond pulse width at a repetition rate of 20 Hz. This near-infrared laser output was then passed through a Laservision (Bellevue, WA) Optical Parametric Generator (OPG)/Optical Parametric Amplifier (OPA) optical system. The OPG/OPA system produced both a 532 nm visible beam, and a tunable infrared beam with an output of 2800 - 3600  $\text{cm}^{-1}$ , which were directly used in SFG measurements. The prismatic sample substrates used in the SFG experiments were placed on top of a PBS/biomolecule solution filled Viton o-ring in a clean Petri dish. The resulting SFG signal generated at the solution-prism surface was detected by a photomultiplier tube before being processed and recorded on a desktop computer. All SFG measurements were conducted in the  $S_{\text{SFG}}S_{\text{VIS}}P_{\text{IR}}$  polarization combination and were carried out at room temperature and atmospheric pressure. The resulting SFG spectra were fit to the Equation 6.2:<sup>21</sup>

$$I_{\text{SFG}} \propto |\chi^{(2)}|^2 = \left| \chi_{\text{NR}}^{(2)} + \sum_q \int d\omega_q \frac{A_q}{\omega_{\text{IR}} - \omega_q + i\Gamma_q} * \exp\left(-\frac{\omega_q - \omega_{q_0}}{\Delta_q^2}\right) \right|^2 \quad (6.2)$$

In this equation,  $\chi^{(2)}$  represents is the second-order nonlinear susceptibility which is composed of both a resonant and non-resonant component,  $\chi_{\text{R}}^{(2)}$  and  $\chi_{\text{NR}}^{(2)}$ , respectively. Additionally, the parameters  $A_q$ ,  $\omega_q$ ,  $\Gamma_q$ ,  $\omega_{q_0}$ ,  $\Delta_q$  represent the strength, infrared frequency of the vibrational mode, phenomenological damping factor, central frequency, and Gaussian width of the  $q^{\text{th}}$  vibrational mode, respectively. The theoretical background of the SFG process is provided in Chapter 2,<sup>22</sup> and a complete description of the Laservision OPG/OPA system as well as SFG sample arrangement and experimental beam geometries are provided in Chapter 3.<sup>23</sup>

## 6.2.3. Chemicals

All experiments were conducted at pH 7.4 and all solutions were made using phosphate buffered saline (PBS) (Sigma-Aldrich). Biomolecule solutions were made with L-lysine at 16.5 mg/mL, poly-L-lysine at 12.5 mg/mL, L-proline at 500 mg/mL, and poly-L-proline at 0.5 mg/mL. All amino acids and peptides used were purchased directly from Sigma-Aldrich and

were used as received. The experimental concentrations used were selected to maximize SFG signal while still maintaining biomolecule solubility. For all experiments the solution concentration of side chains was higher for the amino acids than the polypeptides.

#### 6.2.4. Sample Preparation

Quartz crystal microbalance measurements were performed using gold and SiO<sub>2</sub> coated Q-Sense (Glen Burnie, MD) sensors. Prior to each experimental measurement QCM sensor crystals were cleaned with a Herrick (Ithaca, NY) oxygen plasma cleaner for 60 s (18 W RF, 200 mtorr O<sub>2</sub>) to remove any organic surface contaminants. Additionally, plasma treatment was utilized to also ensure the full surface oxidation of the SiO<sub>2</sub> coated QCM sensor crystals. After plasma treatment, SiO<sub>2</sub> coated sensor crystals were used directly and gold coated sensor crystal surfaces were coated with polystyrene (PS) thin films. The hydrophobic PS surfaces were prepared on the clean gold coated sensor crystals by spin coating with a 2 % weight solution of polystyrene (MW  $\approx$  280,000) (Aldrich) in toluene (Sigma-Aldrich). The spin-coating conducted with a Specialty Coating Systems (Indianapolis, IN) instrument operated at 3000 rpm and spun for 45 s. The resulting PS thin films were annealed for 12 hours at 120 °C to ensure surface flatness and to fully remove any residual toluene solvent from the spin coating solution. Ellipsometry measurements and atomic force microscopy were conducted on the PS coated QCM substrates and the resulting thin films were determined to have  $\sim$ 95 nm thicknesses.

SFG sample substrates were prepared from fused silica equilateral prisms which were cleaned by soaking for 12 hours in a solution of concentrated H<sub>2</sub>SO<sub>4</sub> (97%) (Sigma-Aldrich) and Nochromix (Godax). Subsequently, the SiO<sub>2</sub> prism substrates were washed with distilled, de-ionized water prior to being cleaned using an oxygen plasma treatment as previously described for the QCM sensor crystals. Deuterated polystyrene (*d*<sub>8</sub>-PS) thin films were prepared on the SFG prism substrates by spin-coating 3 % weight solution of *d*<sub>8</sub>-PS (MW  $\approx$  300,000) (Polymer Source) dissolved in toluene (Sigma-Aldrich). The spin-coating and annealing procedures carried out for the SFG substrates were identical to those used for the QCM sensors. The thickness of the *d*<sub>8</sub>-PS films on the SFG substrates were determined to be  $\sim$ 105 nm by ellipsometry and atomic force microscopy.

### 6.3. Results and Discussion

#### 6.3.1. QCM Data and Analysis

QCM experiments were carried out on both PS and SiO<sub>2</sub> surfaces for both amino acids and their corresponding homopeptides. Amino acid and homopeptide surface concentrations were directly determined from 3<sup>rd</sup> harmonic frequency data collected by the QCM instrument using the Sauerbrey Equation. A plot of raw 3<sup>rd</sup> harmonic frequency and dissipation data for poly-L-proline (0.5 mg/mL) on SiO<sub>2</sub> is presented in Figure 6.1 as a representative example of all QCM measurements conducted in this study. Minor linear instrument drift was present in all QCM-D measurements, but this was corrected for by conducting a linear regression of the 3<sup>rd</sup> overtone frequency data in pure PBS immediately prior addition of each biomolecule solution.

A summary of the QCM experiment results are included in Table 6.1 and Figure 6.2. Despite being at lower solution concentrations than its corresponding amino acid, a greater amount of poly-L-lysine homopeptide adsorbed on the both the SiO<sub>2</sub> and PS surfaces than did L-lysine amino acid. The opposite trend was observed in the case of poly-L-proline which was found to adsorb to both the hydrophilic and the hydrophobic surfaces less extensively than its corresponding amino acid, L-proline.

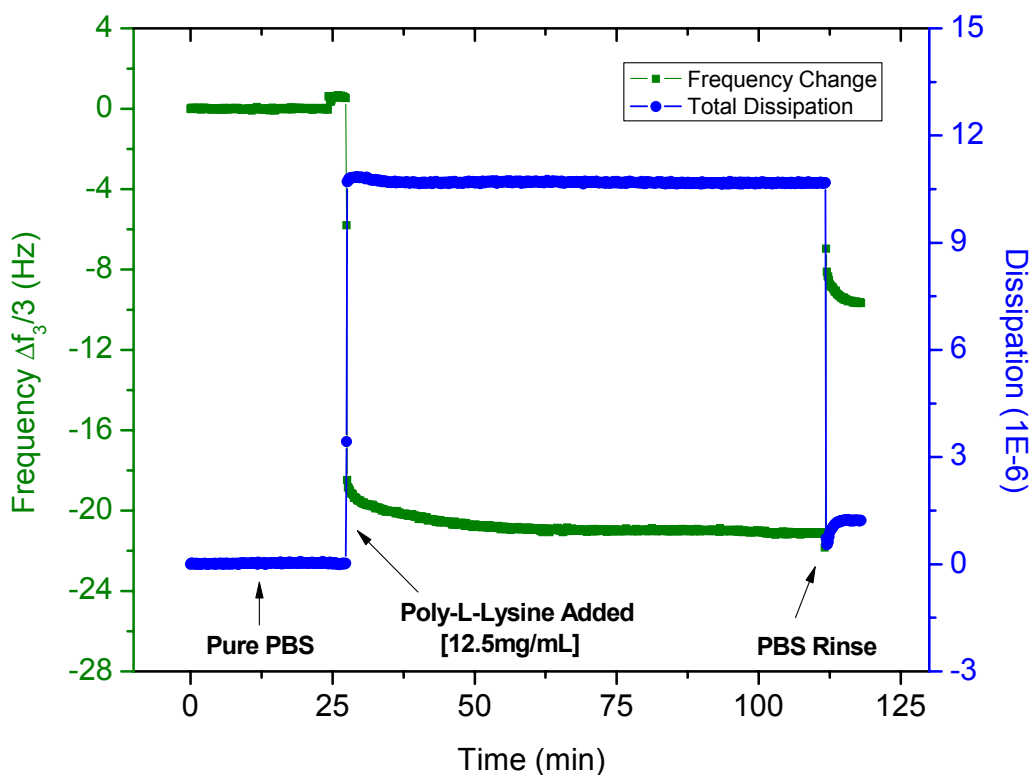


Figure 6.1. Raw QCM measurement data for the frequency (green squares) and dissipation (blue circles) values for the third harmonic of a SiO<sub>2</sub> coated sensor crystal in PBS prior to, during, and after addition of a solution of poly-L-lysine homopeptide.

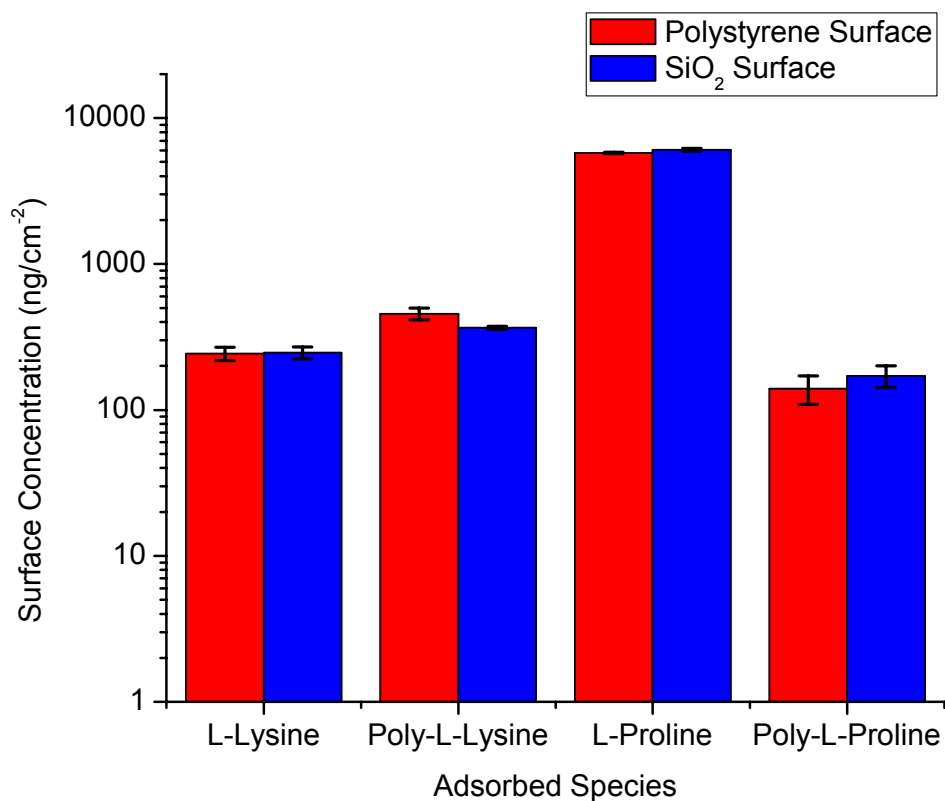


Figure 6.2. Plot summarizing biomolecule surface concentrations upon adsorption on polystyrene (red bars) and SiO<sub>2</sub> (blue bars) surfaces as determined by QCM experiment. For each individual biomolecule, the amount adsorbed was approximately the same between both the hydrophobic polystyrene and the hydrophilic SiO<sub>2</sub> surfaces.

Species (Solution Conc.)	<i>d</i> <sub>8</sub> -Polystyrene Surface Concentration	SiO <sub>2</sub> Surface Concentration
L-Lysine (16.5 mg/mL)	243 ± 25 ng/cm <sup>-2</sup>	248 ± 23 ng/cm <sup>-2</sup>
Poly-L-Lysine (12.5 mg/mL)	457 ± 42 ng/cm <sup>-2</sup>	365 ± 9 ng/cm <sup>-2</sup>
L-Proline (500 mg/mL)	5770 ± 60 ng/cm <sup>-2</sup>	6070 ± 130 ng/cm <sup>-2</sup>
Poly-L-Proline (0.5 mg/mL)	140 ± 31 ng/cm <sup>-2</sup>	171 ± 29 ng/cm <sup>-2</sup>

Table 6.1. Summary QCM data quantifying the surface concentration of each adsorbed biomolecule on the polystyrene and SiO<sub>2</sub> substrate surfaces.

### 6.3.2. SFG Data and Analysis

The SFG spectrum of a solution of poly-L-lysine (12.5 mg/mL) in PBS at the hydrophobic  $d_8$ -PS liquid-solid interface is presented in Figure 6.3. In this spectrum, C-H vibrational modes appear at  $2870\text{ cm}^{-1}$  and  $2935\text{ cm}^{-1}$  which are attributed to  $\text{CH}_2$  symmetric and  $\text{CH}_2$  asymmetric stretches from the lysine side chains, respectively.<sup>12</sup> Similarly, the spectrum of L-lysine amino acid (16.5 mg/mL) in PBS shown in Figure 6.4 also has the same spectral peaks as the homopeptide at  $2870\text{ cm}^{-1}$  from  $\text{CH}_2$  (s) and at  $2935\text{ cm}^{-1}$  from the  $\text{CH}_2$  (as). However, the vibrational modes from the poly-L-lysine are of substantially of higher intensity than of the L-lysine amino acid despite the latter being at higher solution concentration. Both of these spectra also show a broad continuum of SFG signal centered around  $3050\text{ cm}^{-1}$  which is attributed to O-H stretching modes of interfacial water at the  $d_8$ -polystyrene-PBS solid-liquid interface. The presence of this peak agrees with previous SFG studies of aqueous solutions at hydrophobic surfaces under similar experimental conditions.<sup>24</sup> As shown in Figure 6.3, the addition of poly-L-

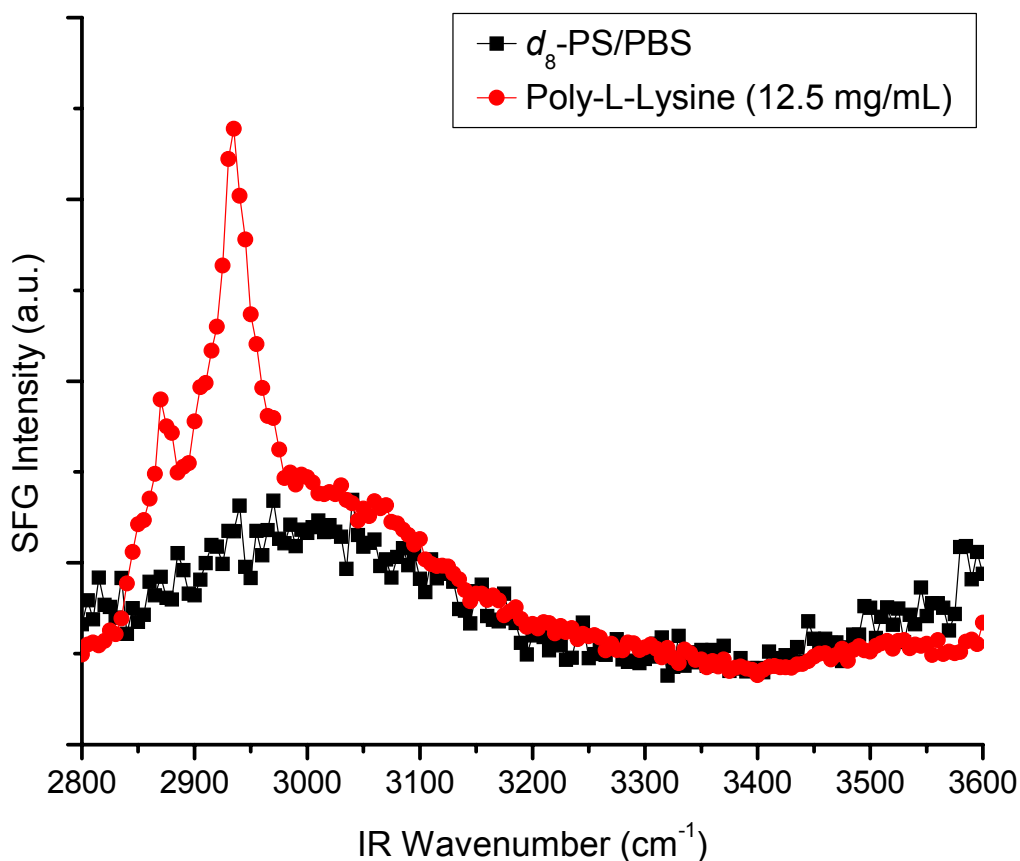
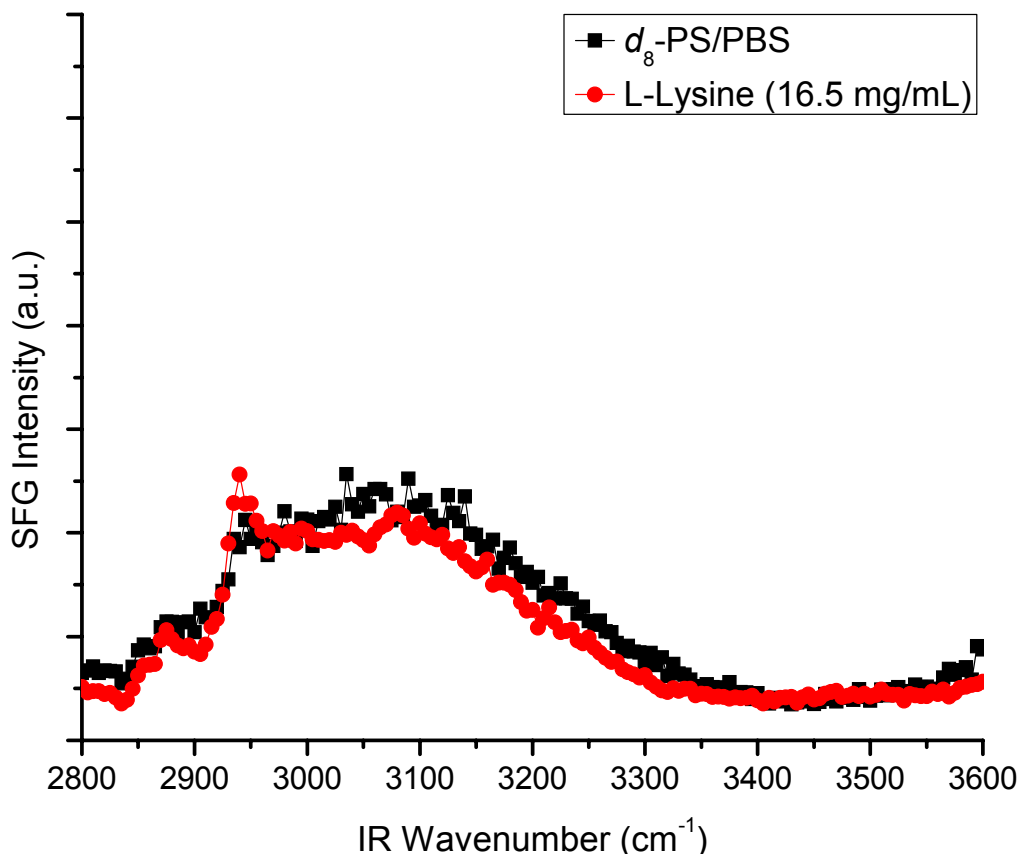


Figure 6.3. The SFG spectrum of the  $d_8$ -PS/PBS interface before (black squares) and after the addition of poly-L-lysine (12.5 mg/mL) (red circles). The broad peak centered around  $\sim 3050\text{ cm}^{-1}$  is attributed to interfacial water. Addition of the homopeptide, two intense C-H peaks are observed at  $2870\text{ cm}^{-1}$  and  $2935\text{ cm}^{-1}$  which are attributed to  $\text{CH}_2$  symmetric and  $\text{CH}_2$  asymmetric vibrational modes, respectively. The SFG intensity in the water region is slightly increased in the presence of adsorbed poly-L-lysine.

lysine peptide slightly enhances the signal from interfacial water when compared to the spectrum of pure PBS. In the case of the L-lysine (Figure 6.4), the SFG signal from O-H stretching modes of water is similar in the spectra of both pure buffer and the amino acid solution indicating the presence of the amino acid does not disturb the previously adsorbed interfacial water.



**Figure 6.4.** The SFG spectrum of the  $d_8$ -PS/PBS interface before (black squares) and after the addition of L-lysine amino acid (red circles) at a solution concentration of 16.5 mg/mL. The broad peak centered on  $\sim 3050$   $\text{cm}^{-1}$  is attributed to an O-H stretching mode of interfacial water. Upon adsorption of L-lysine, the water structure is not perturbed but two modes of smaller intensity attributed to  $\text{CH}_2$  symmetric and  $\text{CH}_2$  asymmetric stretches are observed at  $2870$   $\text{cm}^{-1}$  and  $2935$   $\text{cm}^{-1}$ , respectively.

The SFG spectra of solutions of poly-L-proline homopeptide (0.5 mg/mL) and L-proline amino acid (500 mg/mL) at the  $d_8$ -PS/PBS solid-liquid interface are included in Figure 6.5 and Figure 6.6, respectively. Both spectra show similar C-H vibrational modes at  $2875$   $\text{cm}^{-1}$ ,  $2935$   $\text{cm}^{-1}$ , and  $2980$   $\text{cm}^{-1}$ , as well as the broad continuum of peaks attributed to O-H stretches of interfacial water at  $\sim 3050$   $\text{cm}^{-1}$ . The vibrational mode centered at  $2875$   $\text{cm}^{-1}$  is identified as a combination of  $\text{C}_\beta\text{H}_2$ ,  $\text{C}_\gamma\text{H}_2$ , and  $\text{C}_\delta\text{H}_2$  symmetric stretching modes (see Figure 6.5 for nomenclature details).<sup>25</sup> The peak at  $2935$   $\text{cm}^{-1}$  is attributed to a combination of  $\text{C}_\beta\text{H}_2$  (s) and  $\text{C}_\gamma\text{H}_2$  (s) vibrational modes, and the peak at  $2980$   $\text{cm}^{-1}$  originates from asymmetric C-H stretching modes of the  $\text{C}_\beta\text{H}_2$  and  $\text{C}_\gamma\text{H}_2$  portions of the strained, five-member proline ring.

Interestingly, the intensity of the SFG signal from the amino acid is substantially less than for the homopeptide despite being at a solution concentration four orders of magnitude greater than that of poly-L-proline peptide. This difference in SFG signal is attributed, in part, to the secondary structure of poly-L-proline which is known to exhibit a left-handed helical conformation.<sup>26-29</sup> Additionally, the presence of the homopeptide dramatically changes the SFG signal attributed to interfacial water when compared to the background spectrum of pure PBS as shown in Figure 6.5. However, similar to L-lysine at the  $d_8$ -PS interface, the SFG spectrum of L-proline at the hydrophobic interface indicates only a marginal change in the interfacial O-H signal when compared to the background spectrum of PBS only thus indicating the adsorbed water is left largely unchanged upon the addition of the biomolecule (Figure 6.6).

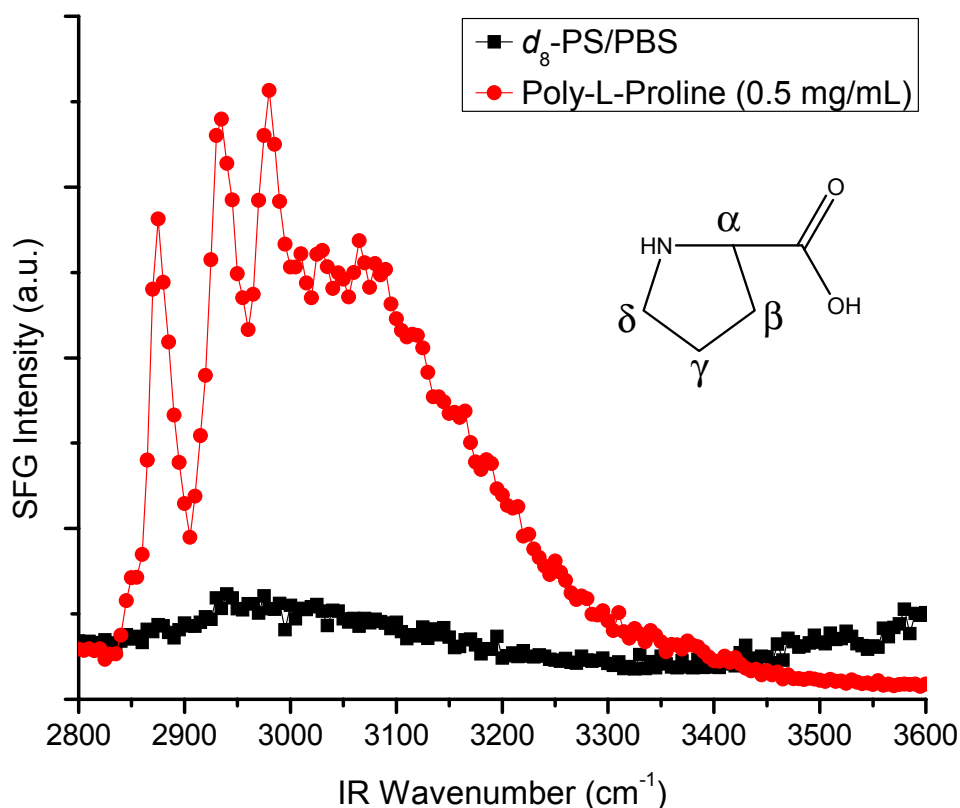


Figure 6.5. The SFG spectrum of the  $d_8$ -PS/PBS interface before (black squares) and after (red circles) the addition of a solution of poly-L-proline at a concentration of 0.5 mg/mL. The broad peak centered on  $\sim 3050$   $\text{cm}^{-1}$  is attributed to interfacial water and is found to increase upon peptide adsorption. Three intense peaks are seen at  $2875$   $\text{cm}^{-1}$ ,  $2935$   $\text{cm}^{-1}$ , and  $2980$   $\text{cm}^{-1}$ . These three modes are assigned to a combination of  $C_\delta\text{H}_2$  (s),  $C_\beta\text{H}_2$  (s), and  $C_\gamma\text{H}_2$  (s); a combination of  $C_\gamma\text{H}_2$  (s) and  $C_\beta\text{H}_2$  (s); and a combination of  $C_\gamma\text{H}_2$  (as) and  $C_\beta\text{H}_2$  (as), respectively. The inset diagram of shows L-proline amino acid with labeled carbons.

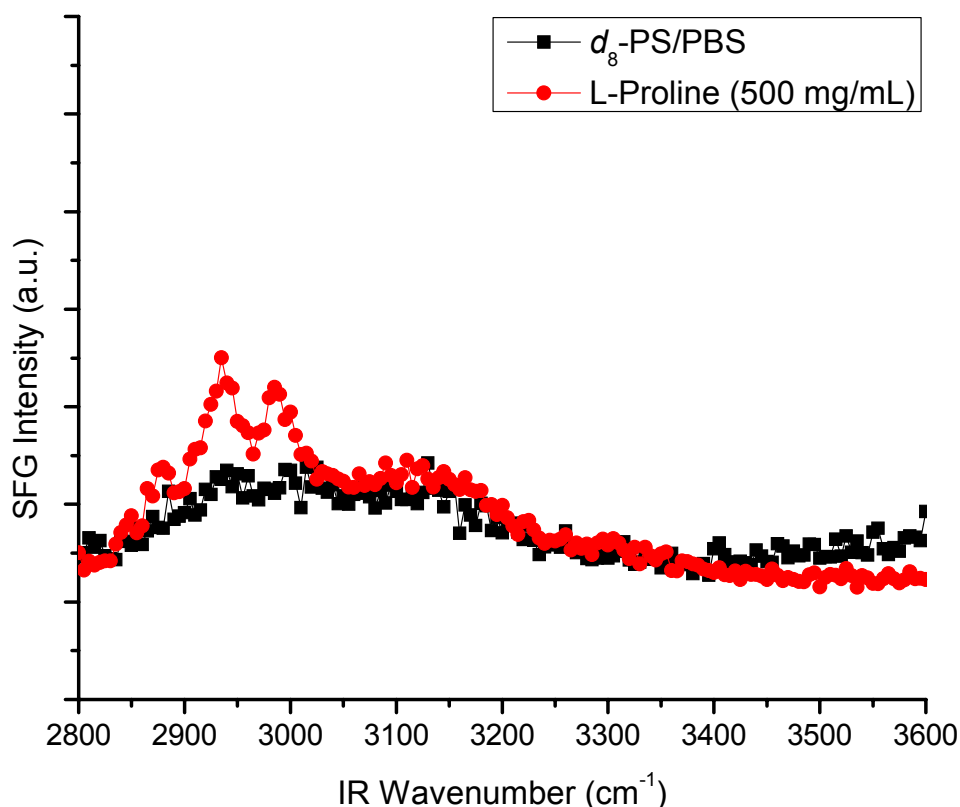


Figure 6.6. The SFG spectrum of the  $d_8$ -PS/PBS interface before (black squares) and after (red circles) the addition of L-proline amino acid at a final solution concentration of 500 mg/mL. The broad peak centered at approximately 3050  $\text{cm}^{-1}$  is attributed to interfacial water and remains upon amino acid adsorption. Three peaks are seen at 2875  $\text{cm}^{-1}$ , 2935  $\text{cm}^{-1}$ , and 2980  $\text{cm}^{-1}$ . These three C-H vibrational modes are assigned to a combination of  $\text{C}_\beta\text{H}_2$  (s),  $\text{C}_\gamma\text{H}_2$  (s), and  $\text{C}_\delta\text{H}_2$  (s); a combination of  $\text{C}_\beta\text{H}_2$  (s) and  $\text{C}_\gamma\text{H}_2$  (s); and a combination of  $\text{C}_\beta\text{H}_2$  (as) and  $\text{C}_\gamma\text{H}_2$  (as), respectively.

At the hydrophilic  $\text{SiO}_2$  surface, the SFG spectra (Figures 6.7 - 6.10) of PBS shows two broad peaks at  $\sim 3200 \text{ cm}^{-1}$  and  $\sim 3400 \text{ cm}^{-1}$  from O-H stretches of “ice-like” tetrahedrally coordinated water and “liquid-like” less than tetrahedrally coordinated water, respectively.<sup>30, 31</sup> These vibrational modes originating from interfacial water are much stronger and frequency shifted from those observed at the hydrophobic  $d_8$ -PS/PBS interface. This increase in the SFG intensity of water is attributed to an enhanced ordering of the polar water molecules at the hydrophilic  $\text{SiO}_2$  surface which is itself polar and has been shown to exhibit a negative surface charge in aqueous solutions at pH values above  $\sim 2$ .<sup>32</sup> Upon the addition of poly-L-lysine peptide (12.5 mg/mL), the SFG spectrum at the  $\text{SiO}_2$ -PBS interface shows a single, weak C-H vibrational mode at approximately 2960  $\text{cm}^{-1}$  as presented in Figure 6.7. The origin of this peak is attributed to an asymmetric stretch from  $\text{CH}_2$  groups which are perturbed due to electrostatic interactions between the positively charged protonated L-lysine side chains and the negatively charged  $\text{SiO}_2$  surface. However, this assignment is not definitive as previous SFG studies of L-lysine residues did not report this vibrational mode.<sup>4, 12, 24, 33</sup> Additionally, the intensity of the spectral peaks attributed to “ice-like” and “liquid-like” interfacial water species at the  $\text{SiO}_2$

interface are dramatically reduced upon the addition of the peptide. Furthermore, the “ice-like” tetrahedrally coordinated water peak is red shifted by more than  $100\text{ cm}^{-1}$  in the presence of the poly-L-lysine homopeptide. This spectral peak is a strong indication that the presence of the large biomolecule at the hydrophilic solid-liquid interface causes a dramatic reorganization of the water species adsorbed on the silica surface. The  $2960\text{ cm}^{-1}$  vibrational mode observed from poly-L-lysine at the  $\text{SiO}_2$  interface is not present in the SFG spectrum of L-lysine ( $16.5\text{ mg/mL}$ ) in PBS at the same interface as shown in Figure 6.8. In fact, no C-H vibrational modes are resolved for L-lysine amino acid at the hydrophilic  $\text{SiO}_2$  interface. However, the continuum of peaks attributed to interfacial water at approximately  $3200\text{ cm}^{-1}$  and  $3400\text{ cm}^{-1}$  are more than three fold enhanced in the SFG spectrum of L-lysine amino acid when compared to the spectrum of pure PBS. Similar to the case of the poly-L-lysine at the  $\text{SiO}_2$  interface, this change in the signal from interfacial water species demonstrates the structural and conformational sensitivity of adsorbed water molecules to their chemical environment at the hydrophilic solid-liquid interface.

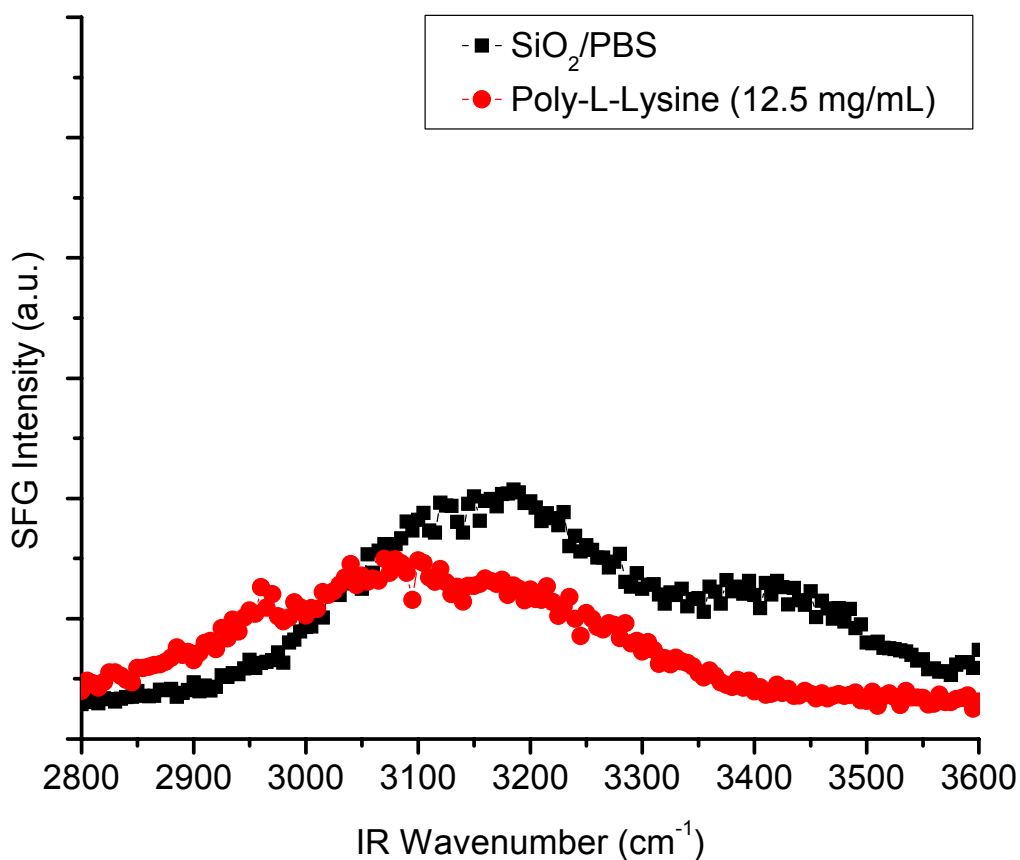
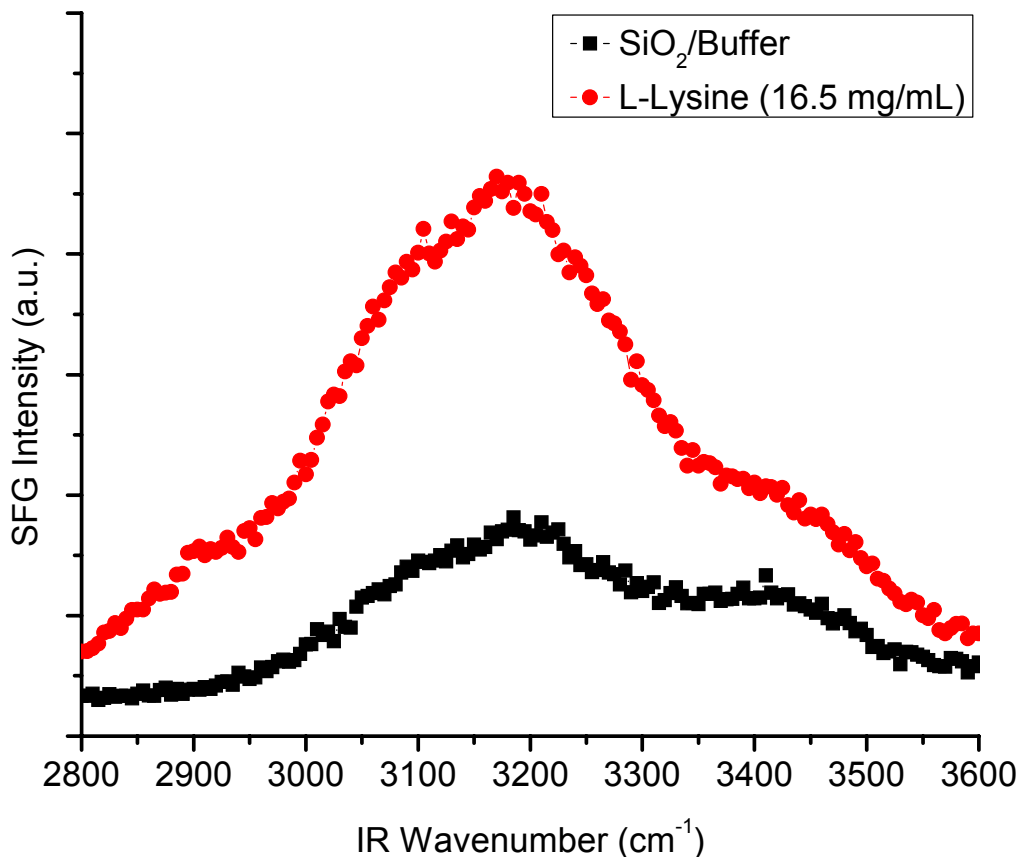
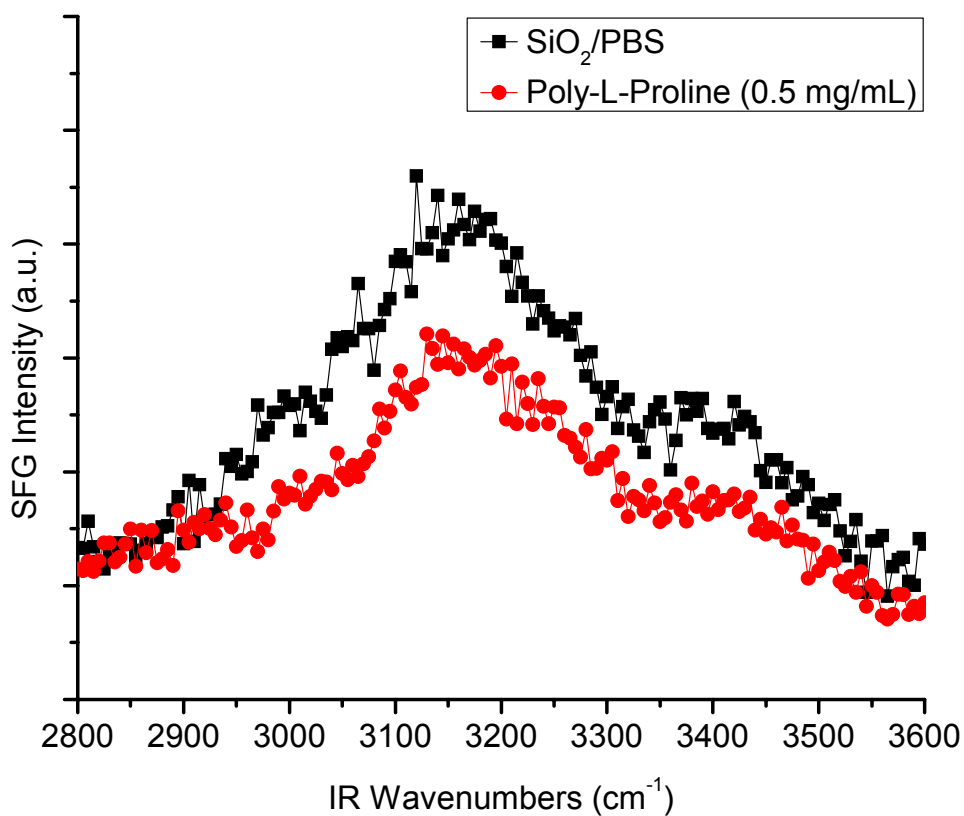


Figure 6.7. The SFG spectrum of the  $\text{SiO}_2/\text{PBS}$  interface before (black squares) and after (red circles) the addition of poly-L-lysine at a concentration of  $12.5\text{ mg/mL}$ . The  $\text{SiO}_2/\text{PBS}$  interfacial water structure shows two very large peaks around  $\sim 3200\text{ cm}^{-1}$  and  $\sim 3400\text{ cm}^{-1}$ , attributed to “ice-like” tetrahedrally and “liquid-like” less than tetrahedrally coordinated hydrogen bonded water, respectively. Upon adsorption of poly-L-lysine, the overall SFG intensity in the water region is reduced, especially around  $3400\text{ cm}^{-1}$ . The C-H vibrational mode seen around  $\sim 2960\text{ cm}^{-1}$  is attributed the asymmetric stretch of highly perturbed methylene groups on the adsorbed poly-L-lysine.



**Figure 6.8.** The SFG spectrum of the SiO<sub>2</sub>/PBS interface before (black squares) and after (red circles) the addition of L-lysine amino acid at a solution concentration of 16.5 mg/mL. The water structure shows two very large peaks around ~3200 cm<sup>-1</sup> and ~3400 cm<sup>-1</sup>, where are attributed to “ice-like” tetrahedrally and “liquid-like” less than tetrahedrally coordinated hydrogen bonded water, respectively. Note the increase in water signal upon L-lysine adsorption.

The SFG spectrum of a solution of poly-L-proline (0.5 mg/mL) in PBS at the SiO<sub>2</sub> interface is presented in Figure 6.9 and does not have any resolvable C-H vibrational modes. However, the intensity of the O-H peaks at 3200 cm<sup>-1</sup> and 3400 cm<sup>-1</sup> present in the spectrum of pure PBS decrease by about a factor of 2 after the addition of the homopeptide. As shown in Figure 6.10, the intensity of these O-H peaks from interfacial water similarly decrease substantially at the silica interface upon the addition of L-proline amino acid (500 mg/mL) to the PBS solution at the hydrophilic interface. Additionally, this spectrum shows a weak C-H vibrational mode at 3000 cm<sup>-1</sup> attributed to a combination of asymmetric stretches from the C<sub>β</sub>H<sub>2</sub> and C<sub>γ</sub>H<sub>2</sub> portions of adsorbed L-proline molecules which are slightly perturbed due to electrostatic interactions with the highly charged SiO<sub>2</sub> surface.



**Figure 6.9.** The SFG spectrum of the SiO<sub>2</sub>/PBS interface before (black squares) and after (red circles) the addition of poly-L-proline at a solution concentration of 0.5 mg/mL. The water structure shows two very broad peaks around ~3200 cm<sup>-1</sup> and ~3400 cm<sup>-1</sup>, attributed to “ice-like” tetrahedrally and “liquid-like” less than tetrahedrally coordinated hydrogen bonded water, respectively. There is little change in the water signal upon poly-L-proline adsorption.

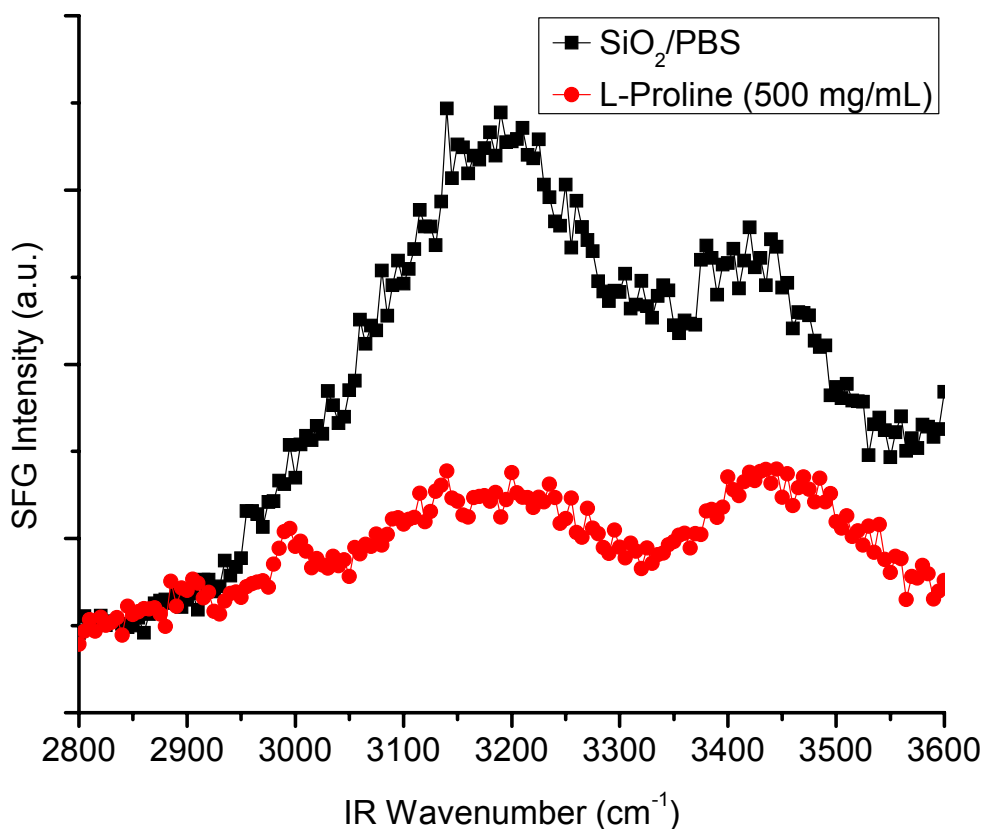


**Figure 6.10.** The SFG spectrum of the SiO<sub>2</sub>/PBS interface before (black squares) and after (red circles) the addition of L-proline amino acid at a solution concentration of 500 mg/mL. One small C-H vibrational mode is observed at ~3000 cm<sup>-1</sup> attributed to a combination of C<sub>β</sub>H<sub>2</sub> and C<sub>γ</sub>H<sub>2</sub> asymmetric stretches and possibly blue-shifted due to interactions with the surface. The water structure shows two very broad peaks around ~3200 cm<sup>-1</sup> and ~3400 cm<sup>-1</sup> which are attributed to “ice-like” tetrahedrally and “liquid-like” less than tetrahedrally coordinated hydrogen bonded water, respectively. There is a decrease in the water signal upon L-proline amino acid adsorption.

### 6.3.3. Discussion of Combined QCM and SFG Results

The broad range of peptide and amino acid solubilities as well as SFG responses for the chemical species studied required that QCM and SFG experiments be conducted over a range of solution concentrations. The experimental data collected in this study can provide definitive information as to whether a monolayer, well organized multilayers, or laterally aggregated clumps were present on the surfaces studied. Nonetheless, it is a reasonable assumption that the bulk concentrations used during SFG and QCM measurements were sufficiently high for the complete coverage of the sample surfaces with adsorbate based solely on geometric arguments. Therefore, the results presented here are interpreted as being free of any constraints imposed by insufficient biomolecule availability to achieve substantial surface adsorption.

While the SFG signal intensity at the hydrophobic solid-liquid interface is approximately one order of magnitude weaker for L-proline than for poly-L-proline, the surface concentration

for the amino acid was determined to be more than an order of magnitude greater by QCM. This finding is unexpected because the SFG intensity is proportional to square of the number density of the surface species.<sup>34</sup> Therefore, this finding can only be interpreted as evidence that L-proline is much less ordered than poly-L-proline at the  $d_8$ -PS/PBS interface. The physical origin of this effect is not clear from these experiments, but is postulated that the decreased ordering of the interfacial L-proline species compared to poly-L-proline at this interface is caused by weak intermolecular forces interactions between the adsorbate and the surface. This would mean that the driving forces for adsorption are probably not due to direct electrostatic or van der Waals attraction forces between the adsorbate and surface. Instead, the extent of ordering exhibited by the interfacial species may be driven by the reorganization of solvent water molecules around both the adsorbates and substrate surface.<sup>35, 36</sup> In the absence of strong intermolecular forces, L-proline is likely to adsorb in a number of different conformations which could explain the SFG data where the amino acid has weak signal and thus appears disordered. Poly-L-proline has many fewer degrees of freedom than the amino acid because of its structural rigidity and thus would be expected to have fewer available conformations when adsorbed on the surface. The case of L-lysine and poly-L-lysine at the hydrophobic  $d_8$ -PS/PBS interface is somewhat different. In this case the SFG intensity of the poly-L-lysine is also greater than the corresponding amino acid by a factor of approximately ten. However, the interfacial concentration of poly-L-lysine measured by QCM is higher than L-lysine meaning that the stronger signal of poly-L-lysine may be due to either a higher interfacial concentration or a higher level of ordering. This data leads to the hypothesis that the driving force for adsorption onto a hydrophobic surface such as polystyrene will be similar for lysine (and poly-L-lysine) and proline (and poly-L-proline). Since the QCM data indicates the surface concentration of L-lysine is approximately only half that of the poly-L-lysine peptide on the  $d_8$ -PS surface, the substantially smaller SFG signal from L-lysine is attributed to both reduced interfacial ordering and a lower surface concentration.

At the hydrophilic SiO<sub>2</sub>/PBS interface, the overall SFG signal from the peptides and amino acids is much lower at the hydrophilic  $d_8$ -PS/buffer interface.<sup>10</sup> The interfacial concentrations of the molecules measured by QCM were not substantially different between the two interfaces. Therefore, the cause of the reduced SFG signal with the SiO<sub>2</sub> substrate is attributed to reduced biomolecule ordering at this interface relative to the hydrophobic  $d_8$ -PS/PBS interface. There is not currently a complete molecular level understanding of why there is less orientational ordering of adsorbates at this SiO<sub>2</sub> interface. However, a possible explanation is that the driving force for adsorption at this interface is dominated by electrostatic interactions between the SiO<sub>2</sub> surface and the solvated biomolecules. This hypothesis is supported by the observation that, unlike the hydrophobic  $d_8$ -PS surface, SiO<sub>2</sub> is negatively charged at pH 7.4 where these experiments were conducted.<sup>32</sup> In such an environment, these short range and relatively strong electrostatic forces could possibly trap adsorbates in the configuration in which they initially adsorb.<sup>37, 38</sup> In contrast to the thermodynamic arguments given in the explanation of the adsorbate behavior at the  $d_8$ -PS surface, it is possible that the relatively slow kinetics of adsorption and desorption processes are primarily responsible for the lack of interfacial ordering of these adsorbates. Interestingly, Paszti and co-workers also did not observe *in-situ* SFG signal of amino acids at the SiO<sub>2</sub>/aqueous interface although their experimental conditions were slightly different and they used the  $P_{\text{SFG}}P_{\text{VIS}}P_{\text{IR}}$  SFG polarization combination instead of the  $S_{\text{SFG}}S_{\text{VIS}}P_{\text{IR}}$  configuration used in this study.<sup>15</sup>

The structure of interfacial water at remains an active area of research and robust debate.<sup>30, 39, 40</sup> The largely featureless SFG spectrum of the hydrophobic  $d_8$ -PS/PBS interface contains only a small, broad signal from a continuum of coordinated O-H modes between 3000-3200  $\text{cm}^{-1}$ . Using the common nomenclature in the field for the  $\text{SiO}_2/\text{H}_2\text{O}$  and air/water interfaces, this peak is assigned as “ordered” water. However, this assignment is not intended to imply the chemical nature of coordinated water at the  $d_8$ -PS/PBS interface is identical to “ice-like” tetrahedrally coordinated water at the  $\text{SiO}_2/\text{water}$  interface. At the hydrophobic  $d_8$ -PS/PBS interface, the SFG spectrum of water does not contain a free O-H mode and it shows minimal intensity around  $\sim 3400 \text{ cm}^{-1}$ .<sup>24</sup> Furthermore, the sensitivity of this hydrophobic solid-liquid interface to contamination makes characterization of the water structure at the  $d_8$ -PS/PBS interface challenging.<sup>41</sup> The SFG spectra from the  $d_8$ -PS/PBS interface in this study are quite similar to the dichloroethane/ $\text{H}_2\text{O}$  interface that has been previously investigated by Richmond and co-workers.<sup>42, 43</sup> In those studies, the water structure observed in the SFG spectra was determined to originate from an increased water penetration in the organic phase, which is unlikely in this study, as well as a general disorder of the water molecules at the interface. Interestingly, the poly-L-lysine and L-lysine results from this study are in dramatic contrast to previous studies on amphiphilic peptides adsorbed on hydrophobic and hydrophilic surfaces.<sup>5, 11, 24, 33</sup> In those earlier studies the hydrophobic portion of the peptides were ordered and observed in the SFG spectra on the hydrophobic  $d_8$ -PS.<sup>11</sup> In this study, the opposite is observed in that both hydrophilic L-lysine and poly-L-lysine biomolecules were found to exhibit ordered hydrocarbon chains on the  $d_8$ -PS surface.

In an earlier SFG study of interfacial biomolecules, an N-H vibrational mode was observed in the spectrum of a 14-residue  $\alpha$ -helical amphiphilic peptide, composed of L-lysine and L-leucine subunits, at the  $\text{SiO}_2/\text{PBS}$  interface.<sup>24</sup> The N-H mode was attributed to either the backbone Amide A of an  $\alpha$ -helix or the terminal amine on the hydrophilic, positively charged L-lysine residues’ side chains. Interestingly, the same vibrational mode is not clearly apparent in the SFG spectra of L-lysine, poly-L-lysine, poly-L-proline, or L-proline on  $\text{SiO}_2$  obtained in this study. Furthermore, a C-H mode is observed in the SFG spectrum of both poly-L-lysine and L-proline amino acid at the  $\text{SiO}_2/\text{PBS}$  interface. These findings are a strong indication that the ordering adsorbed peptides is highly sensitive to the chemical nature of the peptide.

QCM measurements showed a greater mass of L-proline amino acid adsorbed than poly-L-proline on both the hydrophilic and hydrophobic surfaces. This observation could be a result of solvated L-proline species at pH 7.4 being zwitterionic with an overall neutral charge balance thus making possible the formation of stacked layers on the surface because of electrostatic attractions between neighboring amino acids. In contrast, poly-L-proline species do not have this electrostatic driving force because the both amine and acidic portions of each proline unit are replaced with amide bonds along the peptide backbone leaving only the weaker intermolecular forces to drive adsorption and cohesion at the interface. In the case of L-lysine, QCM experiments indicated that its homopeptide, poly-L-lysine, adsorbed more extensively than the amino acid on both the hydrophobic  $d_8$ -PS and the hydrophilic  $\text{SiO}_2$  surfaces. This phenomenon may be explained by both the L-lysine amino acid and the corresponding homopeptide having positively charged side chains in solution at pH 7.4. Subsequently, both the amino acid and homopeptide are expected to experience an increasing number of repulsive electrostatic interactions between the positively charged side chains of neighboring adsorbed species with increasing surface concentration. However, because the molecular mass of an individual poly-L-lysine molecule is orders of magnitude greater than that of an individual L-lysine amino acid it is

reasonable to expect a larger mass of the homopeptide would be bound to on per unit of substrate surface area. While these arguments may explain the observed QCM results on a molecular level, the fact remains that the experimental solution concentration of poly-L-proline was three orders of magnitude smaller than that of L-proline while the solution concentrations of poly-L-lysine and L-lysine were nearly identical.

#### 6.4. Conclusions

This study demonstrated the utility of comparing the adsorption and surface structures of amino acids and their corresponding homopeptides at the hydrophobic polystyrene/PBS and hydrophilic SiO<sub>2</sub>/PBS solid-liquid interfaces using SFG vibrational spectroscopy and QCM. This investigation found that L-lysine, L-proline, and their homopeptides adsorb on polystyrene surfaces and subsequently exhibit sufficient surface ordering to generate SFG signal at the hydrophobic solid/PBS interface. At this biointerface, both poly-L-lysine and poly-L-proline showed higher SFG signal intensity than did their matching amino acid monomers. This trend is interpreted as evidence that the homopeptides exhibit a higher degree of surface ordering than the amino acids at the hydrophobic solid-liquid interface which is likely augmented by the capacity of these peptides to assume organized secondary structures. At the hydrophilic SiO<sub>2</sub>-PBS solid-liquid interface no clear trend was observed establishing a clear relationship between SFG signal intensity and biomolecule chain length or solution concentration. The side function groups of the poly-L-lysine peptides were observed to exhibit interfacial ordering at the hydrophilic SiO<sub>2</sub>/PBS solid-liquid interface while the side functional groups of the poly-L-proline peptides did not. Finally, QCM measurements indicate that the extent to which the poly-L-proline and poly-L-lysine homopeptides adsorb relative to their constituent amino acids on both hydrophilic SiO<sub>2</sub> and hydrophobic polystyrene surfaces depends significantly on the solution concentration of the biomolecules as well as the constituent amino acids' side functional group mass and polarity in solution at pH 7.4.

## References

1. Castner, D. G.; Ratner, B. D., *Surface Science* **2002**, *500* (1-3), 28-60.
2. Kasemo, B., *Current Opinion in Solid State & Materials Science* **1998**, *3* (5), 451-459.
3. Somorjai, G. A.; York, R. L.; Butcher, D.; Park, J. Y., *Physical Chemistry Chemical Physics* **2007**, *9* (27), 3500-3513.
4. York, R. L.; Browne, W. K.; Geissler, P. L.; Somorjai, G. A., *Israel Journal of Chemistry* **2007**, *47* (1), 51-58.
5. Mermut, O.; York, R. L.; Phillips, D. C.; McCrea, K. R.; Ward, R. S.; Somorjai, G. A., *Biointerphases* **2006**, *1* (2), P5-P11.
6. Wang, J.; Clarke, M. L.; Chen, X. Y.; Even, M. A.; Johnson, W. C.; Chen, Z., *Surface Science* **2005**, *587* (1-2), 1-11.
7. Chen, X. Y.; Clarke, M. L.; Wang, J.; Chen, Z., *International Journal of Modern Physics B* **2005**, *19* (4), 691-713.
8. Koffas, T. S.; Amitay-Sadovsky, E.; Kim, J.; Somorjai, G. A., *Journal of Biomaterials Science-Polymer Edition* **2004**, *15* (4), 475-509.
9. Wang, J.; Buck, S. M.; Even, M. A.; Chen, Z., *Journal of the American Chemical Society* **2002**, *124* (44), 13302-13305.
10. Kim, G.; Gurau, M.; Kim, J.; Cremer, P. S., *Langmuir* **2002**, *18* (7), 2807-2811.
11. Phillips, D. C.; York, R. L.; Mermut, O.; McCrea, K. R.; Ward, R. S.; Somorjai, G. A., *Journal of Physical Chemistry C* **2007**, *111* (1), 255-261.
12. Watry, M. R.; Richmond, G. L., *Journal of Physical Chemistry B* **2002**, *106* (48), 12517-12523.
13. Ji, N.; Shen, Y. R., *Journal of Chemical Physics* **2004**, *120* (15), 7107-7112.
14. Kim, J.; Chou, K. C.; Somorjai, G. A., *Journal of Physical Chemistry B* **2002**, *106* (36), 9198-9200.
15. Paszti, Z.; Keszthelyi, T.; Hakkel, O.; Guzzi, L., *Journal of Physics-Condensed Matter* **2008**, *20* (224014), -.
16. Sauerbrey, G., *Zeitschrift Fur Physik* **1959**, *155* (2), 206-222.
17. Marx, K. A., *Biomacromolecules* **2003**, *4* (5), 1099-1120.
18. Rodahl, M.; Kasemo, B., *Review of Scientific Instruments* **1996**, *67* (9), 3238-3241.
19. Arnau, A., *Sensors* **2008**, *8* (1), 370-411.
20. Rodahl, M.; Kasemo, B., *Sensors and Actuators a-Physical* **1996**, *54* (1-3), 448-456.
21. Bain, C. D.; Davies, P. B.; Ong, T. H.; Ward, R. N.; Brown, M. A., *Langmuir* **1991**, *7* (8), 1563-1566.
22. Lambert, A. G.; Davies, P. B.; Neivandt, D. J., *Applied Spectroscopy Reviews* **2005**, *40* (2), 103-145.
23. York, R. L.; Li, Y. M.; Holinga, G. J.; Somorjai, G. A., *Journal of Physical Chemistry A* **2009**, *113* (12), 2768-2774.
24. Mermut, O.; Phillips, D. C.; York, R. L.; McCrea, K. R.; Ward, R. S.; Somorjai, G. A., *Journal of the American Chemical Society* **2006**, *128* (11), 3598-3607.
25. Reva, I. D.; Stepanian, S. G.; Plokhotnichenko, A. M.; Radchenko, E. D.; Sheina, G. G.; Blagoi, Y. P., *Journal of Molecular Structure* **1994**, *318*, 1-13.
26. Burge, R. E.; Mcgavin, S.; Harrison, P. M., *Acta Crystallographica* **1962**, *15* (Sep), 914-&.
27. Cowan, P. M.; Mcgavin, S., *Nature* **1955**, *176* (4480), 501-503.

28. Adzhubei, A. A.; Sternberg, M. J. E., *Journal of Molecular Biology* **1993**, 229 (2), 472-493.
29. Arnott, S.; Dover, S. D., *Acta Crystallographica Section B-Structural Crystallography and Crystal Chemistry* **1968**, B 24, 599-&.
30. Shen, Y. R.; Ostroverkhov, V., *Chemical Reviews* **2006**, 106 (4), 1140-1154.
31. Miranda, P. B.; Shen, Y. R., *Journal of Physical Chemistry B* **1999**, 103 (17), 3292-3307.
32. Yeganeh, M. S.; Dougal, S. M.; Pink, H. S., *Physical Review Letters* **1999**, 83 (6), 1179-1182.
33. York, R. L.; Mermut, O.; Phillips, D. C.; McCrea, K. R.; Ward, R. S.; Somorjai, G. A., *J. Phys. Chem. C* **2007**, 111 (25), 8866-8871.
34. Shen, Y. R., *Nature* **1989**, 337 (6207), 519-525.
35. Wahlgren, M.; Arnebrant, T., *Trends in Biotechnology* **1991**, 9 (6), 201-208.
36. Chandler, D., *Nature* **2005**, 437 (7059), 640-647.
37. Shaffer, J. S.; Chakraborty, A. K.; Tirrell, M.; Davis, H. T.; Martins, J. L., *Journal of Chemical Physics* **1991**, 95 (11), 8616-8630.
38. Chakraborty, A. K.; Shaffer, J. S.; Adriani, P. M., *Macromolecules* **1991**, 24 (18), 5226-5229.
39. Tian, C. S.; Shen, Y. R., *Physical Review Letters* **2008**, 101 (13), -.
40. Sovago, M.; Campen, R. K.; Wurfel, G. W. H.; Muller, M.; Bakker, H. J.; Bonn, M., *Physical Review Letters* **2008**, 101 (13), -.
41. Seo, Y. S.; Satija, S., *Langmuir* **2006**, 22 (17), 7113-7116.
42. Walker, D. S.; Brown, M.; McFearin, C. L.; Richmond, G. L., *Journal of Physical Chemistry B* **2004**, 108 (7), 2111-2114.
43. Walker, D. S.; Moore, F. G.; Richmond, G. L., *Journal of Physical Chemistry C* **2007**, 111 (16), 6103-6112.

## Chapter 7

### **A SFG and QCM Investigation of the Influence of Temperature, Concentration, Competitive Adsorption, Amino Acid Residue Structure, Electrical Bias, and Equilibration Time on the Adsorption and Interfacial Organization of Several Amino Acids and Peptides**

This chapter focuses on a number of exploratory sum frequency generation (SFG) vibrational spectroscopy and quartz crystal microbalance (QCM) studies of biological molecules at model liquid-solid interfaces. Specifically, these investigations explored the influence of several important experimental parameters including temperature, concentration, competitive adsorption, amino acid residue structure, electrical bias, and equilibration time on the adsorption and interfacial organization of several amino acids and peptides. The research findings included herein provide insights and perspectives about several exciting and promising future directions for research at the solid-liquid biointerface.

#### **7.1. Introduction**

This chapter is unique in that it is written to provide experimental evidence for the influence of a broad range variables typically fixed in the SFG and QCM study of a biointerface system. Specifically, the role of interfacial temperature, chemical equilibration time, biomolecule concentration and diversity, electrical surface bias, and peptide primary structure are explored as they pertain to the adsorption and interfacial organization of several biomolecules at the liquid-solid interface. Additionally, the data included from these studies provide insights about the displacement and coadsorption of amino acids on model surfaces and new methods for monitoring these fundamentally important processes. Furthermore, a portion of this research includes evidence for the formation of amino acid monolayers on both a hydrophilic and a hydrophobic model surface in solution and under physiological conditions. Other experimental studies included in this chapter provide data suggesting that the SFG spectrum obtained from an amino acid solution at the liquid-solid interface can vary significantly with the amount of time elapsed between the addition of the biomolecules and collection of SFG data. This chapter also provides new data indicating that the signal strength of SFG active vibrational modes from an adsorbed amino acid may be strongly influenced by a change in interfacial temperature of only 10 °C. Additional experiments included herein produced evidence for the SFG activity of a collagen-like model peptide under physiological conditions. This finding is particularly important and biologically relevant as collagen is commonly found in nature including the skin, muscle, bone, and organ tissues of humans and other mammals. Finally, this chapter includes SFG spectra of the Pt electrode surface under aqueous conditions as a function of electrode bias in the presence of H<sub>2</sub>O, phosphate buffered saline (PBS), and L-arginine amino acid. In conclusion, these studies provided several surprising and important results that provide evidence for new and exciting approaches for future research projects in biological surface science.

## 7.2. Experimental

### 7.2.1. QCM Experimental Measurements

Quartz crystal microbalance experiments in these studies were carried out using a commercial Q-sense (Glen Burnie, MD) model E4 QCM instrument. The resonance and dissipation values of each individual sensor crystal was measured and recorded in pure phosphate buffered saline (PBS) solution at pH 7.4 at the beginning of each QCM experiment. During the entire measurement process for each experiment, the fundamental, 3<sup>rd</sup>, 5<sup>th</sup>, and 7<sup>th</sup> harmonic frequencies and dissipations were monitored at approximately 5 MHz, 15 MHz, 25 MHz, and 35 MHz, respectively. After a stable baseline value for sensor each resonance frequency and dissipation in PBS was established, the sensor crystals were then exposed to solutions of biomolecules dissolved in PBS. Data collection was performed inside a temperature controlled QCM measurement chamber maintained at a constant temperature to within  $\pm 0.1$  °C. Biomolecule surface concentrations were determined from the experimentally measured 3<sup>rd</sup> harmonic frequency data using the Sauerbrey relationship.<sup>1</sup> A detailed theoretical background for the QCM technique and a description of the Q-sense QCM instrument, sensor crystals, and specific experimental procedures implemented in these experiments are provided in Chapter 4.<sup>2-6</sup>

### 7.2.2. SFG Experimental Measurements

Sum Frequency Generation (SFG) experiments were conducted using a 20 Hz pulsed Continuum (Santa Clara, CA) Leopard D-20 Nd:YAG laser with a 1064 nm output at 22 picosecond pulse widths. This near-infrared laser output was then passed through a Laservision (Bellevue, WA) Optical Parametric Generator (OPG)/Optical Parametric Amplifier (OPA) optical system producing a 532 nm visible beam and a tunable infrared beam with an output of 2800 - 3600  $\text{cm}^{-1}$ . Both of these beams were directly used in SFG measurements at energies of approximately 200  $\mu\text{J}$  per pulse. Equilateral prism sample substrates made of fused  $\text{SiO}_2$  were utilized at experimental beam orientations of 65° (visible) and 42° (infrared) off surface normal. These angles were specifically implemented to maximize the collection of SFG signal generated at the liquid-solid interface while minimizing wavelength dependent fluctuations of Fresnel coefficients due to the varying index of refraction of  $\text{H}_2\text{O}$  in the mid-infrared frequency region.<sup>7</sup> The prism substrates were set on top of a PBS/biomolecule solution filled Viton o-ring which was then placed in a clean Petri dish to prevent solvent evaporation and contamination during measurement. The Petri dish rested on top of an aluminum block that could be heated and cooled as necessary using a temperature controlled water bath allowing the collection of SFG spectra at temperatures other than room temperature. During experiments, the SFG signal generated at the solution-prism interface was detected by a photomultiplier tube before being processed and recorded on a desktop computer. All SFG measurements were conducted in the  $S_{\text{SFG}}S_{\text{VIS}}P_{\text{IR}}$  laser beam polarization combination. A detailed theoretical background of the SFG process is provided in Chapter 2,<sup>8</sup> and a description of the Laservision OPG/OPA system and the experimental SFG sample substrate arrangement are provided in Chapter 3.

### 7.2.3. Chemicals

All QCM and SFG experiments were conducted at pH 7.4 and solutions were made with phosphate buffered saline (PBS) (Sigma-Aldrich). Amino acids investigated were purchased from Sigma-Aldrich and were directly used as received. The collagen-like peptide, Ac-(PPG)<sub>4</sub>-NH<sub>2</sub>, was synthesized using by previous members of the Somorjai Group solid-phase peptide synthesis and details of this common synthetic technique can be found elsewhere.<sup>9</sup>

### 7.2.4. Sample Surface Preparation

QCM measurements were performed utilizing gold and SiO<sub>2</sub> coated Q-Sense (Glen Burnie, MD) sensors. Prior to each experiment, the QCM sensor crystals were cleaned with a Herrick (Ithaca, NY) O<sub>2</sub> plasma cleaner for 60 s (18 W RF, 200 mtorr O<sub>2</sub>) to remove organic surface contaminants. Additionally, plasma treatment was utilized to also ensure full oxidation of the SiO<sub>2</sub> coated QCM sensor crystal surfaces. After O<sub>2</sub> plasma treatment, the SiO<sub>2</sub> coated sensor crystals were used directly while gold coated sensor crystal surfaces were coated with hydrophobic polystyrene (PS) thin films. The PS surfaces were prepared on the clean gold coated QCM crystals by spin coating with a 2 % weight solution of polystyrene (MW ≈ 280,000) (Aldrich) in toluene (Sigma-Aldrich). The spin-coating procedure was conducted utilizing a Specialty Coating Systems (Indianapolis, IN) instrument operated at 3000 rpm for 45 s. The resulting PS thin films were then annealed for 12 hours at a temperature of 120 °C to ensure surface flatness and to remove any residual toluene solvent from the spin coating solution. Ellipsometry measurements and atomic force microscopy (AFM) were conducted on the annealed, PS coated QCM sensor crystals. The resulting thin films on the sensor surfaces were determined to have ~95 nm thicknesses.

SFG sample substrates were prepared from fused SiO<sub>2</sub> equilateral prisms which were soaked for 12 hours in a solution of concentrated H<sub>2</sub>SO<sub>4</sub> (97%) (Sigma-Aldrich) and Nochromix (Godax) to remove organic surface contaminants. Next, the SiO<sub>2</sub> prism substrates were washed with distilled, de-ionized water prior to being cleaned using an O<sub>2</sub> plasma treatment as previously described for the QCM sensor crystals. Deuterated *d*<sub>8</sub>-polystyrene (*d*<sub>8</sub>-PS) thin films were prepared on the SFG prism substrate surfaces by spin-coating 3 % weight solution of *d*<sub>8</sub>-PS (MW ≈ 300,000) (Polymer Source) dissolved in toluene (Sigma-Aldrich). The spin-coating and annealing procedures conducted for the SFG substrates were identical to those used for the QCM sensors. The thickness of the *d*<sub>8</sub>-PS films on the SFG substrates were determined to be ~105 nm by AFM and ellipsometry.

## 7.3. Results and Discussion

### 7.3.1. SFG Investigation of Amino Acid Coadsorption on Hydrophilic and Hydrophobic Surfaces

SFG vibrational spectroscopy was utilized to investigate the competitive adsorption and interfacial organization of solutions of two amino acids at the hydrophilic SiO<sub>2</sub> and hydrophobic *d*<sub>8</sub>-polystyrene (*d*<sub>8</sub>-PS) surfaces. The goal of this study was to observe a difference in the SFG

spectrum of an individual amino acid species before and after the addition of another amino acid species and to potentially explain any spectral differences using arguments based on surface-adsorbate and adsorbate-adsorbate affinities. L-arginine and L-proline amino acids were first selected for this displacement and coadsorption study due to their differing chemical nature (L-arginine is polar and hydrophilic while L-proline is more hydrophobic and non-polar)<sup>10</sup> and differing SFG spectra as presented in Figure 7.1 at the hydrophobic  $d_8$ -PS/PBS interface. The SFG spectra of L-arginine and L-proline at the hydrophobic solid-liquid interface both show vibrational modes at  $2850\text{ cm}^{-1}$ ,  $2870\text{ cm}^{-1}$ , and  $2935\text{ cm}^{-1}$ , and an additional mode unique to L-proline is observed at  $2990\text{ cm}^{-1}$  as explained in detail in Chapter 5.

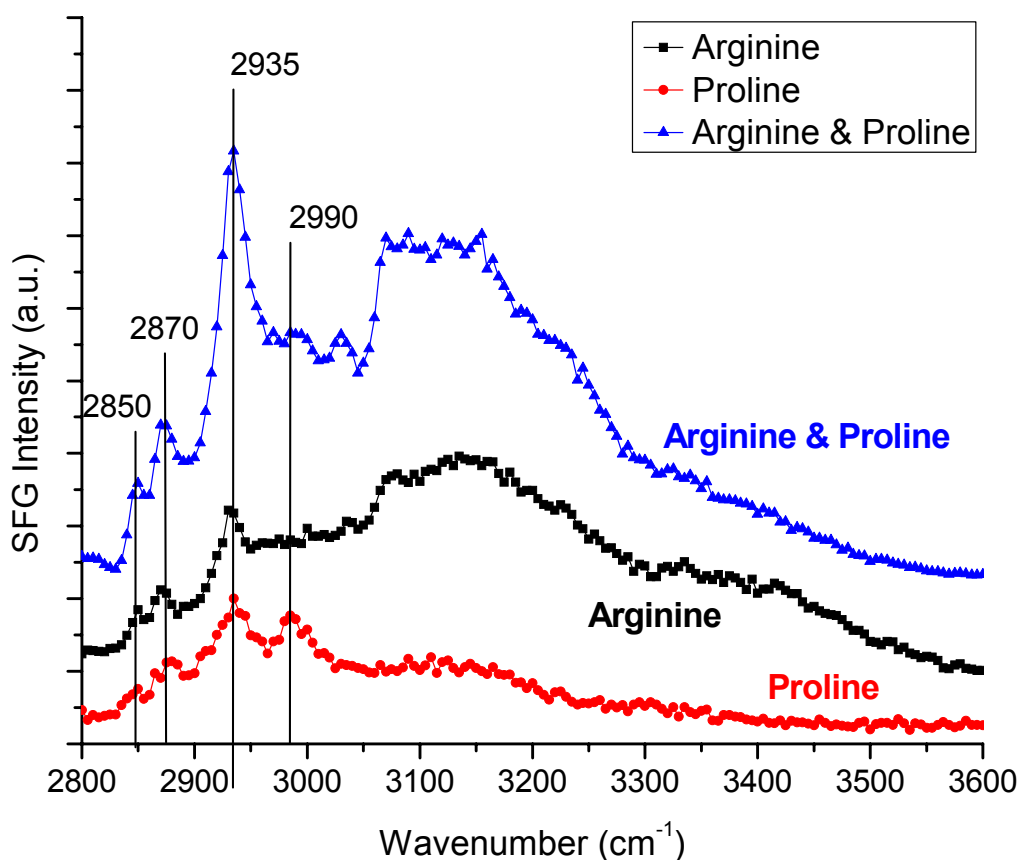


Figure 7.1. SFG spectrum of the hydrophobic  $d_8$ -PS/PBS interface in the presence of pure L-proline (red circles), pure L-arginine (back squares), and an equal concentration mixture of L-proline and L-arginine (blue triangles). While both proline and arginine show C-H vibrational modes at  $2850\text{ cm}^{-1}$ ,  $2870\text{ cm}^{-1}$ , and  $2935\text{ cm}^{-1}$ , proline has an additional and unique spectral feature centered at  $2990\text{ cm}^{-1}$  respectively. The spectra included in this plot are not to scale relative to each other and are intended only for qualitative comparison.

The SFG spectrum of the  $d_8$ -PS/PBS interface in the presence of only L-arginine shows three C-H vibrational modes as presented in Figure 7.2. Subsequently, when L-proline amino acid was added to the system the SFG intensity of the three peaks are dramatically enhanced from their initial levels and a fourth vibrational mode at  $2990\text{ cm}^{-1}$  is observed indicating the

presence of interfacial L-proline species. The origin of this dramatic SFG signal enhancement is not clear as either a higher interfacial concentration or ordering of either or both amino acids could be responsible for this phenomenon. When the SFG experiment was conducted first only with L-proline and then with a mixture of L-proline and L-arginine, a similar but less dramatic SFG signal enhancement was observed in the latter case as presented in Figure 7.3. However, in this case the  $2990\text{ cm}^{-1}$  vibrational mode from L-proline was present in both scans. This observation indicates that while the presence of the second amino acid enhances the overall SFG signal, the addition of L-arginine does not result in the complete displacement of the initially adsorbed L-proline species from the  $d_8$ -PS surface. This result is not surprising as the more hydrophobic L-proline species would be expected to adsorb more strongly to the hydrophobic surface and thus be harder to displace than L-arginine would be. While these findings provide some insight into the nature of amino acid adsorption, the relative similarity between the SFG vibrational spectra of L-arginine and L-proline makes a more thorough spectral analysis prohibitively challenging.

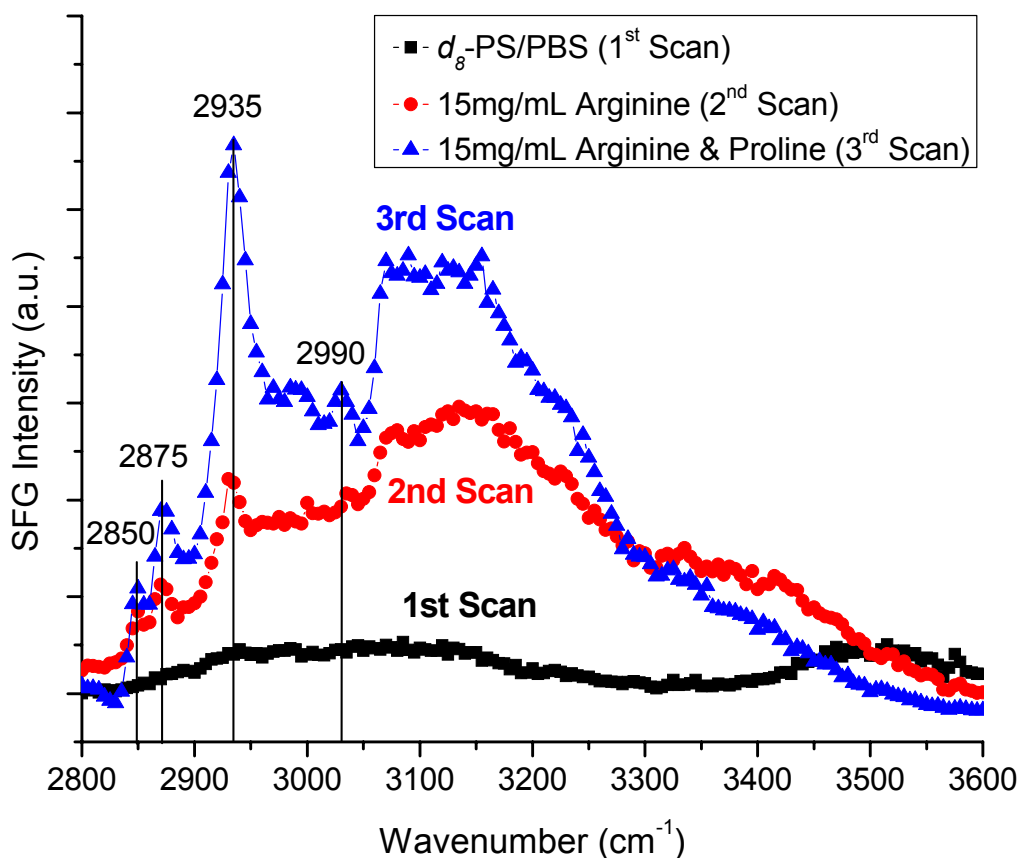


Figure 7.2. SFG spectrum of the hydrophobic  $d_8$ -PS/PBS interface in the presence of pure PBS (black squares), with 15 mg/mL L-arginine (red circles), and subsequently an equal concentration mixture (both 15 mg/mL) of L-proline and L-arginine (blue triangles). The spectrum of L-arginine shows C-H vibrational modes at  $2850\text{ cm}^{-1}$ ,  $2870\text{ cm}^{-1}$ , and  $2935\text{ cm}^{-1}$ , which is enhanced in magnitude upon the addition of L-proline. Also, the presence of L-proline is accompanied by an additional spectral feature centered at  $2990\text{ cm}^{-1}$  from the amino acid's strained five member ring. These spectra provide show that the addition of a second amino acid increases SFG signal and is suggestive of coadsorption of both amino acids on the hydrophobic surface.

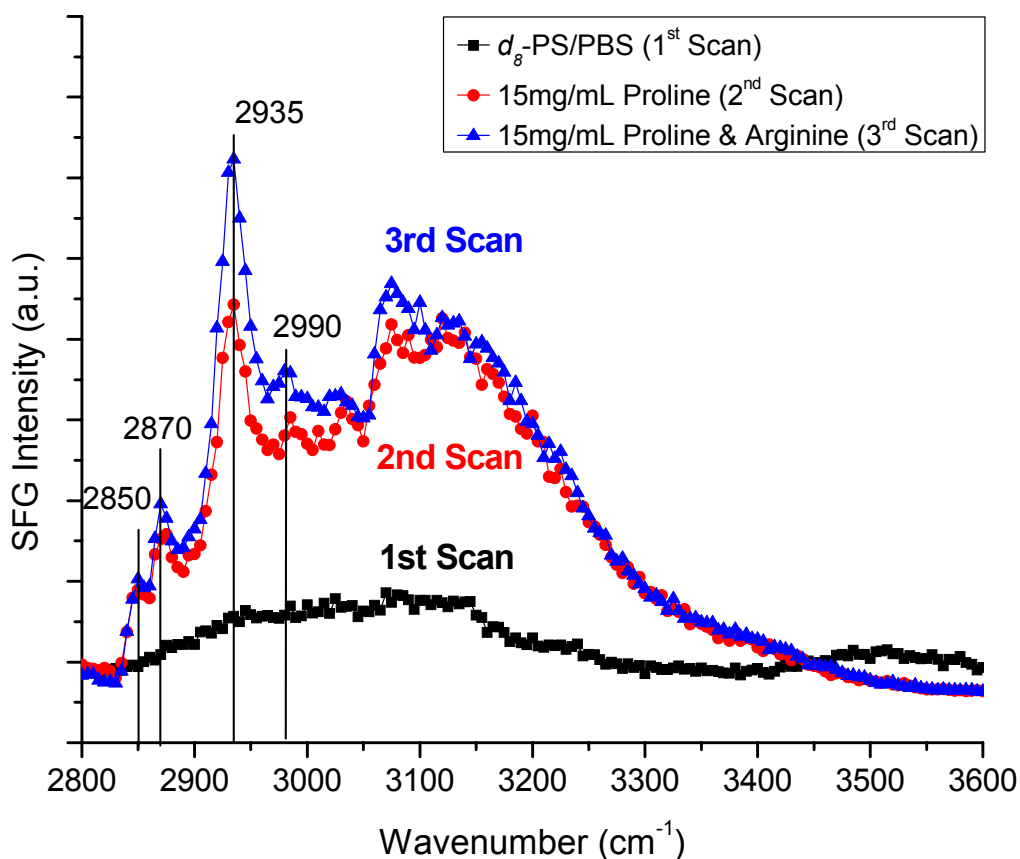


Figure 7.3. SFG spectrum of the hydrophobic  $d_8$ -PS/PBS interface in the presence of pure PBS (black squares), with L-proline at 15 mg/mL (red circles), and subsequently a solution of equal concentrations of L-proline and L-arginine at 15 mg/mL (blue triangles). The spectrum of L-proline shows C-H vibrational modes at 2850  $\text{cm}^{-1}$ , 2870  $\text{cm}^{-1}$ , 2935  $\text{cm}^{-1}$ , and 2990  $\text{cm}^{-1}$ . The SFG spectrum is enhanced a small amount upon the addition of L-arginine, but not as much as when the order of addition is reversed. The presence of L-arginine does not eliminate the L-proline peak at 2990  $\text{cm}^{-1}$  from the spectrum suggesting the coadsorption of both amino acids on the hydrophobic surface in this case.

Several similar SFG experiments with L-proline and L-arginine were conducted at the hydrophilic  $\text{SiO}_2$ /PBS interface as shown in Figures 7.4 and 7.5. The SFG spectrum of the pure  $\text{SiO}_2$ /PBS interface is presented in Figure 7.4 and spectral features from “ice-like” tetrahedrally coordinated and “liquid-like” less than tetrahedrally coordinated interfacial water are observed.<sup>7, 11-13</sup> Upon the addition of L-proline, the intensity of these O-H vibrational modes from water decrease suggesting the disruption and/or the displacement of the surface water molecules by the presence adsorbed L-proline. However, after the subsequent addition of the polar, hydrophilic L-arginine amino acid these vibrational modes from interface water are restored and enhanced in the SFG spectrum to levels well above those observed with pure PBS.<sup>10</sup> This observation is suggestive of the solvated L-arginine restoring the organization of interfacial water and perhaps increasing its surface concentration. Such a phenomenon is expected to be accompanied by a displacement of some or all of the adsorbed L-proline amino acid from the hydrophilic surface.

When the reverse experiment was conducted where first L-arginine was added to the PBS/SiO<sub>2</sub> interface before L-proline as presented in Figure 7.5. In this case, the presence of L-arginine slightly enhances the SFG signal from interfacial water above background levels and subsequently remains unchanged with the introduction of L-proline. This finding may be an indication that the L-arginine seeds the organization of interfacial water and has a higher affinity for the negatively charged SiO<sub>2</sub> surface at pH 7.4 than the L-proline,<sup>14</sup> but further experiments are needed to support this hypothesis.

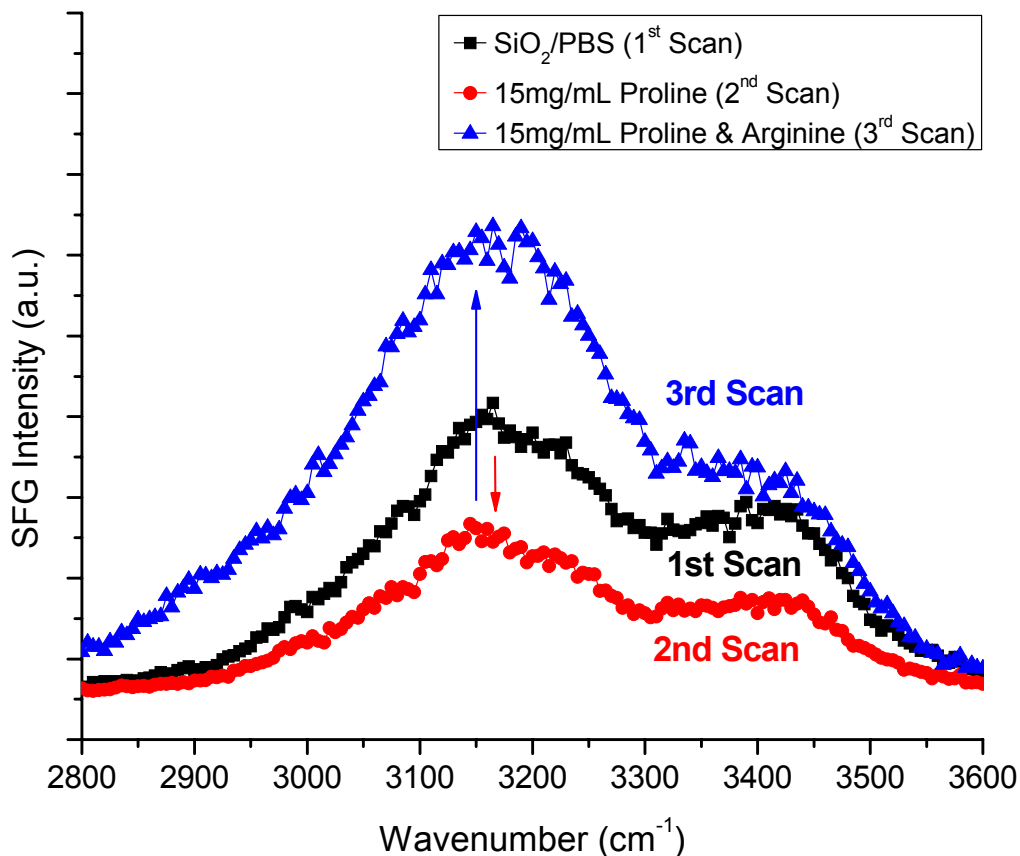


Figure 7.4. SFG spectrum of the hydrophilic SiO<sub>2</sub>/PBS interface in the presence of pure PBS (black squares), with L-proline at 15 mg/mL (red circles), and an equal concentrations mixture of L-proline and L-arginine at 15 mg/mL (blue triangles). The spectrum of L-proline shows a decrease in the SFG intensity from the O-H vibrational modes of interfacial water at ~3200 cm<sup>-1</sup> and ~3400 cm<sup>-1</sup> from background levels. After the addition of L-arginine, the SFG signal from these water peaks is enhanced above initial levels suggesting an increase in the order and/or the concentration of interfacial H<sub>2</sub>O molecules.

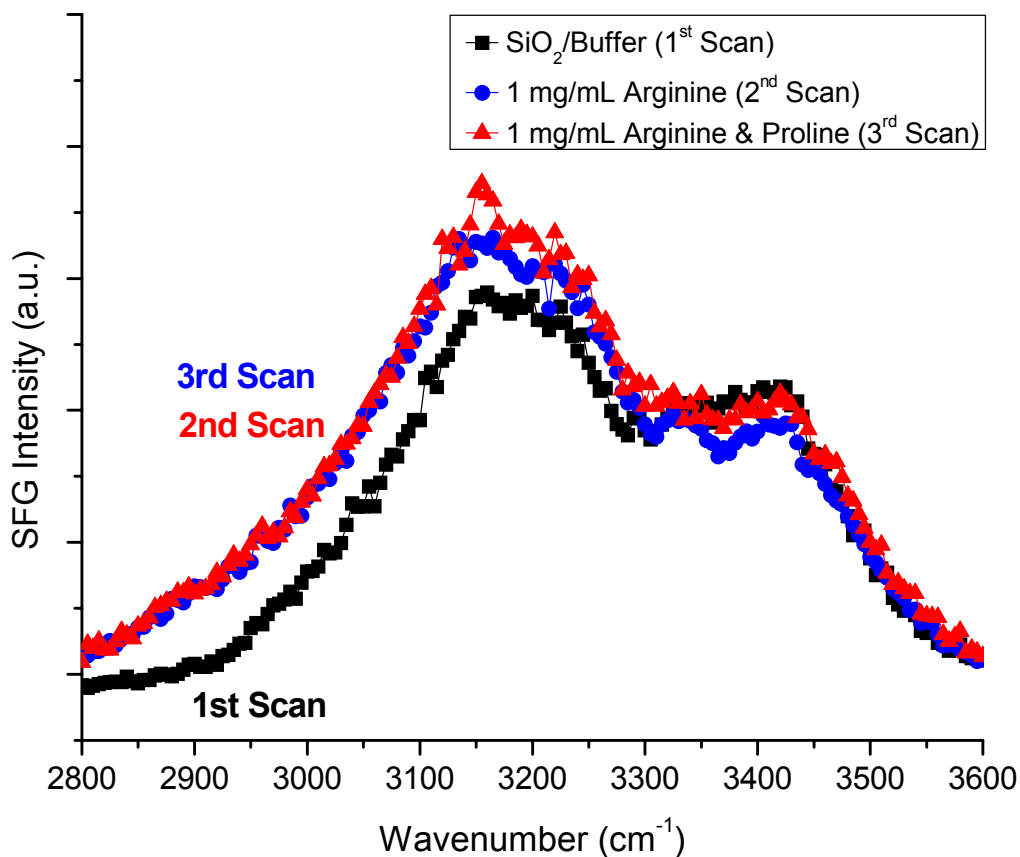


Figure 7.5. SFG spectrum of the hydrophilic SiO<sub>2</sub>/PBS interface in the presence of pure PBS (black squares), with L-arginine amino acid at 1 mg/mL (red circles), and an equal concentration mixture of L-arginine and L-proline both at 1 mg/mL (blue triangles). The spectrum of L-arginine shows a slight increase in the SFG intensity from the O-H vibrational modes of interfacial water at ~3200 cm<sup>-1</sup> and ~3400 cm<sup>-1</sup> from background levels. After the addition of L-proline, the SFG signal from these water peaks remains unchanged. This observation suggests L-proline amino acid has a minimal influence on the order and/or concentration of interfacial H<sub>2</sub>O molecules in the presence of L-arginine.

While these experiments provide some evidence that the coadsorption and displacement of one amino acid species by another may be monitored by SFG at the liquid-solid interface, the relatively small differences in the vibrational spectra presented show more technique sensitivity may be necessary for further investigation. However, this experimental challenge may overcome at the hydrophobic *d*<sub>8</sub>-PS/PBS interface by the substitution of L-phenylalanine amino acid for L-proline as demonstrated in Figure 7.6. In this case, the use of L-phenylalanine is spectrally advantageous due to its distinct  $\nu_2$  vibrational mode from its aromatic ring centered at 3070 cm<sup>-1</sup>.<sup>15, 16</sup> While less conclusive than at the hydrophobic surface, this substitution of L-phenylalanine for L-proline may also be made at the hydrophilic SiO<sub>2</sub>/PBS interface as presented in Figure 7.7. In this plot, the presence of L-phenylalanine is found to decrease the SFG signal from interfacial water below initial levels observed in pure PBS. Upon the subsequent addition of L-arginine, the water signal is restored to background levels supporting the hypothesis that L-

arginine may induce an organized restructuring of interfacial water at the hydrophilic SiO<sub>2</sub>/PBS interface. This argument is supported by analogous QCM experiments conducted at 5 mg/mL solution concentrations which found the total adsorbed mass on the SiO<sub>2</sub> surface increased from background levels upon the introduction of L-phenylalanine and again upon introduction of a mixture of L-arginine and L-phenylalanine. These exploratory experimental findings provide evidence that further study of a two amino acid/adsorbate system may prove a rich, model biointerface for examining physiologically important processes such as the Vroman effect which involves selective displacement and coadsorption of peptides and proteins in the body.<sup>17, 18</sup>

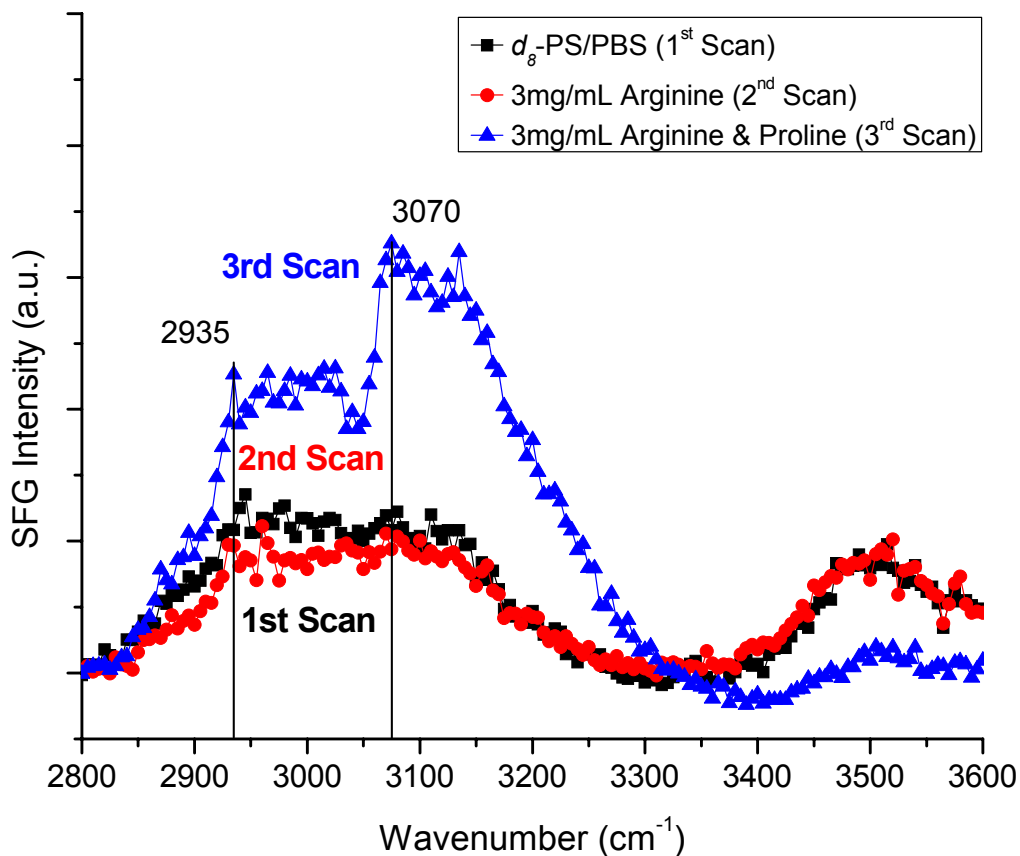
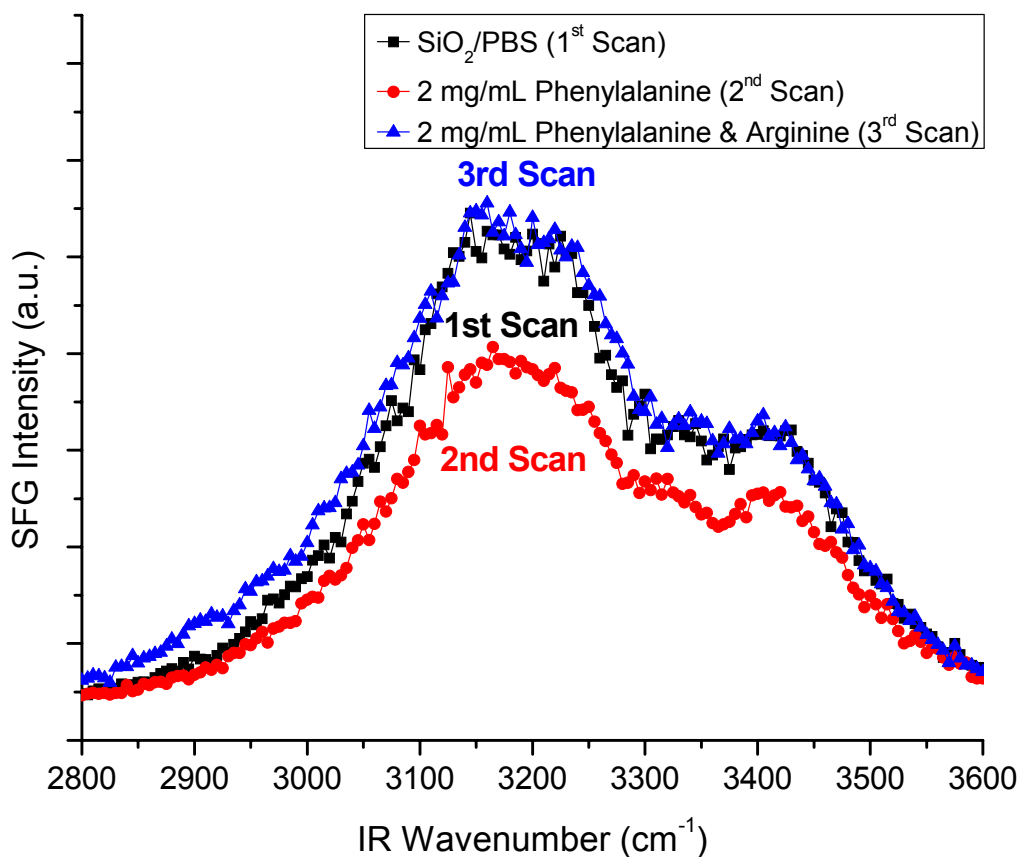


Figure 7.6. SFG spectrum of the hydrophobic *d*<sub>8</sub>-PS/PBS interface in the presence of pure PBS (black squares), L-arginine (red circles) at 3 mg/mL concentration, and an equal concentration mixture of L-arginine and L-phenylalanine both at 3 mg/mL (blue triangles). The spectrum of L-arginine shows a minimal change in the SFG intensity in the C-H vibrational region. However, after the addition of L-phenylalanine the distinctive  $\nu_2$  vibrational mode from the amino acid's five member ring become strongly apparent at a frequency of 3070 cm<sup>-1</sup> indicating the utility of L-phenylalanine as an SFG active amino acid surface marker.



**Figure 7.7.** SFG spectrum of the hydrophilic SiO<sub>2</sub>/PBS interface in the presence of pure PBS (black squares), with 2 mg/mL L-phenylalanine (red circles), and an equal concentration mixture of L-arginine and L-phenylalanine both at 2 mg/mL (blue triangles). The spectrum of L-phenylalanine shows a decrease in the SFG intensity from the O-H vibrational modes of interfacial water at ~3200 cm<sup>-1</sup> and ~3400 cm<sup>-1</sup> from background levels indicating a disruption in the organization of interfacial water on the SiO<sub>2</sub> surface. This disruption is subsequently reversed after the addition of L-arginine suggesting the presence of the highly polar amino acid reorganizes the interfacial water back into its original conformation prior to the addition of biomolecules.

### 7.3.2. Langmuir-Type Adsorption Behavior of Amino Acids as a Function of Side Chain, Solution Concentration, and Interface Character

A QCM study was conducted to investigate whether or not three amino acids will adsorb on model hydrophilic and hydrophobic surfaces in well-ordered monolayers or poorly organized surface films. Specifically, the deposition of L-leucine, L-proline, and L-arginine from PBS solutions at pH 7.4 was quantified by QCM as a function of amino acid solution concentration on hydrophilic SiO<sub>2</sub> and hydrophobic polystyrene (PS) surfaces. These three amino acids were specifically chosen as representatives of the broad spectrum of hydrophilic and hydrophobic amino acids found in nature. L-proline was selected for this study because of its moderate hydrophilic/hydrophobic nature while L-arginine and L-leucine were chosen for their strong

hydrophilic and hydrophobic natures, respectively.<sup>19</sup> In the case of the highly polar L-arginine on the hydrophilic SiO<sub>2</sub>, a relationship between the amount of amino acid adsorbed and amino acid solution concentration was found to be non-linear overall as shown in Figure 7.8. However, the amount of L-arginine adsorbed on the SiO<sub>2</sub> surface was found to increase linearly in two separate sub-regions: the lower concentration range of 0.5 - 3 mg/mL (Regime 1), and the higher concentration range of 3 - 10 mg/mL (Regime 2). This finding is suggestive of Langmuir-type adsorption behavior at low concentrations where adsorption events happen primarily at open surface sites until a monolayer is apparently formed at a solution concentration of 3 mg/mL and a surface concentration of  $57 \pm 8$  ng/cm<sup>2</sup>.<sup>20, 21</sup> Following apparent monolayer formation, the thermodynamically preferable adsorption of L-arginine species is no longer possible and the amount of amino acid adsorbed on top of the bimolecular monolayer increases linearly but at a lower rate than observed at lower surface coverage.

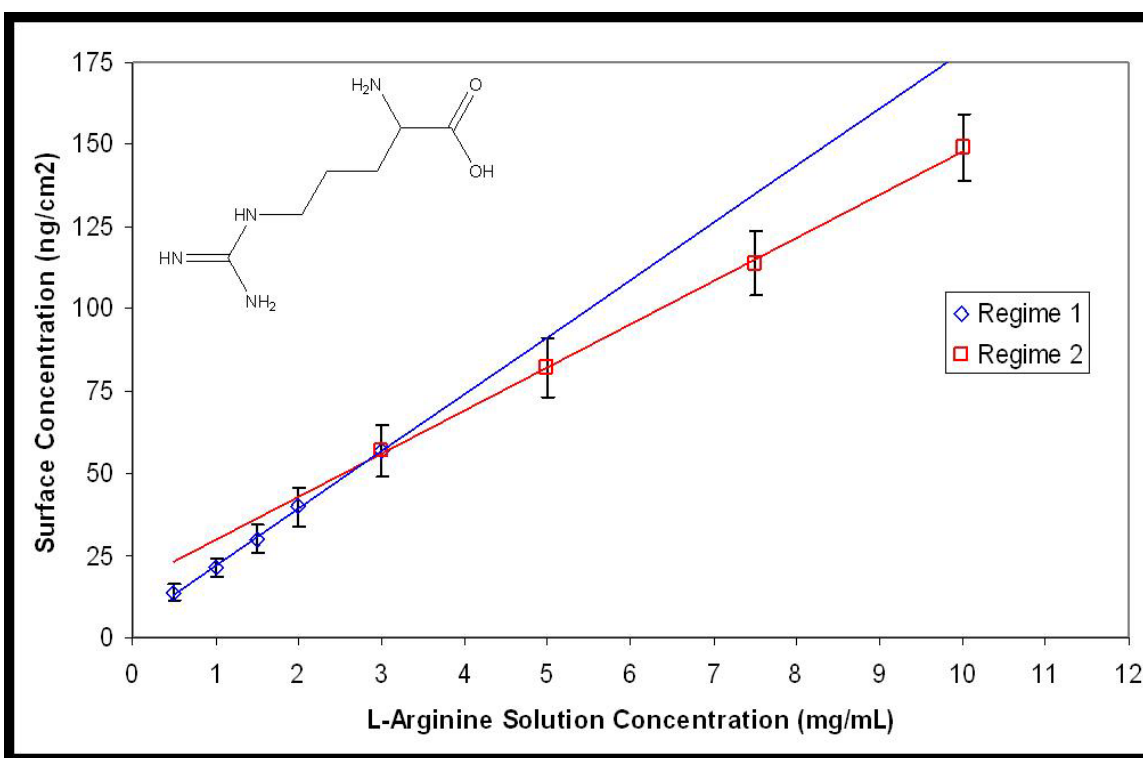


Figure 7.8. QCM data of L-arginine adsorption on the hydrophilic SiO<sub>2</sub> surface as a function of amino acid concentration in PBS at pH 7.4 and 24 °C. Isotherm-like behavior suggests L-arginine monolayer formation at a surface density of  $\sim 57$  ng/cm<sup>2</sup> and solution concentration of 3 mg/mL on the SiO<sub>2</sub> surface.

The hydrophobic L-leucine amino acid shows a bimodal adsorption behavior at the hydrophobic PS-PBS interface as presented in Figure 7.9 which is similar to the case of L-arginine at the hydrophilic SiO<sub>2</sub>/PBS interface. At lower solution concentrations ranging from 0.5 - 2 mg/mL in PBS the amount of L-leucine adsorbed on the hydrophobic surface grows linearly (Regime 1). However, at the higher L-leucine concentration range of 2 - 10 mg/mL in PBS, the relationship between amino acid solution concentration and PS surface coverage also increases linearly but at a lesser rate than before (Regime 2). Similar to the case of L-arginine at the SiO<sub>2</sub> surface, the QCM data from L-leucine adsorption at the hydrophobic PS surface is

suggestive of a monolayer formation at a solution concentration of 2 mg/mL in PBS and a surface concentration of  $41 \pm 5 \text{ ng/cm}^2$ .

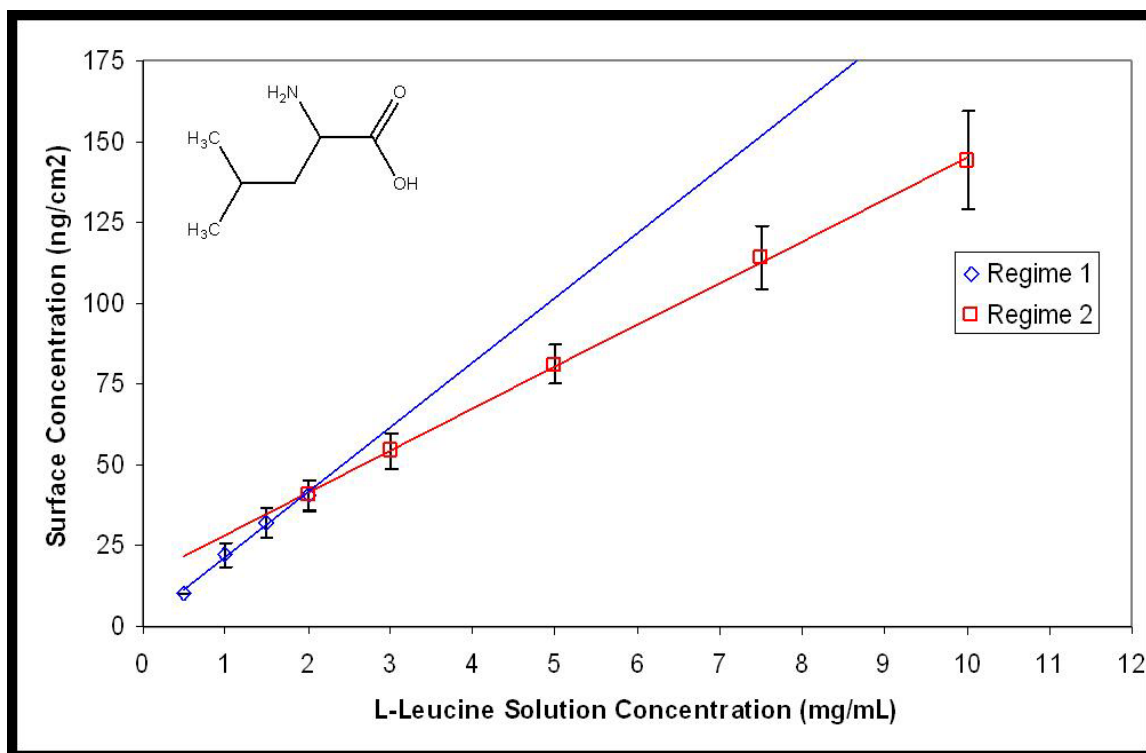
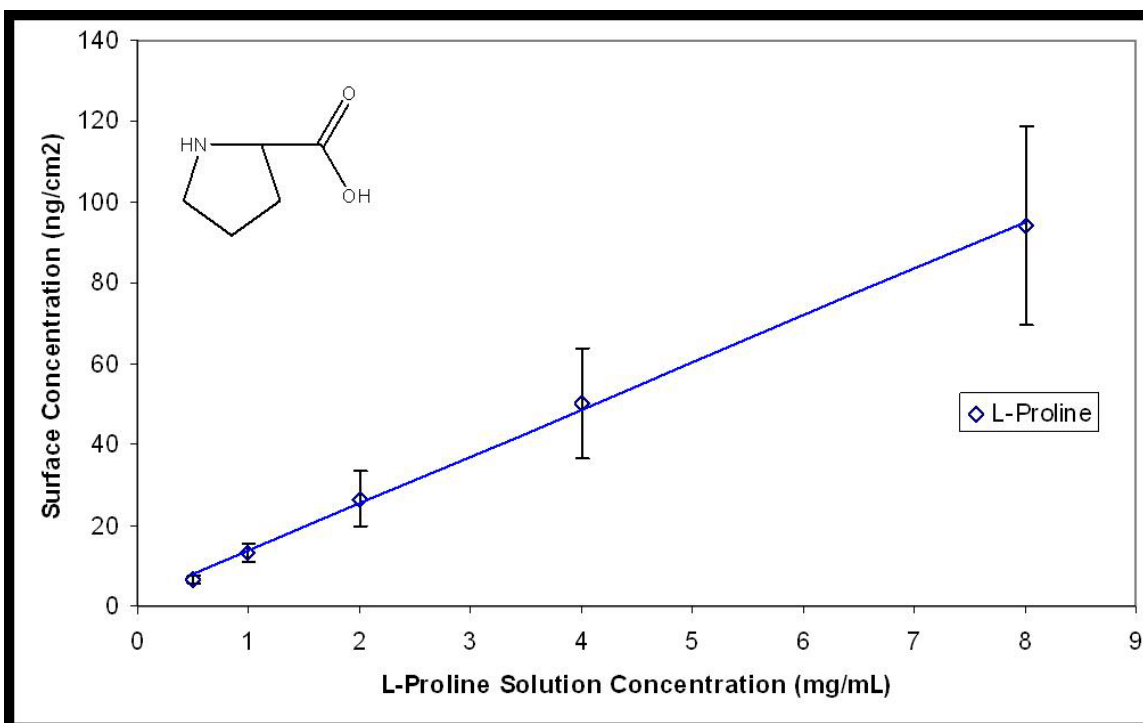


Figure 7.9. QCM data of L-leucine adsorption on the hydrophobic PS surface as a function of amino acid concentration in PBS at pH 7.4 and 24 °C. Isotherm-like behavior suggests a L-leucine monolayer forms at a surface density of  $\sim 41 \text{ ng/cm}^2$  and solution concentration of 2 mg/mL on the PS surface.

Additional QCM concentration experiments were conducted for L-arginine at the hydrophobic PS surface, L-leucine at the hydrophilic  $\text{SiO}_2$  surface, and L-proline at both surfaces. However, in all of these cases, no monolayer type behavior was observed. This finding is explained as the multiple competing driving forces for adsorption and desorption are generally of similar magnitude except in the case where both species exhibit the same, strong hydrophilic or hydrophobic nature such as the L-arginine/ $\text{SiO}_2$  (charged/charged) and L-leucine/PS (hydrophobic/hydrophobic) systems. Interestingly, in the cases of the adsorption of L-arginine on  $\text{SiO}_2$  and L-leucine on PS the discontinuous relationships observed between solution and surface concentration agree roughly with predictions for monolayer coverages which were estimated to be approximately  $10 \text{ ng/cm}^2$  using simple geometric arguments. A plot of L-proline surface concentration on PS as a function of solution concentration is included in Figure 7.10. In this case, the relationship between surface and solution concentration is linear across the range studied suggesting the driving force for adsorption on the surface is not substantially different than that for proline-proline aggregate formation or solvent cage disruption. While this data is not conclusive and further experimentation is necessary, these findings are strongly suggestive of amino acid monolayer formation in cases where there are strong attractive interactions between the adsorbate and the surface.



**Figure 7.10.** QCM data of L-proline adsorption on the hydrophobic PS surface as a function of amino acid concentration in PBS at pH 7.4 and 20 °C. No isotherm-like behavior is observed in this case suggesting on the PS surface the driving force for L-proline adsorption and biomolecule-biomolecule aggregation are roughly equivalent thermodynamically.

SFG spectra of pure PBS and solutions of L-arginine at the hydrophilic SiO<sub>2</sub> surface are presented in Figure 7.11. This data provides additional experimental evidence for bimodal, concentration dependent L-arginine adsorption behavior where molecule-surface interactions dominate the system at low concentrations and intermolecular amino acid aggregation occurs at higher concentrations. At 0.5 mg/mL concentration in PBS (well below the apparent monolayer formation conditions from QCM measurements) L-arginine appears to decrease SFG signal from interfacial “ice-like” and “liquid-like” water at 3200 cm<sup>-1</sup> and 3400 cm<sup>-1</sup>, respectively. This observation is evidence for the presence of adsorbed arginine species disrupting the order of interfacial water and/or displacing a portion of the surface water. This behavior is expected as arginine has a highly positively charged guanidino side chain and SiO<sub>2</sub> has a negative surface charge when both are in an aqueous environment at pH 7.4. In such a circumstance, the electrostatic attractions between the hydrophilic surface and the aqueous amino acid are expected to be stronger than the competing charge-dipole attractive forces between the SiO<sub>2</sub> and H<sub>2</sub>O solvent. At the slightly higher amino acid solution concentration of 1 mg/mL, the SFG spectrum of the L-arginine/PBS/SiO<sub>2</sub> interface shows a restoration and slight increase in the water signal above background levels. This is attributed to an increase in the concentration of interfacial L-arginine which is capable of pulling water molecules out of the bulk solution and onto the surface due to its charged side chain. Additionally, the adsorption of L-arginine may induce a reorganization of surface water in to a more ordered interfacial configuration. After addition of a 15 mg/mL L-arginine solution well above expected monolayer threshold a dramatic increase in the SFG spectrum is observed centered at approximately 3200 cm<sup>-1</sup>. This increase in SFG signal is indicative of an elevated surface concentration of the amino acid as well as the water

molecules that solvate the charged biomolecule. This enhanced peak is centered at  $3200\text{ cm}^{-1}$  where “ice-like” tetrahedral water is observed in the spectra of pure PBS and low concentration amino acid. However, this signal enhancement may also be due, in part, to the Amide A and Amide B modes of L-arginine which are typically broad and located roughly at  $3300\text{ cm}^{-1}$  and  $3100\text{ cm}^{-1}$ , respectively.<sup>22-24</sup>

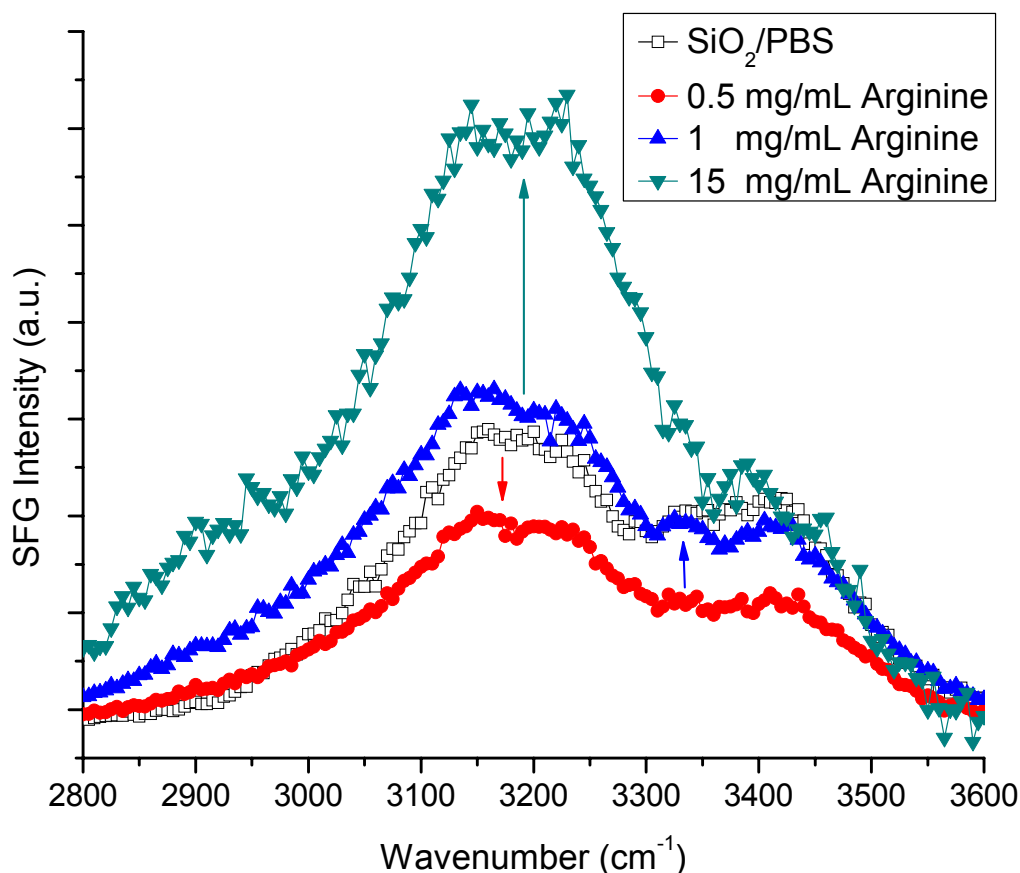


Figure 7.11. SFG spectrum of the hydrophilic  $\text{SiO}_2/\text{PBS}$  interface before (white boxes), and after addition of L-arginine solutions at  $0.5\text{ mg/mL}$  (red circles),  $1\text{ mg/mL}$  (blue triangles), and  $15\text{ mg/mL}$  (olive triangles). The spectrum of pure PBS shows O-H vibrational modes of “ice-like” and “liquid-like” ordered interfacial water at  $3200\text{ cm}^{-1}$  and  $3400\text{ cm}^{-1}$ , respectively. In the presence of  $0.5\text{ mg/mL}$  L-arginine, the water SFG signal decreases below the level observed for the pure PBS solution. However, as more arginine amino acid is added the water signal is restored and enhanced above background levels. At the highest L-arginine concentration studied ( $15\text{ mg/mL}$ ), the peak centered at  $\sim 3200\text{ cm}^{-1}$  is observed to broaden suggestive of a combination of “ice-like” O-H, Amide A, and Amide B vibrational modes.

### 7.3.3. SFG Spectrum of L-Proline Amino Acid as a Function of Interface Temperature

A SFG investigation of L-proline amino acid as a function of temperature modulation was conducted at the hydrophobic  $d_8\text{-PS}/\text{PBS}$  interface at pH 7.4. When a solution of L-proline ( $5\text{ mg/mL}$ ) was added to the  $d_8\text{-PS}$  interface at an initial temperature of  $20\text{ }^\circ\text{C}$  two strong C-H

vibrational modes were observed at  $2875\text{ cm}^{-1}$  and  $2935\text{ cm}^{-1}$  as presented in Figure 7.12. (A thorough identification and explanation of the origin of these modes is included in Chapter 5.<sup>25</sup>) Subsequently, the temperature of the sample substrate and biomolecule was increased to  $30\text{ }^{\circ}\text{C}$  and the SFG spectrum was again measured. At the elevated temperature of  $30\text{ }^{\circ}\text{C}$ , the SFG spectrum of L-proline remained unchanged from that observed at  $20\text{ }^{\circ}\text{C}$ . In a complementary experiment, the SFG spectrum of the L-proline solution was first measured at  $30\text{ }^{\circ}\text{C}$  before and the sample substrate and solution were cooled down to  $20\text{ }^{\circ}\text{C}$  and the SFG spectrum was collected again as shown in Figure 7.13. Similar to the first experiment, C-H vibrational modes were observed at  $2875\text{ cm}^{-1}$  and  $2935\text{ cm}^{-1}$ . However, when the sample was first heated to  $30\text{ }^{\circ}\text{C}$  and then cooled to  $20\text{ }^{\circ}\text{C}$  an enhancement the SFG signal was observed in the second, lower temperature spectrum. This observation is explained as the elevation in interface temperature providing sufficient energy for the adsorbed amino acid species to overcome a small energy barrier thus allowing the L-proline molecules to relax into a more thermodynamically favorable surface conformation upon cooling. In the case where the initial adsorption of L-proline occurs at  $20\text{ }^{\circ}\text{C}$  there may not be sufficient energy to overcome this small barrier to surface relaxation or

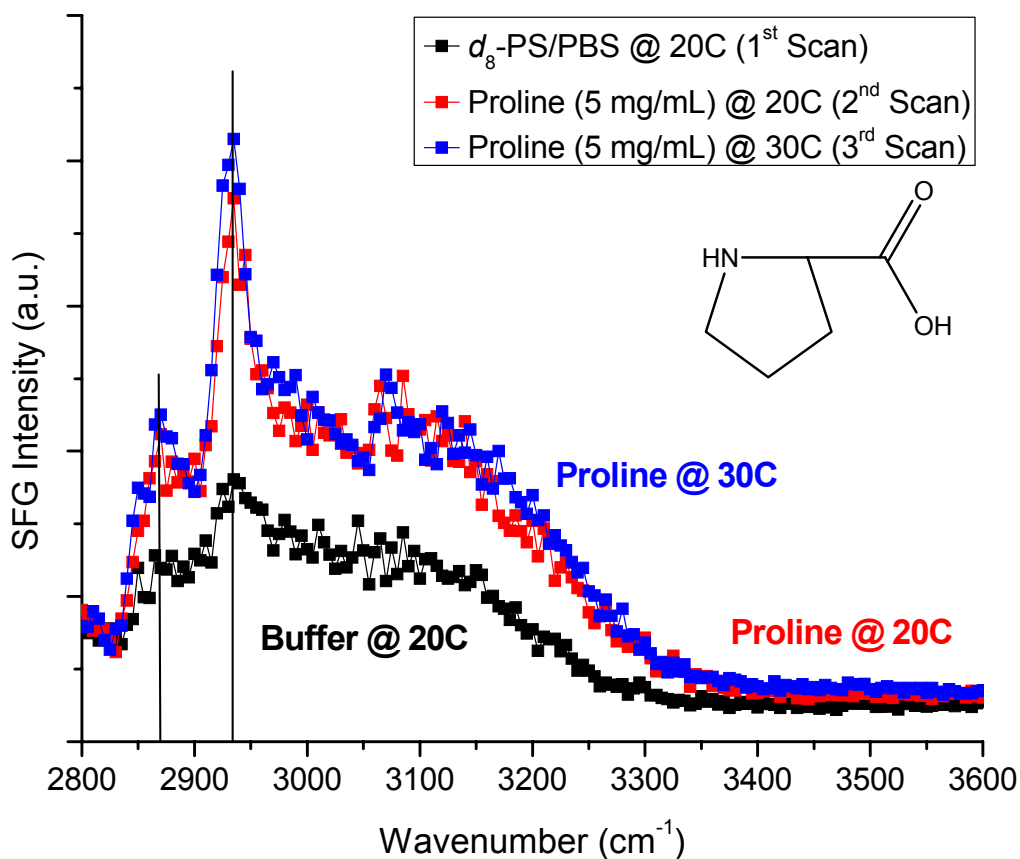


Figure 7.12. SFG spectrum of the hydrophobic  $d_8$ -PS/PBS interface before (black squares) and after addition of L-proline at 5 mg/mL (red squares) at  $20\text{ }^{\circ}\text{C}$ , and again after the subsequent elevation of interface temperature to  $30\text{ }^{\circ}\text{C}$  (blue squares). The spectra of L-proline at  $20\text{ }^{\circ}\text{C}$  and  $30\text{ }^{\circ}\text{C}$  are similar, and both SFG spectra show C-H vibrational modes at  $2875\text{ cm}^{-1}$  and  $2935\text{ cm}^{-1}$ . Both SFG spectra show C-H vibrational modes at  $2875\text{ cm}^{-1}$  and  $2935\text{ cm}^{-1}$  of comparable intensity suggesting no change in interfacial order of the amino acid population upon heating.

reorganization. Therefore, the lack of SFG signal enhancement after heating from 20 °C to 30 °C is hypothesized to be the result of the increase in available energy for the competing processes of surface reorganization and desorption from the hydrophobic  $d_8$ -PS surface. Subsequently, QCM measurements were conducted on similar solutions of L-proline (5 mg/mL in PBS at pH 7.4) to test this hypothesis and allow quantification of amino acid surface concentrations at 20 °C and 30 °C. As presented in Table 7.1, the data collected from the temperature dependent QCM experiments indicated that L-proline was present on the hydrophobic surface at a concentration of  $25 \pm 2$  ng/cm<sup>2</sup> at 20 °C and at a surface concentration of  $36 \pm 4$  ng/cm<sup>2</sup> at 30 °C. These findings were unexpected as a higher surface concentration was expected at a lower temperature where less energy is available to allow for the desorption of amino acids from the hydrophobic surface. Nonetheless, this QCM result supports the hypothesis that the SFG signal enhancement originates from an increase in surface ordering and not from an increase in surface concentration of L-proline. These results provide evidence of the temperature sensitivity of the SFG technique to the net orientation of a population of interfacial species.

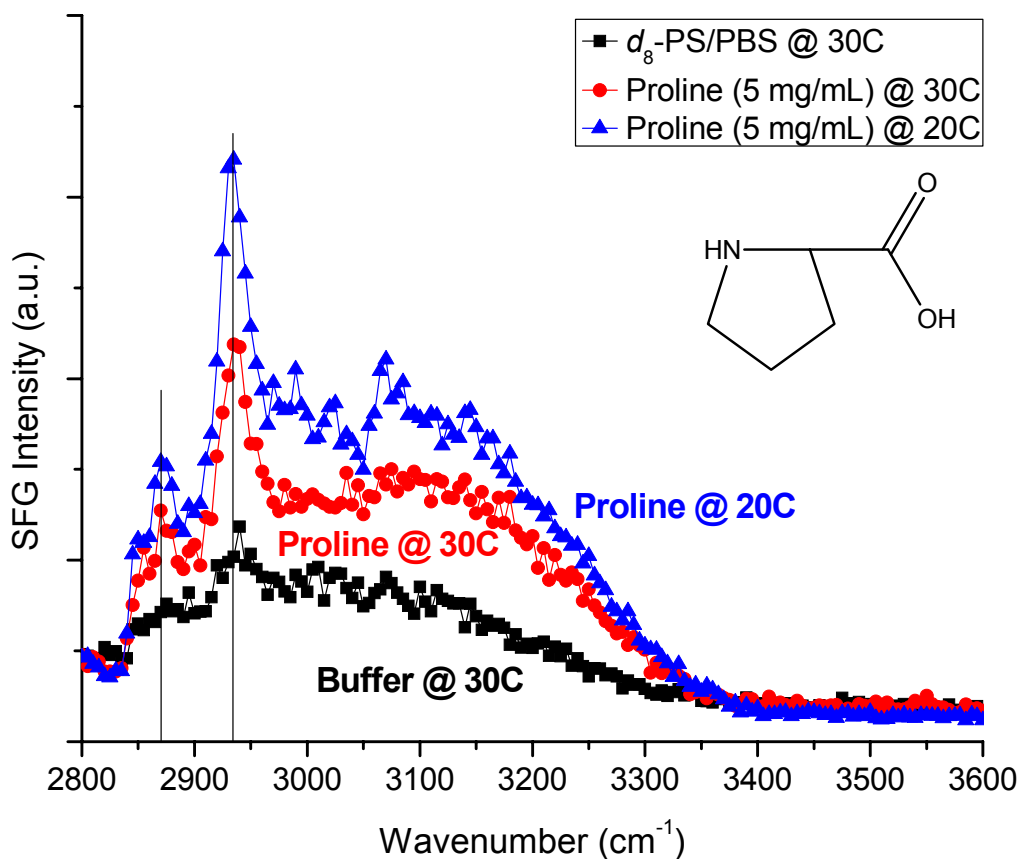


Figure 7.13. SFG spectrum of the hydrophobic  $d_8$ -PS/PBS interface before (black squares) and after addition of L-proline at 5 mg/mL (red circles) at 30 °C, and again after the subsequent reduction of interface temperature to 20 °C (blue triangles). While both SFG spectra show C-H vibrational modes at 2875 cm<sup>-1</sup> and 2935 cm<sup>-1</sup>, the spectral features observed from L-proline at 20 °C are more intense than at the initial temperature of 30 °C suggesting an increase in interfacial order of the amino acid population upon cooling.

Interface Temperature	L-Proline Adsorbed
20 °C	$25 \pm 2 \text{ ng/cm}^2$
30 °C	$36 \pm 4 \text{ ng/cm}^2$

**Table 7.1. Summary of QCM data quantifying the surface concentration of L-proline adsorbed on the hydrophobic polystyrene surface as a function of interface temperature.**

#### **7.3.4. The Time-Dependent Nature of SFG Experiments in the Laboratory**

The SFG spectrum of a mixture of L-arginine and L-proline amino acids (15 mg/mL each) in PBS at the hydrophobic  $d_8$ -PS/PBS (pH 7.4) interface as a function of time is presented in Figure 7.14. Each data point presented in this figure is the average of 600 laser shots and the SFG sample and solution were maintained at 24 °C. While no clear C-H vibrational modes are resolved in this spectrum, this spectrum does show an increase in SFG signal intensity as time progresses in the infrared frequency region 2800 - 3200  $\text{cm}^{-1}$ . The SFG signal increases from its level at 45 minutes after the addition of the amino acid solution to a higher level at approximately 90 minutes. After 90 minutes exposure to the biomolecule solution, the SFG signal appears to remain at a constant level over the subsequent 75 minutes. While further study of this phenomenon is needed, Figure 7.15 provides a valuable insight into the nature and timescale of amino acid adsorption onto the  $d_8$ -PS/PBS surface. Furthermore, this data serves as a cautionary example underscoring the importance of allowing sample solutions sufficient time to reach equilibrium with the substrate of interest during SFG experiments in the laboratory.

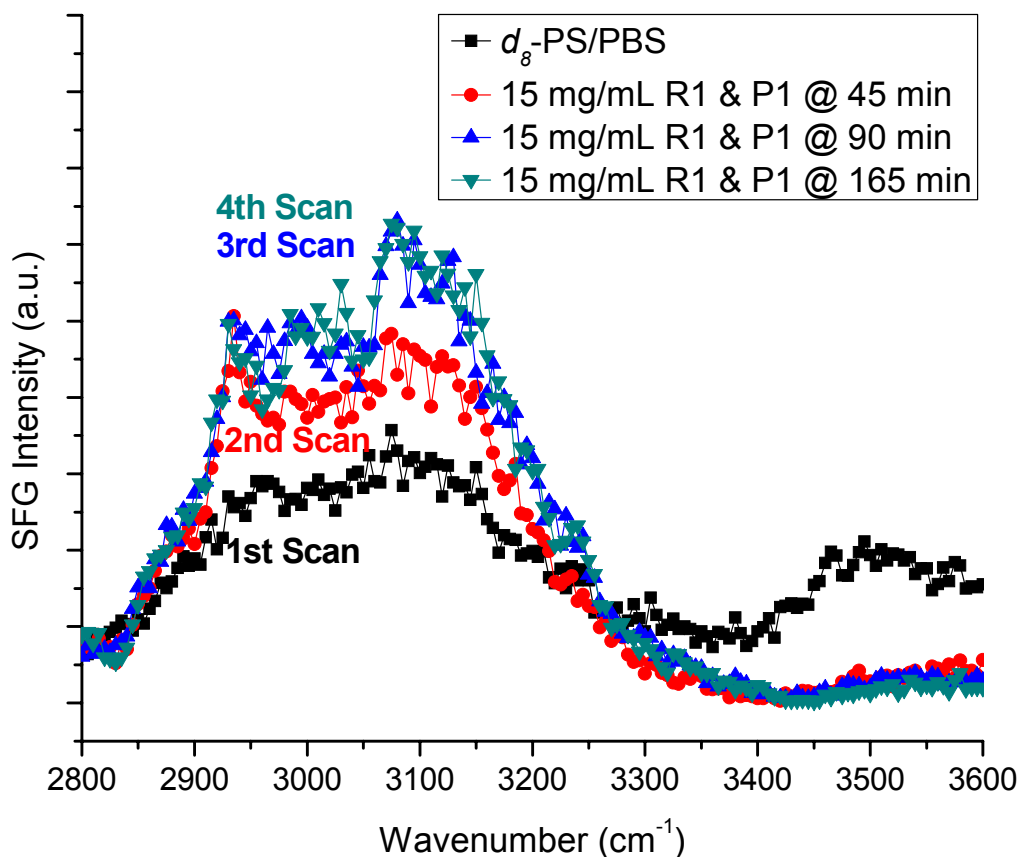


Figure 7.14. The SFG spectrum of the  $d_8$ -PS/PBS solid-liquid interface before (black squares) and at 45 minutes (red circles), 90 minutes (blue triangles), and 165 minutes (olive triangles) after the addition of L-arginine and L-proline (15 mg/mL each). The SFG intensity in the region 2800 - 3200  $\text{cm}^{-1}$  increases to a final and maximal intensity between 45 and 90 minutes after addition of the biomolecule solution. This result emphasizes the importance of allowing SFG sample systems to reach equilibrium prior to measurement.

### 7.3.5. SFG Comparison of Poly-L-Proline and the Collagen-Like Peptide Ac-(PPG)<sub>4</sub>-NH<sub>2</sub>

The SFG spectra of a solution of poly-L-proline (0.5 mg/mL in PBS) and the collagen-like peptide Ac-(PPG)<sub>4</sub>-NH<sub>2</sub> (also 0.5 mg/mL in PBS) are presented in Figure 7.15. These spectra are strikingly similar as both show the same three, sharp spectral features in the C-H region at 2875  $\text{cm}^{-1}$ , 2935  $\text{cm}^{-1}$ , and 2985  $\text{cm}^{-1}$  which are attributed to the proline residues in each peptide. While a detailed identification and explanation of each of these C-H vibrational modes are provided in Chapter 5 and Chapter 6, this finding is important as it provides important evidence for the feasibility of an SFG investigation of collagen and collagen-like peptides.<sup>26</sup> This is significant because collagen is a fundamental chemical component of a wide range of important human biological tissues and structures including skin, muscle fiber, organs, bone, and hair.<sup>27</sup>

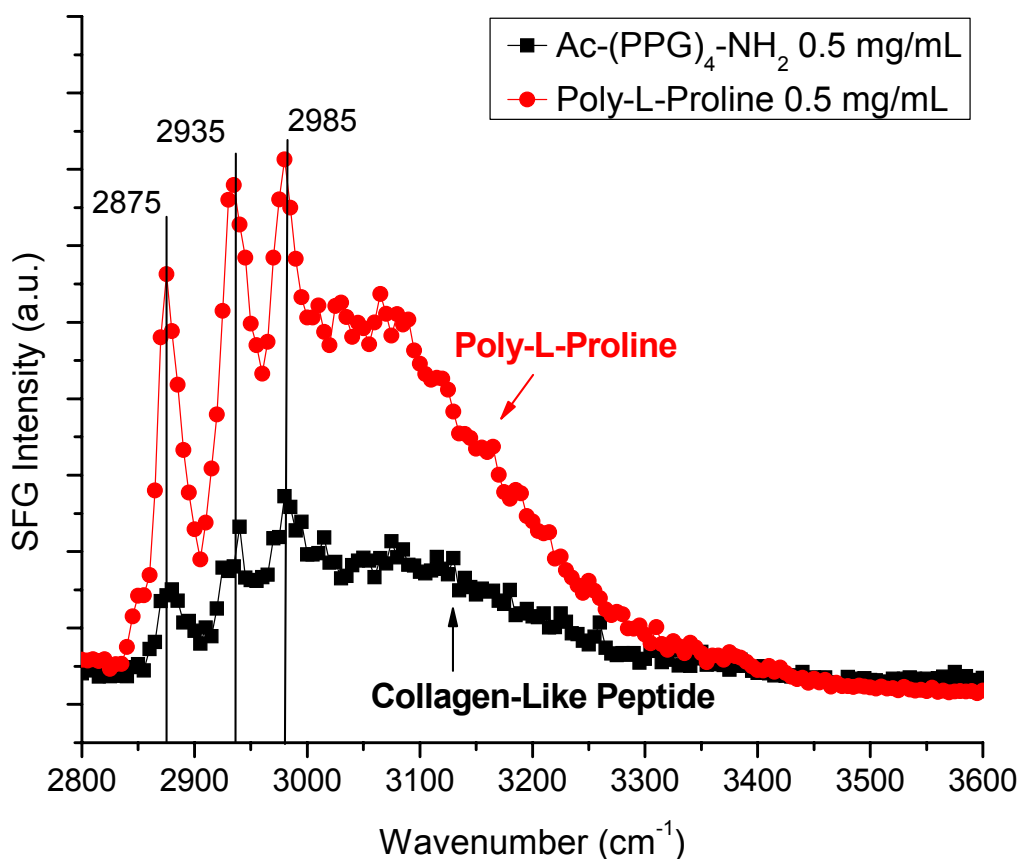


Figure 7.15. The SFG spectra of 0.5 mg/mL solutions of the collagen-like peptide Ac-(PPG)<sub>4</sub>-NH<sub>2</sub> (black squares) and poly-L-proline at the *d*<sub>8</sub>-PS/PBS solid-liquid interface. Both spectra share the SFG active C-H vibrational modes of interfacial L-proline at 2875 cm<sup>-1</sup>, 2935 cm<sup>-1</sup>, and 2985 cm<sup>-1</sup>. The similarity between these spectra provides evidence for the feasibility of utilizing SFG vibrational spectroscopy to investigate the interaction of solutions of collagen and collagen-like peptides with hydrophobic surfaces under physiological conditions.

### 7.3.6. SFG Investigation of H<sub>2</sub>O, PBS, and L-Arginine at the Platinum Electrode Surface

SFG vibrational spectroscopy was conducted of the platinum electrode-aqueous solution interface to probe the sensitivity of interfacial water, PBS, and L-arginine amino acid signal to an applied DC electric field. To conduct these experiments, a fused SiO<sub>2</sub> prism surface was coated with a ~7 nm adhesion layer of titania before a ~10nm layer of platinum was evaporated on the prism surface to form an electrode surface. The titania and platinum layers were sufficiently thick to provide robust adhesion to the SiO<sub>2</sub> prism surface while being thin enough to remain transparent to both the visible and infrared laser beams used during SFG experiments. The resulting prism platinum electrode substrate was then connected to a potentiostat and exposed to aqueous solutions in a Petri dish. The polystyrene Petri dish was situated above a gold electrode such that the platinum and gold electrodes were not in a closed circuit as in previous electrochemical experiments utilizing SFG spectroscopy.<sup>28, 29</sup> Instead, these flat electrodes were

positioned in such a manner that there was an electric field between their 2 mm separation in a manner similar to that of a classical capacitor. A schematic of this SFG electrode setup as utilized during experiment is provided in Figure 7.16.

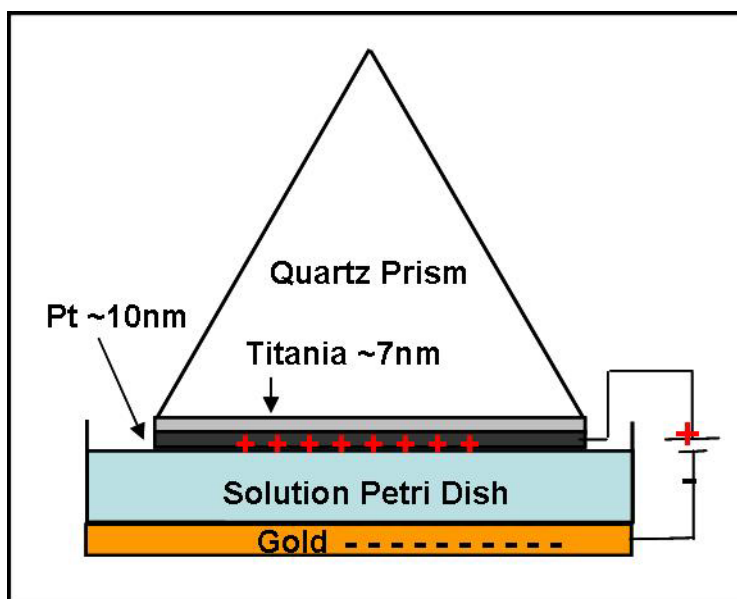
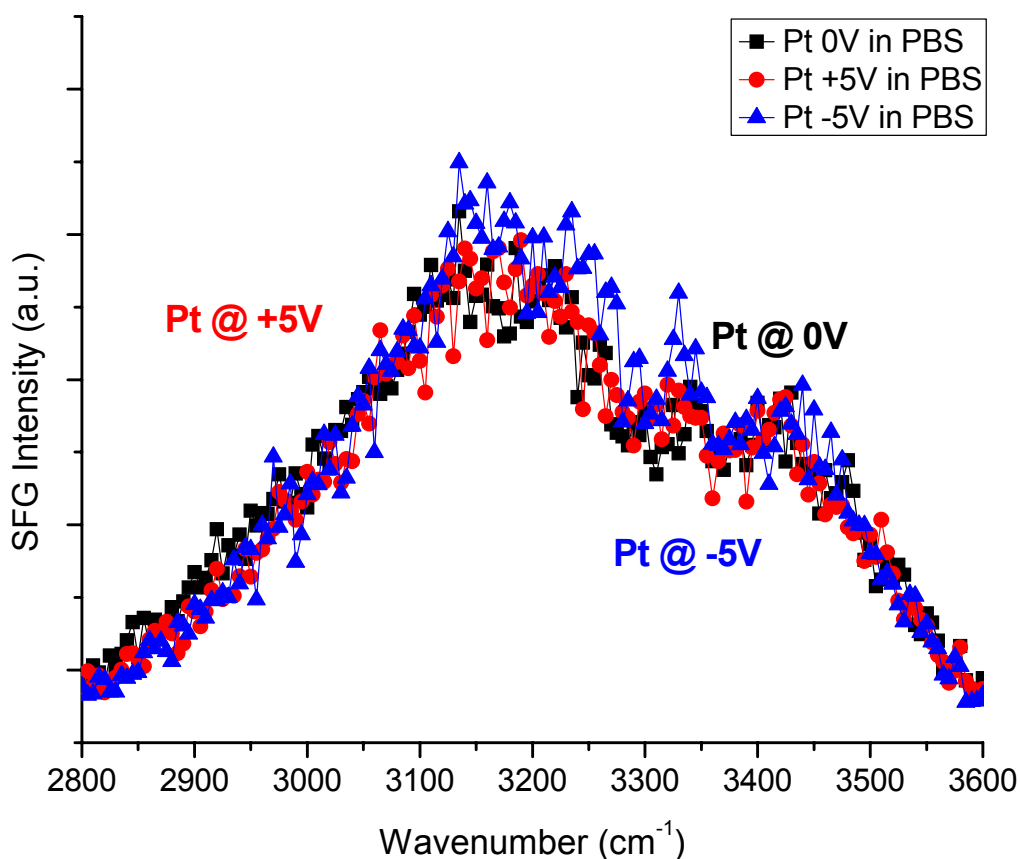


Figure 7.16. Schematic of the platinum electrode prism and experimental arrangement during SFG measurement. A thin film of titania (~7 nm) was evaporated on the surface of the prism substrate to provide an adhesion layer between the fused SiO<sub>2</sub> substrate and the 10 nm thick platinum electrode layer. Subsequently the prism was connected to a potentiostat and submerged in aqueous solution contained in a Petri dish. This dish was placed on top of a gold electrode which served as the complementary electrode for this capacitor-like sample arrangement.

The SFG spectrum of the Pt electrode-PBS interface is provided in Figure 7.17 at no applied voltage as well as +5 V and -5 V potentials at 20 °C. These vibrational spectra show two broad peaks from the O-H stretches of “ice-like” and “liquid-like” interfacial water species at ~3200 cm<sup>-1</sup> and ~3400 cm<sup>-1</sup>, respectively.<sup>11</sup> Additionally, there is no apparent change in the structure of interfacial PBS solution as a function of applied potential. The lack of differences in the SFG spectra is attributed to the high ionic strength of the PBS solution which was calculated to have a Debye screening length of only ~8 Å due to the high salt content of the buffer solution.<sup>30</sup> With such a short screening length it is not unreasonable to suspect that any electric field at the Pt electrode surface would be strongly masked by salt ions thus minimizing the capacity of the applied voltage to influence the structure of the interfacial water species.



**Figure 7.17.** The SFG spectra of the Pt electrode-PBS interface at zero bias (black squares), at +5 V potential (red circles), and at -5 V potential (blue triangles). The spectrum shows only interfacial water structure of at  $3200\text{ cm}^{-1}$  and  $3400\text{ cm}^{-1}$  which do not change with applied electrode potential. The lack of change in the SFG activity of the aqueous solution is attributed to its short Debye screening length of approximately  $\sim 8\text{ \AA}$  due to the high salt concentration of the PBS.

Next, the previous SFG experiment was repeated using pure  $18.2\text{ M}\Omega$  water instead of the buffer solution to extend the predicted screening length of the electric field at the Pt surface to  $\sim 250\text{ \AA}$ . Furthermore, the applied voltages were increased from  $\pm 5\text{ V}$  in the case of PBS, to  $\pm 10\text{ V}$  in the case of pure water. The SFG spectrum of the Pt electrode- $\text{H}_2\text{O}$  interface is presented in Figure 7.18. Similar to the case of Pt-PBS interface, the SFG spectrum of the Pt- $\text{H}_2\text{O}$  interface shows broad features from “ice-like” tetrahedrally coordinated and “liquid-like” less than tetrahedrally coordinated water at  $3200\text{ cm}^{-1}$  and  $3400\text{ cm}^{-1}$ , respectively, neither of which change with applied potential at the Pt electrode surface.

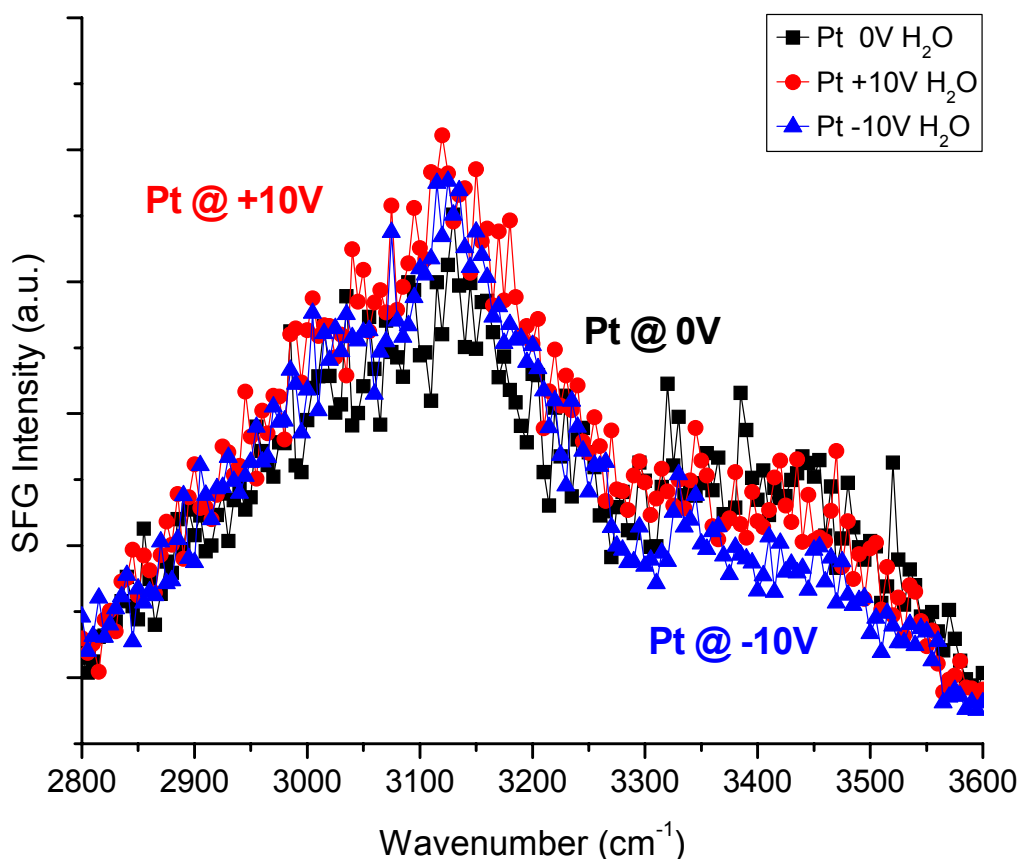


Figure 7.18. SFG spectra of the Pt electrode-H<sub>2</sub>O interface at zero bias (black squares), at +10 V potential (red circles), and at -10 V potential (blue triangles). The spectrum shows only interfacial water structure of at 3200 cm<sup>-1</sup> and 3400 cm<sup>-1</sup>. These spectral features from interfacial water do not change with applied electrode potential. The lack of change in the SFG activity of the aqueous solution is unexpected to the system's predicted Debye screening length of approximately ~250 Å because of its to low ionic strength.

The SFG spectrum of the Pt electrode-H<sub>2</sub>O interface in the presence of L-arginine amino acid (2 mg/mL) is presented in Figure 7.19. Interestingly, the SFG signal from O-H stretches of interfacial water observed at 3200 cm<sup>-1</sup> and 3400 cm<sup>-1</sup> are observed to slightly reduce from background levels at +10 V bias, and substantially reduce at -10 V Pt electrode bias. This finding is unexpected as L-arginine is well documented to become positively charged in aqueous solution at moderate pH.<sup>10</sup> This observation suggests the presence of a negative surface charge could reasonably be anticipated to enhance adsorption and ordering of interfacial water and amino acid species thus resulting in an increase in SFG signal. However the opposite of this expected effect suggests that the structure of interfacial species at the Pt-H<sub>2</sub>O interface may be depend upon a number of similarly influential parameters such as solvent cage networks and intermolecular forces between neighboring adsorbate species.

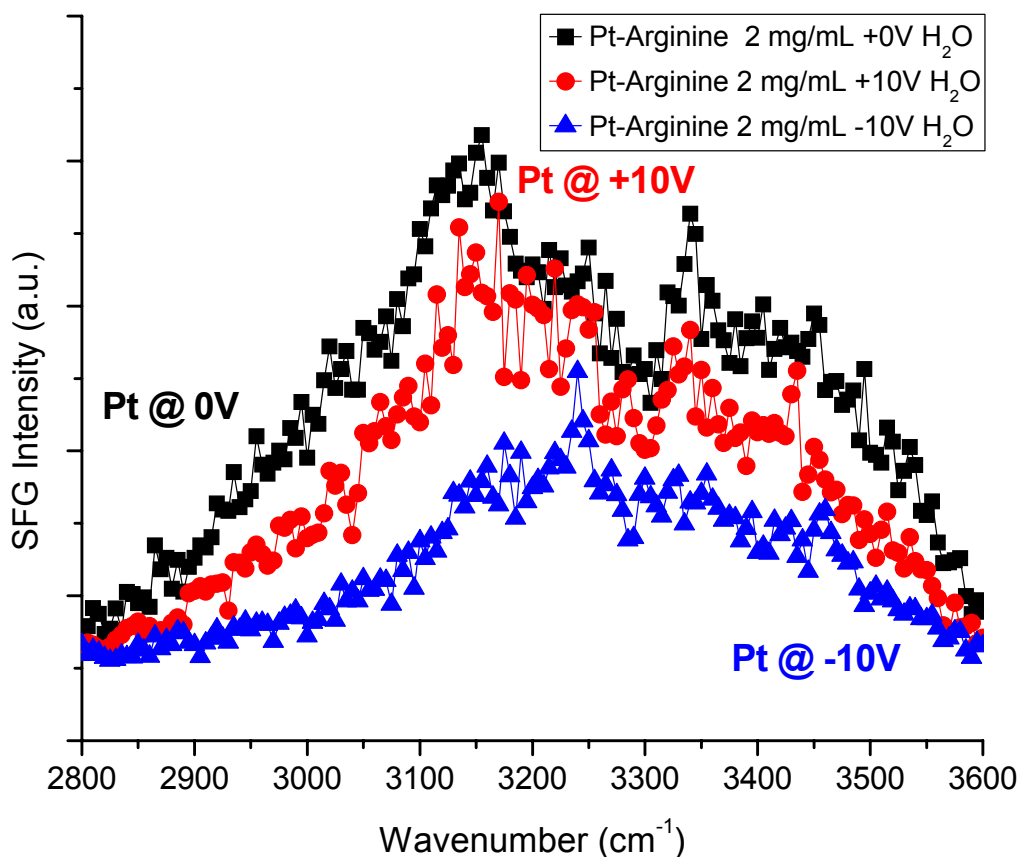


Figure 7.19. SFG spectra of the Pt electrode-H<sub>2</sub>O interface in the presence of L-arginine amino acid (2 mg/mL) at zero bias (black squares), at +10 V potential (red circles), and at -10 V potential (blue triangles). The spectrum shows only interfacial water structure of at 3200 cm<sup>-1</sup> and 3400 cm<sup>-1</sup>. These spectral features change substantially with applied electrode potential, and while the origin of this effect is unclear the presence of L-arginine appears to have a strong influence on the structure of interfacial water with applied potential at the Pt electrode surface. The SFG signal is found to decrease from background and positive bias levels at -10 V applied potential. This result is unexpected due to the positively charged nature of solvated arginine at moderate pH values which would be expected to increase adsorption and organization (and thus SFG signal) of interfacial water and amino acid molecules.

## 7.4. Conclusions

These exploratory studies provided insights into the role of several important experimental parameters and their influence on the adsorption and interfacial organization of several amino acids and peptides using surface sensitive SFG and QCM techniques. Each of these six investigations yielded results indicating scientifically rich and promising areas for future biointerface research projects and the primary finding of each of study is summarized as follows:

1. The coadsorption of amino acids was observed on model hydrophilic  $\text{SiO}_2$  and hydrophobic polystyrene surfaces. These coadsorption events were observed to strongly influence the organization of water at the solid-liquid interface.
2. QCM experiments conducted on solutions of amino acids at the solid-liquid interface showed evidence of amino acid monolayer formation on model surfaces which shared chemical properties with the biomolecule species of interest.
3. The SFG spectrum of L-proline at the hydrophilic  $d_8$ -PS/PBS solid-liquid was found to be strongly influenced by the amount of time the system has to reach chemical equilibrium concentrations during measurement.
4. The SFG signal intensity of vibrational modes from a solution of L-proline amino acid was found to increase with a decrease in interfacial temperature.
5. A collagen-like peptide was studied at the hydrophobic solid/liquid interface under physiological conditions and found to have an SFG vibrational spectrum similar to that of poly-L-proline.
6. The SFG spectra of an amino acid dissolved in pure water was measured at the Pt electrode surface and found to be only weakly dependent on the magnitude of the applied potential.

## References

1. Sauerbrey, G., *Zeitschrift Fur Physik* **1959**, 155 (2), 206-222.
2. Marx, K. A., *Biomacromolecules* **2003**, 4 (5), 1099-1120.
3. Rodahl, M.; Kasemo, B., *Review of Scientific Instruments* **1996**, 67 (9), 3238-3241.
4. Rodahl, M.; Kasemo, B., *Sensors and Actuators a-Physical* **1996**, 54 (1-3), 448-456.
5. Arnau, A., *Sensors* **2008**, 8 (1), 370-411.
6. Rodahl, M.; Hook, F.; Kasemo, B., *Analytical Chemistry* **1996**, 68 (13), 2219-2227.
7. York, R. L.; Li, Y. M.; Holinga, G. J.; Somorjai, G. A., *Journal of Physical Chemistry A* **2009**, 113 (12), 2768-2774.
8. Lambert, A. G.; Davies, P. B.; Neivandt, D. J., *Applied Spectroscopy Reviews* **2005**, 40 (2), 103-145.
9. Merrifield, R., *Advances in Enzymology and Related Areas of Molecular Biology* **1969**, 32, 221-&.
10. Voet, D.; Voet, J. G.; Pratt, C. W., *Fundamentals of biochemistry upgrade*. [Rev. ed.; Wiley: New York, 2002; p 1 v. (various pagings).
11. Shen, Y. R.; Ostroverkhov, V., *Chemical Reviews* **2006**, 106 (4), 1140-1154.
12. York, R. L.; Mermut, O.; Phillips, D. C.; McCrea, K. R.; Ward, R. S.; Somorjai, G. A., *J. Phys. Chem. C* **2007**, 111 (25), 8866-8871.
13. Phillips, D. C.; York, R. L.; Mermut, O.; McCrea, K. R.; Ward, R. S.; Somorjai, G. A., *Journal of Physical Chemistry C* **2007**, 111 (1), 255-261.
14. Yeganeh, M. S.; Dougal, S. M.; Pink, H. S., *Physical Review Letters* **1999**, 83 (6), 1179-1182.
15. Briggman, K. A.; Stephenson, J. C.; Wallace, W. E.; Richter, L. J., *Journal of Physical Chemistry B* **2001**, 105 (14), 2785-2791.
16. Watry, M. R.; Richmond, G. L., *Journal of Physical Chemistry B* **2002**, 106 (48), 12517-12523.
17. Castner, D. G.; Ratner, B. D., *Surface Science* **2002**, 500 (1-3), 28-60.
18. Anderson, J. M., *Annual Review of Materials Research* **2001**, 31, 81-110.
19. Kyte, J.; Doolittle, R. F., *Journal of Molecular Biology* **1982**, 157 (1), 105-132.
20. Rusanov, A. I., *Surf. Sci. Rep.* **2005**, 58 (5-8), 111-239.
21. Somorjai, G. A.; Li, Y., *Introduction to surface chemistry and catalysis*. 2nd ed.; WILEY: Hoboken, N.J., 2010.
22. Krimm, S.; Dwivedi, A. M., *Journal of Raman Spectroscopy* **1982**, 12 (2), 133-137.
23. Miyazawa, T., *Journal of Molecular Spectroscopy* **1960**, 4 (2), 168-172.
24. Krimm, S.; Bandekar, J., *Advances in Protein Chemistry* **1986**, 38, 181-364.
25. Reva, I. D.; Stepanian, S. G.; Plokhotnichenko, A. M.; Radchenko, E. D.; Sheina, G. G.; Blagoi, Y. P., *Journal of Molecular Structure* **1994**, 318, 1-13.
26. Woodcock, S. E.; Johnson, W. C.; Chen, Z., *Journal of Colloid and Interface Science* **2005**, 292 (1), 99-107.
27. Nimni, M. E.; Bernick, S.; Cheung, D. T.; Ertl, D. C.; Nishimoto, S. K.; Paule, W. J.; Salka, C.; Strates, B. S., *Calcif. Tissue Int.* **1988**, 42 (5), 313-320.
28. Kim, J.; Chou, K. C.; Somorjai, G. A., *Journal of Physical Chemistry B* **2002**, 106 (36), 9198-9200.
29. Baldelli, S., *Accounts of Chemical Research* **2008**, 41 (3), 421-431.

30. Dobrynin, A. V.; Colby, R. H.; Rubinstein, M., *Macromolecules* **1995**, 28 (6), 1859-1871.

## Chapter 8

### An SFG and QCM Study of Biologically Active Heparin Functionalized Surfaces

This investigation of heparin coated surfaces utilized the surface-sensitive quartz crystal microbalance (QCM) technique to quantify the biological activity of heparin functionalized surfaces. The surface binding capacities of both heparin and polystyrene coated surfaces for two biologically important proteins, tumor necrosis factor alpha and antithrombin-III (AT-III), were quantitatively determined under physiological conditions. Additionally, the surface-sensitive sum frequency generation (SFG) vibrational spectrum of a heparin functionalized surface was collected for the first time. These findings provide important evidence for the experimental feasibility of future quantitative studies of the heparin/thrombin/AT-III biocatalytic mechanism for the regulation of blood clotting using surface-sensitive analytical techniques in real-time and under physiological conditions. Furthermore, this research suggests that heparin functionalized surfaces hold promise as a powerful tool for the removal of pathogens and the purification of blood.

#### 8.1. Introduction

A fundamental characteristic determining the biocompatibility of a material is its ability to adsorb proteins and other biomolecules without simulating a strong unfavorable immune response in the host.<sup>1, 2</sup> The functionalizing of material surfaces is an important approach to making a foreign material in the body biocompatible while maintaining its bulk properties and functionality.<sup>3-8</sup> Specifically, biomaterials can be designed to be biocompatible even in situations of flowing fluids such as the case with catheters, artificial heart valves, stents, and angioplasty balloons. Photographs of used, surgically implanted angioplasty balloons with and without surface modification to enhance biocompatibility are presented in Figure 8.1. The balloon that was not surface modified is heavily coated with clotted blood and adsorbed proteins while the surface modified balloon appears relatively free of accumulated blood and biofouling.

The purpose of this study was to quantify the biological activity and binding capacity of a synthetically produced heparin surface using QCM as a simple, direct, real-time, and quantitative alternative to enzyme immunoassay (ELISA) techniques.<sup>9</sup> Additionally, this investigation was intended to explore the potential use of heparin coatings as biocompatibility enhancing surface

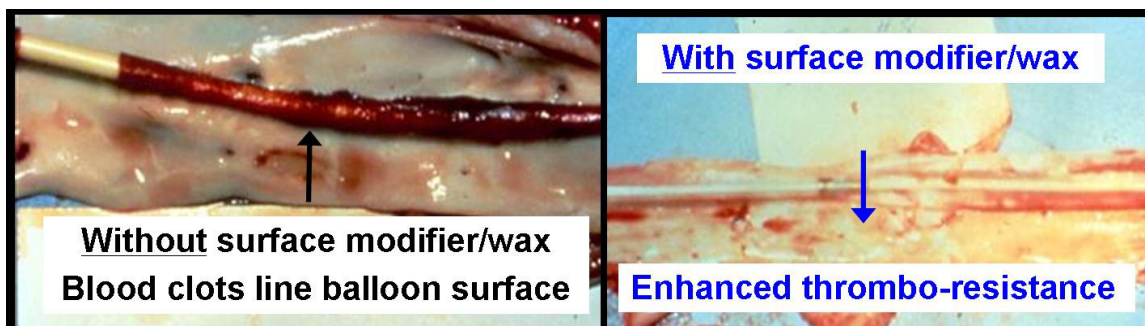
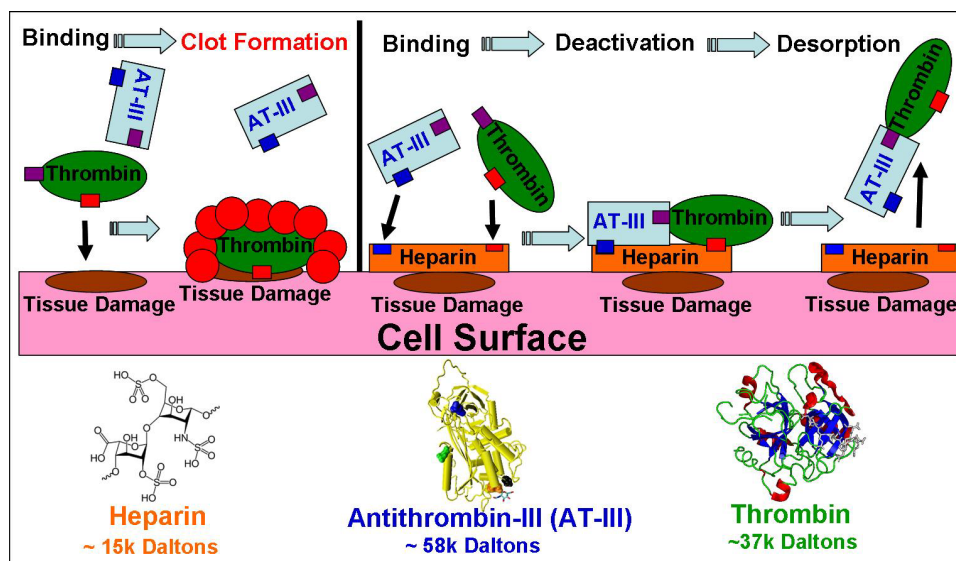


Figure 8.1. Angioplasty balloons with and without surface treatment to minimize blood clotting. The untreated surface has substantial clot accumulation while the modified surface shows minimal clotting.

treatments. Heparin is ubiquitous in animal cells and is a highly structurally varied, acidic polysaccharide ranging in size from approximately 3,000 - 37,500 Daltons.<sup>10-12</sup> It is synthesized in the Golgi apparatus within the cell and found in nearly all mammalian cells.<sup>13</sup> The heparin molecule plays an active role in a number of critically important biological processes including the regulation of blood clotting as well as the binding of cytokines that trigger the immune response and pathogens alike.<sup>10, 12, 14-17</sup> Most commonly, heparin has been used for decades as a medical treatment for the regulation of blood clotting.<sup>18, 19</sup> Specifically, heparin acts as a biocatalyst by deactivating thrombin, an important blood clotting factor, when it simultaneously binds antithrombin-III and thrombin shown in Figure 8.2.<sup>10, 12, 17</sup> In addition to participating in the regulation of clotting heparin can irreversibly bind tumor necrosis factor alpha (TNF- $\alpha$ ), a 17 kDa protein responsible for triggering apoptosis in unhealthy cells.<sup>20-22</sup> TNF- $\alpha$  is an incredibly important protein in the protection and preservation of a healthy organism. However, when it is produced by the body in high concentrations in response to the presence (or perceived presence) to a particularly harmful pathogen it can cause for sepsis and even death.<sup>23</sup>



**Figure 8.2.** Schematic of the biocatalytic action of heparin for the deactivation of thrombin clotting factor by the simultaneous binding of the antithrombin-III and thrombin. After AT-III and thrombin bind together irreversibly and are deactivated, they desorb from heparin and thus regenerate the biocatalytic surface.

This investigation of heparin coated surfaces demonstrated the capability of the QCM technique for quantitatively determining the reversible and irreversible binding of proteins to biologically active heparin coated surfaces under physiological conditions. Additionally, the binding capacities of bare polystyrene and heparinized surfaces for both TNF- $\alpha$  and AT-III proteins were determined in this study. Finally, surface-sensitive sum frequency generation (SFG) vibrational spectroscopy was performed on a heparin coated surface providing the first known SFG spectrum of this biologically important molecule.

## 8.2. Experimental

### 8.2.1. QCM Experimental Measurements

Quartz crystal microbalance measurements in this investigation were conducted with a commercial Q-sense (Glen Burnie, MD) model E4 QCM instrument. The resonance and dissipation values of each individual sensor crystal was measured and recorded in pure phosphate buffered saline (PBS) solution at pH 7.4 at the start of every QCM experiment. Throughout the QCM data collection process the fundamental, 3<sup>rd</sup>, and 5<sup>th</sup> harmonic frequencies and dissipations were continuously monitored at approximately 5 MHz, 15 MHz, and 25 MHz frequency ranges, respectively. After establishing a stable baseline values for sensor resonance frequencies and dissipations in pure PBS, the sensor crystals were then exposed to degassed solutions of biomolecules dissolved in PBS. QCM experiments were performed inside of a temperature controlled measurement chamber which was maintained at a constant temperature of  $37.0 \pm 0.1$  °C to replicate human body temperature for the model biological system. Quantitative surface concentrations for the biomolecules adsorbed on the QCM sensor surfaces were determined from experimentally measured 3<sup>rd</sup> harmonic frequency data using the Sauerbrey relationship as shown in Equation (8.1).<sup>24</sup>

$$\Delta m = -\frac{C}{n} \Delta f_n \quad (8.1)$$

The Sauerbrey equation correlates the change in a QCM resonator's  $n^{\text{th}}$  harmonic frequency,  $\Delta f_n$ , to the harmonic number of the resonance of interest,  $n$ , and a constant dependant upon the physical properties of the resonator,  $C$ , to the mass adsorbed on to the resonator's surface,  $\Delta m$ , during an experiment. Both the heparinized and unheparinized gold and SiO<sub>2</sub> coated QCM sensor crystals used during these measurements were manufactured by Q-sense to have a resonator constant of  $C = 17.7 \text{ ng s cm}^{-2}$ . A more detailed theoretical background for the QCM technique is provided in Chapter 4 along with a more detailed description of the quartz sensor crystals, the QCM instrument, and specific experimental procedures implemented in this study.<sup>24-28</sup>

### 8.2.2. SFG Experimental Measurements

Sum Frequency Generation (SFG) experiments were conducted using a 20 Hz pulsed Continuum (Santa Clara, CA) Leopard D-20 Nd:YAG laser with an output of 1064 nm light at a 22 picosecond pulse width. The near-infrared beam was then passed through to a Laservision (Bellevue, WA) Optical Parametric Generator (OPG)/Optical Parametric Amplifier (OPA) optical system which produced a 532 nm visible beam and a tunable infrared beam at 2800 - 3600  $\text{cm}^{-1}$ . Both of these output laser beams were used directly in SFG experiments at energies of  $\sim 200 \mu\text{J/pulse}$ . A flat, glass microscope cover slip with a heparin surface coating was used in measurements at a beam geometry of 65° and 42° off surface normal for the incoming visible and infrared beams, respectively. The heparinized cover slip substrates were placed on top of a Viton o-ring in a clean Petri dish during measurement. SFG signal generated at the air-solid interface was detected using a photomultiplier tube before being processed and recorded on a

desktop computer. These SFG measurements were conducted in the *ssp* laser polarization combination. Additional theoretical background of the SFG process is included in Chapter 2,<sup>29</sup> and a thorough description of the Laservision OPG/OPA system setup is provided in Chapter 3.

### 8.2.3. Chemicals

All QCM experiments were conducted at pH 7.4 and solutions were made with phosphate buffered saline (PBS) (Fisher). Human tumor necrosis factor- $\alpha$  (TNF- $\alpha$ ) and bovine antithrombin III (AT-III) were purchased from Sigma-Aldrich and used as received. TNF- $\alpha$  solutions were made and used at 83  $\mu\text{g/L}$  concentrations in PBS, and solutions AT-III were made and studied at concentrations of 200 mg/L (1 UN) in PBS. All QCM measurements were carried out in pure PBS or biomolecules/PBS solutions maintained at 37.0 °C to replicate human body temperature, while all SFG measurements were conducted in air at a temperature of 20 °C.

### 8.2.4. Heparin Functionalized Surface Preparation

QCM measurements were performed utilizing SiO<sub>2</sub> coated and polystyrene coated gold Q-Sense (Glen Burnie, MD) sensors as described in detail Chapters 3, 6, and 7. However, after cleaning and surface preparation the clean PS and SiO<sub>2</sub> coated QCM sensors were provided to industrial collaborators at Emergence Venture Partners LLC. (Berkeley, CA) and DSM Biomedical Inc. (Berkeley, CA) for surface heparinization. Similarly, SFG sample substrates were prepared from glass microscope slide cover slips (VWR) which were cleaned using an O<sub>2</sub> plasma treatment as previously described for the SiO<sub>2</sub> coated QCM sensor crystals in Chapters 3, 6, and 7 before being surrendered for heparinization. The exact procedure implemented for surface heparinization of these samples is currently an industrial trade secret controlled by Carmeda AB (Sweden). Nonetheless, other experimental procedures for heparinizing surfaces have been previously published.<sup>30-32</sup> The heparin coating process is suspected to include the use of a thin layer of polyethyleneimine or a similar polymer to covalently anchor the large, polysaccharide heparin molecules to the surface of interest. The successful completion of the heparinization process was confirmed by the treatment of a small, representative portion of QCM and SFG substrates with toluidine blue dye (Fischer). In the presence of this dye the surfaces coated with heparin turned purple while uncoated control sample surfaces remained their original color. Successfully heparinized QCM and SFG sample substrates were then thoroughly rinsed with distilled, de-ionized water before being dried. All heparinized QCM and SFG substrate surfaces were stored in the dark and inside of a desiccator to prevent sample degradation prior to experimental use.

## 8.3. Results and Discussion

### 8.3.1. QCM Data and Analysis

The binding capacity of both heparinized and bare PS-coated “control” QCM sensor crystals to tumor necrosis factor alpha (TNF- $\alpha$ ) was experimentally determined with QCM. This experiment was performed because the 17,000 Dalton TNF- $\alpha$  protein is well known to irreversibly bind heparin (but not polystyrene) and this property can be exploited to titrate the active loading capacity of a heparin functionalized surface as depicted in Figure 8.3.<sup>13-15</sup> During the QCM experiment a  $37.0 \pm 0.1$  °C solution of TNF- $\alpha$  ( $83 \mu\text{g/L}$  in PBS) was flowed across the PS and heparin coated crystals at a rate of  $100 \mu\text{L/min}$  over a period of 20 hours as presented in Figure 4. The heparin coated QCM sensor crystals were found to bind an average TNF- $\alpha$  surface concentration of  $1260 \text{ ng/cm}^2$  after approximately 16 hours of exposure. The bare polystyrene coated surfaces were found to bind a small amount of TNF- $\alpha$  averaging only  $\sim 40 \text{ ng/cm}^2$ . A summary of these results is included in Table 8.1. Measurement of the PS coated QCM surfaces was made challenging by the periodic nucleation, growth, and desorption of air bubbles from the TNF- $\alpha$ /PBS solution on the hydrophobic QCM sensor surface. The frequency of phenomenon’s occurrence was reduced by degassing dissolved  $\text{CO}_2/\text{O}_2$  with nitrogen bubbling and the subsequent gentle heating of PBS solutions prior to introduction to the QCM flow chambers.

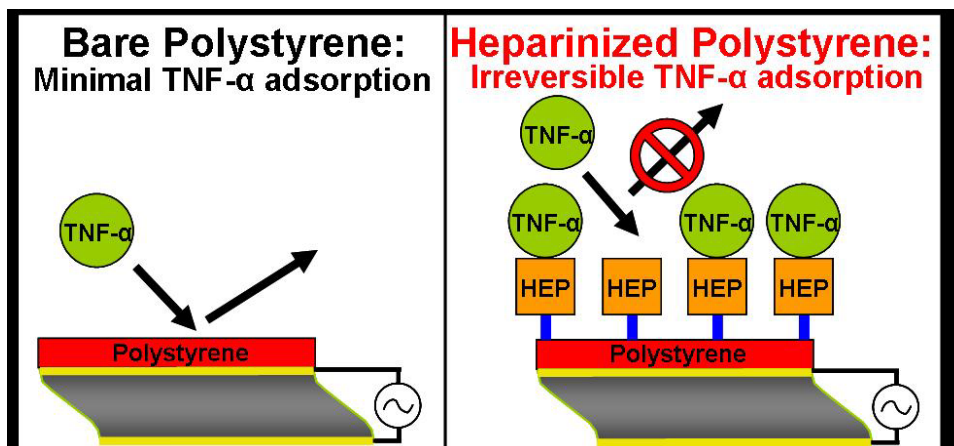


Figure 8.3. Schematic of QCM binding experiment performed for the determination of surface loading capacity of bare polystyrene and heparin coated surfaces for TNF- $\alpha$ . The PS coated surface was used as an experimental control surface as the TNF- $\alpha$  protein has been previously reported to irreversibly bind to heparin.

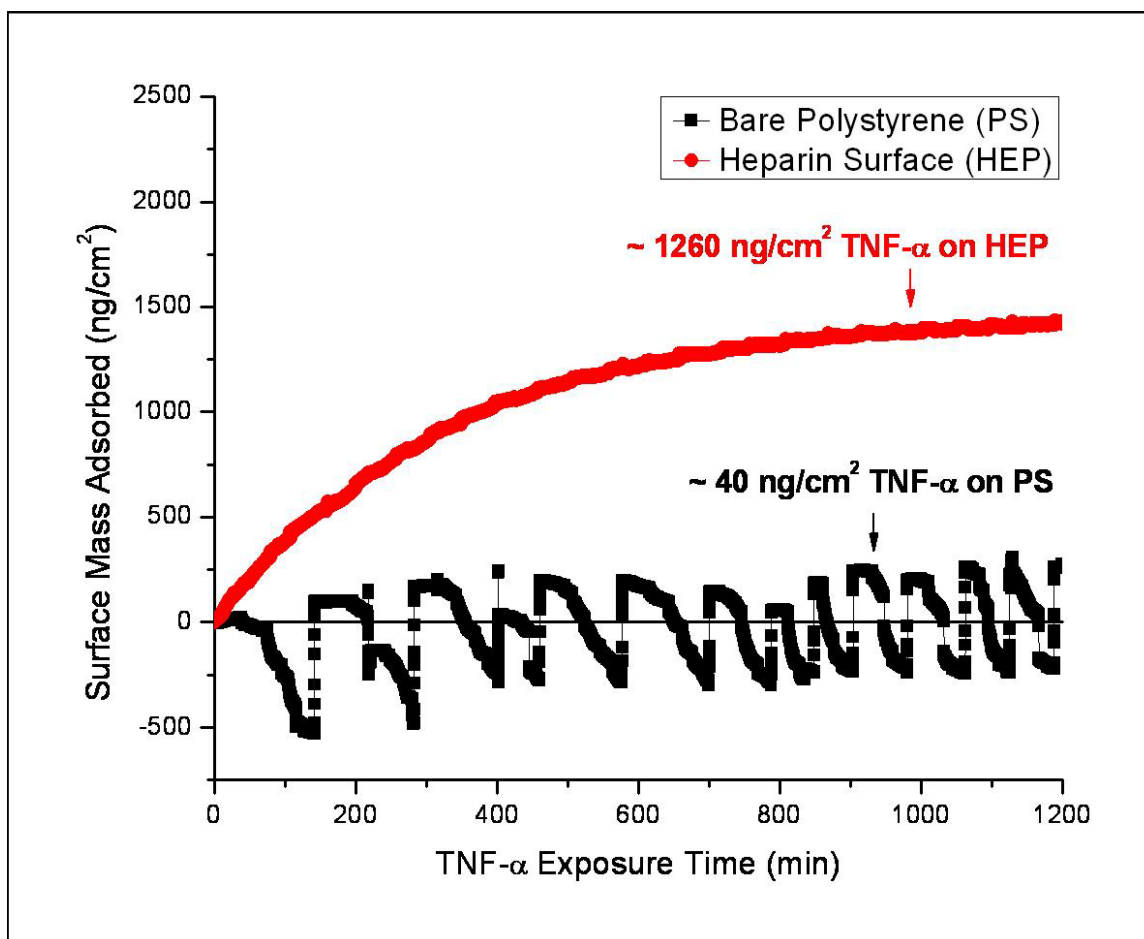


Figure 8.4. QCM experimental data of showing TNF- $\alpha$  binding from a protein solution (83  $\mu\text{g/L}$  in PBS) flowed across bare polystyrene and heparin coated surfaces (100  $\mu\text{L/min}$ ) at 37  $^{\circ}\text{C}$ . The TNF- $\alpha$  protein appears to saturate the heparin surface after approximately 16 hours at a surface concentration of  $\sim 1260$   $\text{ng/cm}^2$  while only  $\sim 40$   $\text{ng/cm}^2$  of protein was found to bind to the PS surface.

Surface	TNF- $\alpha$ Bound
HEP on PS	1260 $\text{ng/cm}^2$
Bare PS	40 $\text{ng/cm}^2$

Table 8.1. Summary of TNF- $\alpha$  binding capacity of polystyrene and heparin coated surfaces as determined by QCM measurements at 37  $^{\circ}\text{C}$ .

A second set of QCM experiments were conducted to determine the binding capacity of the heparin coated surface for antithrombin-III (AT-III), a 58 kDa protein responsible for the deactivation of the thrombin blood clotting factor.<sup>10-12, 14-17, 33-35</sup> In these experiments a solution of AT-III was flowed across heparin coated and polystyrene coated QCM sensor crystals before another solution of TNF- $\alpha$  was exposed to the surfaces. This procedure was performed to quantify the amount of AT-III that would reversibly bind to both surfaces in the absence and presence of presence of the TNF- $\alpha$  protein as shown in Figure 8.5. Specifically, this experiment

was conducted by the exposure of a solution of AT-III (1 UN or 200 mg/L in PBS) flowed across the QCM sensor surfaces at a rate of 50  $\mu\text{L}/\text{min}$  for two hours. Subsequently, a solution of TNF- $\alpha$  (83  $\mu\text{g}/\text{L}$  in PBS) was flowed through the QCM measurement chambers for one additional hour at a rate of 50  $\mu\text{L}/\text{min}$ . The QCM instrument was maintained at a temperature of  $37.0 \pm 0.1$   $^{\circ}\text{C}$  throughout the entire experiment. A plot of the data collected during this QCM binding experiment is presented in Figure 8.6. Interestingly the heparin coated surfaces were found to bind an average of 178  $\text{ng}/\text{cm}^2$  AT-III in the absence of TNF- $\alpha$  while the polystyrene surfaces accumulated a final AT-III surface concentration of 459  $\text{ng}/\text{cm}^2$ . This result was unexpected as the PS surface was expected to bind substantially less AT-III than the heparin coated surface and only a minimal amount of protein. However, this may be explained by the non-specific binding and subsequent denaturation of the AT-III protein on the PS surface. In such a circumstance, upon adsorption a protein could unfold from its native structure and spread across the hydrophobic surface thus allowing the accumulation of additional non-specific binding events. This is a reasonable hypothesis as the non-specific binding of large proteins is an immediate and crucial process in the body's immune response to the presence of foreign materials.<sup>1, 2</sup> Further supporting this hypothesis is the observation that the accumulation of biomolecules on the PS surface occurs rapidly but only after nearly an hour of exposure to the AT-III solution as shown in Figure 8.6. After equilibrium concentrations of AT-III accumulated on both surfaces, the introduction of a solution of TNF- $\alpha$  resulted in a subsequent reduction in the total surface mass adsorbed on the polystyrene and heparin surfaces of 25  $\text{ng}/\text{cm}^2$  and 34  $\text{ng}/\text{cm}^2$ , respectively. This observation is explained as the displacement of AT-III species from both surfaces by adsorbed TNF- $\alpha$  species. A quantitative summary of the surface concentration data collected during this QCM experiment is provided in Table 8.2.

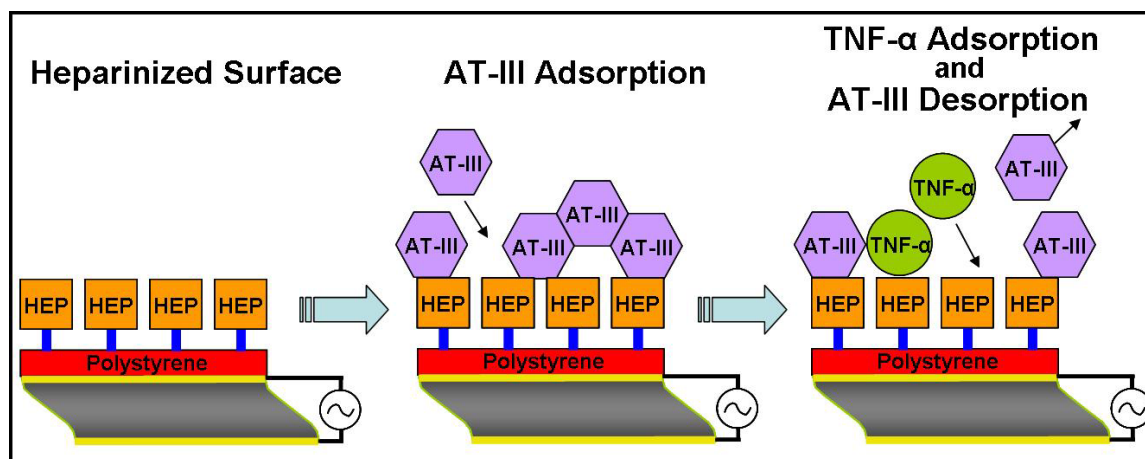


Figure 8.5. Schematic of QCM binding experiment performed for the determination of surface loading capacity of bare polystyrene and heparin coated surfaces for AT-III before and after the introduction of a solution of TNF- $\alpha$ .

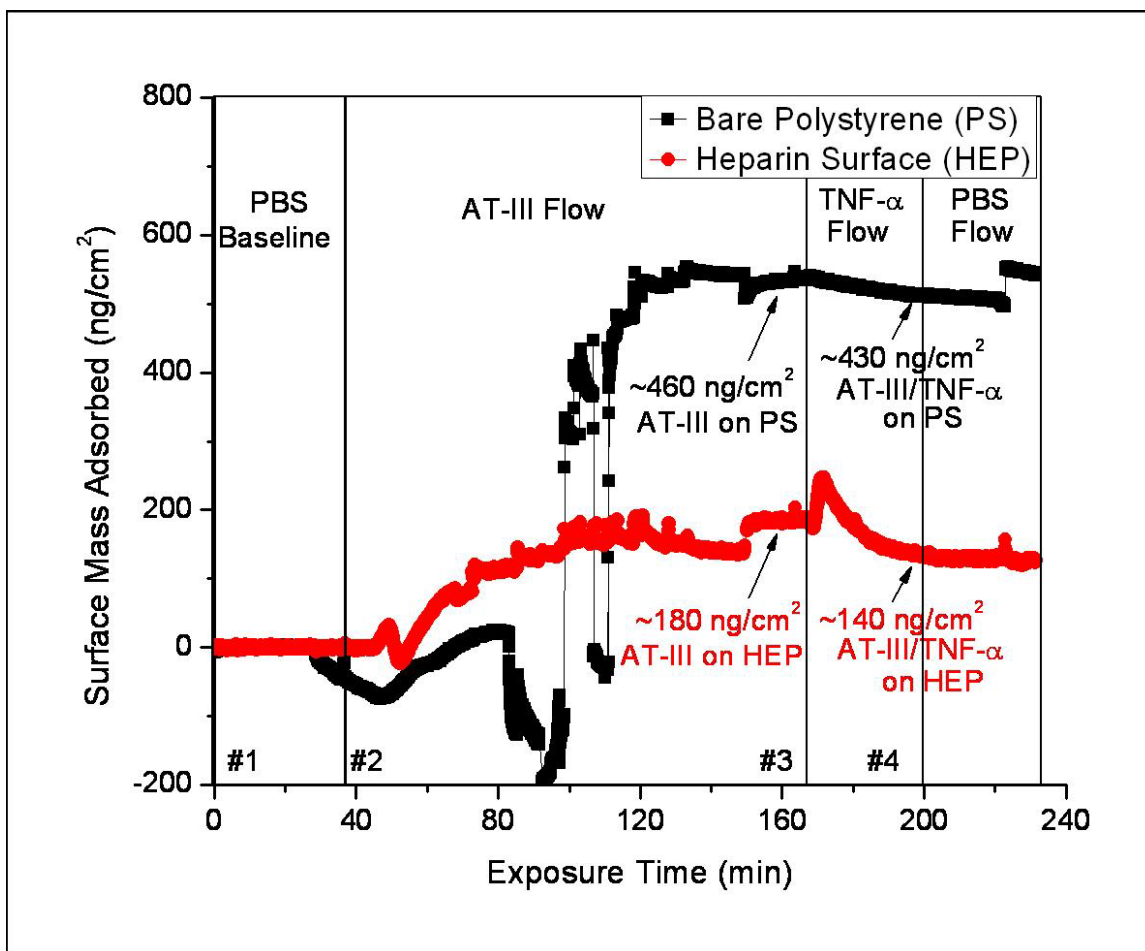


Figure 8.6. QCM experimental data showing the binding AT-III from a solution (1 UN or 200 mg/L in PBS) flowed across bare polystyrene and heparin coated surfaces (50  $\mu\text{L}/\text{min}$ ) at 37  $^{\circ}\text{C}$ . The AT-III protein appears to saturate the PS and heparin surfaces after approximately 2 hours at surface concentrations of 459  $\text{ng}/\text{cm}^2$  and 178  $\text{ng}/\text{cm}^2$ , respectively. Interestingly, the AT-III protein appears to accumulate to a greater extent on the bare PS surface indicating non-specific protein adsorption process. Upon the subsequent addition of a solution of TNF- $\alpha$  (83  $\mu\text{g}/\text{L}$  in PBS flowed at a rate of 100  $\mu\text{L}/\text{min}$ ), the total mass adsorbed on both QCM sensor surfaces is observed to decrease slightly from previous levels indicating the displacement of adsorbed AT-III by TNF- $\alpha$  molecules.

Surface	AT-III Bound	Surface Mass w/ TNF- $\alpha$
HEP on PS	178 $\text{ng}/\text{cm}^2$	144 $\text{ng}/\text{cm}^2$
Bare PS	459 $\text{ng}/\text{cm}^2$	434 $\text{ng}/\text{cm}^2$

Table 8.2. Summary of the AT-III and subsequent TNF- $\alpha$  binding capacity of polystyrene and heparin coated surfaces as determined by QCM measurements at 37  $^{\circ}\text{C}$ .

### 8.3.2. SFG Data and Analysis

SFG experiments were conducted on heparin coated glass microscope cover slips to provide information about the surface structure of the biologically active surface as presented in Figure 8.7. This vibrational spectrum was collected at 20 °C in air and each data point is the average of 640 measurements. The data included in Figure 8.7 shows three C-H vibrational modes centered at 2850  $\text{cm}^{-1}$ , 2905  $\text{cm}^{-1}$ , and 2945  $\text{cm}^{-1}$  as well as a broad spectral feature centered at approximately 3315  $\text{cm}^{-1}$ . The structural origin of these C-H peaks apparent in the SFG spectrum of is somewhat ambiguous due to the high molecular weight of heparin (~15 kDa) and as well as the structural diversity of the large polysaccharide chains. Nonetheless, the spectral peak at 2850  $\text{cm}^{-1}$  is identified as a  $\text{CH}_2$  symmetric stretching mode from the polyethyleneimine polymer anchoring the heparin molecules to the glass surface. The vibrational mode observed at 2905  $\text{cm}^{-1}$  is suspected to originate from a CH stretching mode of tri-substituted carbon atoms on the heparin polysaccharide chains. However, the assignment of this peak is nontrivial and it may also be indicative of a  $\text{CH}_2$  Fermi resonance from the polymer anchoring. The strongest of the three C-H modes observed in the SFG spectrum of the heparin surface is centered at a frequency of 2945  $\text{cm}^{-1}$  and is assigned as either a  $\text{CH}_2$  asymmetric stretch from the polymer attaching the heparin to the surface or it may be indicative of a  $\text{CH}_3$  Fermi resonance from methyl terminated heparin sub-units. Finally, the vibrational mode centered at approximately 3315  $\text{cm}^{-1}$  is attributed to the N-H amide A vibrational mode of the polyethyleneimine polymer linking the heparin molecules to the solid substrate surface. While the assignment of these SFG active vibrational modes is only preliminary, this spectrum is an important experimental achievement as it is the first known SFG spectrum of a heparin surface despite unpublished attempts by other research groups. Therefore, this spectrum provides evidence supporting the further study of heparin and heparin coated surfaces using the surface-sensitive SFG vibrational spectroscopy technique.

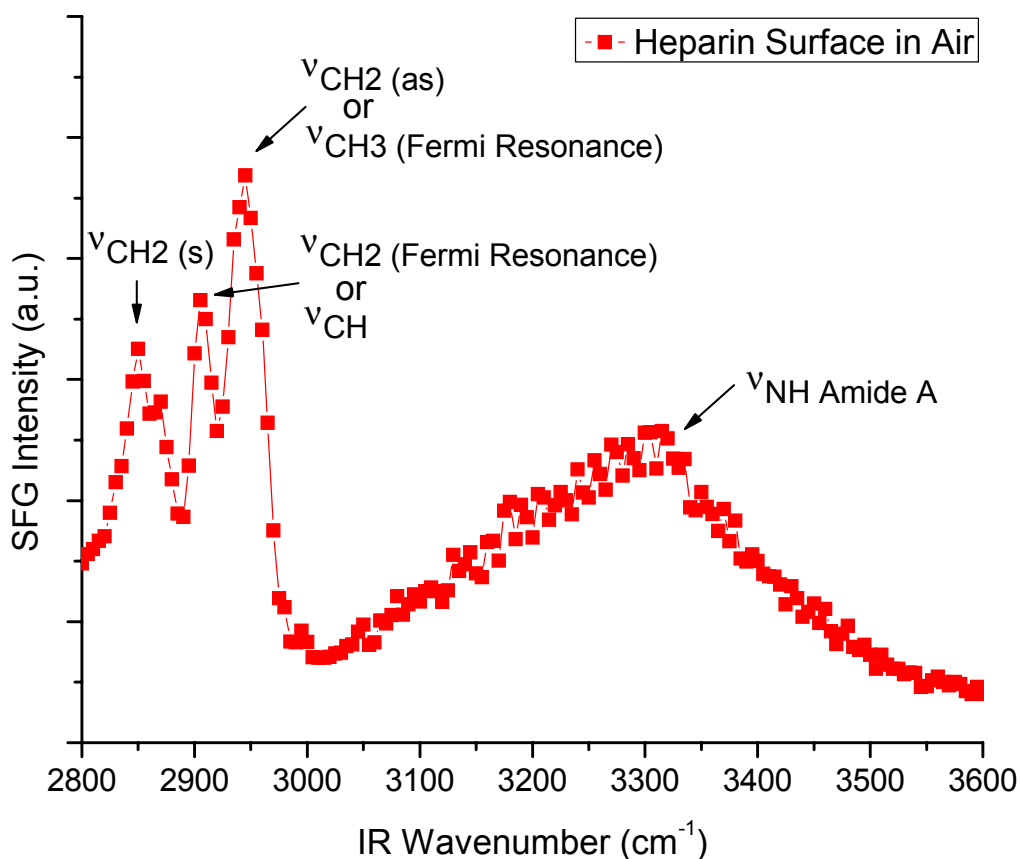


Figure 8.7. SFG spectrum of heparin coated glass microscope cover slip in air. Three SFG active C-H vibrational modes are observed at  $2850\text{ cm}^{-1}$ ,  $2905\text{ cm}^{-1}$ , and  $2945\text{ cm}^{-1}$  as well as an N-H amide A mode from the polyethyleneimine anchoring layer at  $3315\text{ cm}^{-1}$ . The peak centered at  $2850\text{ cm}^{-1}$  is identified as a  $\text{CH}_2$  (s) mode from polyethyleneimine. The vibrational modes centered at  $2905\text{ cm}^{-1}$  and  $2945\text{ cm}^{-1}$  are attributed to a  $\text{CH}_2$  Fermi resonance and a  $\text{CH}_2$  asymmetric stretch, respectively, from the polymer layer attaching the long heparin chains to the glass surface. Alternatively, these SFG peaks may originate from a CH stretching mode ( $2905\text{ cm}^{-1}$ ) and a  $\text{CH}_3$  Fermi resonance ( $2945\text{ cm}^{-1}$ ) on some of the heparin polysaccharide chains.

#### 8.4. Conclusions

This investigation of heparin coated surfaces demonstrated the capability of the QCM technique for quantitatively determining the reversible and irreversible binding of biologically active heparin coated surfaces in real-time. Furthermore, the binding capacities of bare polystyrene and heparinized surfaces for both TNF- $\alpha$  and AT-III proteins were determined under physiological conditions and without the use of ELISA type techniques. Additionally, the first known successful SFG spectrum of a heparin surface was obtained in this study. This progress suggests the experimental feasibility of conducting surface-sensitive vibrational spectroscopic investigations of the scientifically important biocatalytic heparin/thrombin/AT-III blood clotting system in the future. Finally, this research provides strong evidence for the reproducible and quantifiable biological activity of heparin functionalized surfaces made in the laboratory.

## References

1. Anderson, J. M., *Annual Review of Materials Research* **2001**, *31*, 81-110.
2. Castner, D. G.; Ratner, B. D., *Surface Science* **2002**, *500* (1-3), 28-60.
3. Chen, Z.; Ward, R.; Tian, Y.; Malizia, F.; Gracias, D. H.; Shen, Y. R.; Somorjai, G. A., *Journal of Biomedical Materials Research* **2002**, *62* (2), 254-264.
4. Chen, Z.; Shen, Y. R.; Somorjai, G. A., *Annual Review of Physical Chemistry* **2002**, *53*, 437-465.
5. Kim, J.; Koffas, T. S.; Lawrence, C. C.; Somorjai, G. A., *Langmuir* **2004**, *20* (11), 4640-4646.
6. Opdahl, A.; Koffas, T. S.; Amitay-Sadovsky, E.; Kim, J.; Somorjai, G. A., *Journal of Physics-Condensed Matter* **2004**, *16* (21), R659-R677.
7. Chen, Z.; Ward, R.; Tian, Y.; Baldelli, S.; Shen, Y. R.; Somorjai, G. A., *Abstracts of Papers of the American Chemical Society* **2000**, *219*, U525-U525.
8. Chen, Z.; Ward, R.; Tian, Y.; Eppler, A. S.; Shen, Y. R.; Somorjai, G. A., *Journal of Physical Chemistry B* **1999**, *103* (15), 2935-2942.
9. Voller, A.; Bartlett, A.; Bidwell, D. E., *Journal of Clinical Pathology* **1978**, *31* (6), 507-520.
10. Jaques, L. B., *Science* **1979**, *206* (4418), 528-533.
11. Nader, H. B.; Chavante, S. F.; dos-Santos, E. A.; Oliveira, F. W.; de-Paiva, J. F.; Jeronimo, S. M. B.; Medeiros, G. F.; de-Abreu, L. R. D.; Leite, E. L.; de-Sousa, J. F.; Castro, R. A. B.; Toma, T.; Tersariol, I. L. S.; Porcionatto, M. A.; Dietrich, C. P., *Brazilian Journal of Medical and Biological Research* **1999**, *32* (5), 529-538.
12. Hirsh, J.; Warkentin, T. E.; Shaughnessy, S. G.; Anand, S. S.; Halperin, J. L.; Raschke, R.; Granger, C.; Ohman, E. M.; Dalen, J. E., *Chest* **2001**, *119* (1), 64s-94s.
13. Garg, H. G.; Linhardt, R. J.; Hales, C. A., *Chemistry and biology of heparin and heparan sulfate*. Elsevier: Amsterdam ; London, 2005; p xviii, 774.
14. Day, J. R. S.; Landis, R. C.; Taylor, K. M., *Journal of Cardiothoracic and Vascular Anesthesia* **2004**, *18* (1), 93-100.
15. Byun, Y.; Jacobs, H. A.; Kim, S. W., *Journal of Biomaterials Science-Polymer Edition* **1994**, *6* (1), 1-13.
16. Byun, Y.; Jacobs, H. A.; Kim, S. W., *Biotechnology Progress* **1996**, *12* (2), 217-225.
17. Byun, Y.; Jacobs, H. A.; Kim, S. W., *Journal of Biomedical Materials Research* **1996**, *30* (4), 423-427.
18. Hull, R. D.; Raskob, G. E.; Hirsh, J.; Jay, R. M.; Leclerc, J. R.; Geerts, W. H.; Rosenbloom, D.; Sackett, D. L.; Anderson, C.; Harrison, L.; Gent, M., *New England Journal of Medicine* **1986**, *315* (18), 1109-1114.
19. Basu, D.; Cade, J.; Gallus, A.; Hirsh, J., *New England Journal of Medicine* **1972**, *287* (7), 324-&.
20. Wollenberg, G. K.; Lamarre, J.; Rosendal, S.; Gonias, S. L.; Hayes, M. A., *American Journal of Pathology* **1991**, *138* (2), 265-272.
21. Hoffmann, J. N.; Hartl, W. H.; Faist, E.; Jochum, M.; Inthorn, D., *Inflammation Research* **1997**, *46* (9), 342-347.
22. Fujita, M.; Ishihara, M.; Ono, K.; Hattori, H.; Kurita, A.; Shimizu, M.; Mitsumaru, A.; Segawa, D.; Hinokiyama, K.; Kusama, Y.; Kikuchi, M.; Maehara, T., *Artificial Organs* **2002**, *26* (12), 1020-1025.

23. Abbas, A. K.; Lichtman, A. H.; Pober, J. S., *Cellular and molecular immunology*. 4th ed.; W.B. Saunders: Philadelphia, 2000; p vii, 553 p.
24. Sauerbrey, G., *Zeitschrift Fur Physik* **1959**, *155* (2), 206-222.
25. Marx, K. A., *Biomacromolecules* **2003**, *4* (5), 1099-1120.
26. Rodahl, M.; Kasemo, B., *Review of Scientific Instruments* **1996**, *67* (9), 3238-3241.
27. Arnau, A., *Sensors* **2008**, *8* (1), 370-411.
28. Rodahl, M.; Kasemo, B., *Sensors and Actuators a-Physical* **1996**, *54* (1-3), 448-456.
29. Lambert, A. G.; Davies, P. B.; Neivandt, D. J., *Applied Spectroscopy Reviews* **2005**, *40* (2), 103-145.
30. Larm, O.; Larsson, K.; Scholander, E., *Carbohydr. Res.* **1979**, *73* (AUG), 332-336.
31. Larm, O.; Larsson, R.; Olsson, P., *Biomaterials Medical Devices and Artificial Organs* **1983**, *11* (2-3), 161-173.
32. Olsson, P.; Larm, O., *Int. J. Artif. Organs* **1991**, *14* (8), 453-456.
33. Shapiro, S. S.; Martinez, J., *Journal of Clinical Investigation* **1969**, *48* (7), 1292-&.
34. Sakr, Y.; Reinhart, K.; Hagel, S.; Kientopf, M.; Brunkhorst, F., *Anesthesia and Analgesia* **2007**, *105* (3), 715-723.
35. Butenas, S.; van't Veer, C.; Mann, K. G., *Blood* **1999**, *94* (7), 2169-2178.

## Chapter 9

### The Development and Implementation of a Novel Optical Parametric Amplifier Utilizing Lithium Thioindate to Probe the Amide I Mode of a Model Amphiphilic Peptide

A new optical parametric amplifier using lithium thioindate has been developed and used to study the interfacial secondary structure of a model peptide by sum frequency generation (SFG) vibrational spectroscopy in the amide I spectral region. The 14 residue model peptide, LK<sub>14</sub>, was composed of L-lysine (K) and L-leucine (L) amino acid subunits in the sequence Ac-LKKLLKLLKLLKLL-NH<sub>2</sub> resulting in a peptide with an  $\alpha$ -helical secondary structure in high ionic strength bulk buffer solutions and a random coil backbone structure in low ionic strength bulk buffer solutions. The LK<sub>14</sub> peptide dissolved in high ionic strength buffer solutions was studied on both the hydrophobic deuterated polystyrene (*d*<sub>8</sub>-PS) and the hydrophilic calcium fluoride (CaF<sub>2</sub>) solid-liquid interfaces, as well as at the *d*<sub>8</sub>-PS surface at low ionic strength buffer conditions. The amide I mode at on *d*<sub>8</sub>-PS at both high and low ionic strength solution conditions was found to be centered at 1655 cm<sup>-1</sup> indicating the adsorbed peptide backbone maintained an  $\alpha$ -helical structure from high ionic strength solutions, and it transformed from a random coil to an  $\alpha$ -helix upon adsorption at low ionic strengths. On the CaF<sub>2</sub> surface, the SFG spectrum of the LK<sub>14</sub> peptide solution had a weak amide I mode at 1670 cm<sup>-1</sup> suggesting that upon adsorption the backbone secondary structure changed from an  $\alpha$ -helix to a random coil conformation.

#### 9.1. Introduction

The capacity of a substrate to change a peptide or protein's interfacial conformation or secondary structure and subsequently change or inhibit its function is well known.<sup>1-4</sup> However, monitoring changes in the interfacial secondary structure of these biomolecules at a molecular level has been experimentally challenging due to a lack of surface specific techniques that can be implemented under the physiological conditions at which these species exist and function in nature. Several research groups have recently begun utilizing sum frequency generation (SFG) vibrational spectroscopy, a surface-specific nonlinear optical technique, to probe the structure and conformation of peptides and proteins on solid surfaces.<sup>5-7</sup> In this study, we implement a novel type of optical parametric amplifier (OPA) built using lithium thioindate (LIS) frequency conversion crystals, LiInS<sub>2</sub>, to generate intense infrared laser light in the spectroscopic region 1500 cm<sup>-1</sup> to 2000 cm<sup>-1</sup> more easily than using the other commercially available frequency conversion crystals for this region.<sup>8,9</sup> This technique development makes it possible to more easily use SFG spectroscopy to monitor the amide I vibrational mode which is sensitive to the secondary structure (specifically backbone conformation) of interfacial peptides and proteins which are typically observed between 1600 - 1700 cm<sup>-1</sup>.<sup>10, 11</sup> Specifically, Raman and infrared spectroscopy have been implemented to establish the characteristic amide I vibrational frequency of a peptide or protein with an  $\alpha$ -helix secondary structure at 1650 - 1660 cm<sup>-1</sup> and a  $\beta$ -sheet structure at both 1630 cm<sup>-1</sup> and 1690 cm<sup>-1</sup>. However, biomolecules with a random coil

secondary structure show infrared activity at all of these frequencies as they may include multiple internal domains each of which has a different local conformation.

While a majority of SFG studies of interfacial biomolecules have investigated vibrational modes of these species in the infrared region 2800 - 3100  $\text{cm}^{-1}$ , Chen and co-workers began actively interrogating the amide I vibrational band of a number of biomolecules in 2003.<sup>12-15</sup> In 2005, Chen *et al* demonstrated that nonlinear SFG experiments conducted in the amide I region could be implemented to detect and differentiate the secondary structure of an interfacial biomolecule just as with Raman and infrared linear spectroscopic techniques.<sup>14</sup> Their SFG study found that an aqueous  $\alpha$ -helical peptide at a hydrophobic solid-liquid interface had a single peak in the middle of the amide I region at 1650  $\text{cm}^{-1}$ .

In this study we investigated a model peptide, LK<sub>14</sub>, in solution at the solid-liquid interface using SFG vibrational spectroscopy in the amide I region.<sup>16</sup> These SFG experiments were made possible through the use of a novel, LIS crystal based OPA. The LK<sub>14</sub> peptide is made up of only L-leucine (L) and L-lysine (K) amino acid residues which are hydrophobic and hydrophilic, respectively. These amino acids are arranged in the sequence, Ac-LKKLLKLLKLLKL-NH<sub>2</sub> which causes the resulting peptide to assume an  $\alpha$ -helical secondary structure in phosphate buffered saline (PBS) at pH 7.4 and high ionic strength; at lower ionic strengths, the LK<sub>14</sub> peptide will adopt a random coil secondary structure in PBS at pH 7.4.<sup>17-20</sup> Using the LIS based OPA, we found a solution of LK<sub>14</sub> in PBS at both high and low ionic strengths to have an SFG active vibrational mode at 1655  $\text{cm}^{-1}$  at the hydrophobic deuterated polystyrene (*d*<sub>8</sub>-PS)/PBS solid-liquid interface. The observation of this amide I peak at 1655  $\text{cm}^{-1}$  is expected at high ionic strength solid-liquid interfaces as a vibrational mode at this frequency corresponds to an  $\alpha$ -helical conformation of LK<sub>14</sub> species on the surface. However, detection of an  $\alpha$ -helical amide I peak is surprising from low ionic strength solutions where the peptide has been reported to exhibit a random coil conformation in bulk solutions.<sup>17</sup> This finding suggests that interactions between the surface and peptide upon adsorption induces the LK<sub>14</sub> to adopt an  $\alpha$ -helical secondary structure not present in solution phase species. When the same peptide was studied at high ionic strength solution conditions and at the hydrophilic calcium fluoride (CaF<sub>2</sub>)/PBS interface a peak was observed in the SFG spectrum at 1670  $\text{cm}^{-1}$ . This data indicates an  $\alpha$ -helix secondary structure exists at the hydrophilic solid-liquid interface. The blue-shift of this SFG vibrational mode 15  $\text{cm}^{-1}$  from the frequency observed on *d*<sub>8</sub>-PS is attributed to differences in interfacial structure of the peptide resulting from either the dissimilar nature of the two surfaces and their capacity to interact with solvent, ions, and adsorbate molecules via van der Waals interactions, or the peptide backbone assuming a random coil conformation on the CaF<sub>2</sub> surface.

## 9.2. Experimental

### 9.2.1. SFG Experimental Details

Sum Frequency Generation (SFG) vibrational spectroscopy is a surface-sensitive nonlinear optical laser technique which can provide surface-sensitive vibrational spectra of interfaces under a broad range of conditions. The SFG process is accomplished by spatially and temporally overlapping two intense, pulsed laser beams at frequencies  $\omega_1$  and  $\omega_2$  at a surface or interface of interest, which for an appropriately chosen system will result in the emission of light

at a frequency equal to the sum of the two input frequencies ( $\omega_1 + \omega_2 = \omega_3$ ), or sum frequency,  $\omega_3 = \omega_{\text{SFG}}$ .

In the picosecond infrared-visible SFG experiments described herein, both the visible beam at 532 nm ( $\omega_1 = \omega_{\text{vis}}$ ) and the tunable infrared beam ( $\omega_2 = \omega_{\text{IR}}$ ) are generated by pumping a series of nonlinear crystals with the output of a Nd:YAG laser producing pulses of light at 1064 nm. The Nd:YAG laser used in these experiments was an Ekspla PL2143A (Vilnius, Lithuania) laser with a pulse width of 25 picoseconds and a repetition rate of 10 Hz. A schematic for the optical parametric generation (OPG) and optical parametric amplification (OPA) stages used in these experiments is included in Figure 9.1. The 1064 nm infrared output of the Nd:YAG laser is split into two beams. One 1064 nm beam is converted into visible 532 nm pulses by passing it through a potassium di-deuterium phosphate (KD\*P),  $\text{KD}_2\text{PO}_4$ , crystal. A portion of the resulting beam is directly sent to the SFG sample surface, and the remainder is then passed through the OPG stage consisting of a pair of phase matched KTP crystals. These KTP crystals are mounted on stages which can be synchronously rotated. When the beam of 532 nm light passes through these crystals two tunable laser beams are generated, a signal beam ( $\sim 900$  nm) at shorter wavelengths and an idler beam ( $\sim 1300$  nm) at longer wavelengths so that energy is conserved. The signal beam is then dumped, and the idler beam is then sent to the OPA stage where difference frequency generation (DFG) occurs. (OPA and DFG are synonymous.<sup>21</sup>)

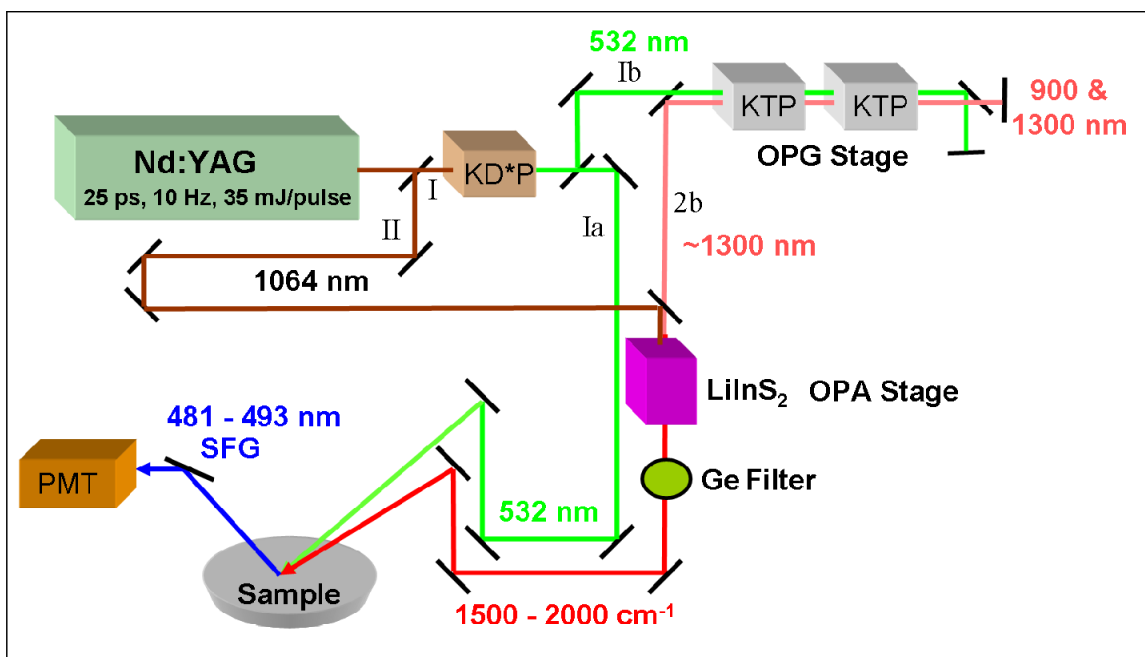
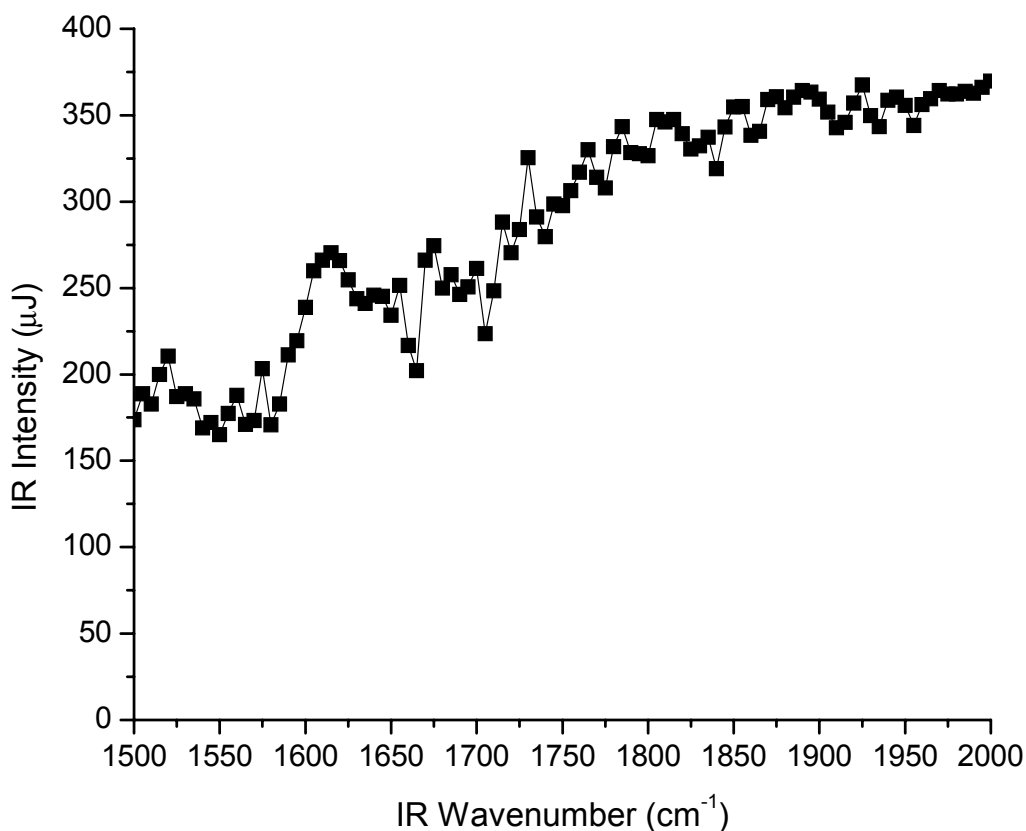


Figure 9.1. Diagram of OPG/OPA laser setup utilizing LIS crystals. A picosecond ND:YAG laser with 1064 nm output and split into two beams, I and II. Beam I is passed through a KD\*P crystal where it is frequency doubled producing 532 nm output which is split into beams Ia and Ib. Beam Ia is sent directly to the sample where it is used as the visible beam in the experiment. Beam Ib is sent through the OPG stage where it passes through two angle tunable KTP crystals twice producing two new beams, a signal and an idler beam. The higher energy signal beam is dumped, and the lower energy beam (2b) is then send to the OPA stage. Beam II and beam 2b are overlapped and simultaneously passed through the LIS crystal mounted on an angle tunable mount in the OPA stage. The idler light exiting the LIS crystal at the difference frequency of the two input beams ranges between 5000 nm and 7000 nm. Before being sent directly to the sample as the infrared beam used in the SFG experiment, the idler from the LIS is passed through a germanium window to filter out any unconverted input laser light from beams II and 2b.

While the OPA stage for many picosecond SFG experiments is composed of potassium titanyl arsenate (KTA) or lithium niobate ( $\text{LiNbO}_3$ ) crystals due to being able to efficiently produce wavelengths between  $2500 - 4000 \text{ cm}^{-1}$ , they have poor conversion efficiency for producing light in the amide I region ( $1600 - 1700 \text{ cm}^{-1}$ ). Light in the amide I frequency region can be produced using a combination of KTA and either silver gallium selenide,  $\text{AgGaSe}_2$ , (AGSe) crystals or silver gallium sulfide,  $\text{AgSeS}_2$  (AGS) crystals. However, the relatively low damage threshold of the AGS, as well as the need to use of two OPA stages (both KTA and AGS) results in poor overall energy conversion efficiency making this method experimentally non-ideal. OPAs based on KTP and AGSe stages have limited applicability due to the signal and idler outputs of the second crystal not being phase-matchable with a  $1064 \text{ nm}$  pump beam. Alternatively, in this study we have implemented the use of an OPA consisting of only one OPA crystal, LIS, which has a substantially increased damage threshold, higher conversion efficiency, lower cost, and better beam quality.



**Figure 9.2. Infrared energy output for LIS based OPA. The input energy for the  $1064 \text{ nm}$  beam pumping the LIS crystal was  $12 \text{ mJ/pulse}$ .**

As the conversion efficiency of a nonlinear crystal increases with input energy, it was necessary to determine the damage threshold of the LIS crystal so that it could be operated at the highest energy possible while minimizing the crystal damage and degradation with prolonged

use. We began pumping the LIS with increasing energy until reaching a pump power of 15mJ/pulse ( $\sim 1 \text{ J/cm}^2$ ) at which point we observed immediate surface damage consisting of clouding and small regions of opacity. We then determined the maximal safe pumping energy to be 80% of this immediate damage threshold at 12 mJ/pulse. A spectrum of the LIS based OPA output at a pump energy of 12 mJ is included in Figure 9.2. While AGS can be pumped at 15mJ/pulse, we have observed it to degrade on timescales of tens of hours of use and have observed gradual damage at pumping energies as low as 7 mJ/pulse.

### 9.2.2. Peptide Synthesis and Sample Preparation Details

The LK<sub>14</sub> peptide synthesis and experimental details aside from sample substrate material used in these experiments were identical to our previous publications.<sup>19, 20</sup> In these experiments, calcium fluoride, CaF<sub>2</sub>, substrates were used instead of fused silica, SiO<sub>2</sub>, because the latter is not transparent to infrared wavelengths used in this study. LK<sub>14</sub> peptide solutions (0.15 mg/mL) were made with PBS at pH 7.4 at both 1X and 0.01X concentrations. Theoretical and experimental details about SFG measurements can be found in the literature.<sup>22-26</sup> The laser polarization combination used in these experiments was s-polarized SFG, s-polarized visible, and p-polarized infrared (*ssp*, commonly). All experiments were carried out at a temperature of 20 °C.

### 9.3. Results and Discussion

The amide I SFG spectrum of LK<sub>14</sub> peptide in 1X PBS (0.15 mg/mL) at the hydrophobic *d*<sub>8</sub>-PS solid-liquid interface is presented in Figure 9.3. The spectrum shows an amide I mode centered at 1655 cm<sup>-1</sup> indicative of the peptide backbone assuming an  $\alpha$ -helical secondary structure. This peak assignment is consistent with the peptide's known secondary structure under similar conditions and buffer strength, as well as the published infrared and Raman vibrational mode frequencies for  $\alpha$ -helical peptides and proteins at 1650 cm<sup>-1</sup>.<sup>10, 17, 20</sup> This is interpreted as strong evidence that the LK<sub>14</sub> peptide retains its  $\alpha$ -helix structure upon adsorption to the *d*<sub>8</sub>-PS surface.

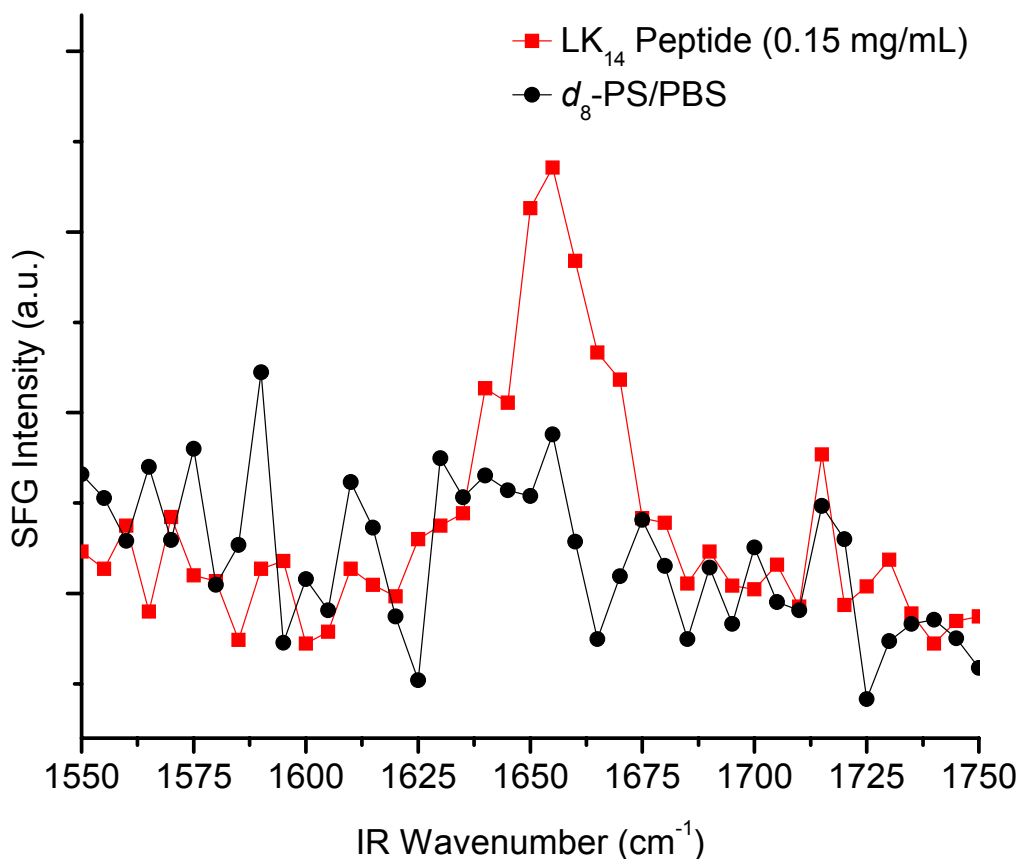
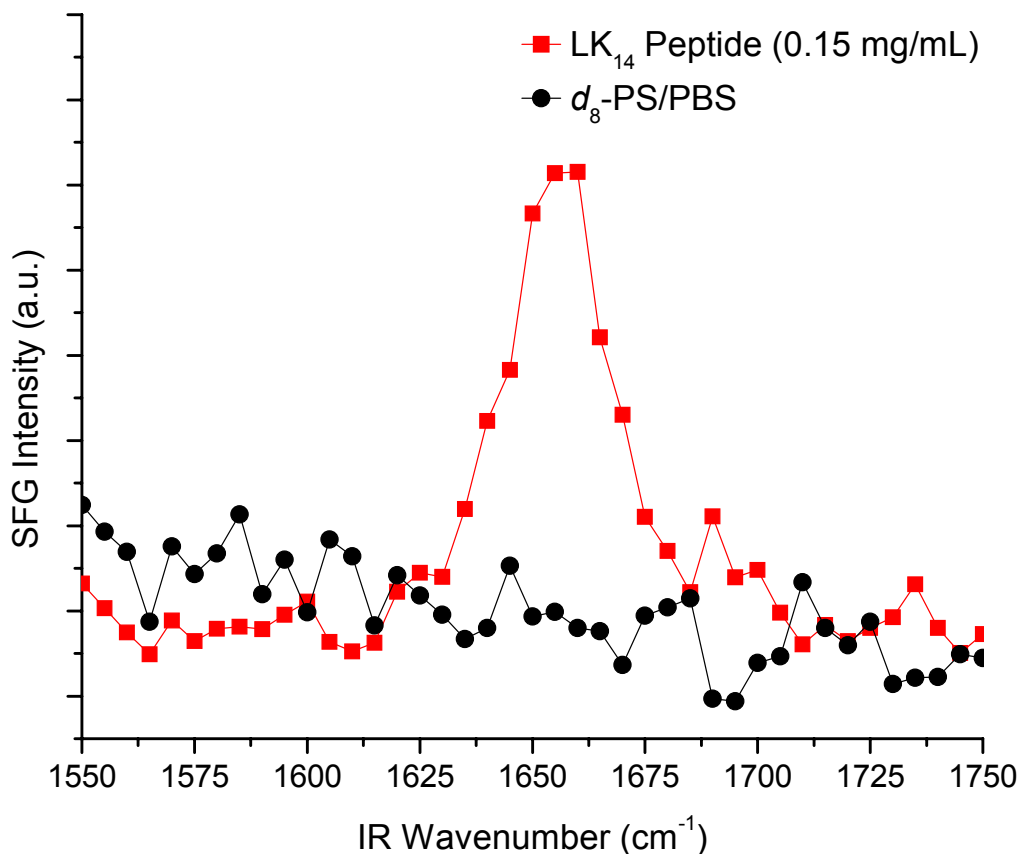


Figure 9.3. Amide I SFG spectrum of 1X PBS (high ionic strength) the hydrophobic  $d_8$ -PS solid-liquid interface before (black circles) and after (red squares) the addition of LK<sub>14</sub> peptide (0.15mg/mL). The amide I mode centered at 1655  $\text{cm}^{-1}$  is indicative of an  $\alpha$ -helical peptide backbone structure at the interface. This data supports measurements of the bulk solutions of LK<sub>14</sub> under similar conditions.

The SFG spectrum of a 0.15 mg/mL solution of LK<sub>14</sub> peptide in low ionic strength 0.01X PBS at the  $d_8$ -PS solid-liquid interface is shown in Figure 9.4. Similar to the spectrum of the same peptide at 1X PBS (Figure 9.3), Figure 9.4 has an amide I mode centered at 1655  $\text{cm}^{-1}$ . Again this peak is attributed to the peptide backbone assuming an  $\alpha$ -helix structure upon adsorbing to the  $d_8$ -PS surface. However, this finding is surprising because under these low ionic strength conditions the peptide is known to adopt a random coil conformation in bulk solution.<sup>17</sup> Thus the observation of the 1655  $\text{cm}^{-1}$  peak is interpreted as an indication that upon adsorption the peptide secondary structure transforms from a random coil to an  $\alpha$ -helix. However, it should be noted that the term “random coil” secondary structure is used to indicate a molecule that does not possess a well-defined global secondary structure, but it may possess one or more small regions of local secondary structure ( $\alpha$ -helix,  $\beta$ -sheet, etc.). Therefore it is possible that the 1655  $\text{cm}^{-1}$  vibrational mode from adsorbed peptide at low ionic strength may be from a species exhibiting only a partial helical structure. Nonetheless, this scenario is not

expected due to the short chain length of the peptide containing only 14 amino acid subunits in total and the number of amino residues needed to form an  $\alpha$ -helix being minimally five.



**Figure 9.4.** The SFG amide I spectrum of the low ionic strength (0.01X PBS) buffer at the  $d_8$ -PS hydrophobic solid-liquid interface before (black circles) and after (red squares) the addition of LK<sub>14</sub> peptide (0.15 mg/mL). The presence of a peak at 1655 cm<sup>-1</sup> is indicative of an  $\alpha$ -helical peptide backbone, despite the peptide exhibiting a random coil in bulk solution under similar conditions. This suggests the LK<sub>14</sub> species transforms from a random coil structure in solution to a helical secondary structure upon adsorption. Despite differences in ionic strength of PBS buffer solutions, the amide I mode in this spectrum is similar to that presented in Figure 9.3.

The SFG spectrum for a solution of LK<sub>14</sub> peptide at 0.15 mg/mL in 1X PBS at the hydrophilic CaF<sub>2</sub> solid-liquid interface is presented in Figure 9.5. This amide I spectrum in shows a single weak vibrational mode centered at 1670 cm<sup>-1</sup>. The origin of this of this peak from the peptide backbone is non-trivial because it is approximately 20 cm<sup>-1</sup> and equidistant from the frequencies expected for either an  $\alpha$ -helix (1650 cm<sup>-1</sup>) or a  $\beta$ -sheet (1690 cm<sup>-1</sup>). However, this mode may originate from the peptide backbone assuming a random-coil secondary structure which would explain the peak center being equidistant from the typical frequencies of the each of the two secondary structures. Alternatively, the difference in frequency could also be attributed simply to differences in interfacial structure of the peptide resulting from the dissimilar

nature of the two surfaces and their capacity to interact with the PBS and peptide molecules through van der Waals forces.<sup>27</sup> While there is not sufficient data for a conclusive assignment of this  $1670\text{ cm}^{-1}$  peak's origin, the difference between the amide I mode of LK<sub>14</sub> solutions at high ionic strength on the hydrophobic and hydrophilic surfaces (Figure 9.3 and Figure 9.5, respectively) is attributed to a difference in the secondary structure of the peptide upon adsorption to each surface.

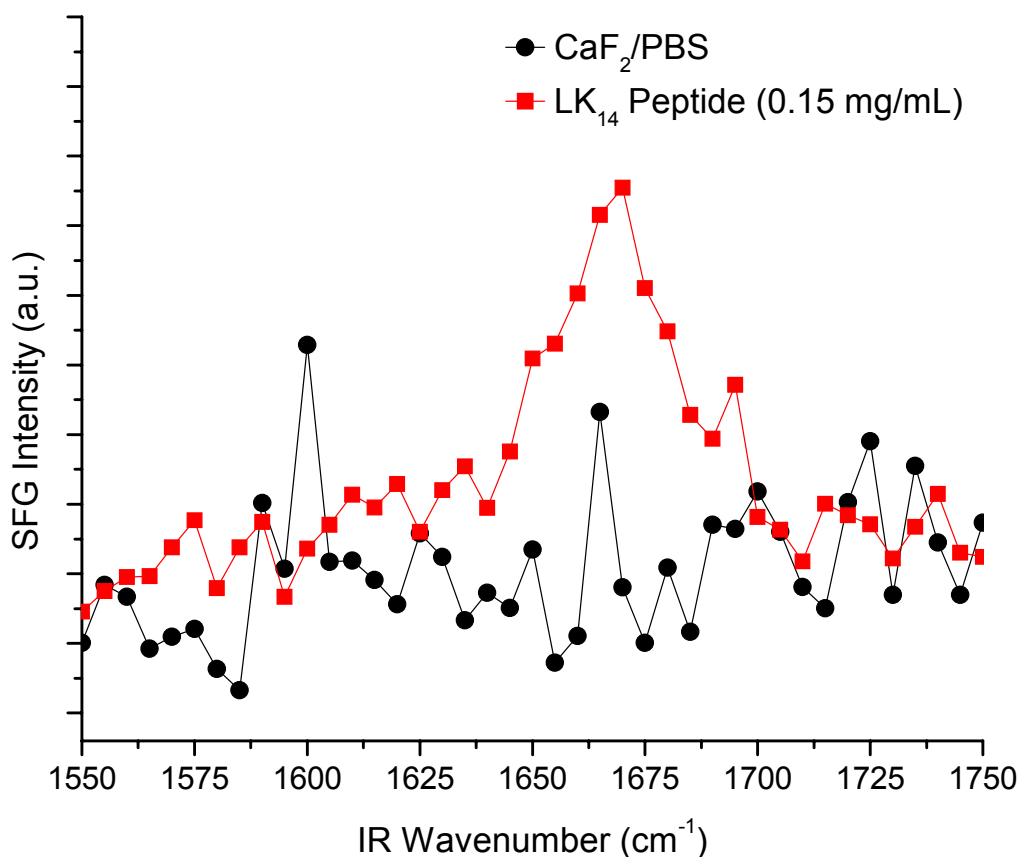


**Figure 9.5.** The amide I SFG spectrum of 1X PBS (high ionic strength) at the hydrophilic CaF<sub>2</sub> solid-liquid interface before (black circles) and after (red squares) addition of LK<sub>14</sub> peptide (0.15 mg/mL). A weak vibrational mode is observed at  $1670\text{ cm}^{-1}$  and is preliminarily assigned to a random coil peptide backbone secondary structure. The location of this peak is  $15\text{ cm}^{-1}$  blue-shifted from the amide I mode of LK<sub>14</sub> peptide on *d*<sub>8</sub>-PS in Figure 9.3 (high ionic strength, 1X PBS) and Figure 9.4 (low ionic strength, 0.01X PBS).

## 9.4. Conclusions

We have developed and implemented a new optical parametric amplifier (OPA) based on lithium thioindate (LIS) nonlinear crystals. This LIS based OPA was used to produce infrared laser wavelengths between  $1500\text{ cm}^{-1}$  and  $2000\text{ cm}^{-1}$  with improved energy conversion and beam quality than alternative OPAs utilizing AGS or AGSe crystals. We used this new OPA system to conduct SFG experiments investigating the amide I mode of a solution of a model peptide, LK<sub>14</sub> adsorbed on *d*<sub>8</sub>-PS and CaF<sub>2</sub> surfaces. The SFG spectra show an amide I peak for the amino acid at  $1655\text{ cm}^{-1}$  at the *d*<sub>8</sub>-PS solid-liquid interface independent of PBS buffer strength and indicative of interfacial peptide species possessing an  $\alpha$ -helix secondary structure. On the CaF<sub>2</sub> surface, the amide I SFG spectrum showed a weak spectral peak at  $1670\text{ cm}^{-1}$  indicating the LK<sub>14</sub> peptide backbone exhibits a different secondary structure on the hydrophilic surface than on the hydrophobic surface. The secondary structure of the interfacial peptide on the CaF<sub>2</sub> was preliminarily assigned as a random coil secondary structure, but additional study needs to be done to confirm this assignment.

## References

1. Castner, D. G.; Ratner, B. D., *Surface Science* **2002**, *500* (1-3), 28-60.
2. Horbett, T. A.; Brash, J. L.; American Chemical Society. Division of Colloid and Surface Chemistry.; American Chemical Society. Meeting, *Proteins at interfaces II : fundamentals and applications*. American Chemical Society: Washington, DC, 1995; p xiv, 561
3. Kasemo, B., *Current Opinion in Solid State & Materials Science* **1998**, *3* (5), 451-459.
4. Somorjai, G. A.; York, R. L.; Butcher, D.; Park, J. Y., *Physical Chemistry Chemical Physics* **2007**, *9* (27), 3500-3513.
5. Chen, X. Y.; Clarke, M. L.; Wang, J.; Chen, Z., *International Journal of Modern Physics B* **2005**, *19* (4), 691-713.
6. Wang, J.; Clarke, M. L.; Chen, X. Y.; Even, M. A.; Johnson, W. C.; Chen, Z., *Surface Science* **2005**, *587* (1-2), 1-11.
7. York, R. L.; Browne, W. K.; Geissler, P. L.; Somorjai, G. A., *Israel Journal of Chemistry* **2007**, *47* (1), 51-58.
8. Fossier, S.; Salaun, S.; Mangin, J.; Bidault, O.; Thenot, I.; Zondy, J. J.; Chen, W. D.; Rotermund, F.; Petrov, V.; Petrov, P.; Henningsen, J.; Yelisseyev, A.; Isaenko, L.; Lobanov, S.; Balachninaite, O.; Slekys, G.; Sirutkaitis, V., *Journal of the Optical Society of America B-Optical Physics* **2004**, *21* (11), 1981-2007.
9. Isaenko, L.; Vasilyeva, I.; Yelisseyev, A.; Lobanov, S.; Malakhov, V.; Dovlitova, L.; Zondy, J. J.; Kavun, I., *Journal of Crystal Growth* **2000**, *218* (2-4), 313-322.
10. Krimm, S.; Bandekar, J., *Advances in Protein Chemistry* **1986**, *38*, 181-364.
11. Socrates, G., *Infrared and Raman characteristic group frequencies : tables and charts*. 3rd ed.; Wiley: Chichester ; New York, 2001; p xv, 347 p.
12. Wang, J.; Even, M. A.; Chen, X. Y.; Schmaier, A. H.; Waite, J. H.; Chen, Z., *Journal of the American Chemical Society* **2003**, *125* (33), 9914-9915.
13. Wang, J.; Chen, X. Y.; Clarke, M. L.; Chen, Z., *Proceedings of the National Academy of Sciences of the United States of America* **2005**, *102* (14), 4978-4983.
14. Chen, X. Y.; Wang, J.; Sniadecki, J. J.; Even, M. A.; Chen, Z., *Langmuir* **2005**, *21* (7), 2662-2664.
15. Chen, X. Y.; Chen, Z., *Biochimica Et Biophysica Acta-Biomembranes* **2006**, *1758* (9), 1257-1273.
16. York, R. L.; Holinga, G. J.; Guyer, D. R.; McCrea, K. R.; Ward, R. S.; Somorjai, G. A., *Applied Spectroscopy* **2008**, *62* (9), 937-940.
17. Degrado, W. F.; Lear, J. D., *Journal of the American Chemical Society* **1985**, *107* (25), 7684-7689.
18. Long, J. R.; Oyler, N.; Drobny, G. P.; Stayton, P. S., *Journal of the American Chemical Society* **2002**, *124* (22), 6297-6303.
19. Mermut, O.; Phillips, D. C.; York, R. L.; McCrea, K. R.; Ward, R. S.; Somorjai, G. A., *Journal of the American Chemical Society* **2006**, *128* (11), 3598-3607.
20. York, R. L.; Mermut, O.; Phillips, D. C.; McCrea, K. R.; Ward, R. S.; Somorjai, G. A., *J. Phys. Chem. C* **2007**, *111* (25), 8866-8871.
21. Boyd, R. W., *Nonlinear optics*. 2nd ed.; Academic Press: San Diego, CA, 2003; p xvii, 578 p.
22. Wang, H. F.; Gan, W.; Lu, R.; Rao, Y.; Wu, B. H., *International Reviews in Physical Chemistry* **2005**, *24* (2), 191-256.

23. Wei, X.; Hong, S. C.; Zhuang, X. W.; Goto, T.; Shen, Y. R., *Physical Review E* **2000**, *62* (4), 5160-5172.
24. Miranda, P. B.; Shen, Y. R., *Journal of Physical Chemistry B* **1999**, *103* (17), 3292-3307.
25. Zhuang, X.; Miranda, P. B.; Kim, D.; Shen, Y. R., *Physical Review B* **1999**, *59* (19), 12632-12640.
26. Lambert, A. G.; Davies, P. B.; Neivandt, D. J., *Applied Spectroscopy Reviews* **2005**, *40* (2), 103-145.
27. Smith, J. D.; Saykally, R. J.; Geissler, P. L., *Journal of the American Chemical Society* **2007**, *129* (45), 13847-13856.